A FRAMEWORK FOR MODELING LARGE DEFORMATIONS AND STRESS WAVE MECHANICS IN SOFT BIOLOGICAL TISSUE

A Dissertation

by

SHAHLA ZAMANI

Submitted to the Graduate and Professional School of
Texas A&M University
in partial fulfillment of the requirements for the degree of

DOCTOR OF PHILOSOPHY

Chair of Committee,	Alan D. Freed
Co-Chair of Committee,	J. N. Reddy
Committee Members,	John C. Criscione
	Alan Palazzolo
Head of Department,	Andreas A. Polycarpou

August 2021

Major Subject: Mechanical Engineering

ABSTRACT

An oblique, Cartesian, coordinate system arises from the geometry affiliated with a Gram-Schmidt (**QR**) factorization of the deformation gradient $\boldsymbol{F}$, wherein **Q** is a proper orthogonal matrix and **R** is an upper-triangular matrix.

First, a cube deforms into a parallelepiped whose edges are oblique and serve as the base vectors for a convected coordinate system. Components for the metric tensor, its dual, and their rates, evaluated in this convected coordinate system, are established for *any* state of deformation. Strains and strain rates are defined and quantified in terms of these metrics and their rates. Quotient laws and their affiliated Jacobians are constructed that govern how vector and tensor fields transform between this oblique coordinate system, where constitutive equations are ideally cast, and the reference, rectangular, Cartesian, coordinate system described in terms of Lagrangian variables, where boundary value problems are solved.

Then, we derived two sets of thermodynamically admissible stress-strain pairs. They are quantified in terms of physical components extracted from a convected stress and a convected velocity gradient, with elastic models being presented for both sets. The first model supports two modes of deformation: elongation and shear. The second model supports three modes of deformation: dilatation, squeeze and shear. These models are distinguished by their pure- and simple-shear responses. They contain the coupling effects of Lord Kelvin [1], Poisson [2] and Poynting [3].

The Eulerian formulation, consists of a lower-triangular stretch postmultiplied by a different rotation tensor is studied. The corresponding stretch tensors is denoted as the Eulerian Laplace stretches. Kinematics (with physical interpretations) and work conjugate stress measures are analyzed. The Eulerian formulation, which may be advantageous for modeling isotropic solids and fluids with no physically identifiable reference configuration, does not seem to have been used elsewhere in a continuum mechanical setting.

As the application of our work, we introduced a dodecahedron to model an alveolus. Its

geometric properties are derived in detail with regard to its three geometric features: 1D septal chords, 2D septal membranes, and the 3D alveolar sac. The kinematics are derived for us to model a deforming dodecahedron, including the shape functions needed for interpolating each geometry. Constitutive models are derived that are suitable for describing the thermomechanical response for the structural constituents of an alveolus: its septal chords, its permeable membranes, and its volume. Numerical methods are advanced for solving first- and second-order ordinary differential equations (ODEs) and spatial integrations along a bar, across a pentagon, and throughout a tetrahedron using Gaussian quadrature schemes designed for each geometry. A variational formulation is used to create our structural modeling of an alveolus. Constitutive equations suitable for modeling biological tissues are derived from thermodynamics using the theory of implicit elasticity, presented in an appendix.

DEDICATION

To my parents and my spouse.

ACKNOWLEDGMENTS

There are many who helped me along the way on this journey. I want to take a moment to thank them.

First and foremost, I have to thank my research supervisor, Professor Alan D. Freed. Without his assistance and dedicated involvement in every step throughout the process, this dissertation would have never been accomplished. Your insightful feedback pushed me to sharpen my thinking and brought my work to a higher level. You have taught me more than I could ever give you credit for here. I would like to thank you very much for your support and understanding.

I would like to express my gratitude to my Co-Chair, Professor J.N. Reddy, who supported me and offered deep insight into the study. I have been honored to study with Professor Reddy, who has dedicated to the field of applied and computational mechanics.

I would also like to show gratitude to my committee, including Dr. John C. Criscione and Dr. Alan Palazzolo for providing me extensive personal and professional guidance.

I am grateful for the financial support that was provided me during my Ph.D. studies by U.S. Army Combat Capabilities Development Command (CCDC) Army Research Laboratory. I am thankful to all my seniors and colleagues at the Advanced Computational Mechanics Laboratory (ACML).

Getting through my dissertation required more than academic support. It is a pleasure to thank Mrs. Karen Freed who gave me the necessary distractions from my research and made my stay in the USA memorable.

Most importantly, none of this could have happened without my family. My parents and my siblings, whose love and guidance are with me in whatever I pursue. They are the ultimate role models. To my spouse, who provide unending inspiration. He was always around at times I thought that it is impossible to continue, he helped me to keep things in perspective. This dissertation stands as a testament to your unconditional love and encouragement.

TABLE OF CONTENTS

Page

LIST OF FIGURES

1. INTRODUCTION

1.1 Background

It was in his 1951 paper entitled "On the use of convected coordinate systems in the mechanics of continuous media" published in the *Proceedings of the Cambridge Philosophical Society* where Arthur Lodge introduced body fields—a formalism he made precise in his 1974 book on *Body Tensor Fields in Continuum Mechanics* [10]. Lodge showed that a connection exists between convected space-tensor fields and body-tensor fields, viz., their components are equivalent at that instant when their coordinate axes become coincident [11].

A common conjecture betwixt Brillouin [12], Hencky [13], Oldroyd [14], Lodge [11], Green & Zerna [15] and others is: It is within a convected coordinate system where an application of the calculus will be independent of spatial considerations, and therefore, it is there where constitutive equations will take on their simplest representation. Lamé [16] was the first to use curvilinear coordinate systems in his analysis of shells.

1.2 Introduction

We construct our analysis using convected space-coordinate systems derived from the geometry of a parallelepiped generated out of a Gram decomposition of the deformation gradient that, itself, is generated from the motion of a body traveling through space.

Our analysis is based upon the hypothesis: *Deformation is homogeneous at a particle in a continuum.*

The partially embedded coordinate system arrived at in our analysis is oblique Cartesian. It convects with the motion, but only within a neighborhood surrounding a particle. The coordinate axes defining this system are comprised of tangents to an embedded curvilinear triad whose origin is located at the particle $\mathcal{P}$ whereat deformation gradient $\mathbf{F}(\mathcal{P})$ is evaluated, see Fig. 2.1.

A convected metric with local reach is derived in this study that describes a homogeneous state of deformation in terms of an oblique, Cartesian, coordinate system, provided one knows components of the deformation gradient.

We also use the two Jacobians arising from our convected kinematic analysis to arrive at two sets of thermodynamic conjugate pairs. Each pair is comprised of two fields: a stress and a strain, both measures being scalar fields. From these thermodynamic co-ordinates, constitutive equations can be derived. One set of conjugate pairs associates with two distinct modes of deformation: elongation and shear. The second set associates with three distinct modes of deformation: dilatation, squeeze and shear. Elastic models that describe Kelvin, Poisson and Poynting coupling effects are put forward for both sets of conjugate pairs. These models are not restricted to infinitesimal strains and/or rotations. The Lodge-Meissner [17] relation from rheology and the Poynting [3] effect from solid mechanics are shown to describe the same physics.

We studied a different triangular decomposition of deformation gradient that splits the deformation gradient tensor into a rotation tensor followed (premultiplied) by a lower-triangular stretch tensor. This construction is referred to as the Eulerian formulation of the triangular decomposition of deformation.

In general, Lagrangian formulations, that is studied in chapter 2 and 3 (e.g., constitutive models based on Lagrangian measures of strain) are preferred for modeling anisotropic solids, as-well-as certain isotropic solids, that have a clearly defined initial, stress-free, or 'reference' state. This is readily apparent for single crystals, for example, whereby a reference state is identified with the regular lattice geometry occupied by atoms in their minimum energy (ground) state. Hyperelasticity is usually invoked in this context [18, 19], whereby an energy potential depending on a Lagrangian stretch tensor is prescribed. Eulerian formulations, in contrast, are often preferred for modeling isotropic solids (and fluids) that have no obvious initial or reference state. For example, many biological tissues, in vivo, are perpetually under tension, and a stress-free reference state is never physically realized. Eulerian forms are also

used for hypoelastic constitutive modeling that is often more popular than hyperelasticity for solving initial-boundary value problems numerically.

These models and metrics whose parameters are physical and unique, and whose numeric implementation will be efficient and stable are used for modeling large deformations and stress wave mechanics in soft biological tissue. Injuries that occur after a blast wave impacts a person wearing personal protective equipment (PPE) or a non-penetrating ballistic projectile impacts a person wearing PPE are referred to as behind armor blunt trauma (BABT). The kinetic energy from such an impact is absorbed by the PPE, and the bony and soft tissues. Verification is through experiments where, typically, a suit of body armor is placed over a "body" subjected to a ballistic impact from a projectile fired by a weapon, all in accordance with a standard. Current practice is to use clay (usually Roma Plastilina No. 1 clay) as a surrogate for the human body in these tests.

BABT occurs at the microscopic level of alveoli, which make up the parenchyma, i.e., the spongy tissue of lung that comprises around 90% of lung by volume, cf. Fig. 1.1, there being some 500 million alveoli in a typical human lung. We develop a mechanistic multi-scale model that is capable of describing the deformation and damage that occur at an alveolar level, caused by a shock wave traveling through the parenchyma, induced through either a blast or a ballistic impact to PPE.

Performing experiments for the purpose of model characterization is extremely difficult when it comes to modeling lung. Lung is a structure; parenchyma is a material. Therefore, one would normally choose to test the parenchyma, and from these data extract one's model parameters but, because of its spongy nature, we are challenged to do so in a physically meaningful way. Consequently, one typically tests whole lungs, or lobes thereof, and from these structural experiments we are tasked to extract material parameters through an inverse analysis. An alternative approach whereby one could, in principle, acquire parameters for the continuum models would be to homogenize a microscopic structural response for the alveoli of the parenchyma. The work presented here addresses this approach in our modeling of

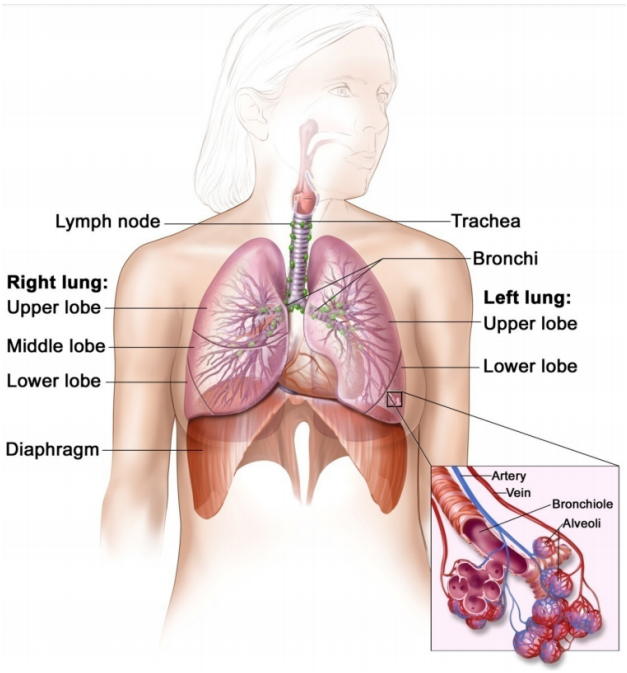

Figure 1.1: A medical drawing of the respiratory system [8].

deformation, damage, and injury in alveolar structures.

The primary purpose of this work is to provide a microscopic model for lung tissue that can be used as an aid in the parameterization of a macroscopic model for lung that will be reasonably accurate yet efficient to run in full torso finite element analyses to study BABT for the purpose of improving PPE.

Figure 1.2 shows micrographs from a rat lung taken at different magnifications. In the lower-resolution image, one sees numerous alveoli that became exposed because of the sectioning process. Also present are several alveolar ducts that connect individual alveoli to a bronchial tree. In the higher-resolution image we observe the faceted structure of these alveoli, wherein one can see the septal chords and membranes, the latter being traversed by capillaries through which gas exchange occurs. Gas exchange is not modeled here.

Alveolar geometry is modeled here as a dodecahedron, i.e., a soccer-ball like structure comprising 12 pentagonal facets bordered by 30 septal cords that are connected at 20 vertices. Each vertex links three neighboring cords of the alveolus with a fourth chord from a

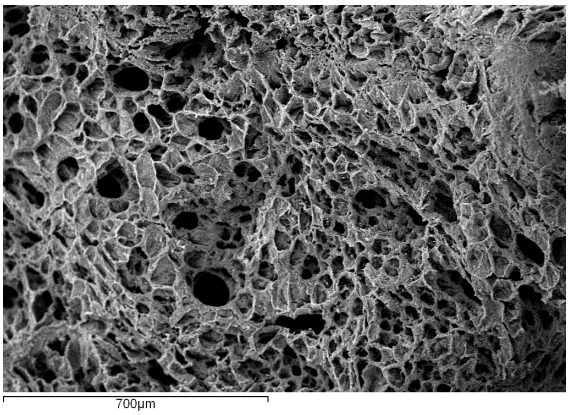

(a) Magnification at 100X. This is Fig. 5 in Freed *et al.* [20].

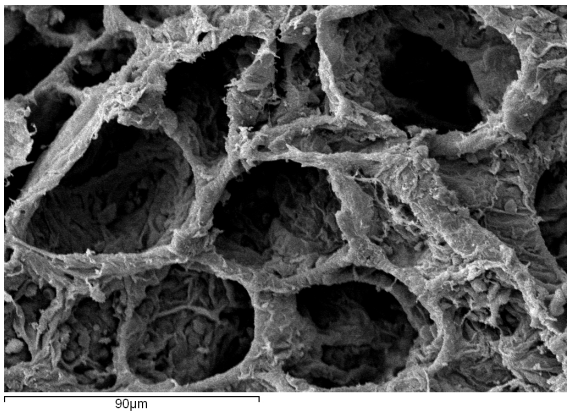

(b) Magnification at 750X. This is Fig. 7 in Freed *et al.* [20].

Figure 1.2: SEM photographs from a sectioned rat lung. The alveolar diameter in rat lung is about one quarter the alveolar diameter in human lung.

neighboring alveolus.

This hypothesis was tested and confirmed in an experimental study done by Butler *et al.* [21] where they used light scattering to study changes in geometry of the septal planes in alveoli, from which they concluded: "the microscopic strain field does not differ significantly from the macroscopic field." We employ this hypothesis by taking the deformation gradient from, say, a Gauss point in a finite element model of lung, and imposing it as a far-field deformation onto our dodecahedral model of an alveolus. From this kinematic input we arrive at an upper bound on the macroscopic stress/stiffness response, akin to a Voigt approximation, through a homogenization of the microscopic forces created within our structural model for an alveolus.

In this research we set out to develop a constitutive framework for alveolar mechanics, fully cognizant of the aforementioned challenges. Our objectives are different from those of prior studies in alveolar mechanics in that we seek to describe the response/injury of a human lung that has been subjected to a stress wave propagating across the thorax region caused by an impact from either a blunt object or a blast wave. Consequently, some important aspects in the modeling of a breathing lung are thought to be less impactful here, e.g., the

effect of surfactant in keeping alveoli from collapsing at the end of expiration.

1.3 Motivation and Scope of the Study

The contribution of the proposed study is novel and significant in the following respects:

1. A long-standing challenge is resolved to quantify the relevant, convected, tensor fields for any arbitrary state of deformation as they would arise in a finite element analysis.

2. A general kinematic description for a deformable body in terms of a locally, convected, coordinate system as a platform is provided.

3. The covariant and contravariant base-vectors, metrics, strains, and their differential rates in the convected coordinate system, in the sense of Lodge [11, 22, 23, 24] are derived that describe the geometry of Laplace stretch.

4. Stresses are quantified and constitutive equations are constructed in this convected coordinate system that is oblique Cartesian.

5. An Eulerian lower-triangular decomposition in the context of continuum mechanics for modeling isotropic solids (and fluids) that have no obvious initial or reference state has been derived.

6. An accurate material models for the human body that are also efficient in the finite element implementation is developed, which facilitate the study Behind Armor Blunt Trauma (BABT) in an effort to improve the designs of Personal Protective Equipment (PPE).

2. ON THE USE OF CONVECTED COORDINATE SYSTEMS IN THE MECHANICS OF CONTINUOUS MEDIA FROM LAGRANGIAN LAPLACE STRETCH [4]

A body $\mathcal{B}$ is an open set in a topological space with a non-negative Borel measure introduced to describe mass [25]. Elements $\{\mathcal{P}\}$ of set $\mathcal{B}$ are called particles. Supplied with a rigid frame of reference, any motion $\boldsymbol{\chi}$ of body $\mathcal{B}$ can be described as $\boldsymbol{x} = \boldsymbol{\chi}(\mathcal{P}, t)$ at particle $\mathcal{P} \in \mathcal{B}$ at time t. At each instant t, a motion $\boldsymbol{\chi}(\cdot, t)$ is the placement of particle $\mathcal{P}$ into body $\mathcal{B}$.

2.1 Base Vector

In this chapter we utilize four coordinates systems that associate with four sets of base vectors. Three coordinate systems are rectangular Cartesian with orthonormal base vectors. The fourth coordinate system is oblique Cartesian with base vectors that are neither orthogonal nor of unit length.

A rectangular Cartesian triad with base vectors $(\vec{\mathbf{e}}_1, \vec{\mathbf{e}}_2, \vec{\mathbf{e}}_3)$, denoted as $\{\vec{\mathbf{e}}_i\}$, establishes the first coordinate system considered. It describes an Eulerian frame of reference $\S$ that spans Euclidean point space $\mathcal{E}$. A different, rectangular, Cartesian triad of base vectors $(\vec{\boldsymbol{E}}_1, \vec{\boldsymbol{E}}_2, \vec{\boldsymbol{E}}_3)$, denoted as $\{\vec{\boldsymbol{E}}_i\}$, establishes the second coordinate system considered. These are the Lagrangian base vectors. Base vectors $\{\vec{\boldsymbol{E}}_i\}$ rotate from the Eulerian base vectors $\{\vec{\mathbf{e}}_i\}$ according to an orthogonal tensor $\mathbf{R}$ that arises from a polar decomposition of the deformation gradient, viz., $\boldsymbol{F} = \mathbf{RU}$ where $\mathbf{U}$ is the symmetric Stretch tensor. Another rectangular Cartesian triad of base vectors $\{\tilde{\mathbf{e}}_1, \tilde{\mathbf{e}}_2, \tilde{\mathbf{e}}_3\}$, denoted as $\{\tilde{\mathbf{e}}_i\}$, establishes the third coordinate system considered, see Fig. 2.1.

The left-hand graphic is of a unit cube representing a material element oriented with respect to a set of orthonormal base vectors $\{\tilde{\mathbf{e}}_1, \tilde{\mathbf{e}}_2, \tilde{\mathbf{e}}_3\}$ originating from some particle $\mathcal{P}$. This spatial triad coincides with a set of material lines $\{\vec{\boldsymbol{\xi}}_1, \vec{\boldsymbol{\xi}}_2, \vec{\boldsymbol{\xi}}_3\}$ that become material curves in the deformed state, the right-hand graphic. Tangents to these material curves $\{\vec{\boldsymbol{g}}_1, \vec{\boldsymbol{g}}_2, \vec{\boldsymbol{g}}_3\}$

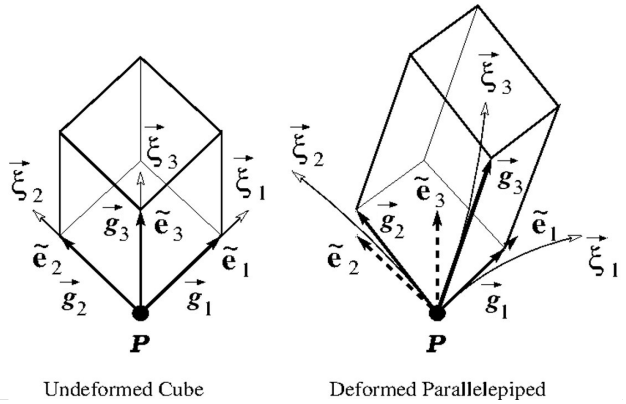

Figure 2.1: Deformation of a cube to a parallelepiped

describe the edges of a parallelepiped. As volume of the parallelepiped approaches zero, i.e., the volume of particle $\mathcal{P}$, differences between the material curves $\{\vec{\boldsymbol{\xi}}_1, \vec{\boldsymbol{\xi}}_2, \vec{\boldsymbol{\xi}}_3\}$ and the oblique, Cartesian, tangent vectors $\{\vec{\boldsymbol{g}}_1, \vec{\boldsymbol{g}}_2, \vec{\boldsymbol{g}}_3\}$ become negligible. The oblique, Cartesian, coordinate system becomes coincident with the embedded, curvilinear, coordinate system within a neighborhood surrounding $\mathcal{P}$. Deformation becomes homogeneous as the volume of a material element shrinks to a particle, and the convected coordinate system becomes oblique Cartesian.

2.2 Lagrangian Laplace Stretch

To describe kinematics of a planar membrane, an upper-triangular Gram–Schmidt decomposition of the deformation gradient $\boldsymbol{F}$ is used in lieu of the symmetric polar decomposition that is commonly adopted [26, 27, 28, 5, 29]. McLellan [30, 18] was the first to propose a triangular decomposition of $\boldsymbol{F}$, to prove its uniqueness and existence, and to establish many of its physical properties. This idea has been rediscovered several times since then.

A Lagrangian Gram–Schmidt factorization of the deformation gradient $\boldsymbol{F}$ is written here as $\boldsymbol{F} = \boldsymbol{\mathcal{R}}\boldsymbol{\mathcal{U}}$, where the rotation $\boldsymbol{\mathcal{R}}$ is orthogonal, and where the Lagrangian Laplace Stretch $\boldsymbol{\mathcal{U}}$ is upper-triangular [29].[1] This triangular measure of stretch possesses an inherent property

[1]The **QR** rotation $\boldsymbol{\mathcal{R}}$ and Lagrangian Stretch $\boldsymbol{\mathcal{U}}$ tensors are distinct from those that arise from a polar decomposition of a deformation gradient, typically denoted as $\boldsymbol{R}$ and $\boldsymbol{U}$, as found in any, modern, continuum mechanics text. McLellan [30, 18] introduced the Lagrangian Laplace Stretch in 1976, which he denoted as

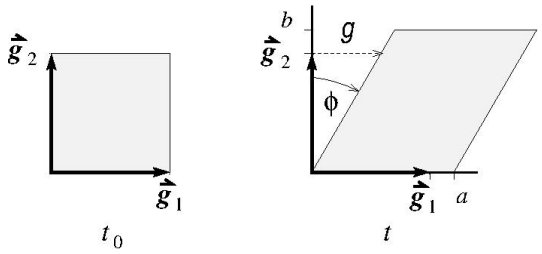

Figure 2.2: Physical attributes of a planar deformation

in two space: the direction aligned with the rotated 1-axis, denoted as $\vec{\boldsymbol{g}}_1$, remains invariant under transformation $\boldsymbol{\mathcal{U}}$ [18], i.e., it is a material vector in a neighborhood surrounding that particle whereat $\boldsymbol{F}$ is evaluated [4].

2.2.1 2D Factorization of Deformation Gradient

The 2×2 deformation gradient associated with a planar membrane has a Gram–Schmidt decomposition expressed in terms of four physical attributes. Three of these attributes describe deformation. They are defined as [28]

$$a = \sqrt{F_{11}^2 + F_{21}^2}, \quad b = \frac{F_{11}F_{22} - F_{12}F_{21}}{\sqrt{F_{11}^2 + F_{21}^2}}, \quad g = \frac{F_{11}F_{12} + F_{22}F_{21}}{F_{11}^2 + F_{21}^2} \tag{2.1}$$

thereby populating Lagrangian Laplace Stretch $\boldsymbol{\mathcal{U}}$ and its inverse $\boldsymbol{\mathcal{U}}^{-1}$ with components

$$\boldsymbol{\mathcal{U}} = \begin{bmatrix} a & ag \\ 0 & b \end{bmatrix} \qquad \text{and} \qquad \boldsymbol{\mathcal{U}}^{-1} = \begin{bmatrix} 1/a & -g/b \\ 0 & 1/b \end{bmatrix} \tag{2.2}$$

where a and b are the principal elongations (ratios of current lengths to reference lengths) and g is the extent of in-plane shear, as measured in a co-ordinate frame $(\vec{\boldsymbol{g}}_1, \vec{\boldsymbol{g}}_2)$ illustrated in Fig. 2.2.

Orthogonal tensor $\boldsymbol{\mathcal{R}} = \left[\vec{\boldsymbol{g}}_1 \;\middle|\; \vec{\boldsymbol{g}}_2\right] = \delta_{ij}\, \vec{\boldsymbol{g}}_i \otimes \vec{\boldsymbol{e}}_j = \mathcal{R}_{ij}\, \vec{\boldsymbol{e}}_i \otimes \vec{\boldsymbol{e}}_j$ rotates the reference co-ordinate axes $(\vec{\boldsymbol{e}}_1, \vec{\boldsymbol{e}}_2)$ into a physical co-ordinate system $(\vec{\boldsymbol{g}}_1, \vec{\boldsymbol{g}}_2)$ through an angle θ, which

$\boldsymbol{H}$, while Srinivasa [26] denoted it as $\tilde{\boldsymbol{F}}$ in his 2012 paper.

is the fourth physical attribute arising from a **QR** factorization of $\boldsymbol{F}$. This angle of rotation describes a proper orthogonal matrix, specifically

$$\boldsymbol{\mathcal{R}} = \begin{bmatrix} \cos\theta & -\sin\theta \\ \sin\theta & \cos\theta \end{bmatrix} \tag{2.3}$$

with

$$\sin\theta = \frac{F_{21}}{\sqrt{F_{11}^2 + F_{21}^2}}, \quad \cos\theta = \frac{F_{11}}{\sqrt{F_{11}^2 + F_{21}^2}} \quad \therefore \quad \theta = \tan^{-1}\left(\frac{F_{21}}{F_{11}}\right) \tag{2.4}$$

where a positive angle θ corresponds with a counterclockwise rotation of physical axes $(\vec{\boldsymbol{g}}_1, \vec{\boldsymbol{g}}_2)$ about reference axes $(\vec{\boldsymbol{e}}_1, \vec{\boldsymbol{e}}_2)$.

2.2.1.1 Dilemma

Until recently, [31] there has been a tacit assumption in prior applications of Gram–Schmidt factorizations of $\boldsymbol{F}$: Specifically, the physical base vectors $(\vec{\boldsymbol{g}}_1, \vec{\boldsymbol{g}}_2)$ satisfy a geometric condition whereby the physical 1-direction $\vec{\boldsymbol{g}}_1$ rotates out of the reference 1-direction $\vec{\boldsymbol{e}}_1$, but this need not always be the case. Physical vector $\vec{\boldsymbol{g}}_1$ could equally likely rotate out of the 2-direction $\vec{\boldsymbol{e}}_2$ of the reference frame. At issue is not: How the physical base vectors orient in space? That is managed by Gram's procedure. Rather, at issue is: How do the physical base vectors index with respect to the reference base vectors? This topic is addressed in Appendix C for the 3D case; below, we address this topic for the 2D case.

To illustrate the concern, consider two deformation histories, as drawn in Fig. 2.3, each of which describes a simple shear taking place in the plane of a membrane. In one case shear occurs in the 1-direction, while in the other case shear occurs in the 2-direction. The left graphic designates a reference configuration while the right two graphics designate deformed configurations, both in basis $(\vec{\boldsymbol{g}}_1, \vec{\boldsymbol{g}}_2)$. There are no elongations. These motions lead to different Gram–Schmidt factorizations of the deformation gradient. When following the

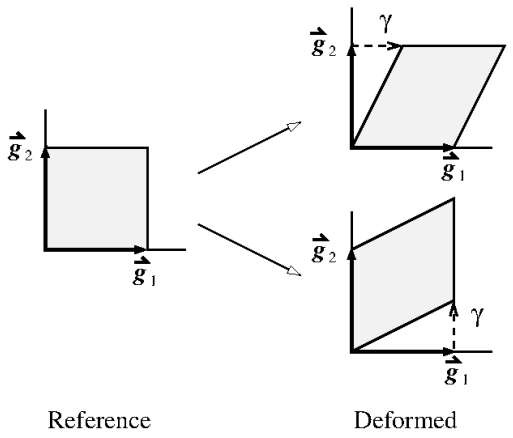

Figure 2.3: Reference and deformed configuration associated with Eqns. (2.5a) and (2.5b).

protocol of Eqns. (2.1–2.4), these factorizations are found to be

$$\boldsymbol{F} = \begin{bmatrix} 1 & \gamma \\ 0 & 1 \end{bmatrix} \implies \boldsymbol{\mathcal{R}} = \begin{bmatrix} 1 & 0 \\ 0 & 1 \end{bmatrix}, \quad \boldsymbol{\mathcal{U}} = \begin{bmatrix} 1 & \gamma \\ 0 & 1 \end{bmatrix} \tag{2.5a}$$

and

$$\boldsymbol{F} = \begin{bmatrix} 1 & 0 \\ \gamma & 1 \end{bmatrix} \implies \begin{cases} \boldsymbol{\mathcal{R}} = \dfrac{1}{\sqrt{1+\gamma^2}} \begin{bmatrix} 1 & -\gamma \\ \gamma & 1 \end{bmatrix} \\ \boldsymbol{\mathcal{U}} = \begin{bmatrix} \sqrt{1+\gamma^2} & \gamma \\ 0 & 1 \,/\, \sqrt{1+\gamma^2} \end{bmatrix} \end{cases} \tag{2.5b}$$

respectively, where we see that shear $\mathcal{U}_{12}$ has the same physical interpretation in both cases, viz., γ, but elongations $\mathcal{U}_{11}$ and $\mathcal{U}_{22}$ do not, viz., $\mathcal{U}_{11} = 1$ and $\mathcal{U}_{22} = 1$ in Eqn. (2.5a), whereas $\mathcal{U}_{11} = \sqrt{1+\gamma^2}$ and $\mathcal{U}_{22} = 1/\sqrt{1+\gamma^2}$ for the motion described in Eqn. (2.5b). Consequently, two geometric interpretations are produced for just one physical mode of deformation. This cannot be!

The only difference between the motions that lead to the two deformation gradients presented in Eqn. (2.5) is one's choice for labeling the co-ordinate directions. Matrix oper-

ations of row and column pivoting, taken from linear algebra, allow one to transform the lower-triangular form of Eqn. (2.5b) into an upper-triangular form like Eqn. (2.5a); hence, producing an unified physical interpretation for both shearing motions, and thereby providing a means for establishing a remedy to this dilemma.

2.2.1.2 Remedy

For 2D membranes, there are only two co-ordinate re-indexings that are possible (for 3D solids there are six, Appendix C). The default is no re-indexing at all, in which case

$$[\boldsymbol{P}] = [\boldsymbol{P}_0] := \begin{bmatrix} 1 & 0 \\ 0 & 1 \end{bmatrix} \qquad \Longrightarrow \qquad \begin{bmatrix} \mathcal{F}_{11} & \mathcal{F}_{12} \\ \mathcal{F}_{21} & \mathcal{F}_{22} \end{bmatrix} := \begin{bmatrix} F_{11} & F_{12} \\ F_{21} & F_{22} \end{bmatrix} \tag{2.6a}$$

while in the second case there is a re-indexing specified by

$$[\boldsymbol{P}] = [\boldsymbol{P}_1] := \begin{bmatrix} 0 & 1 \\ 1 & 0 \end{bmatrix} \qquad \Longrightarrow \qquad \begin{bmatrix} \mathcal{F}_{11} & \mathcal{F}_{12} \\ \mathcal{F}_{21} & \mathcal{F}_{22} \end{bmatrix} := \begin{bmatrix} F_{22} & F_{21} \\ F_{12} & F_{11} \end{bmatrix} \tag{2.6b}$$

where components $\mathcal{F}_{ij} = P_{ki} F_{k\ell} P_{\ell j}$ are the components to be used in the Gram–Schmidt factorization, and where $\boldsymbol{P} \in \{\boldsymbol{P}_0, \boldsymbol{P}_1\}$ is orthogonal, i.e., $\boldsymbol{P}\boldsymbol{P}^{\mathsf{T}} = \boldsymbol{P}^{\mathsf{T}}\boldsymbol{P} = \boldsymbol{I}$ with $\det \boldsymbol{P} = \pm 1$; specifically, $\det \boldsymbol{P}_0 = +1$ while $\det \boldsymbol{P}_1 = -1$.

The challenge in implementing such a strategy is to determine when to switch from $\boldsymbol{P}_0$ (case 1) to $\boldsymbol{P}_1$ (case 2), or back again, viz., from $\boldsymbol{P}_1$ to $\boldsymbol{P}_0$. To this end, it is useful to represent the components of a planar deformation gradient as

$$\begin{bmatrix} \mathcal{F}_{11} & \mathcal{F}_{12} \\ \mathcal{F}_{21} & \mathcal{F}_{22} \end{bmatrix} = \begin{cases} \text{case 1}: & \begin{bmatrix} F_{11} & F_{12} \\ F_{21} & F_{22} \end{bmatrix} = \begin{bmatrix} x & \beta y \\ \alpha x & y \end{bmatrix} \\ \text{case 2}: & \begin{bmatrix} F_{22} & F_{21} \\ F_{12} & F_{11} \end{bmatrix} = \begin{bmatrix} y & \alpha x \\ \beta y & x \end{bmatrix} \end{cases} \tag{2.7}$$

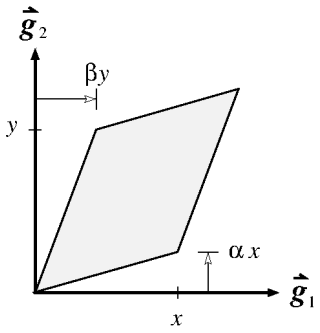

Figure 2.4: A general description for homogeneous planar deformation

The physical attributes for Lagrangian Laplace Stretch, as they pertain to the two cases in Eqn. (2.6), written in terms of components F_{ij} from $\boldsymbol{F} = F_{ij}\,\vec{\boldsymbol{e}}_i \otimes \vec{\boldsymbol{e}}_j$ as defined in Eqn. (2.7), are respectively given by

$$\tilde{a} = x\sqrt{1+\alpha^2} \qquad\qquad \hat{a} = y\sqrt{1+\beta^2} \tag{2.8a}$$

$$\tilde{b} = y(1-\alpha\beta) \,/\, \sqrt{1+\alpha^2} \qquad\qquad \hat{b} = x(1-\alpha\beta) \,/\, \sqrt{1+\beta^2} \tag{2.8b}$$

$$\tilde{g} = y(\alpha+\beta) \,/\, x(1+\alpha^2) \qquad\qquad \hat{g} = x(\alpha+\beta) \,/\, y(1+\beta^2) \tag{2.8c}$$

$$\tilde{\theta} = \tan^{-1}(-\alpha) \qquad\qquad \hat{\theta} = \tan^{-1}(-\beta) \tag{2.8d}$$

where attributes in the left column apply to case 1 (i.e., Eqn. 2.6a) while those in the right column apply to case 2 (viz., Eqn. 2.6b). The actual set of physical attributes $\{a, b, g, \theta\}$ that are to be used when quantifying Lagrangian Laplace Stretch and its inverse, according to Eqn. (2.2), are then selected via the strategy

$$\text{if } |\tilde{g}| \geqslant |\hat{g}| : \qquad\qquad \{\tilde{a}, \tilde{b}, \tilde{g}, \tilde{\theta}\} \mapsto \{a, b, g, \theta\} \tag{2.9a}$$

$$\text{else } |\tilde{g}| \leqslant |\hat{g}| : \qquad\qquad \{\hat{a}, \hat{b}, \hat{g}, \hat{\theta}\} \mapsto \{a, b, g, \theta\} \tag{2.9b}$$

where it is easily verified that $\tilde{a} = \hat{a}$ and $\tilde{b} = \hat{b}$ whenever $\tilde{g} = \hat{g}$.

2.2.1.3 Thermodynamic Strains and Strain Rates

In terms of the above physical attributes for Lagrangian Stretch, i.e., a, b and g, and their reference values, viz., a_0, b_0 and g_0, one can define a set of strain attributes derived from thermodynamics, specifically [32]

$$\xi := \ln\left(\sqrt{\frac{a}{a_0}\frac{b}{b_0}}\right) \qquad \mathrm{d}\xi = \frac{1}{2}\left(\frac{\mathrm{d}a}{a} + \frac{\mathrm{d}b}{b}\right) \tag{2.10a}$$

$$\varepsilon := \ln\left(\sqrt{\frac{a}{a_0}\frac{b_0}{b}}\right) \qquad \mathrm{d}\varepsilon = \frac{1}{2}\left(\frac{\mathrm{d}a}{a} - \frac{\mathrm{d}b}{b}\right) \tag{2.10b}$$

$$\gamma := g - g_0 \qquad \mathrm{d}\gamma = \mathrm{d}g \tag{2.10c}$$

whose rates are exact differentials, i.e., they are independent of path—a tacit requirement from thermodynamics [33]. Here ξ denotes dilation (uniform areal stretch), ε denotes squeeze (pure shear), and γ denotes (simple) shear.

2.2.1.4 Stretch Rates

The following approximations for stretch rates were derived by Freed & Zamani [4]. From these, the various strain rates listed in Eqn. (2.10) can be established.

A forward difference formula is used to approximate rates in the reference configuration for the various stretch attributes, as obtained from $\mathrm{d}\boldsymbol{\mathcal{U}}_0 = (\boldsymbol{\mathcal{U}}_1 - \boldsymbol{\mathcal{U}}_0)/\mathrm{d}t + \mathcal{O}(\mathrm{d}t)$ that, neglecting higher-order terms, produces

$$\mathrm{d}a_0 = \frac{a_1 - a_0}{\mathrm{d}t}, \quad \mathrm{d}b_0 = \frac{b_1 - b_0}{\mathrm{d}t}, \quad \mathrm{d}g_0 = \frac{a_1}{a_0}\left(\frac{g_1 - g_0}{\mathrm{d}t}\right) \tag{2.11}$$

where $\mathrm{d}t = t_1 - t_0$ is the applied time step. A backward difference formula $\mathrm{d}\boldsymbol{\mathcal{U}}_1 = (\boldsymbol{\mathcal{U}}_1 - \boldsymbol{\mathcal{U}}_0)/\mathrm{d}t + \mathcal{O}(\mathrm{d}t)$ is used to estimate rates for the various stretch attributes at the end of its first integration step that, neglecting higher-order terms, give

$$\mathrm{d}a_1 = \frac{a_1 - a_0}{\mathrm{d}t}, \quad \mathrm{d}b_1 = \frac{b_1 - b_0}{\mathrm{d}t}, \quad \mathrm{d}g_1 = \frac{a_0}{a_1}\left(\frac{g_1 - g_0}{\mathrm{d}t}\right). \tag{2.12}$$

Equations (2.11 & 2.12) are first-order approximations for these derivatives. Second-order approximations can be established whenever $i > 0$ provided the stepsize for step $[i, i+1]$ equals the stepsize for step $[i-1, i]$, where state $i = 0$ associates with an initial condition. The backward difference formula $\mathrm{d}\boldsymbol{\mathcal{U}}_{i+1} = (3\boldsymbol{\mathcal{U}}_{i+1} - 4\boldsymbol{\mathcal{U}}_{i} + \boldsymbol{\mathcal{U}}_{i-1})/2\mathrm{d}t + \mathcal{O}\big((\mathrm{d}t)^2\big)$ then produces rates for the stretch attributes of

$$\begin{aligned} \mathrm{d}a_{i+1} &= \frac{3a_{i+1} - 4a_i + a_{i-1}}{2\mathrm{d}t} \\ \mathrm{d}b_{i+1} &= \frac{3b_{i+1} - 4b_i + b_{i-1}}{2\mathrm{d}t} \\ \mathrm{d}g_{i+1} &= \frac{2a_i}{a_{i+1}}\left(\frac{g_{i+1} - g_i}{\mathrm{d}t}\right) - \frac{a_{i-1}}{a_{i+1}}\left(\frac{g_{i+1} - g_{i-1}}{2\mathrm{d}t}\right) \end{aligned} \tag{2.13}$$

which require stretch attributes a_{i-1}, b_{i-1} and g_{i-1} to be stored in a finite element setting.

2.2.2 3D Factorization of Deformation Gradient

Taking the approach of Srinivasa [26] in 3 dimensional problem and melding it with the co-ordinate selection methodology of Freed & Rajagopal [34], the components for Lagrangian Laplace Stretch $\mathcal{U}_{ij}$ are readily gotten through a Cholesky factorization of the right Cauchy-Green deformation tensor $\boldsymbol{C} = \mathcal{C}_{ij}\,\vec{\boldsymbol{E}}_i \otimes \vec{\boldsymbol{E}}_j$ with tensor components $\mathcal{C}_{ij} = \mathcal{F}_{ki}\,\mathcal{F}_{kj}$ that relate to their physical attributes via [32]

$$\boldsymbol{\mathcal{U}} = \begin{bmatrix} a & a\gamma & a\beta \\ 0 & b & b\alpha \\ 0 & 0 & c \end{bmatrix} \quad \text{with inverse} \quad \boldsymbol{\mathcal{U}}^{-1} = \begin{bmatrix} 1/a & -\gamma/b & -(\beta - \alpha\gamma)/c \\ 0 & 1/b & -\alpha/c \\ 0 & 0 & 1/c \end{bmatrix} \tag{2.14}$$

with tensor components $\mathcal{U}_{ij}$ being evaluated according to formulæ [26]

$$\begin{aligned} &\mathcal{U}_{11} = \sqrt{C_{11}} \quad && \mathcal{U}_{12} = \frac{C_{12}}{\mathcal{U}_{11}} && \mathcal{U}_{13} = \frac{C_{13}}{\mathcal{U}_{11}} \\ &\mathcal{U}_{21} = 0 && \mathcal{U}_{22} = \sqrt{C_{22} - \mathcal{U}_{12}^2} && \mathcal{U}_{23} = \frac{C_{23} - \mathcal{U}_{12}\mathcal{U}_{13}}{\mathcal{U}_{22}} \\ &\mathcal{U}_{31} = 0 && \mathcal{U}_{32} = 0 && \mathcal{U}_{33} = \sqrt{C_{33} - \mathcal{U}_{13}^2 - \mathcal{U}_{23}^2} \end{aligned} \tag{2.15}$$

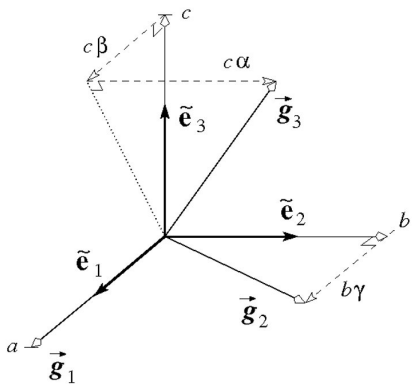

Figure 2.5: Geometric interpretation of Lagrangian Laplace Stretch in a 3D solid

whose elements have physical interpretation, see Fig. 2.5, when defined as

$$a := \mathcal{U}_{11}, \quad b := \mathcal{U}_{22}, \quad c := \mathcal{U}_{33}, \quad \alpha := \frac{\mathcal{U}_{23}}{\mathcal{U}_{22}}, \quad \beta := \frac{\mathcal{U}_{13}}{\mathcal{U}_{11}}, \quad \gamma := \frac{\mathcal{U}_{12}}{\mathcal{U}_{11}} \tag{2.16}$$

where a, b, c are three, positive, elongation ratios, and where α, β, γ are three shear magnitudes, cf. Fig. 2.5, with $\boldsymbol{\mathcal{U}} = \mathcal{U}_{ij} \tilde{\mathbf{e}}_i \otimes \vec{\boldsymbol{E}}_j$ and $\boldsymbol{\mathcal{U}}^{-1} = \mathcal{U}_{ij}^{-1} \vec{\boldsymbol{E}}_i \otimes \tilde{\mathbf{e}}_j$.

One can deconstruct the Lagrangian Laplace Stretch $\boldsymbol{\mathcal{U}}$ into a product between an extensional stretch $\boldsymbol{\Lambda}$ and a shear deformation $\boldsymbol{\Gamma}$ as [26]

$$\boldsymbol{\mathcal{U}} = \boldsymbol{\Lambda}\boldsymbol{\Gamma} = \underbrace{\begin{bmatrix} a & 0 & 0 \\ 0 & b & 0 \\ 0 & 0 & c \end{bmatrix}}_{\text{extension } \boldsymbol{\Lambda}} \underbrace{\begin{bmatrix} 1 & \gamma & \beta \\ 0 & 1 & \alpha \\ 0 & 0 & 1 \end{bmatrix}}_{\text{shear } \boldsymbol{\Gamma}} = \underbrace{\begin{bmatrix} a & a\gamma & a\beta \\ 0 & b & b\alpha \\ 0 & 0 & c \end{bmatrix}}_{\text{Lagrangian Laplace Stretch } \boldsymbol{\mathcal{U}}} \tag{2.17}$$

This is an Iwasawa [35] decomposition of the deformation gradient $\boldsymbol{F}$; namely: extension $\boldsymbol{\Lambda}$ is diagonal with positive elements and shear $\boldsymbol{\Gamma}$ is unit upper triangular.

2.3 Convected Base Vectors

Edges of the deformed parallelepiped depicted in Figs. 2.1 & 2.5 describe a set of oblique base vectors $\{\vec{\boldsymbol{g}}_i\}$ whose components obey a linear map of

$$\begin{Bmatrix} \vec{\boldsymbol{g}}_1 \\ \vec{\boldsymbol{g}}_2 \\ \vec{\boldsymbol{g}}_3 \end{Bmatrix} = \begin{bmatrix} a & 0 & 0 \\ b\gamma & b & 0 \\ c\beta & c\alpha & c \end{bmatrix} \begin{Bmatrix} \tilde{\mathrm{e}}_1 \\ \tilde{\mathrm{e}}_2 \\ \tilde{\mathrm{e}}_3 \end{Bmatrix} \tag{2.18}$$

or $\{\vec{\boldsymbol{g}}_i\} = \boldsymbol{\Lambda}\boldsymbol{\Gamma}^{\mathsf{T}}\{\tilde{\mathrm{e}}_i\}$, cf. Eq. (2.17). These base vectors describe a relative volume of

$$V_{\{\vec{\boldsymbol{g}}_i\}} = \vec{\boldsymbol{g}}_1 \cdot \vec{\boldsymbol{g}}_2 \times \vec{\boldsymbol{g}}_3 = abc \tag{2.19}$$

which is the volume of distortion in that $\det \boldsymbol{F} = \det \boldsymbol{\mathcal{U}} = abc$. Collectively, these formulæ describe the shape of a homogeneously deformed mass element located at particle $\mathcal{P}$ whereat $\boldsymbol{F}$ is evaluated, see Fig. 2.1. The convected base vectors $\{\vec{\boldsymbol{g}}_i\}$ are not the actual curvilinear base vectors; rather, they are tangents to the curvilinear base vectors. The theory is therefore local; nevertheless, it is suitable, e.g., for finite element analysis.

Dual vectors $\{\vec{\boldsymbol{g}}^i\}$ to the convected basis $\{\vec{\boldsymbol{g}}_i\}$ are acquired through [36]

$$\vec{\boldsymbol{g}}^1 := \frac{\vec{\boldsymbol{g}}_2 \times \vec{\boldsymbol{g}}_3}{\vec{\boldsymbol{g}}_1 \cdot \vec{\boldsymbol{g}}_2 \times \vec{\boldsymbol{g}}_3}, \quad \vec{\boldsymbol{g}}^2 := \frac{\vec{\boldsymbol{g}}_3 \times \vec{\boldsymbol{g}}_1}{\vec{\boldsymbol{g}}_1 \cdot \vec{\boldsymbol{g}}_2 \times \vec{\boldsymbol{g}}_3}, \quad \vec{\boldsymbol{g}}^3 := \frac{\vec{\boldsymbol{g}}_1 \times \vec{\boldsymbol{g}}_2}{\vec{\boldsymbol{g}}_1 \cdot \vec{\boldsymbol{g}}_2 \times \vec{\boldsymbol{g}}_3} \tag{2.20}$$

which are described by $\{\vec{\boldsymbol{g}}^i\} = \boldsymbol{\Lambda}^{-1}\boldsymbol{\Gamma}^{-1}\{\tilde{\mathrm{e}}^i\}$. Base vectors $\{\vec{\boldsymbol{g}}_i\}$ and their duals $\{\vec{\boldsymbol{g}}^i\}$ convect with the motion, locally at a particle, and by their vary definition, viz. Eq. (2.20), obey $\vec{\boldsymbol{g}}^i \cdot \vec{\boldsymbol{g}}_j = \delta^i_j$. which are described by the linear map

$$\begin{Bmatrix} \vec{\boldsymbol{g}}^1 \\ \vec{\boldsymbol{g}}^2 \\ \vec{\boldsymbol{g}}^3 \end{Bmatrix} = \begin{bmatrix} 1/a & -\gamma/a & -(\beta - \alpha\gamma)/a \\ 0 & 1/b & -\alpha/b \\ 0 & 0 & 1/c \end{bmatrix} \begin{Bmatrix} \tilde{\mathrm{e}}^1 \\ \tilde{\mathrm{e}}^2 \\ \tilde{\mathrm{e}}^3 \end{Bmatrix} \tag{2.21}$$

or $\{\vec{\boldsymbol{g}}^i\} = \boldsymbol{\Lambda}^{-1}\boldsymbol{\Gamma}^{-1}\{\tilde{\mathbf{e}}^i\}$.

2.4 Convected Metrics

The ability to work with an oblique, Cartesian, coordinate system instead of having to work with a general, curvilinear, coordinate system, in accordance with our hypothesis, affords a practical utility to the convected tensor analysis presented herein. *The convected metric tensor can be quantified given any spatially smooth description for motion*—a capability that has been absent until now.

Convected metric $\boldsymbol{\gamma} = \gamma_{ij}\,\vec{\boldsymbol{g}}^i \otimes \vec{\boldsymbol{g}}^j$ has components $\gamma_{ij} := \vec{\boldsymbol{g}}_i \cdot \vec{\boldsymbol{g}}_j$, $\gamma_{ij} = \gamma_{ji}$, that, according to Eq. (2.18), populate as a symmetric matrix with elements

$$\boldsymbol{\gamma} = \begin{bmatrix} a^2 & ab\gamma & ac\beta \\ ab\gamma & b^2(1+\gamma^2) & bc(\alpha+\beta\gamma) \\ ac\beta & bc(\alpha+\beta\gamma) & c^2(1+\alpha^2+\beta^2) \end{bmatrix} \tag{2.22}$$

whose dual $\boldsymbol{\gamma}^{-1} = \gamma^{ij}\,\vec{\boldsymbol{g}}_i \otimes \vec{\boldsymbol{g}}_j$ has components $\gamma^{ij} := \vec{\boldsymbol{g}}^i \cdot \vec{\boldsymbol{g}}^j$, $\gamma^{ij} = \gamma^{ji}$, that, populate as a symmetric matrix which obey $\boldsymbol{\gamma}^{-1}\boldsymbol{\gamma} = \boldsymbol{\delta}$.

When expressed in terms of Jacobian $\mathbf{Y}$, and its fundamental constituents $\boldsymbol{\Lambda}$ and $\boldsymbol{\Gamma}$, viz., $\mathbf{Y} = \boldsymbol{\Gamma}\boldsymbol{\Lambda}$, one finds that

$$\boldsymbol{\gamma} = \mathbf{Y}^{\mathsf{T}}\mathbf{Y} \qquad \text{and} \qquad \boldsymbol{\gamma}^{-1} = \mathbf{Y}^{-1}\mathbf{Y}^{-\mathsf{T}} \tag{2.23}$$

neither of which can be constructed directly out of the Lagrangian Laplace Stretch $\boldsymbol{\mathcal{U}} = \boldsymbol{\Lambda}\boldsymbol{\Gamma}$, because matrices $\boldsymbol{\Lambda}$ and $\boldsymbol{\Gamma}$ do not commute. Convected metric $\boldsymbol{\gamma} = \mathbf{Y}^{\mathsf{T}}\mathbf{Y}$ resembles Lagrangian metric $\mathbf{C} = \boldsymbol{F}^{\mathsf{T}}\boldsymbol{F} \equiv \boldsymbol{\mathcal{U}}^{\mathsf{T}}\boldsymbol{\mathcal{U}} = C_{ij}\,\vec{\boldsymbol{E}}^i \otimes \vec{\boldsymbol{E}}^j$ which does not look like Eq. (2.22).

2.4.1 Convected Velocity Gradient

There is an analog to the Eulerian velocity gradient that exists in our convected coordinate system with oblique base vectors $\{\vec{\boldsymbol{g}}_i\}$. It is a mixed tensor $\mathrm{d}\boldsymbol{\eta}$ defined by

$$\mathrm{d}\boldsymbol{\eta} = \mathrm{d}\eta^i_j \, \vec{\boldsymbol{g}}_i \otimes \vec{\boldsymbol{g}}^j \qquad \text{with} \qquad \mathrm{d}\eta^i_j := \frac{\partial \xi^i}{\partial \tilde{x}^k} \frac{\partial \mathrm{d}\tilde{x}^k}{\partial \xi^j} \tag{2.24}$$

The velocity gradient in the experimentor's basis defined in Eq. (A.3) is $\mathrm{d}\mathbf{H} = \mathrm{d}H^i_j \, \tilde{\mathbf{e}}_i \otimes \tilde{\mathbf{e}}^j$ with $\mathrm{d}\mathbf{H} = \mathrm{d}\mathbf{Y} \cdot \mathbf{Y}^{-1}$. It maps to a velocity gradient of the convected basis $\mathrm{d}\boldsymbol{\eta}$ as $\mathrm{d}\boldsymbol{\eta} = \mathbf{Y}^{-1} \cdot \mathrm{d}\mathbf{H} \cdot \mathbf{Y}$, i.e., $\mathrm{d}\boldsymbol{\eta} \hookleftarrow \mathrm{d}\mathbf{H}$. Consequently, velocity gradients $\mathrm{d}\mathbf{H}$ and $\mathrm{d}\boldsymbol{\eta}$ represent the same physical field, they are just defined on different manifolds.

2.5 Convected Strains

From our analysis of a cube being transformed into a parallelepiped, the convected, covariant, strain tensor $\boldsymbol{\varepsilon}$ of Lodge [24, 10] has components

$$\boldsymbol{\varepsilon} := \tfrac{1}{2}(\boldsymbol{\gamma} - \boldsymbol{\gamma}_0) = \frac{1}{2} \begin{bmatrix} a^2 - 1 & ab\gamma & ac\beta \\ ab\gamma & b^2(1+\gamma^2) - 1 & bc(\alpha + \beta\gamma) \\ ac\beta & bc(\alpha + \beta\gamma) & c^2(1 + \alpha^2 + \beta^2) - 1 \end{bmatrix} \tag{2.25}$$

while the convected, contravariant, strain tensor $\boldsymbol{\mathcal{E}}$ of Lodge has components

$$\boldsymbol{\mathcal{E}} := \tfrac{1}{2}(\boldsymbol{\gamma}_0^{-1} - \boldsymbol{\gamma}^{-1}) = \frac{1}{2} \begin{bmatrix} \big(a^2 - 1 - \gamma^2 - (\beta - \alpha\gamma)^2\big)/a^2 & \big(\gamma(1+\alpha^2) - \alpha\beta\big)/ab & (\beta - \alpha\gamma)/ac \\ \big(\gamma(1+\alpha^2) - \alpha\beta\big)/ab & (b^2 - 1 - \alpha^2)/b^2 & \alpha/bc \\ (\beta - \alpha\gamma)/ac & \alpha/bc & (c^2 - 1)/c^2 \end{bmatrix} \tag{2.26}$$

whenever $\boldsymbol{\gamma}_0 = \delta_{ij}\,\vec{\boldsymbol{g}}_0^{\,i} \otimes \vec{\boldsymbol{g}}_0^{\,j}$ and $\boldsymbol{\gamma}_0^{-1} = \delta^{ij}\,(\vec{\boldsymbol{g}}_0)_i \otimes (\vec{\boldsymbol{g}}_0)_j$, i.e., $a_0 = b_0 = c_0 = 1$ and $\alpha_0 = \beta_0 = \gamma_0 = 0$.

2.5.1 Properties of Convected Strains

Convected strain $\boldsymbol{\varepsilon} = \varepsilon_{ij}\,\vec{\boldsymbol{g}}^{\,i} \otimes \vec{\boldsymbol{g}}^{\,j}$ has the physical interpretation of being a measure of change in the squared distance separating two neighboring particles. Convected strain $\boldsymbol{\mathcal{E}} = \mathcal{E}^{ij}\,\vec{\boldsymbol{g}}_i \otimes \vec{\boldsymbol{g}}_j$ has the physical interpretation of being a measure of change in the squared distance separating two, neighboring but non-intersecting, material planes [24].

Consider an ordered sequence in time $t_0 < t_1 < t_2 < \cdots < t_{n-1} < t_n$ for which fields $a, b, c, \alpha, \beta, \gamma$ are normalized in that $a(t_0) = b(t_0) = c(t_0) = 1$ and $\alpha(t_0) = \beta(t_0) = \gamma(t_0) = 0$. The convected strain tensors $\boldsymbol{\varepsilon}$ and $\boldsymbol{\mathcal{E}}^{-1}$ of LODGE, presented in Eqs. (2.25 & 2.26), generalize to

$$\begin{aligned} \boldsymbol{\varepsilon}(t_i, t_j) &:= \tfrac{1}{2}\big(\boldsymbol{\gamma}(t_i) - \boldsymbol{\gamma}(t_j)\big) \\ \boldsymbol{\mathcal{E}}(t_i, t_j) &:= \tfrac{1}{2}\big(\boldsymbol{\gamma}^{-1}(t_j) - \boldsymbol{\gamma}^{-1}(t_i)\big) \end{aligned} \qquad \forall \quad i, j = 0, 1, 2, \ldots, n. \tag{2.27}$$

For any subset of times t_i, t_j, t_k belonging to the above sequence, LODGE's generalized strain tensors possess the following important properties:

$$\boldsymbol{\varepsilon}(t_i, t_i) = \mathsf{0} \qquad\qquad \boldsymbol{\mathcal{E}}(t_i, t_i) = \mathsf{0} \tag{2.28a}$$

$$\boldsymbol{\varepsilon}(t_i, t_j) = -\boldsymbol{\varepsilon}(t_j, t_i) \qquad\qquad \boldsymbol{\mathcal{E}}(t_i, t_j) = -\boldsymbol{\mathcal{E}}(t_j, t_i) \tag{2.28b}$$

$$\boldsymbol{\varepsilon}(t_i, t_j) = \boldsymbol{\varepsilon}(t_i, t_k) + \boldsymbol{\varepsilon}(t_k, t_j) \qquad\qquad \boldsymbol{\mathcal{E}}(t_i, t_j) = \boldsymbol{\mathcal{E}}(t_i, t_k) + \boldsymbol{\mathcal{E}}(t_k, t_j) \tag{2.28c}$$

Equation (2.27) says strain is a two-state field, independent of the path traversed between these two states. Equation (2.28a) says a reference state for strain exists, and furthermore, that its selection is arbitrary. Equation (2.28b) says that strain is anti-symmetric in its assignment of state. Equation (2.28c) says that two strains will add whenever there is a state in common between them, irrespective of the states selected, and therefore, irrespective of the extent of strain. These remarkable properties are unique to convected strain fields.

3. ELASTIC KELVIN-POISSON-POYNTING SOLIDS DESCRIBED THROUGH SCALAR CONJUGATE STRESS/STRAIN PAIRS DERIVED FROM LAGRANGIAN LAPLACE STRETCH [5]

In this chapter an observer assigned frame of reference is considered. It is represented by an orthonormal triad of base vectors $(\vec{\boldsymbol{\imath}}, \vec{\boldsymbol{\jmath}}, \vec{\boldsymbol{k}})$ describing a rectangular, Cartesian, co-ordinate system spanning a fixed, Euclidean, point space through which an embedded body $\mathcal{B}$ moves with time where we called Eulerian basis $(\vec{\mathbf{e}}_1, \vec{\mathbf{e}}_2, \vec{\mathbf{e}}_3)$ and Lagrangian basis $(\vec{\boldsymbol{E}}_1, \vec{\boldsymbol{E}}_2, \vec{\boldsymbol{E}}_3)$ in the previous chapter, and what we called an experimentor's basis $(\tilde{\mathbf{e}}_1, \tilde{\mathbf{e}}_2, \tilde{\mathbf{e}}_3)$ we now refer to as the *physical basis* $(\vec{\boldsymbol{e}}_1, \vec{\boldsymbol{e}}_2, \vec{\boldsymbol{e}}_3)$, because it is within this co-ordinate system that the components of convected vector and tensor fields find their physical components.

In previous chapter we decomposed the Lagrangian Laplace stretch $\boldsymbol{\mathcal{U}}$ into a product of two gradients, viz., $\boldsymbol{\mathcal{U}} = \mathbf{YZ}$. When evaluated in our reference frame for analysis $(\vec{\boldsymbol{E}}_1, \vec{\boldsymbol{E}}_2, \vec{\boldsymbol{E}}_3)$, Jacobian $\mathbf{F}$ will have components $\hat{F}_{ij} = \partial\hat{\chi}_{i,\kappa}(\boldsymbol{X}, t)/\partial\hat{X}_j$ with $\hat{x}_i = \hat{\chi}_{i,\kappa}(\boldsymbol{X}, t)$ describing the motion in $(\vec{\boldsymbol{E}}_1, \vec{\boldsymbol{E}}_2, \vec{\boldsymbol{E}}_3)$. How the Jacobians describe the mapping of a tangent vector, for example, between these various configurations is illustrated in Fig. 3.1. There are three reference configurations and three current configurations that one can work with in a convected analysis with basis $(\vec{\boldsymbol{g}}_1, \vec{\boldsymbol{g}}_2, \vec{\boldsymbol{g}}_3)$. The deformation gradient F_{ij} maps the Lagrangian components of a tangent vector belonging to a reference configuration $\boldsymbol{\kappa}_r$ into its Eulerian components belonging to the current configuration $\boldsymbol{\kappa}_t$. The co-ordinate relabeling P_{ij} (one of six variants) transforms one from an observer's frame of reference, i.e., $(\vec{\boldsymbol{\imath}}, \vec{\boldsymbol{\jmath}}, \vec{\boldsymbol{k}})$, into a frame better suited for **QR** analysis, viz., $(\vec{\boldsymbol{E}}_1, \vec{\boldsymbol{E}}_2, \vec{\boldsymbol{E}}_3)$. The Lagrangian Laplace stretch $\mathcal{U}_{ij}$ maps tangent vectors from the **QR** reference configuration $\hat{\boldsymbol{\kappa}}_r$ into their counterparts in the physical frame of reference $\tilde{\boldsymbol{\kappa}}_t$. The distortion Z_{ij} transforms tangent vectors from the **QR** reference configuration $\hat{\boldsymbol{\kappa}}_r$ into tangent vectors in the convected frame of reference $\boldsymbol{\kappa}_c$, while the convected stretch Y_{ij} continues this mapping into the physical frame of reference $\tilde{\boldsymbol{\kappa}}_t$ out of which Q_{ij} rotates them back into the current configuration for analysis $\hat{\boldsymbol{\kappa}}_t$. Matrix P_{ij}

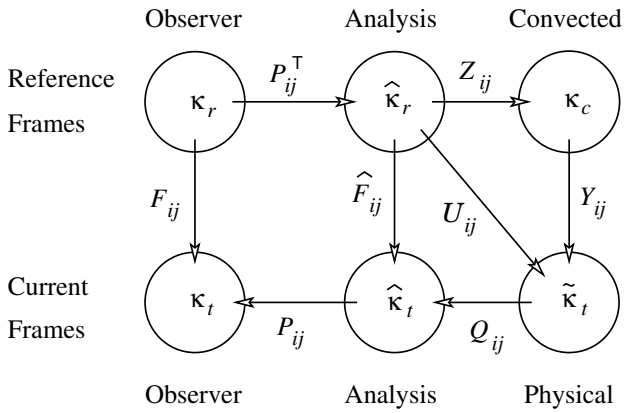

Figure 3.1: Mapping between reference and current configurations by Jacobians

then relabels the co-ordinate axes to those assigned by the observer, returning one to the current configuration $\boldsymbol{\kappa}_t$.

The upper-triangular components for the Jacobians in this decomposition of Lagrangian Laplace stretch, i.e., $\mathbf{YZ}$ $(=\boldsymbol{\mathcal{U}})$, and its inverse, viz., $\mathbf{Z}^{-1}\mathbf{Y}^{-1}$ $(=\boldsymbol{\mathcal{U}}^{-1})$, can be written out in terms of the physical attributes of deformation $a, b, c, \alpha, \beta, \gamma$ established in Eq. (2.16)

$$\mathbf{Y} = \boldsymbol{\Gamma}\boldsymbol{\Lambda} = \begin{bmatrix} a & b\gamma & c\beta \\ 0 & b & c\alpha \\ 0 & 0 & c \end{bmatrix} \qquad \mathbf{Z} = \begin{bmatrix} 1 & \frac{a-b}{a}\,\gamma & \frac{a-c}{a}\,\beta - \frac{b-c}{a}\,\alpha\gamma \\ 0 & 1 & \frac{b-c}{b}\,\alpha \\ 0 & 0 & 1 \end{bmatrix} \tag{3.1}$$

where $\det \mathbf{Z} = 1$ while $\det \mathbf{Y} = \det \boldsymbol{\mathcal{U}} = \det \mathbf{F} = abc$.

3.1 Stress Power

The internal mechanical power $\dot{W}$ exerted upon a material particle, caused by stressing a deformable body, is a frame-indifferent [37, 38] physical property described by [39]

$$\dot{W} = \mathrm{tr}(\mathbf{TL}) \tag{3.2}$$

where $\mathbf{T}$ is the symmetric Cauchy stress and $\mathbf{L} := \dot{\mathbf{F}}\mathbf{F}^{-1}$ is the non-symmetric velocity gradient, with $\dot{\mathbf{F}}$ representing a material derivative of the deformation gradient $\mathbf{F}$. These

fields are defined in the current configuration $\boldsymbol{\kappa}_t$, see Fig. 3.1.

For our purposes, it is advantageous to map $\mathbf{L}$ and $\mathbf{T}$ as mixed tensor fields, first pulling their Eulerian components back into their associated Lagrangian components, and then pushing these Lagrangian components forward into their convected components. The reason for using mixed tensor components is because Eulerian components L^i_j for the velocity gradient will map into upper-triangular components $\dot{\eta}^i_j$ for the convected velocity gradient. As a consequence, the expression for stress power used in the construction of constitutive equations is vastly simplified, hence the motivation. This property of triangularity would be lost if either covariant or contravariant tensor components had been selected.

The mechanical power caused by stressing a deformable body, i.e., Eq. (3.2), can also be expressed as

$$\dot{W} = \operatorname{tr}(\boldsymbol{\sigma}\,\dot{\boldsymbol{\eta}}) = \operatorname{tr}(\boldsymbol{\mathcal{T}}\boldsymbol{\mathcal{L}}) = \operatorname{tr}(\mathbf{T}\,\mathbf{L}) \tag{8a}$$

whose convected and physical fields for stress, i.e., $\boldsymbol{\sigma}$ and $\boldsymbol{\mathcal{T}}$, and velocity gradient, viz., $\dot{\boldsymbol{\eta}}$ and $\boldsymbol{\mathcal{L}}$, are described by

$$\begin{aligned} &\boldsymbol{\sigma} = \sigma^i_j\,\vec{\boldsymbol{g}}_i \otimes \vec{\boldsymbol{g}}^j, \quad \boldsymbol{\mathcal{T}} = \mathcal{T}_{ij}\,\vec{\mathbf{e}}_i \otimes \vec{\mathbf{e}}_j \qquad \text{with} \qquad \mathcal{T}_{ij} = \mathcal{T}^i_j = Y^i_k \sigma^k_\ell [Y^{-1}]^\ell_j \\ &\dot{\boldsymbol{\eta}} = \dot{\eta}^i_j\,\vec{\boldsymbol{g}}_i \otimes \vec{\boldsymbol{g}}^j, \quad \boldsymbol{\mathcal{L}} = \mathcal{L}_{ij}\,\vec{\mathbf{e}}_i \otimes \vec{\mathbf{e}}_j \qquad\qquad\quad \mathcal{L}_{ij} = \mathcal{L}^i_j = Y^i_k \dot{\eta}^k_\ell [Y^{-1}]^\ell_j \end{aligned} \tag{8b}$$

wherein

$$\begin{aligned} \dot{\eta}^i_j &= [Y^{-1}]^i_k \dot{Y}^k_j + \dot{Z}^i_k [Z^{-1}]^k_j \\ \mathcal{L}_{ij} = \mathcal{L}^i_j &= \dot{Y}^i_k [Y^{-1}]^k_j + Y^i_k \dot{Z}^k_\ell [Z^{-1}]^\ell_m [Y^{-1}]^m_j \end{aligned} \tag{8c}$$

establish the oblique and physical components for the velocity gradient.

In terms of the physical tensors $\boldsymbol{\mathcal{T}}$ and $\boldsymbol{\mathcal{L}}$ that are affiliated with convected tensors $\boldsymbol{\sigma}$ and $\dot{\boldsymbol{\eta}}$, the work expended by stressing a deformable body becomes

$$\dot{W} = \mathcal{T}_{ij}\mathcal{L}_{ji} = \operatorname{tr}\left(\begin{bmatrix} \mathcal{T}_{11} & \mathcal{T}_{12} & \mathcal{T}_{13} \\ \mathcal{T}_{21} & \mathcal{T}_{22} & \mathcal{T}_{23} \\ \mathcal{T}_{31} & \mathcal{T}_{32} & \mathcal{T}_{33} \end{bmatrix} \begin{bmatrix} \mathcal{L}_{11} & \mathcal{L}_{12} & \mathcal{L}_{13} \\ \mathcal{L}_{21} & \mathcal{L}_{22} & \mathcal{L}_{23} \\ \mathcal{L}_{31} & \mathcal{L}_{32} & \mathcal{L}_{33} \end{bmatrix} \right) \tag{8d}$$

wherein $\boldsymbol{\mathcal{T}} = \boldsymbol{\mathcal{T}}^{\mathsf{T}}$ and $\boldsymbol{\mathcal{L}} = \dot{\boldsymbol{\mathcal{U}}}\boldsymbol{\mathcal{U}}^{-1}$.

3.2 Stress/Strain Base Pairs

3.2.1 Two-Mode Theory

Hypothesis 1: Trace $\mathrm{tr}(\boldsymbol{\mathcal{T}}\boldsymbol{\mathcal{L}}) = \mathcal{T}_{ij}\,\mathcal{L}_{ji}$ establishes stress power $\mathrm{d}W$ in terms of physical components, thereby describing a convected stress tensor and a convected velocity-gradient tensor that can be decomposed into a set of six, conjugate, stress-strain pairs:

$$\mathrm{d}W = \mathrm{tr}\left(\begin{bmatrix} \mathcal{T}_{11} & \mathcal{T}_{12} & \mathcal{T}_{13} \\ \mathcal{T}_{21} & \mathcal{T}_{22} & \mathcal{T}_{23} \\ \mathcal{T}_{31} & \mathcal{T}_{32} & \mathcal{T}_{13} \end{bmatrix} \begin{bmatrix} \mathrm{d}a/a & a\,\mathrm{d}\gamma/b & a(\mathrm{d}\beta - \alpha\,\mathrm{d}\gamma)/c \\ 0 & \mathrm{d}b/b & b\,\mathrm{d}\alpha/c \\ 0 & 0 & \mathrm{d}c/c \end{bmatrix}\right) = \sum_{i=1}^{3}\big(\sigma_i\,\mathrm{d}\varepsilon_i + \tau_i\,\mathrm{d}\gamma_i\big) \tag{3.3}$$

The definition selected here for assigning strains and their rates is a byproduct of a Gram–Schmidt factorization of the deformation gradient $\mathbf{F}$, specifically, we conjecture that

$$\varepsilon_1 := \ln(a/a_0) \qquad \mathrm{d}\varepsilon_1 = \mathrm{d}a/a \tag{3.4a}$$

$$\varepsilon_2 := \ln(b/b_0) \qquad \mathrm{d}\varepsilon_2 = \mathrm{d}b/b \tag{3.4b}$$

$$\varepsilon_3 := \ln(c/c_0) \qquad \mathrm{d}\varepsilon_3 = \mathrm{d}c/c \tag{3.4c}$$

$$\gamma_1 := \gamma - \gamma_0 \qquad \mathrm{d}\gamma_1 = \mathrm{d}\gamma \tag{3.4d}$$

$$\gamma_2 := \alpha - \alpha_0 \qquad \mathrm{d}\gamma_2 = \mathrm{d}\alpha \tag{3.4e}$$

$$\gamma_3 := \beta - \beta_0 \qquad \mathrm{d}\gamma_3 = \mathrm{d}\beta \tag{3.4f}$$

The thermodynamic stresses conjugate to these strains are therefore

$$\sigma_1 := \mathcal{T}_{11} \qquad \tau_1 := \tfrac{a}{b}\,\mathcal{T}_{21} - \alpha\,\tfrac{a}{c}\,\mathcal{T}_{31} \tag{3.5a}$$

$$\sigma_2 := \mathcal{T}_{22} \qquad \tau_2 := \tfrac{b}{c}\,\mathcal{T}_{32} \tag{3.5b}$$

$$\sigma_3 := \mathcal{T}_{33} \qquad \tau_3 := \tfrac{a}{c}\,\mathcal{T}_{31} \tag{3.5c}$$

Note: From a Lagrangian perspective, a reference configuration $\hat{\boldsymbol{\kappa}}_r$ would be chosen so that, typically, $a_0 = b_0 = c_0 = 1$ and $\alpha_0 = \beta_0 = \gamma_0 = 0$ with their current values a, b, c and α, β, γ being response functions. From an Eulerian perspective, a reference configuration $\hat{\boldsymbol{\kappa}}_r$ would be chosen so that, typically, $a = b = c = 1$ and $\alpha = \beta = \gamma = 0$ with their reference values a_0, b_0, c_0 and $\alpha_0, \beta_0, \gamma_0$ being response functions, cf. Lodge [24, 10].

3.2.2 Three-Mode Theory

Hypothesis 2: Trace $\mathrm{tr}(\boldsymbol{\mathcal{T}}\boldsymbol{\mathcal{L}}) = \mathcal{T}_{ij}\,\mathcal{L}_{ji}$ representing stress power can likewise be decomposed into a set of seven, conjugate, stress-strain, base pairs:

$$\mathrm{d}W = \mathrm{tr}\left(\begin{bmatrix} \mathcal{T}_{11} & \mathcal{T}_{12} & \mathcal{T}_{13} \\ \mathcal{T}_{21} & \mathcal{T}_{22} & \mathcal{T}_{23} \\ \mathcal{T}_{31} & \mathcal{T}_{32} & \mathcal{T}_{13} \end{bmatrix} \begin{bmatrix} \mathrm{d}a/a & a\,\mathrm{d}\gamma/b & a(\mathrm{d}\beta - \alpha\,\mathrm{d}\gamma)/c \\ 0 & \mathrm{d}b/b & b\,\mathrm{d}\alpha/c \\ 0 & 0 & \mathrm{d}c/c \end{bmatrix}\right) = -3p\,\mathrm{d}e + \sum_{i=1}^{3}\left(\sigma_i\,\mathrm{d}\varepsilon_i + \tau_i\,\mathrm{d}\gamma_i\right) \tag{3.6}$$

where $\{p, \sigma_1, \sigma_2, \sigma_3, \tau_1, \tau_2, \tau_3\}$ describes a set of intensive scalar-valued stresses whose thermodynamic conjugates $\{e, \varepsilon_1, \varepsilon_2, \varepsilon_3, \gamma_1, \gamma_2, \gamma_3\}$ describe a set of extensive scalar-valued strains. These strains and their rates are defined as

$$e := \ln \sqrt[3]{abc/a_0b_0c_0} \qquad \mathrm{d}e = \tfrac{1}{3}\left(\mathrm{d}a/a + \mathrm{d}b/b + \mathrm{d}c/c\right) \tag{3.7a}$$

$$\varepsilon_1 := \ln \sqrt[3]{ab_0/a_0b} \qquad \mathrm{d}\varepsilon_1 = \tfrac{1}{3}\left(\mathrm{d}a/a - \mathrm{d}b/b\right) \tag{3.7b}$$

$$\varepsilon_2 := \ln \sqrt[3]{bc_0/b_0c} \qquad \mathrm{d}\varepsilon_2 = \tfrac{1}{3}\left(\mathrm{d}b/b - \mathrm{d}c/c\right) \tag{3.7c}$$

$$\varepsilon_3 := \ln \sqrt[3]{ca_0/c_0a} \qquad \mathrm{d}\varepsilon_3 = \tfrac{1}{3}\left(\mathrm{d}c/c - \mathrm{d}a/a\right) \tag{3.7d}$$

$$\gamma_1 := \gamma - \gamma_0 \qquad \mathrm{d}\gamma_1 = \mathrm{d}\gamma \tag{3.7e}$$

$$\gamma_2 := \alpha - \alpha_0 \qquad \mathrm{d}\gamma_2 = \mathrm{d}\alpha \tag{3.7f}$$

$$\gamma_3 := \beta - \beta_0 \qquad \mathrm{d}\gamma_3 = \mathrm{d}\beta \tag{3.7g}$$

where $a_0, b_0, c_0, \alpha_0, \beta_0, \gamma_0$ are reference values for these kinematic variables, evaluated in a configuration $\hat{\boldsymbol{\kappa}}_r$ affiliated with time t_0.

The stresses conjugate to the above measures for strain become

$$p := -\tfrac{1}{3}\big(\mathcal{T}_{11} + \mathcal{T}_{22} + \mathcal{T}_{33}\big) \tag{3.8a}$$

$$\sigma_1 := \mathcal{T}_{11} - \mathcal{T}_{22} \qquad \tau_1 := \tfrac{a}{b}\,\mathcal{T}_{21} - \alpha\tfrac{a}{c}\,\mathcal{T}_{31} \tag{3.8b}$$

$$\sigma_2 := \mathcal{T}_{22} - \mathcal{T}_{33} \qquad \tau_2 := \tfrac{b}{c}\,\mathcal{T}_{32} \tag{3.8c}$$

$$\sigma_3 := \mathcal{T}_{33} - \mathcal{T}_{11} \qquad \tau_3 := \tfrac{a}{c}\,\mathcal{T}_{31} \tag{3.8d}$$

where the σ_i now denote normal stress differences, instead of normal stresses, while the shear stresses τ_i retain the same physical interpretations as in the first hypothesis. Pressure p and dilatation e are tensor invariants.

Note: This hypothesis supposes there are three separate modes of straining. Only two of the three squeeze modes are independent, because $\varepsilon_3 = -(\varepsilon_1 + \varepsilon_2)$ and $\sigma_3 = -(\sigma_1 + \sigma_2)$.

3.3 Equilibrium Thermodynamics

The internal energy U of a system that is in thermodynamic equilibrium with its surroundings is a function of its extensive variables $\mathcal{E}^1$, $\mathcal{E}^2$, …, $\mathcal{E}^n$ (e.g., S, ε_1, ε_2, ε_3, γ_1, γ_2, γ_3). Conjugate to these extensive variables are the intensive variables $\mathcal{F}_1$, $\mathcal{F}_2$, …, $\mathcal{F}_n$ (e.g., T, σ_1, σ_2, σ_3, τ_1, τ_2, τ_3). At equilibrium, the First Law of Thermodynamics has a mathematical interpretation of

$$\mathrm{d}U = \sum_{\alpha=1}^{n} \mathcal{F}_\alpha\,\mathrm{d}\mathcal{E}^\alpha = T\,\mathrm{d}S + \sum_{\alpha=2}^{n} \mathcal{F}_\alpha\,\mathrm{d}\mathcal{E}^\alpha \tag{3.9}$$

where the sum in the right-hand expression only spans over the deformation variables, as the non-deformation variables $\mathcal{E}^1 := S$ and $\mathcal{F}_1 := T$ have been written out explicitly.

Because $\mathrm{d}U$ is an exact differential, equations of constitution follow

$$\mathcal{F}_\alpha = U_{,\alpha} \quad \therefore \quad \mathrm{d}\mathcal{F}_\alpha = \sum_{\beta=1}^{n} U_{,\alpha\beta}\,\mathrm{d}\mathcal{E}^\beta \quad \text{or} \quad \mathrm{d}\mathcal{E}^\alpha = \sum_{\beta=1}^{n} U^{\alpha\beta}\,\mathrm{d}\mathcal{F}_\beta \tag{3.10}$$

where $U_{,\alpha} := \partial U/\partial\mathcal{E}^\alpha$ and $U_{,\alpha\beta} := \partial^2 U/\partial\mathcal{E}^\alpha\,\partial\mathcal{E}^\beta$ with $\alpha, \beta = 1, 2, \ldots, n$.

3.4 Elastic Model with Kelvin, Poisson and Poynting Strain Effects

Here we consider two such solids. The first adopts the two-mode description for state variables. The second adopts the three-mode description for state variables. Both models incorporate three coupling effects: Lord Kelvin (Sir William Thomson) [1] studied a coupling effect between temperature and elongation; Poisson [2] studied a coupling effect between axial and transverse elongations; and Poynting [3] studied a coupling effect between shear and elongation.

3.4.1 Two-Mode Elastic Solid

A thermoelastic solid that exhibits Kelvin, Poisson and Poynting strain effects has a compliance matrix that looks like

$$\begin{Bmatrix} \mathrm{d}S \\ \mathrm{d}\varepsilon_1 \\ \mathrm{d}\varepsilon_2 \\ \mathrm{d}\varepsilon_3 \\ \frac{1}{2}\mathrm{d}\gamma_1 \\ \frac{1}{2}\mathrm{d}\gamma_2 \\ \frac{1}{2}\mathrm{d}\gamma_3 \end{Bmatrix} = \begin{bmatrix} C/T & \alpha & \alpha & \alpha & 0 & 0 & 0 \\ \alpha & 1/E & -\nu/E & -\nu/E & 0 & 0 & 0 \\ \alpha & -\nu/E & 1/E & -\nu/E & \gamma_1/E & 0 & 0 \\ \alpha & -\nu/E & -\nu/E & 1/E & 0 & \gamma_2/E & \gamma_3/E \\ 0 & 0 & \gamma_1/E & 0 & (1+\nu)/E & 0 & 0 \\ 0 & 0 & 0 & \gamma_2/E & 0 & (1+\nu)/E & 0 \\ 0 & 0 & 0 & \gamma_3/E & 0 & 0 & (1+\nu)/E \end{bmatrix} \begin{Bmatrix} \mathrm{d}T \\ \mathrm{d}\sigma_1 \\ \mathrm{d}\sigma_2 \\ \mathrm{d}\sigma_3 \\ \mathrm{d}\tau_1 \\ \mathrm{d}\tau_2 \\ \mathrm{d}\tau_3 \end{Bmatrix} \tag{3.11}$$

where the material constants include: $C := T\,\mathrm{d}S/\mathrm{d}T$ is the specific heat capacity measured at constant pressure; $\alpha := (1/L)\mathrm{d}L/\mathrm{d}T$ is the coefficient of thermal expansion over a gage length L; $E := \mathrm{d}\sigma/\mathrm{d}\varepsilon$ is the elastic modulus; and $\nu := -\mathrm{d}\varepsilon_{\text{transverse}}/\mathrm{d}\varepsilon_{\text{axial}}$ is Poisson's ratio.

3.4.2 Three-Mode Elastic Solid

A different thermoelastic solid that also exhibits the Kelvin, Poisson and Poynting strain effects has a compliance matrix that looks like

$$\begin{Bmatrix} \mathrm{d}S \\ \mathrm{d}e \\ \mathrm{d}\varepsilon_1 \\ \mathrm{d}\varepsilon_2 \\ \mathrm{d}\varepsilon_3 \\ \frac{1}{2}\mathrm{d}\gamma_1 \\ \frac{1}{2}\mathrm{d}\gamma_2 \\ \frac{1}{2}\mathrm{d}\gamma_3 \end{Bmatrix} = \begin{bmatrix} C/T & \alpha & 0 & 0 & 0 & 0 & 0 & 0 \\ \alpha & 1/3K & 0 & 0 & 0 & 0 & 0 & 0 \\ 0 & 0 & 1/3N & 0 & 0 & -\gamma_1/3N & 0 & 0 \\ 0 & 0 & 0 & 1/3N & 0 & \gamma_1/3N & -\gamma_2/3N & -\gamma_3/3N \\ 0 & 0 & 0 & 0 & 1/3N & 0 & \gamma_2/3N & \gamma_3/3N \\ 0 & 0 & -\gamma_1/3N & \gamma_1/3N & 0 & 1/2G & 0 & 0 \\ 0 & 0 & 0 & -\gamma_2/3N & \gamma_2/3N & 0 & 1/2G & 0 \\ 0 & 0 & 0 & -\gamma_3/3N & \gamma_3/3N & 0 & 0 & 1/2G \end{bmatrix} \begin{Bmatrix} \mathrm{d}T \\ -\mathrm{d}p \\ \mathrm{d}\sigma_1 \\ \mathrm{d}\sigma_2 \\ \mathrm{d}\sigma_3 \\ \mathrm{d}\tau_1 \end{Bmatrix} \tag{3.12}$$

where the material constants include: $C := T\,\mathrm{d}S/\mathrm{d}T$ is the specific heat capacity measured at constant pressure; $\alpha := (1/L)\mathrm{d}L/\mathrm{d}T$ is the coefficient of thermal expansion; $K := -V\,\mathrm{d}p/\mathrm{d}V = -\mathrm{d}p/3\mathrm{d}e$ is the bulk modulus; $N := \mathrm{d}\sigma/3\mathrm{d}\varepsilon$ is the squeeze modulus; and $G := \mathrm{d}\tau/\mathrm{d}\gamma$ is the shear modulus.

4. LAPLACE STRETCH: EULERIAN FORMULATIONS [6]

The deformation gradient admits a number of different triangular decompositions, whereby in each case the full deformation gradient matrix is decomposed into a product of an orthogonal tensor and a triangular stretch tensor. The decomposition studied in this chapter splits the deformation gradient tensor into a rotation tensor followed (premultiplied) by a lower-triangular stretch tensor. This construction is referred to as the Eulerian formulation of the triangular decomposition of deformation.

In general, Eulerian formulations are often preferred for modeling isotropic solids (and fluids) that have no obvious initial or reference state. For example, many biological tissues, in vivo, are perpetually under tension, and a stress-free reference state is never physically realized. Eulerian forms are also used for hypoelastic constitutive modeling that is often more popular than hyperelasticity for solving initial-boundary value problems numerically. However, prior to the present work, no application of the Eulerian lower-triangular decomposition in the context of continuum mechanics seems to have been reported.

4.1 Deformation

We assume that a body is simply connected and its motion $\boldsymbol{\chi}$ is sufficiently differentiable so that $\boldsymbol{F} = \partial\boldsymbol{\chi}(\boldsymbol{X}, t)/\partial\boldsymbol{X}$ exists and therefore

$$F_{ij} = \frac{\partial \chi_i(\boldsymbol{X}, t)}{\partial X_j} = \begin{bmatrix} F_{11} & F_{12} & F_{13} \\ F_{21} & F_{22} & F_{23} \\ F_{31} & F_{32} & F_{33} \end{bmatrix} = \left[\begin{array}{c} \boldsymbol{f}_1^r \\ \hline \boldsymbol{f}_2^r \\ \hline \boldsymbol{f}_3^r \end{array}\right] \tag{4.1}$$

where vectors $\boldsymbol{f}_i^r = F_{ij}\,\vec{\mathbf{e}}_j$ contain the rows of tensor $\boldsymbol{F} = F_{ij}\,\vec{\mathbf{e}}_i \otimes \vec{\mathbf{e}}_j$, $i = 1, 2, 3$, with repeated indices being summed according to Einstein's summation convention. It follows straightaway that the left, Cauchy-Green, deformation tensor $\mathbf{B} := \boldsymbol{F}\boldsymbol{F}^{\mathsf{T}} = B_{ij}\,\vec{\mathbf{e}}_i \otimes \vec{\mathbf{e}}_j$, which is symmetric.

4.1.1 Eulerian Laplace Stretch

Now we describe a Gram–Schmidt like factorization of the deformation gradient, viz., $\boldsymbol{F} = \boldsymbol{\mathcal{V}}\boldsymbol{\mathcal{R}}^E$, wherein $\boldsymbol{\mathcal{V}} = \mathcal{V}_{ij}\,\vec{\mathbf{e}}_i \otimes \vec{\mathbf{e}}_j$ is called the Eulerian Laplace stretch, or the left Laplace stretch. Applying a Cholesky factorization to the symmetric, positive-definite, left, Cauchy-Green, deformation tensor $\mathbf{B} := \boldsymbol{F}\boldsymbol{F}^{\mathsf{T}} = \boldsymbol{\mathcal{V}}\boldsymbol{\mathcal{V}}^{\mathsf{T}}$ with components $\mathbf{B} = B_{ij}\,\vec{\mathbf{e}}_i \otimes \vec{\mathbf{e}}_j$ one can construct a stretch tensor $\boldsymbol{\mathcal{V}} = \mathcal{V}_{ij}\,\vec{\mathbf{e}}_i \otimes \vec{\mathbf{e}}_j$ whereby

$$\begin{array}{lll} \mathcal{V}_{11} = \sqrt{B_{11}} & \mathcal{V}_{12} = 0 & \mathcal{V}_{13} = 0 \\ \mathcal{V}_{21} = B_{21}/\mathcal{V}_{11} & \mathcal{V}_{22} = \sqrt{B_{22} - \mathcal{V}_{21}^2} & \mathcal{V}_{23} = 0 \\ \mathcal{V}_{31} = B_{31}/\mathcal{V}_{11} & \mathcal{V}_{32} = \big(B_{32} - \mathcal{V}_{21}\mathcal{V}_{31}\big)/\mathcal{V}_{22} & \mathcal{V}_{33} = \sqrt{B_{33} - \mathcal{V}_{31}^2 - \mathcal{V}_{32}^2} \end{array} \tag{4.2}$$

A Gram–like factorization of the deformation gradient $\boldsymbol{F} = F_{ij}\,\vec{\mathbf{e}}_i \otimes \vec{\mathbf{e}}_j$ can also describe an Eulerian rotation tensor $\boldsymbol{\mathcal{R}}^E = \delta_{ij}\,\vec{\mathbf{e}}_i \otimes \vec{\mathbf{e}}_j^{\,E} = \mathcal{R}^E_{ij}\,\vec{\mathbf{e}}_i \otimes \vec{\mathbf{e}}_j$ constructed as

$$\mathcal{R}^E_{ij} = \left[\begin{array}{c|c|c} \vec{\mathbf{e}}_1^{\,E} & \vec{\mathbf{e}}_2^{\,E} & \vec{\mathbf{e}}_3^{\,E} \end{array}\right]^{\mathsf{T}} \tag{4.3a}$$

whose rows constitute unit base vectors that can be constructed via

$$\vec{\mathbf{e}}_1^{\,E} := \frac{\boldsymbol{f}_1^r}{\|\boldsymbol{f}_1^r\|} \tag{4.3b}$$

$$\vec{\mathbf{e}}_2^{\,E} := \frac{\boldsymbol{f}_2^r - (\boldsymbol{f}_2^r \cdot \vec{\mathbf{e}}_1^{\,E})\vec{\mathbf{e}}_1^{\,E}}{\|\boldsymbol{f}_2^r - (\boldsymbol{f}_2^r \cdot \vec{\mathbf{e}}_1^{\,E})\vec{\mathbf{e}}_1^{\,E}\|} \tag{4.3c}$$

$$\vec{\mathbf{e}}_3^{\,E} := \frac{\boldsymbol{f}_3^r - (\boldsymbol{f}_3^r \cdot \vec{\mathbf{e}}_1^{\,E})\vec{\mathbf{e}}_1^{\,E} - (\boldsymbol{f}_3^r \cdot \vec{\mathbf{e}}_2^{\,E})\vec{\mathbf{e}}_2^{\,E}}{\|\boldsymbol{f}_3^r - (\boldsymbol{f}_3^r \cdot \vec{\mathbf{e}}_1^{\,E})\vec{\mathbf{e}}_1^{\,E} - (\boldsymbol{f}_3^r \cdot \vec{\mathbf{e}}_2^{\,E})\vec{\mathbf{e}}_2^{\,E}\|} \tag{4.3d}$$

It follows that the Eulerian Laplace stretch has components which can be expressed as

$$\mathcal{V}_{ij} = \begin{bmatrix} \boldsymbol{f}_1^r \cdot \vec{\mathbf{e}}_1^{\,E} & 0 & 0 \\ \boldsymbol{f}_2^r \cdot \vec{\mathbf{e}}_1^{\,E} & \boldsymbol{f}_2^r \cdot \vec{\mathbf{e}}_2^{\,E} & 0 \\ \boldsymbol{f}_3^r \cdot \vec{\mathbf{e}}_1^{\,E} & \boldsymbol{f}_3^r \cdot \vec{\mathbf{e}}_2^{\,E} & \boldsymbol{f}_3^r \cdot \vec{\mathbf{e}}_3^{\,E} \end{bmatrix} \tag{4.4}$$

that provide a means of geometric interpretation for this measure of stretch.

4.2 Physical Interpretation of Laplace Stretch Components

Each Laplace stretch has six, independent, physical attributes. Their Eulerian interpretations are distinguished with an overline, viz., $\overline{a}$, $\overline{b}$, $\overline{c}$, $\overline{\alpha}$, $\overline{\beta}$ and $\overline{\gamma}$ which are distinct from Lagrangian stretch attributes. However, their geometric interpretations are the same.

4.2.1 Eulerian Stretch Attributes

The Eulerian Laplace stretch has geometric interpretations that arise from Eqn. (4.4) whereby one can assign

$$\mathcal{V}_{ij} = \begin{bmatrix} \overline{a} & 0 & 0 \\ \overline{a\gamma} & \overline{b} & 0 \\ \overline{a\beta} & \overline{b\alpha} & \overline{c} \end{bmatrix} = \begin{bmatrix} 1 & 0 & 0 \\ \overline{\gamma} & 1 & 0 \\ 0 & 0 & 1 \end{bmatrix} \begin{bmatrix} 1 & 0 & 0 \\ 0 & 1 & 0 \\ \overline{\beta} & \overline{\alpha} & 1 \end{bmatrix} \begin{bmatrix} \overline{a} & 0 & 0 \\ 0 & \overline{b} & 0 \\ 0 & 0 & \overline{c} \end{bmatrix} \tag{4.5a}$$

whose constituents are measured in a coordinate frame with base vectors

$$\vec{\mathbf{e}}_1^E = \boldsymbol{f}_1^r \,/\, \overline{a} \tag{4.6a}$$

$$\vec{\mathbf{e}}_2^E = \left(\boldsymbol{f}_2^r - \overline{\gamma}\boldsymbol{f}_1^r\right) / \overline{b} \tag{4.6b}$$

$$\vec{\mathbf{e}}_3^E = \left(\boldsymbol{f}_3^r - \overline{\alpha}\boldsymbol{f}_2^r - (\overline{\beta} - \overline{\alpha\gamma})\boldsymbol{f}_1^r\right) / \overline{c} \tag{4.6c}$$

all of which are described in terms of physical attributes defined as

$$\overline{a} := \mathcal{V}_{11}, \quad \overline{b} := \mathcal{V}_{22}, \quad \overline{c} := \mathcal{V}_{33}, \quad \overline{\alpha} := \frac{\mathcal{V}_{32}}{\mathcal{V}_{22}}, \quad \overline{\beta} := \frac{\mathcal{V}_{31}}{\mathcal{V}_{11}}, \quad \overline{\gamma} := \frac{\mathcal{V}_{21}}{\mathcal{V}_{11}} \tag{4.7}$$

According to Eqn. (4.5), the Eulerian Laplace stretch arises from the following sequence of deformations: it starts with three elongations $\overline{a}$, $\overline{b}$ and $\overline{c}$, followed by two out-of-plane shears $\overline{\alpha}$ and $\overline{\beta}$, and then finishes with an in-plane shear $\overline{\gamma}$, as illustrated in Fig. 4.1.

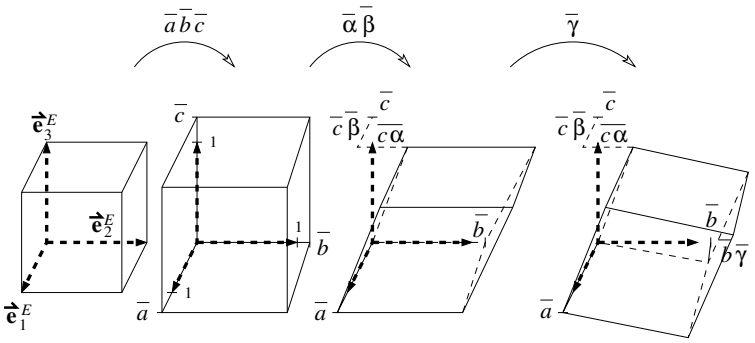

Figure 4.1: A geometric interpretation for Eulerian Laplace stretch.

4.3 Frameworks for Constitutive Development

Here we construct sets of thermodynamic conjugate pairs for Eulerian frameworks when using Laplace stretch as one's kinematic variable.

4.3.1 Eulerian Stress-Strain Attributes

In terms of Eulerian fields, stress power $\dot{W}$ can be written as $\frac{1}{\rho_0}\mathrm{tr}(\boldsymbol{\tau}\mathbf{D})$ wherein $\boldsymbol{\tau} = \boldsymbol{F}\mathbf{S}\boldsymbol{F}^{\mathsf{T}}$ is the Kirchhoff stress, which relates to Cauchy stress $\mathbf{T}$ via $\boldsymbol{\tau} := \det(\boldsymbol{F})\mathbf{T} = \frac{\rho_0}{\rho}\mathbf{T}$, and where $\mathbf{D} := \frac{1}{2}(\mathbf{L} + \mathbf{L}^{\mathsf{T}}) = \boldsymbol{F}^{-\mathsf{T}}\dot{\mathbf{E}}\boldsymbol{F}^{-1}$ is the symmetric part of velocity gradient $\mathbf{L} := \dot{\boldsymbol{F}}\boldsymbol{F}^{-1}$, with ρ being the current mass density.

It can be shown that

$$\dot{W} = \tfrac{1}{\rho_0}\mathrm{tr}(\boldsymbol{\tau}\mathbf{D}) = \tfrac{1}{\rho_0}\mathrm{tr}\big(\boldsymbol{\tau}\boldsymbol{\mathcal{L}}^E\big) \tag{4.8a}$$

given that $\boldsymbol{F} = \boldsymbol{\mathcal{V}}\boldsymbol{\mathcal{R}}^E$, where this Eulerian velocity gradient $\boldsymbol{\mathcal{L}}^E$ is defined by

$$\boldsymbol{\mathcal{L}}^E := \mathring{\boldsymbol{\mathcal{V}}}\boldsymbol{\mathcal{V}}^{-1} \quad \text{wherein} \quad \mathring{\boldsymbol{\mathcal{V}}} := \dot{\boldsymbol{\mathcal{V}}} + \boldsymbol{\mathcal{V}}\boldsymbol{\Omega}^E - \boldsymbol{\Omega}^E\boldsymbol{\mathcal{V}} \tag{4.8b}$$

with $\mathring{\boldsymbol{\mathcal{V}}}$ being an objective co-rotational derivative for this measure of stretch, and $\boldsymbol{\Omega}^E := \dot{\boldsymbol{\mathcal{R}}}^E\boldsymbol{\mathcal{R}}^{E^{\mathsf{T}}}$ being a spin of an Eulerian coordinate axes $(\vec{\mathbf{e}}_1^E, \vec{\mathbf{e}}_2^E, \vec{\mathbf{e}}_3^E)$ about the reference axes.

Consequently, stress power $\rho_0\dot{W} = \mathrm{tr}\big(\boldsymbol{\tau}\boldsymbol{\mathcal{L}}^E\big)$ arises from two sources in this Eulerian

construction, viz. $\dot{W} = \dot{W}_1 + \dot{W}_2$. The first is energetic, i.e.,

$$\dot{W}_1 := \tfrac{1}{\rho_0}\mathrm{tr}\big(\boldsymbol{\tau}\dot{\boldsymbol{\mathcal{V}}}\boldsymbol{\mathcal{V}}^{-1}\big) \tag{4.9a}$$

while the second satifies objectivity, viz.,

$$\dot{W}_2 := \tfrac{1}{\rho_0}\mathrm{tr}\big(\boldsymbol{\tau}\boldsymbol{\mathcal{V}}\boldsymbol{\Omega}^E\boldsymbol{\mathcal{V}}^{-1}\big) \tag{4.9b}$$

noting that $\mathrm{tr}(\boldsymbol{\tau}\boldsymbol{\Omega}^E) = 0$. The objective correction (4.9b) is required to quantify the work being done, but it plays no role when creating our Eulerian stress-strain attributes, as $\dot{W}_2 = 0$ whenever $\boldsymbol{\Omega}^E = \mathbf{0}$.

Because $\dot{\boldsymbol{\mathcal{V}}}\boldsymbol{\mathcal{V}}^{-1} = \dot{\mathcal{V}}_{ik}\mathcal{V}^{-1}_{kj}\,\vec{\mathbf{e}}_i\otimes\vec{\mathbf{e}}_j$ has components that are lower triangular, a consequence of the group that tensor $\boldsymbol{\mathcal{V}}$ belongs to, the first contribution to stress power put forward in Eqn. (4.9a) reduces to a sum of six scalar contributions; specifically,

$$\rho_0\dot{W}_1 \;=\; \tau_{11}\dot{\mathcal{V}}_{1i}\mathcal{V}^{-1}_{i1} + \tau_{12}\dot{\mathcal{V}}_{2i}\mathcal{V}^{-1}_{i1} + \tau_{13}\dot{\mathcal{V}}_{3i}\mathcal{V}^{-1}_{i1} + \tau_{22}\dot{\mathcal{V}}_{2i}\mathcal{V}^{-1}_{i2} + \tau_{23}\dot{\mathcal{V}}_{3i}\mathcal{V}^{-1}_{i2} + \tau_{33}\dot{\mathcal{V}}_{3i}\mathcal{V}^{-1}_{i3} \tag{4.10}$$

wherein

$$\dot{\mathcal{V}}_{ik}\mathcal{V}^{-1}_{kj} = \begin{bmatrix} \frac{\dot{\overline{a}}}{\overline{a}} & 0 & 0 \\ \dot{\overline{\gamma}} + \overline{\gamma}\left(\frac{\dot{\overline{a}}}{\overline{a}} - \frac{\dot{\overline{b}}}{\overline{b}}\right) & \frac{\dot{\overline{b}}}{\overline{b}} & 0 \\ \dot{\overline{\beta}} - \overline{\gamma}\,\dot{\overline{\alpha}} + \overline{\beta}\left(\frac{\dot{\overline{a}}}{\overline{a}} - \frac{\dot{\overline{c}}}{\overline{c}}\right) - \overline{\alpha\gamma}\left(\frac{\dot{\overline{b}}}{\overline{b}} - \frac{\dot{\overline{c}}}{\overline{c}}\right) & \dot{\overline{\alpha}} + \overline{\alpha}\left(\frac{\dot{\overline{b}}}{\overline{b}} - \frac{\dot{\overline{c}}}{\overline{c}}\right) & \frac{\dot{\overline{c}}}{\overline{c}} \end{bmatrix} \tag{4.11}$$

Present here are the squeeze rates $\dot{\overline{\varepsilon}}_1 = \frac{1}{3}\big(\dot{\overline{a}}/\overline{a} - \dot{\overline{b}}/\overline{b}\big)$, etc., which appear in the off-diagonal terms, along with their corresponding shear rates, e.g., $\dot{\overline{\gamma}}$, thereby substantiating our assumed construction of conjugate pairs.

Expressing Eqn. (4.10) in terms of Eulerian, thermodynamic, conjugate pairs, one can write

$$\rho_0\dot{W}_1 = \overline{\pi}\dot{\overline{\delta}} + \sum_{i=1}^{3}\big(\overline{\sigma}_i\dot{\overline{\varepsilon}}_i + \overline{\tau}_i\dot{\overline{\gamma}}_i\big) \tag{4.12}$$

whose seven, conjugate, stress-strain pairs are defined as follows: a uniform bulk response is governed by an Eulerian pressure $\overline{\pi}$ and an Eulerian dilatation $\overline{\delta}$ defined by

$$\overline{\pi} := \tau_{11} + \tau_{22} + \tau_{33} \qquad \overline{\delta} := \ln \sqrt[3]{\frac{\overline{a}}{\overline{a}_0}\frac{\overline{b}}{\overline{b}_0}\frac{\overline{c}}{\overline{c}_0}} \qquad \dot{\overline{\delta}} = \frac{1}{3}\left(\frac{\dot{\overline{a}}}{\overline{a}} + \frac{\dot{\overline{b}}}{\overline{b}} + \frac{\dot{\overline{c}}}{\overline{c}}\right) \tag{4.13a}$$

while the squeeze (pure shear) responses are governed by Eulerian normal-stress differences $\overline{\sigma}_i$ and Eulerian squeezes $\overline{\varepsilon}_i$ defined by

$$\overline{\sigma}_1 := \tau_{11} - \tau_{22} + 3\overline{\gamma}\tau_{12} \qquad \overline{\varepsilon}_1 := \ln \sqrt{\frac{\overline{a}}{\overline{a}_0}\frac{\overline{b}_0}{\overline{b}}} \qquad \dot{\overline{\varepsilon}}_1 = \frac{1}{3}\left(\frac{\dot{\overline{a}}}{\overline{a}} - \frac{\dot{\overline{b}}}{\overline{b}}\right) \tag{4.13b}$$

$$\overline{\sigma}_2 := \begin{cases} \tau_{22} - \tau_{33} \\ \\ \quad + 3\overline{\alpha}(\tau_{23} - \overline{\gamma}\tau_{13}) \end{cases} \qquad \overline{\varepsilon}_2 := \ln \sqrt{\frac{\overline{b}}{\overline{b}_0}\frac{\overline{c}_0}{\overline{c}}} \qquad \dot{\overline{\varepsilon}}_2 = \frac{1}{3}\left(\frac{\dot{\overline{b}}}{\overline{b}} - \frac{\dot{\overline{c}}}{\overline{c}}\right) \tag{4.13c}$$

$$\overline{\sigma}_3 := -\tau_{11} + \tau_{33} - 3\overline{\beta}\tau_{13} \qquad \overline{\varepsilon}_3 := \ln \sqrt{\frac{\overline{c}}{\overline{c}_0}\frac{\overline{a}_0}{\overline{a}}} \qquad \dot{\overline{\varepsilon}}_3 = \frac{1}{3}\left(\frac{\dot{\overline{c}}}{\overline{c}} - \frac{\dot{\overline{a}}}{\overline{a}}\right) \tag{4.13d}$$

of which only two are independent, while the (simple) shear responses are governed by Eulerian shear stresses $\overline{\tau}_i$ and strains $\overline{\gamma}_i$ defined by

$$\overline{\tau}_1 := \tau_{23} - \overline{\gamma}\tau_{13} \qquad \overline{\gamma}_1 := \overline{\alpha} - \overline{\alpha}_0 \qquad \dot{\overline{\gamma}}_1 = \dot{\overline{\alpha}} \tag{4.13e}$$

$$\overline{\tau}_2 := \tau_{13} \qquad \overline{\gamma}_2 := \overline{\beta} - \overline{\beta}_0 \qquad \dot{\overline{\gamma}}_2 = \dot{\overline{\beta}} \tag{4.13f}$$

$$\overline{\tau}_3 := \tau_{12} \qquad \overline{\gamma}_3 := \overline{\gamma} - \overline{\gamma}_0 \qquad \dot{\overline{\gamma}}_3 = \dot{\overline{\gamma}} \tag{4.13g}$$

wherein $\overline{a}_0$, $\overline{b}_0$ and $\overline{c}_0$ are their initial elongation ratios, and where $\overline{\alpha}_0$, $\overline{\beta}_0$ and $\overline{\gamma}_0$ are their initial shear offsets.

The set of thermodynamic conjugate pairs for the Eulerian frameworks is composed of three modes: one pair to describe uniform dilatation, three pairs to describe pure shears, and three pairs to describe simple shears. There are three pure-shear pairs independent, thereby resulting in sets of six, independent, conjugate pairs that have direct connections with the six independent components of stress and stretch rate.

Bijective maps exist to transform tensor components into thermodynamic stress–strain-rate attributes that, for isotropic materials, are described by

$$\begin{Bmatrix} \overline{\pi} \\ \overline{\sigma}_1 \\ \overline{\sigma}_2 \\ \overline{\tau}_1 \\ \overline{\tau}_2 \\ \overline{\tau}_3 \end{Bmatrix} = \begin{bmatrix} 1 & 1 & 1 & 0 & 0 & 0 \\ 1 & -1 & 0 & 0 & 0 & 3\overline{\gamma} \\ 0 & 1 & -1 & 3\overline{\alpha} & -3\overline{\alpha\gamma} & 0 \\ 0 & 0 & 0 & 1 & -\overline{\gamma} & 0 \\ 0 & 0 & 0 & 0 & 1 & 0 \\ 0 & 0 & 0 & 0 & 0 & 1 \end{bmatrix} \begin{Bmatrix} \tau_{11} \\ \tau_{22} \\ \tau_{33} \\ \tau_{32} \\ \tau_{31} \\ \tau_{21} \end{Bmatrix} \tag{4.14a}$$

with

$$\overline{\sigma}_3 = -\overline{\sigma}_1 - \overline{\sigma}_2 + 3\big(\overline{\alpha\tau}_1 - \overline{\beta\tau}_2 + \overline{\gamma\tau}_3\big) \tag{4.14b}$$

and where

$$\begin{Bmatrix} \dot{\overline{\delta}} \\ \dot{\overline{\varepsilon}}_1 \\ \dot{\overline{\varepsilon}}_2 \\ \dot{\overline{\gamma}}_1 \\ \dot{\overline{\gamma}}_2 \\ \dot{\overline{\gamma}}_3 \end{Bmatrix} = \begin{bmatrix} 1/3 & 1/3 & 1/3 & 0 & 0 & 0 \\ 1/3 & -1/3 & 0 & 0 & 0 & 0 \\ 0 & 1/3 & -1/3 & 0 & 0 & 0 \\ 0 & -\overline{\alpha} & \overline{\alpha} & 1 & 0 & 0 \\ -\overline{\beta} & 0 & \overline{\beta} & \overline{\gamma} & 1 & 0 \\ -\overline{\gamma} & \overline{\gamma} & 0 & 0 & 0 & 1 \end{bmatrix} \begin{Bmatrix} \dot{\mathcal{V}}_{1i}\mathcal{V}_{i1}^{-1} \\ \dot{\mathcal{V}}_{2i}\mathcal{V}_{i2}^{-1} \\ \dot{\mathcal{V}}_{3i}\mathcal{V}_{i3}^{-1} \\ \dot{\mathcal{V}}_{2i}\mathcal{V}_{i3}^{-1} \\ \dot{\mathcal{V}}_{1i}\mathcal{V}_{i3}^{-1} \\ \dot{\mathcal{V}}_{1i}\mathcal{V}_{i2}^{-1} \end{Bmatrix} \tag{4.14c}$$

with

$$\dot{\overline{\varepsilon}}_3 = -\dot{\overline{\varepsilon}}_1 - \dot{\overline{\varepsilon}}_2. \tag{4.14d}$$

These strain rates can be integrated to get the Eulerian thermodynamic strains $\overline{\delta}$, $\overline{\varepsilon}_1$, $\overline{\varepsilon}_2$, $\overline{\varepsilon}_3$, $\overline{\gamma}_1$, $\overline{\gamma}_2$ and $\overline{\gamma}_3$ by using initial conditions of $\overline{\delta}|_0 = \overline{\varepsilon}_1|_0 = \overline{\varepsilon}_2|_0 = \overline{\varepsilon}_3|_0 = \overline{\gamma}_1|_0 = \overline{\gamma}_2|_0 = \overline{\gamma}_3|_0 = 0$ provided that the initial elongation ratios have been specified as $\overline{a}_0$, $\overline{b}_0$ and $\overline{c}_0$ and that the initial magnitudes of shear have been specified as $\overline{\alpha}_0$, $\overline{\beta}_0$ and $\overline{\gamma}_0$.

5. A MICROSCOPIC MODEL FOR LUNG TISSUE [7]

Models and metrics whose parameters are physical and unique, and whose numeric implementation will be efficient and stable are used for modeling the Lung tissues.

In this chapter a microscopic model for lung tissue is provided that can be used as an aid in the parameterization of a macroscopic model for lung that will be reasonably accurate yet efficient to run in full torso finite element analyses to study behind armor blunt trauma (BABT) for the purpose of improving personal protective equipment (PPE).

5.1 Dodecahedra: A Model for Alveoli

Typical alveoli are 14 sided polyhedra with one face normally being open as a mouth to an alveolar duct, and whose septal membranes typically become flat at transpulmonary pressures as low as 2 cm H_2O [40]. A dodecahedron is an isotropic structure, and is nearly volume filling [41]. It is one of the five perfectly symmetric solids in geometry, Fig. 5.1(a).

5.1.1 Geometric Properties of a Regular Pentagon

Figure 5.2 presents a regular pentagon drawn in its natural co-ordinate system with co-ordinates designated as (ξ, η). Vertices of such a pentagon are placed at

$$\xi = \cos\left(\frac{2(k-1)\pi}{5} + \frac{\pi}{2}\right) \quad \eta = \sin\left(\frac{2(k-1)\pi}{5} + \frac{\pi}{2}\right) \quad k = 1, 2, \ldots, 5 \tag{5.1}$$

wherein k denotes the vertex number that are numbered counterclockwise, as assigned in Fig. 5.2. Lengths of the five chords in a regular pentagon are all

$$L^p = 2\cos(\omega) \approx 1.176 \tag{5.2}$$

while the area of this pentagon is

$$A^p = \tfrac{5}{4}\tan(\omega)\,(L^p)^2 = 5\sin(\omega)\cos(\omega) \approx 2.378 \tag{5.3}$$

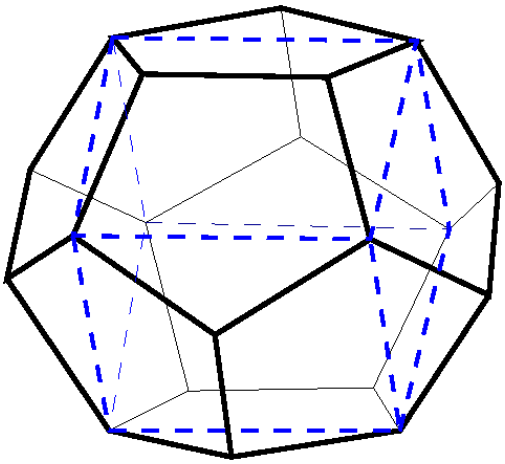

(a) A cube is contained within a dodecahedron, with one of its five possible orientations being displayed.

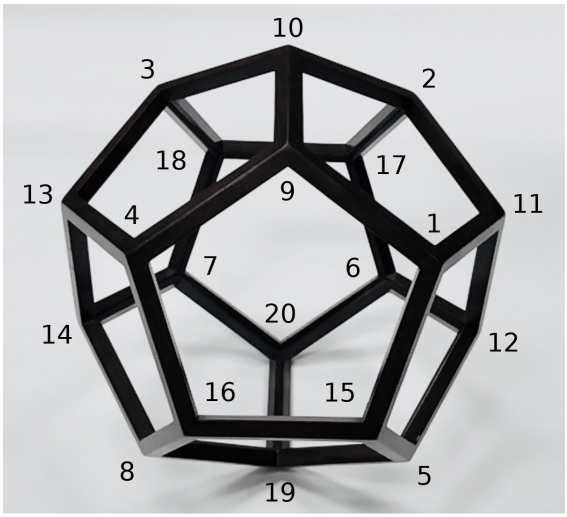

(b) Vertices 1 through 8 are located at the corners of such a cube. Vertices 9 through 20 are corners of the hipped roof lines residing above each face of the cube.

Figure 5.1: Geometric representations for a dodecahedron.

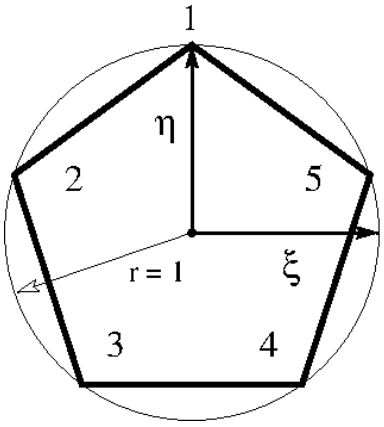

Figure 5.2: A regular pentagon in the natural co-ordinate system

where area of the unit circle that inscribes this pentagon is $\pi r^2 \approx 3.142$, $r = 1$.

5.1.2 Geometric Properties of a Regular Dodecahedron

Here we consider a dodecahedron that inscribes the unit sphere. Let this geometry be described in its natural co-ordinate system with co-ordinates (ξ, η, ζ) whose origin is located at its centroid, the center of the sphere. The 20 vertices of this dodecahedron are placed at

$$\begin{array}{ccc} \xi & \eta & \zeta \\ \hline \pm 1/\sqrt{3} & \pm 1/\sqrt{3} & \pm 1/\sqrt{3} \\ \pm \phi/\sqrt{3} & \pm 1/\sqrt{3}\phi & 0 \\ 0 & \pm \phi/\sqrt{3} & \pm 1/\sqrt{3}\phi \\ \pm 1/\sqrt{3}\phi & 0 & \pm \phi/\sqrt{3} \end{array} \tag{5.4}$$

where $\phi = (1 + \sqrt{5})/2 \approx 1.618$, which is also known as the golden ratio. Lengths of the 30 chords in a regular dodecahedron, when measured in its natural co-ordinate system, are all

$$L^d = \frac{2}{\sqrt{3}\phi} \approx 0.7136 \tag{5.5}$$

while the volume of such a dodecahedron is

$$V^d = \frac{40}{3\sqrt{3}\phi^3} \tan^2(\omega) \sin(\omega) \approx 2.785 \tag{5.6}$$

where volume of the unit sphere that inscribes the dodecahedron is $\frac{4}{3}\pi r^3 \approx 4.189$, $r = 1$.

5.1.3 Dimensions of Human Alveoli

Septal chord length $L(D)$, expressed as a function of alveolar diameter D, can be estimated by considering the areal projection of a dodecahedron onto a plane that contains one of its pentagonal faces, which leads to

$$L = \frac{D}{\tan(\omega)(1 + \cos(\alpha))} \approx \frac{D}{2.685}, \tag{5.7}$$

where $\alpha = \pi/10 = 18^\circ$. Alveolar diameter D is a property that can be measured in histological studies of parenchyma.

5.1.4 Geometric Properties for Irregular Pentagons and Dodecahedra

Formulæ (5.3 & 5.6) only apply for regular pentagons and dodecahedra evaluated in their respective natural co-ordinate systems. For irregular dodecahedra, the areas of its irregular pentagons are calculated via

$$A = \frac{1}{2}\sum_{i=1}^{5}(x_i y_{i+1} - x_{i+1} y_i) \tag{5.8}$$

where $x_6 \Leftarrow x_1$ and $y_6 \Leftarrow y_1$. In order for the predicted area to be positive when using this formula, it is necessary that the vertices (x_i, y_i) index counterclockwise, as drawn in Fig. 5.2. The centroid of this pentagon has co-ordinates[0]

$$c_x = \frac{1}{6A}\sum_{i=1}^{5}(x_i + x_{i+1})(x_i y_{i+1} - x_{i+1} y_i) \tag{5.9a}$$

$$c_y = \frac{1}{6A}\sum_{i=1}^{5}(y_i + y_{i+1})(x_i y_{i+1} - x_{i+1} y_i) \tag{5.9b}$$

wherein the vertex co-ordinates x_i and y_i are quantified in a 2D pentagonal frame of reference, e.g., as established later in Fig. 5.4.

To compute the volume of an irregular dodecahedron, use the formula

$$288\, V_{tet}^2 = \begin{vmatrix} 0 & 1 & 1 & 1 & 1 \\ 1 & 0 & \ell_{12}^2 & \ell_{13}^2 & \ell_{14}^2 \\ 1 & \ell_{21}^2 & 0 & \ell_{23}^2 & \ell_{24}^2 \\ 1 & \ell_{31}^2 & \ell_{32}^2 & 0 & \ell_{34}^2 \\ 1 & \ell_{41}^2 & \ell_{42}^2 & \ell_{43}^2 & 0 \end{vmatrix} \tag{5.10}$$

to calculate each of the 60 individual tetrahedral volumes that collectively fill the volume of an irregular dodecahedron. Here ℓ_{ij} is the length of that tetrahedral edge with vertices i

Table 5.1: Natural co-ordinates for the vertices of a regular dodecahedron, as labeled in Fig. 5.1(b) according to Eqn. (5.4)

Vertex	$\boldsymbol{\xi}$	$\boldsymbol{\eta}$	$\boldsymbol{\zeta}$	**Vertex**	$\boldsymbol{\xi}$	$\boldsymbol{\eta}$	$\boldsymbol{\zeta}$
1	$1/\sqrt{3}$	$1/\sqrt{3}$	$1/\sqrt{3}$	11	$\phi/\sqrt{3}$	$1/\sqrt{3}\phi$	0
2	$1/\sqrt{3}$	$1/\sqrt{3}$	$-1/\sqrt{3}$	12	$\phi/\sqrt{3}$	$-1/\sqrt{3}\phi$	0
3	$-1/\sqrt{3}$	$1/\sqrt{3}$	$-1/\sqrt{3}$	13	$-\phi/\sqrt{3}$	$1/\sqrt{3}\phi$	0
4	$-1/\sqrt{3}$	$1/\sqrt{3}$	$1/\sqrt{3}$	14	$-\phi/\sqrt{3}$	$-1/\sqrt{3}\phi$	0
5	$1/\sqrt{3}$	$-1/\sqrt{3}$	$1/\sqrt{3}$	15	$1/\sqrt{3}\phi$	0	$\phi/\sqrt{3}$
6	$1/\sqrt{3}$	$-1/\sqrt{3}$	$-1/\sqrt{3}$	16	$-1/\sqrt{3}\phi$	0	$\phi/\sqrt{3}$
7	$-1/\sqrt{3}$	$-1/\sqrt{3}$	$-1/\sqrt{3}$	17	$1/\sqrt{3}\phi$	0	$-\phi/\sqrt{3}$
8	$-1/\sqrt{3}$	$-1/\sqrt{3}$	$1/\sqrt{3}$	18	$-1/\sqrt{3}\phi$	0	$-\phi/\sqrt{3}$
9	0	$\phi/\sqrt{3}$	$1/\sqrt{3}\phi$	19	0	$-\phi/\sqrt{3}$	$1/\sqrt{3}\phi$
10	0	$\phi/\sqrt{3}$	$-1/\sqrt{3}\phi$	20	0	$-\phi/\sqrt{3}$	$-1/\sqrt{3}\phi$

and j; $i, j = 1, 2, 3, 4$; $i \neq j$; with $\ell_{ij} = \ell_{ji}$.

5.1.5 Indexing Scheme for Dodecahedra

In order to implement the dodecahedron as a geometric model for an alveolar sac, as suggested by the images in Fig. 1.2, it first becomes necessary to introduce a labeling strategy.

The co-ordinates positioning the 20 vertices of a regular dodecahedron in its natural frame of reference are presented in Table 5.1. According to the labeling scheme of Fig. 5.1(b), the 30 chords of a dodecahedron are given vertex assignments according to Table 5.2, while its 12 pentagons are given vertex assignments according to Table 5.3, which are indexed counterclockwise when viewed looking from the outside in, and labeled according to Fig. 5.1(b).

5.1.6 Co-Ordinate Systems for Chordal Fibers and Pentagonal Membranes

The dodecahedron used to model an alveolus is considered to be regular in its "natural" configuration, with a capability of being irregular in its reference configuration, and certainly becoming irregular after deformation. The co-ordinate frame of its natural state is taken to have its origin positioned at the centroid of this regular dodecahedron, i.e., at the centroid of its enclosed cube (cf. Fig. 5.1).

Table 5.2: Vertices that locate the endpoints of septal chords in a dodecahedron, as labeled in Fig. 5.1(b)

Chord	**Vertices**	**Chord**	**Vertices**	**Chord**	**Vertices**
1	9, 10	11	17, 18	21	7, 18
2	1, 9	12	3, 18	22	7, 14
3	2, 10	13	4, 16	23	13, 14
4	3, 10	14	15, 16	24	8, 14
5	4, 9	15	1, 15	25	8, 16
6	1, 11	16	5, 15	26	5, 19
7	2, 11	17	5, 12	27	6, 20
8	3, 13	18	11, 12	28	7, 20
9	4, 13	19	6, 12	29	8, 19
10	2, 17	20	6, 17	30	19, 20

Table 5.3: Vertices that locate the corners of regular pentagonal surfaces in a regular dodecahedron, and the chords that connect them

Pentagon	**Vertices**	**Chords**
1	11, 2, 10, 9, 1	6, 7, 3, 1, 2
2	10, 2, 17, 18, 3	4, 3, 10, 11, 12
3	13, 4, 9, 10, 3	8, 9, 5, 1, 4
4	9, 4, 16, 15, 1	2, 5, 13, 14, 15
5	15, 5, 12, 11, 1	15, 16, 17, 18, 6
6	17, 2, 11, 12, 6	20, 10, 7, 18, 19
7	18, 7, 14, 13, 3	12, 21, 22, 23, 8
8	16, 4, 13, 14, 8	25, 13, 9, 23, 24
9	12, 5, 19, 20, 6	19, 17, 26, 30, 27
10	14, 7, 20, 19, 8	24, 22, 28, 30, 29
11	20, 7, 18, 17, 6	27, 28, 21, 11, 20
12	19, 5, 15, 16, 8	29, 26, 16, 14, 25

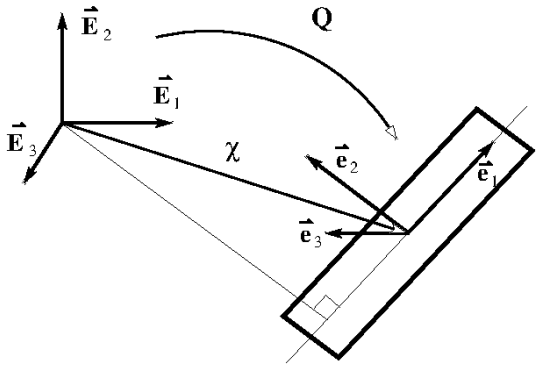

Figure 5.3: The co-ordinate system of a chord $(\vec{e}_1, \vec{e}_2, \vec{e}_3)$ relative to the co-ordinate system of its dodecahedron $(\vec{\boldsymbol{E}}_1, \vec{\boldsymbol{E}}_2, \vec{\boldsymbol{E}}_3)$ with origins located at their respective centroids that are offset by a translation $\boldsymbol{\chi}$.

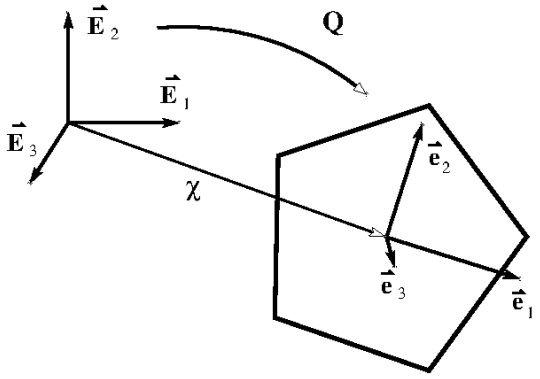

Figure 5.4: The co-ordinate system of a pentagon $(\vec{e}_1, \vec{e}_2, \vec{e}_3)$ relative to the co-ordinate system of its dodecahedron $(\vec{\boldsymbol{E}}_1, \vec{\boldsymbol{E}}_2, \vec{\boldsymbol{E}}_3)$ with origins located at their respective centroids that are offset by a translation $\boldsymbol{\chi}$.

The local co-ordinate system of a chordal fiber, pentagonal membrane, and tetrahedral volume are presented in Figures 5.3, 5.4, and 5.5, respectively. All three, local, co-ordinate systems are denoted as $(\vec{\boldsymbol{e}}_1, \vec{\boldsymbol{e}}_2, \vec{\boldsymbol{e}}_3)$ and each rotates out of the reference co-ordinate system $(\vec{\boldsymbol{E}}_1, \vec{\boldsymbol{E}}_2, \vec{\boldsymbol{E}}_3)$ of the dodecahedron via its own orthogonal rotation tensor $\boldsymbol{Q}$.

5.2 Kinematics

The irregular dodecahedron used here as a model for alveoli describes a 3D structure composing 30 1D rods (the septal chords) joined at twenty nodes (the vertices) that collec-

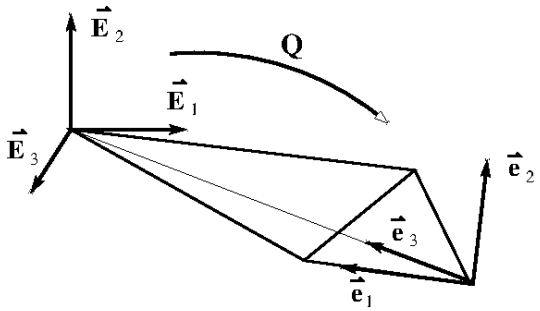

Figure 5.5: The co-ordinate system of a tetrahedron $(\vec{\mathbf{e}}_1, \vec{\mathbf{e}}_2, \vec{\mathbf{e}}_3)$ relative to the co-ordinate system of its dodecahedron $(\vec{\boldsymbol{E}}_1, \vec{\boldsymbol{E}}_2, \vec{\boldsymbol{E}}_3)$ with origins located at their respective centroids.

tively circumscribe 12 2D pentagonal membranes (the alveolar septa) that in turn envelop an alveolar sac whose volume is represented using 60 tetrahedra. To be able to describe the overall mechanical response of this 3D dodecahedral structure, it is conjectured to be sufficient to know the individual mechanical responses of its 1D septal chords, its 2D septal membranes, and the 3D void within.

5.2.1 1D Chords

The stretch of a rod under extension is a ratio of its lengths. Specifically, $\lambda := L/L_0$ where L and L_0 are its current and reference lengths, respectively.

5.2.1.1 Shape Functions for Interpolating a Rod

A two-noded alveolar chord has shape functions N_i, $i = 1, 2$, that, when evaluated in its natural co-ordinate system where $-1 \leqslant \xi \leqslant 1$, describe a matrix with elements

$$\mathbf{N} = \begin{bmatrix} N_1 & N_2 \end{bmatrix} = \begin{bmatrix} \frac{1}{2}(1-\xi) & \frac{1}{2}(1+\xi) \end{bmatrix} \tag{5.11a}$$

that interpolate vector fields according to

$$\boldsymbol{x}(\xi) = \sum_{i=1}^{2} N_i(\xi)\, x_i, \quad \boldsymbol{u}(\xi) = \sum_{i=1}^{2} N_i(\xi)\, u_i \tag{5.11b}$$

wherein ξ is the natural co-ordinate. Components x_i and $u_i := x_i - x_{0i}$, $i = 1, 2$, are their global co-ordinates and displacements, respectively, located at the two nodes of a chord evaluated in the co-ordinate frame $(\vec{\boldsymbol{e}}_1, \vec{\boldsymbol{e}}_2, \vec{\boldsymbol{e}}_3)$ of Fig. 5.3.

5.2.1.2 Deformation Gradient for a Rod

The deformation gradient in this case is simply

$$\boldsymbol{F}(\xi) = 1 + \frac{\partial \boldsymbol{u}}{\partial \xi}\left(\frac{\partial \mathbf{x}_0}{\partial \xi}\right)^{-1} = 1 + \sum_{i=1}^{2} N_{i,\xi} u_i \left(\sum_{i=1}^{2} N_{i,\xi} x_{0i}\right)^{-1}$$
$$= 1 + \frac{u_2 - u_1}{x_{02} - x_{01}}\,\vec{\boldsymbol{e}}_1 \otimes \vec{\boldsymbol{e}}_1 = \frac{x_2 - x_1}{x_{02} - x_{01}}\,\vec{\boldsymbol{e}}_1 \otimes \vec{\boldsymbol{e}}_1 \quad (5.12)$$

which is uniform over the length of a chord, i.e., it is independent of ξ.

5.2.2 2D Triangles

Triangular elements are needed in a support capacity in order to construct our alevolar model; specifically, the four surfaces of a tetrahedron are triangles. What is required of them is a capability to compute the traction acting across such a surface through integration.

5.2.2.1 Shape Functions for Interpolating a Triangle

The shape functions for a triangle expressed in terms of its natural co-ordinates (ξ, η), where $0 \leqslant \xi \leqslant 1$ and $0 \leqslant \eta \leqslant 1 - \xi$, are given by

$$N_1 = 1 - \xi - \eta \qquad N_2 = \xi \qquad N_3 = \eta \qquad (5.13a)$$

so that the area of a triangle in its natural co-ordinates is $1/2$.

5.2.3 2D Irregular Pentagons

The kinematics of an irregular pentagon, on the other hand, are not trivial. Shape functions are required from which deformation gradients can then be constructed. Once a deformation gradient is in hand, the state of stretch occurring within a pentagon at its Gauss

points can finally be derived.

5.2.3.1 Wachspress' Shape Functions for Interpolating an Irregular Pentagon

In 1975, Wachspress [42, 43] derived a set of shape functions N_i that are capable of interpolating convex polyhedra. His shape functions take on the form of rational polynomials, viz., $N_i = A_i/B$ where A_i and B are polynomials.

Let us consider a convex pentagonal domain Ω defined over $\mathbb{R}^2$ whose vertices have global co-ordinates of

$$(x_1, y_1),\ (x_2, y_2),\ (x_3, y_3),\ (x_4, y_4),\ (x_5, y_5)$$

when evaluated in the pentagonal co-ordinate system $(\vec{\boldsymbol{e}}_1, \vec{\boldsymbol{e}}_2)$ of Fig. 5.4, with $\vec{\boldsymbol{e}}_3$ being an outward normal to the pentagon. Associated with this set of global co-ordinates is a set of local or natural co-ordinates

$$(\xi_1, \eta_1),\ (\xi_2, \eta_2),\ (\xi_3, \eta_3),\ (\xi_4, \eta_4),\ (\xi_5, \eta_5)$$

that describe a mapping of interpolation where

$$\begin{aligned} x(\xi,\eta) &= \textstyle\sum_{i=1}^{5} N_i(\xi,\eta)\, x_i \\ y(\xi,\eta) &= \textstyle\sum_{i=1}^{5} N_i(\xi,\eta)\, y_i \end{aligned} \qquad \text{or} \qquad \boldsymbol{x}(\boldsymbol{\xi}) = \sum_{i=1}^{5} N_i(\boldsymbol{\xi})\, \boldsymbol{x}_i \tag{5.14}$$

which relate natural co-ordinates $\boldsymbol{\xi} \equiv (\xi, \eta)$ to global co-ordinates $\boldsymbol{x} \equiv (x, y)$, where $\boldsymbol{x}_i \equiv (x_i, y_i)$ are nodal co-ordinates at the i^{th} vertex, with i indexing counterclockwise around a pentagon according to Fig. 5.2. Displacement $\boldsymbol{u}(\boldsymbol{x}) := \boldsymbol{x} - \boldsymbol{x}_0$, with reference co-ordinates $\boldsymbol{x}_0 \equiv (x_0, y_0)$, also obeys this mapping

$$\begin{aligned} u(\xi,\eta) &= \textstyle\sum_{i=1}^{5} N_i(\xi,\eta)\, u_i \\ v(\xi,\eta) &= \textstyle\sum_{i=1}^{5} N_i(\xi,\eta)\, v_i \end{aligned} \qquad \text{or} \qquad \boldsymbol{u}(\boldsymbol{\xi}) = \sum_{i=1}^{5} N_i(\boldsymbol{\xi})\, \boldsymbol{u}_i \tag{5.15}$$

whose components $\boldsymbol{u}_i \equiv (u_i, v_i)$ designate the nodal displacements.

Shape functions $N_i(\boldsymbol{\xi}) \equiv N_i(\xi, \eta)$ are interpolation functions that place any position P with local co-ordinates $\boldsymbol{\xi} \equiv (\xi, \eta) \in \bar{\Omega}$, where $\bar{\Omega} := \Omega \cup \partial\Omega$, into their global co-ordinates $\boldsymbol{x} \equiv (x, y)$. The shape functions of Wachspress [42, 43] possess the following properties [44]:

1. Partition of unity: $\sum_{i=1}^{5} N_i(\boldsymbol{\xi}) = 1, \quad 0 \leqslant N_i(\boldsymbol{\xi}) \leqslant 1.$
2. Interpolate nodal data: $N_i(\boldsymbol{\xi}_j) = \Xi_{ij}$.
3. Linear completeness: $\sum_{i=1}^{5} N_i(\boldsymbol{\xi})\, \boldsymbol{x}_i = \boldsymbol{x}$.
4. For $\boldsymbol{\xi} \in \Omega$, $N_i(\boldsymbol{\xi})$ is C^∞, but for $\boldsymbol{\xi} \in \partial\Omega$, $N_i(\boldsymbol{\xi})$ is C^0, i.e., interpolation is linear along an edge (or alveolar chord) connecting two neighboring vertices.

Item 4 is often considered a disadvantage of Wachspress shape functions, viz., the linear interpolation along their boundaries. However, this is appropriate for our modeling of alveoli, because the septal boundaries are alveolar chords that are taken to interpolate linearly.

For interpolating a convex, planar, pentagonal shape, the shape functions of Wachspress have polynomials of order three in their numerators, and another polynomial of order two in their denominators; specifically, we write them here as

$$N_{i+1}(\xi, \eta) = \kappa_i\, A_i(\xi, \eta)/B(\xi, \eta), \qquad i = 1, 2, \ldots, 5 \tag{5.16a}$$

using a scaling factor of κ_i, where $N_1 \Leftarrow N_6$. The numerators and denominator for interpolating a pentagon take on the general form of

$$\begin{aligned} A_i(\xi, \eta) = {} & \alpha_{0i} + \alpha_{1i}\xi + \alpha_{2i}\eta + \alpha_{3i}\xi^2 + \alpha_{4i}\xi\eta + \alpha_{5i}\eta^2 \\ & + \alpha_{6i}\xi^3 + \alpha_{7i}\xi^2\eta + \alpha_{8i}\xi\eta^2 + \alpha_{9i}\eta^3 \end{aligned} \tag{5.16b}$$

$$B(\xi, \eta) = \beta_0 + \beta_1\xi + \beta_2\eta + \beta_3\xi^2 + \beta_4\xi\eta + \beta_5\eta^2 \tag{5.16c}$$

Consider a chord c_i that connects vertex $\xi_{i-1} = (\xi_{i-1}, \eta_{i-1})$ with vertex $\xi_i = (\xi_i, \eta_i)$ via a

straight line segment such that $\ell_i = 0$ with $\ell_i := 1 - a_i\xi - b_i\eta$ wherein

$$a_i = \frac{\eta_i - \eta_{i-1}}{\xi_{i-1}\eta_i - \xi_i\eta_{i-1}}, \quad b_i = \frac{\xi_{i-1} - \xi_i}{\xi_{i-1}\eta_i - \xi_i\eta_{i-1}} \tag{5.17a}$$

for which Dasgupta [45] derived the following set of constraints

$$\kappa_i = \kappa_{i-1}\left(\frac{a_{i+1}(\xi_{i-1} - \xi_i) + b_{i+1}(\eta_{i-1} - \eta_i)}{a_{i-1}(\xi_i - \xi_{i-1}) + b_{i-1}(\eta_i - \eta_{i-1})}\right) \tag{5.17b}$$

with recursion starting at $\kappa_1 := 1$. Coefficients κ_i enforce property 4 listed above. The polynomial coefficients for the A_i in Eqn. (5.16b) have values of

$$\alpha_{0i} = 1 \tag{5.18a}$$

$$\alpha_{1i} = -(a_{i+1} + a_{i+2} + a_{i+3}) \tag{5.18b}$$

$$\alpha_{2i} = -(b_{i+1} + b_{i+2} + b_{i+3}) \tag{5.18c}$$

$$\alpha_{3i} = a_{i+1}a_{i+2} + a_{i+2}a_{i+3} + a_{i+3}a_{i+1} \tag{5.18d}$$

$$\alpha_{4i} = a_{i+1}(b_{i+2} + b_{i+3}) + a_{i+2}(b_{i+1} + b_{i+3}) + a_{i+3}(b_{i+1} + b_{i+2}) \tag{5.18e}$$

$$\alpha_{5i} = b_{i+1}b_{i+2} + b_{i+2}b_{i+3} + b_{i+3}b_{i+1} \tag{5.18f}$$

$$\alpha_{6i} = -a_{i+1}a_{i+2}a_{i+3} \tag{5.18g}$$

$$\alpha_{7i} = -(a_{i+1}a_{i+2}b_{i+3} + a_{i+1}b_{i+2}a_{i+3} + b_{i+1}a_{i+2}a_{i+3}) \tag{5.18h}$$

$$\alpha_{8i} = -(a_{i+1}b_{i+2}b_{i+3} + b_{i+1}a_{i+2}b_{i+3} + b_{i+1}b_{i+2}a_{i+3}) \tag{5.18i}$$

$$\alpha_{9i} = -b_{i+1}b_{i+2}b_{i+3} \tag{5.18j}$$

which differ for each shape function via index $i = 1, 2, \ldots, 5$, while the polynomial coefficients for B in Eqn. (5.16c) have values of

$$\beta_i = \sum_{j=1}^{5} \alpha_{ij}\kappa_j, \qquad i = 0, 1, \ldots, 5 \tag{5.19}$$

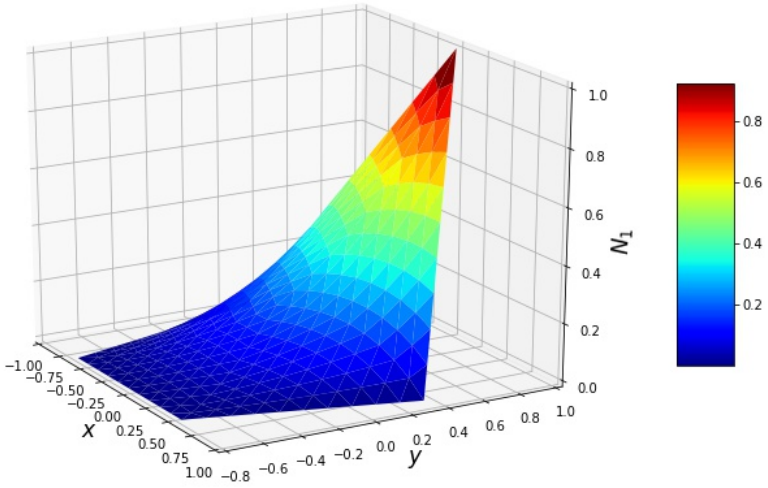

Figure 5.6: Wachspress shape functions for a pentagon, in this case, shape function N_1

which are the same for all five shape functions.

5.2.3.2 First Derivatives of the Shape Functions

The first derivatives of Wachspress' shape functions for a pentagon are

$$N_{i+1,\xi}(\xi,\eta) = \kappa_i \mathcal{N}_{i,\xi}(\xi,\eta)/B^2(\xi,\eta) \tag{5.20a}$$

$$N_{i+1,\eta}(\xi,\eta) = \kappa_i \mathcal{N}_{i,\eta}(\xi,\eta)/B^2(\xi,\eta) \tag{5.20b}$$

where $N_{i+1,\xi}(\xi,\eta) = \partial N_{i+1}(\xi,\eta)/\partial\xi$ and $N_{i+1,\eta}(\xi,\eta) = \partial N_{i+1}(\xi,\eta)/\partial\eta$ with

$$\mathcal{N}_{i,\xi}(\xi,\eta) = B(\xi,\eta)A_{i,\xi}(\xi,\eta) - B_{,\xi}(\xi,\eta)A_i(\xi,\eta) \tag{5.20c}$$

$$\mathcal{N}_{i,\eta}(\xi,\eta) = B(\xi,\eta)A_{i,\eta}(\xi,\eta) - B_{,\eta}(\xi,\eta)A_i(\xi,\eta) \tag{5.20d}$$

which contain the polynomials

$$A_{i,\xi}(\xi,\eta) = \alpha_{1i} + 2\alpha_{3i}\xi + \alpha_{4i}\eta + 3\alpha_{6i}\xi^2 + 2\alpha_{7i}\xi\eta + \alpha_{8i}\eta^2 \tag{5.20e}$$

$$A_{i,\eta}(\xi,\eta) = \alpha_{2i} + \alpha_{4i}\xi + 2\alpha_{5i}\eta + \alpha_{7i}\xi^2 + 2\alpha_{8i}\xi\eta + 3\alpha_{9i}\eta^2 \tag{5.20f}$$

$$B_{,\xi}(\xi,\eta) = \beta_1 + 2\beta_3\xi + \beta_4\eta \tag{5.20g}$$

$$B_{,\eta}(\xi,\eta) = \beta_2 + \beta_4\xi + 2\beta_5\eta \tag{5.20h}$$

from which the deformation and displacement gradients are constructed.

5.2.3.3 Deformation Gradient for an Irregular Pentagon

Derivatives of displacement (u, v) taken with respect to the local co-ordinates (ξ, η) described in terms of gradients of the shape functions $N_{i,\xi}(\xi,\eta)$ and $N_{i,\eta}(\xi,\eta)$ of a pentagon have components

$$\begin{bmatrix} \partial u/\partial\xi & \partial u/\partial\eta \\ \partial v/\partial\xi & \partial v/\partial\eta \end{bmatrix} = \sum\nolimits_{i=1}^{5} \begin{bmatrix} N_{i,\xi}(\xi,\eta)\, u_i & N_{i,\eta}(\xi,\eta)\, u_i \\ N_{i,\xi}(\xi,\eta)\, v_i & N_{i,\eta}(\xi,\eta)\, v_i \end{bmatrix} \tag{5.21a}$$

where $u := x - x_0$ and $v := y - y_0$, while gradients of the global co-ordinates (x, y) evaluated in the current state taken with respect to the local co-ordinates (ξ, η) have components

$$\begin{bmatrix} \partial x/\partial\xi & \partial x/\partial\eta \\ \partial y/\partial\xi & \partial y/\partial\eta \end{bmatrix} = \sum\nolimits_{i=1}^{5} \begin{bmatrix} N_{i,\xi}(\xi,\eta)\, x_i & N_{i,\eta}(\xi,\eta)\, x_i \\ N_{i,\xi}(\xi,\eta)\, y_i & N_{i,\eta}(\xi,\eta)\, y_i \end{bmatrix} \tag{5.21b}$$

whose transpose establishes the Jacobian matrix

$$\mathbf{J} := \begin{bmatrix} \partial x/\partial\xi & \partial y/\partial\xi \\ \partial x/\partial\eta & \partial y/\partial\eta \end{bmatrix} = \sum\nolimits_{i=1}^{5} \begin{bmatrix} N_{i,\xi}(\xi,\eta)\, x_i & N_{i,\xi}(\xi,\eta)\, y_i \\ N_{i,\eta}(\xi,\eta)\, x_i & N_{i,\eta}(\xi,\eta)\, y_i \end{bmatrix} \tag{5.21c}$$

wherein (x_i, y_i) denote the current global co-ordinates at the i^{th} vertex.

From the above matrices, one can construct the deformation gradient $\boldsymbol{F} = \partial\mathbf{x}/\partial\mathbf{x}_0 =$

$\boldsymbol{I} + \partial \boldsymbol{u}/\partial \boldsymbol{x}_0$ for an irregular pentagon via

$$\boldsymbol{F}(\xi,\eta) = \begin{bmatrix} F_{11}(\xi,\eta) & F_{12}(\xi,\eta) \\ F_{21}(\xi,\eta) & F_{22}(\xi,\eta) \end{bmatrix} = \begin{bmatrix} 1 & 0 \\ 0 & 1 \end{bmatrix} + \begin{bmatrix} \partial u/\partial \xi & \partial u/\partial \eta \\ \partial v/\partial \xi & \partial v/\partial \eta \end{bmatrix} \begin{bmatrix} \partial x_0/\partial \xi & \partial x_0/\partial \eta \\ \partial y_0/\partial \xi & \partial y_0/\partial \eta \end{bmatrix}^{-1} \tag{5.22}$$

All are evaluated in the 12 plane belonging to a co-ordinate system $(\vec{\boldsymbol{e}}_2, \vec{\boldsymbol{e}}_2, \vec{\boldsymbol{e}}_3)$ that orients this pentagon, with $\vec{\boldsymbol{e}}_3$ being normal to its surface, as illustrated in Fig. 5.4.

5.2.4 3D Irregular Dodecahedra

The primary kinematic variables needed to describe the deformation of an irregular dodecahedron used as a model for an alveolar sac are its volume V and the differential change in volume $\mathrm{d}V$. Whenever the material filling an alveolar sac is air (its normal healthy condition), no further breakdown of these kinematics is required.

5.2.4.1 Shape Functions for Interpolating an Irregular Tetrahedron

The shape functions associated with the four vertices of a tetrahedron are defined as

$$N_1 = 1 - \xi - \eta - \zeta, \quad N_2 = \xi, \quad N_3 = \eta, \quad N_4 = \zeta \tag{5.23a}$$

where ξ, η and ζ represent natural co-ordinates with $0 \leqslant \xi \leqslant 1$, $0 \leqslant \eta \leqslant 1 - \xi$ and $0 \leqslant \zeta \leqslant 1 - \xi - \eta$. Gradients of these shape functions are

$$\begin{aligned} &N_{1,\xi} = -1, \quad N_{1,\eta} = -1, \quad N_{1,\zeta} = -1 \\ &N_{2,\xi} = 1, \quad N_{2,\eta} = 0, \quad N_{2,\zeta} = 0 \\ &N_{3,\xi} = 0, \quad N_{3,\eta} = 1, \quad N_{3,\zeta} = 0 \\ &N_{4,\xi} = 0, \quad N_{4,\eta} = 0, \quad N_{4,\zeta} = 1 \end{aligned} \tag{5.23b}$$

and consequently the deformation gradient will be constant throughout its volume, like the deformation gradients used for chords and triangles.

5.2.4.2 Deformation Gradient for an Irregular Tetrahedron

The deformation gradient for a volume element is constructed from

$$\boldsymbol{F}(\xi,\eta,\zeta) = \begin{bmatrix} 1 & 0 & 0 \\ 0 & 1 & 0 \\ 0 & 0 & 1 \end{bmatrix} + \begin{bmatrix} \partial u/\partial\xi & \partial u/\partial\eta & \partial u/\partial\zeta \\ \partial v/\partial\xi & \partial v/\partial\eta & \partial v/\partial\zeta \\ \partial w/\partial\xi & \partial w/\partial\eta & \partial w/\partial\zeta \end{bmatrix} \begin{bmatrix} \partial x_0/\partial\xi & \partial x_0/\partial\eta & \partial x_0/\partial\zeta \\ \partial y_0/\partial\xi & \partial y_0/\partial\eta & \partial y_0/\partial\zeta \\ \partial z_0/\partial\xi & \partial z_0/\partial\eta & \partial z_0/\partial\zeta \end{bmatrix}^{-1} \tag{5.24}$$

such that, for the four-node tetrahedron considered here, one has

$$\begin{aligned} \begin{bmatrix} \partial u/\partial\xi & \partial u/\partial\eta & \partial u/\partial\zeta \\ \partial v/\partial\xi & \partial v/\partial\eta & \partial v/\partial\zeta \\ \partial w/\partial\xi & \partial w/\partial\eta & \partial w/\partial\zeta \end{bmatrix} &= \sum_{i=1}^{4} \begin{bmatrix} N_{i,\xi}u_i & N_{i,\eta}u_i & N_{i,\zeta}u_i \\ N_{i,\xi}v_i & N_{i,\eta}v_i & N_{i,\zeta}v_i \\ N_{i,\xi}w_i & N_{i,\eta}w_i & N_{i,\zeta}w_i \end{bmatrix} \\ &= \begin{bmatrix} u_2-u_1 & u_3-u_1 & u_4-u_1 \\ v_2-v_1 & v_3-v_1 & v_4-v_1 \\ w_2-w_1 & w_3-w_1 & w_4-w_1 \end{bmatrix} \end{aligned} \tag{5.25a}$$

whose nodal displacements $\boldsymbol{u}_i := \boldsymbol{x}_i - \boldsymbol{x}_{0i}$, $i = 1,2,3,4$, have components of $\boldsymbol{u}_i = u_i\,\vec{\boldsymbol{E}}_1 + v_i\,\vec{\boldsymbol{E}}_2 + w_i\,\vec{\boldsymbol{E}}_3$ with $u_i := x_i - x_{0i}$, $v_i := y_i - y_{0i}$ and $w_i := z_i - z_{0i}$, evaluated in the reference co-ordinate frame $(\vec{\boldsymbol{E}}_1, \vec{\boldsymbol{E}}_2, \vec{\boldsymbol{E}}_3)$ of the dodecahedron, and

$$\begin{aligned} \begin{bmatrix} \partial x_0/\partial\xi & \partial x_0/\partial\eta & \partial x_0/\partial\zeta \\ \partial y_0/\partial\xi & \partial y_0/\partial\eta & \partial y_0/\partial\zeta \\ \partial z_0/\partial\xi & \partial z_0/\partial\eta & \partial z_0/\partial\zeta \end{bmatrix} &= \sum_{i=1}^{4} \begin{bmatrix} N_{i,\xi}x_{0i} & N_{i,\eta}x_{0i} & N_{i,\zeta}x_{0i} \\ N_{i,\xi}y_{0i} & N_{i,\eta}y_{0i} & N_{i,\zeta}y_{0i} \\ N_{i,\xi}z_{0i} & N_{i,\eta}z_{0i} & N_{i,\zeta}z_{0i} \end{bmatrix} \\ &= \begin{bmatrix} x_{02}-x_{01} & x_{03}-x_{01} & x_{04}-x_{01} \\ y_{02}-y_{01} & y_{03}-y_{01} & y_{04}-y_{01} \\ z_{02}-z_{01} & z_{03}-z_{01} & z_{04}-z_{01} \end{bmatrix} \end{aligned} \tag{5.25b}$$

whose initial nodal positions are $\boldsymbol{x}_{0i} = x_{0i}\,\vec{\boldsymbol{E}}_1 + y_{0i}\,\vec{\boldsymbol{E}}_2 + z_{0i}\,\vec{\boldsymbol{E}}_3$ at vertex i. This matrix is invertible, because the four vertices of a tetrahedron are distinct. The Jacobian matrix is therefore given by

$$\mathbf{J} := \begin{bmatrix} \partial x/\partial\xi & \partial y/\partial\xi & \partial z/\partial\xi \\ \partial x/\partial\eta & \partial y/\partial\eta & \partial z/\partial\eta \\ \partial x/\partial\zeta & \partial y/\partial\zeta & \partial z/\partial\zeta \end{bmatrix} = \sum_{i=1}^{4} \begin{bmatrix} N_{i,\xi}x_i & N_{i,\xi}y_i & N_{i,\xi}z_i \\ N_{i,\eta}x_i & N_{i,\eta}y_i & N_{i,\eta}z_i \\ N_{i,\zeta}x_i & N_{i,\zeta}y_i & N_{i,\zeta}z_i \end{bmatrix} = \begin{bmatrix} x_2 - x_1 & y_2 - y_1 & z_2 - z_1 \\ x_3 - x_1 & y_3 - y_1 & z_3 - z_1 \\ x_4 - x_1 & y_4 - y_1 & z_4 - z_1 \end{bmatrix} \tag{5.25c}$$

whose determinant is used in integrations.

5.2.5 Code Verification: Kinematics

5.2.5.1 Isotropic Motions

Imposing an uniform far-field motion of a volumetric expansion onto our dodecahedral model results in a dodecahedral dilatation ($\Xi := \ln \sqrt[3]{V/V_0}$) that equals its pentagonal dilation ($\xi := \ln \sqrt{A/A_0}$) that equals its chordal strain ($e := \ln(L/L_0)$). Other choices for strain measures do not result in one-to-one relationships when exposed to an isotropic motion like those observed here. This is a particularly useful result in that it establishes a meaningful scaling in terms of strains between the three dimensions, cf. Fig. 5.7.

There are two types of strain measures that one can use to quantify deformation within a pentagon of a dodecahedron: geometric and thermodynamic. For the uniform far-field motion of volumetric expansion, only a thermodynamic strain known as dilation, i.e., $\xi = \ln \sqrt{ab/a_0b_0}$, varies with the motion, and its response equals that of the geometric strain $\ln \sqrt{A/A_0}$, see Fig. 5.8. Also present in this graph is an observation that the thermodynamic strains for squeeze ε and shear γ do not contribute under motions of pure dilatation, as expected.

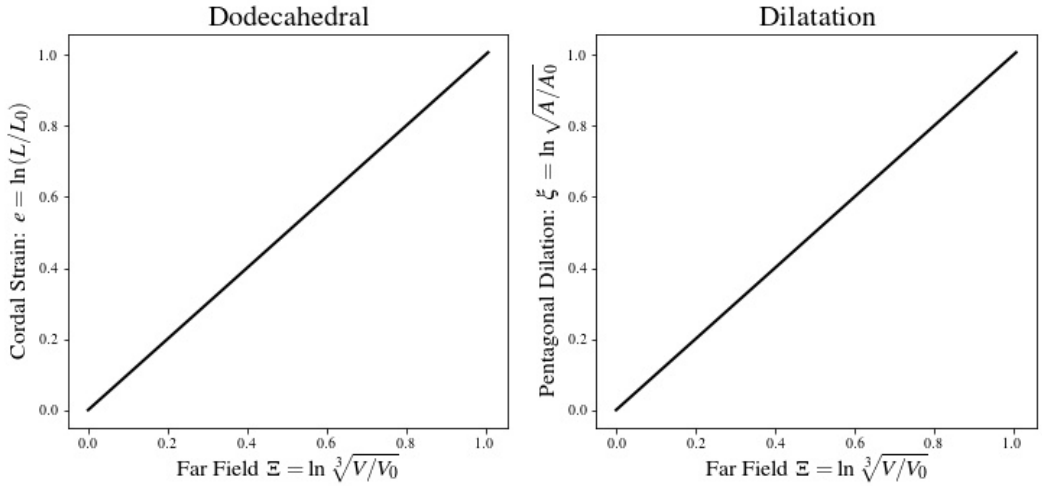

Figure 5.7: Response of a dodecahedron exposed to an isotropic motion of dilatation.

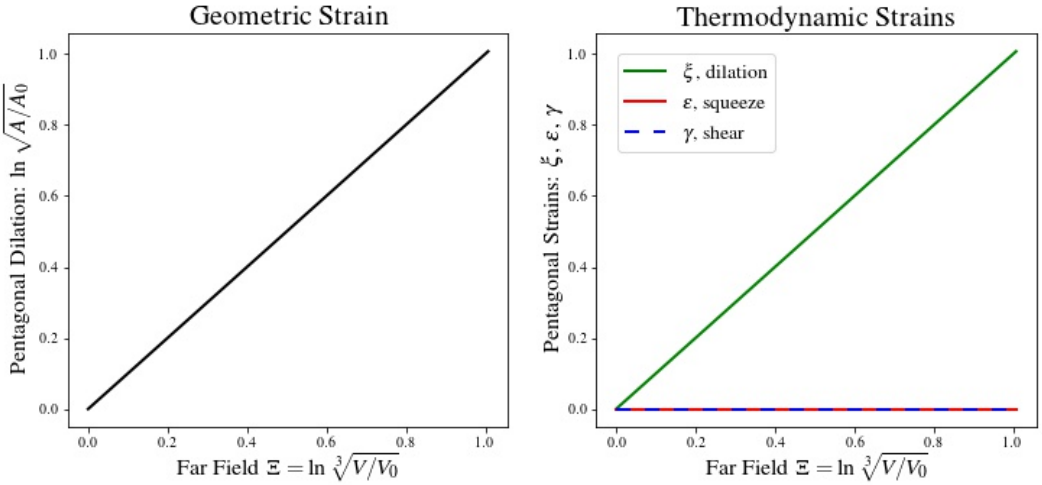

Figure 5.8: Response of a dodecahedron exposed to a far-field isotropic motion of dilatation.

5.2.5.2 Isochoric Motions

How the 30 chords and the 12 irregular pentagons deform under far-field motions of pure shear is displayed in Fig. 5.9. It demonstrates that the individual chordal and pentagonal constituents deform in a non-homogeneous manner, where the strains have been calculated as geometric changes in dodecahedral shape. This result agrees with *in vivo* observations made by Perlman & Bhattacharya [46] where confocal microscopy was used to image a breathing rat lung.

For the chords, there are six independent responses for dodecahedral motions of pure shear: two chords each for three of these lines, and eight chords each for the remaining three curves present in the left images of Fig. 5.9. For pentagons, there are three independent responses with four pentagons responding according to each curve shown in the right images. Although different chords and pentagons deform differently when sheared in different directions, their collective responses are the same regardless of the far-field direction being sheared. Consequently, the local geometric response of a dodecahedron is isotropic under the far-field motions of pure shear.

How the 30 chords and the 12 irregular pentagons deform under far-field motions of simple shear is displayed in Fig. 5.10. It demonstrates that the individual chordal and pentagonal constituents deform in a non-homogeneous manner during simple shears, like they do for pure shears. However, unlike pure shears whose collective chordal and pentagonal responses remain isotropic, here they diverge slightly from isotropy under motions of simple shear. Simple shears in the 12 and 23 planes have the same collective response; whereas, simple shear in the 13 plane has a slightly different response with respect to changes in the shearing direction.

The thermodynamic strains arising from a Gram–Schmidt factorization of the deformation gradient specify three strain measures pertinent to a membrane: dilation $\xi = \ln\sqrt{ab/a_0b_0}$, squeeze $\varepsilon = \ln\sqrt{ab_0/a_0b}$ and shear $\gamma = g - g_0$, where elongations a and b and magnitude of shear g are illustrated in Fig. 2.2.

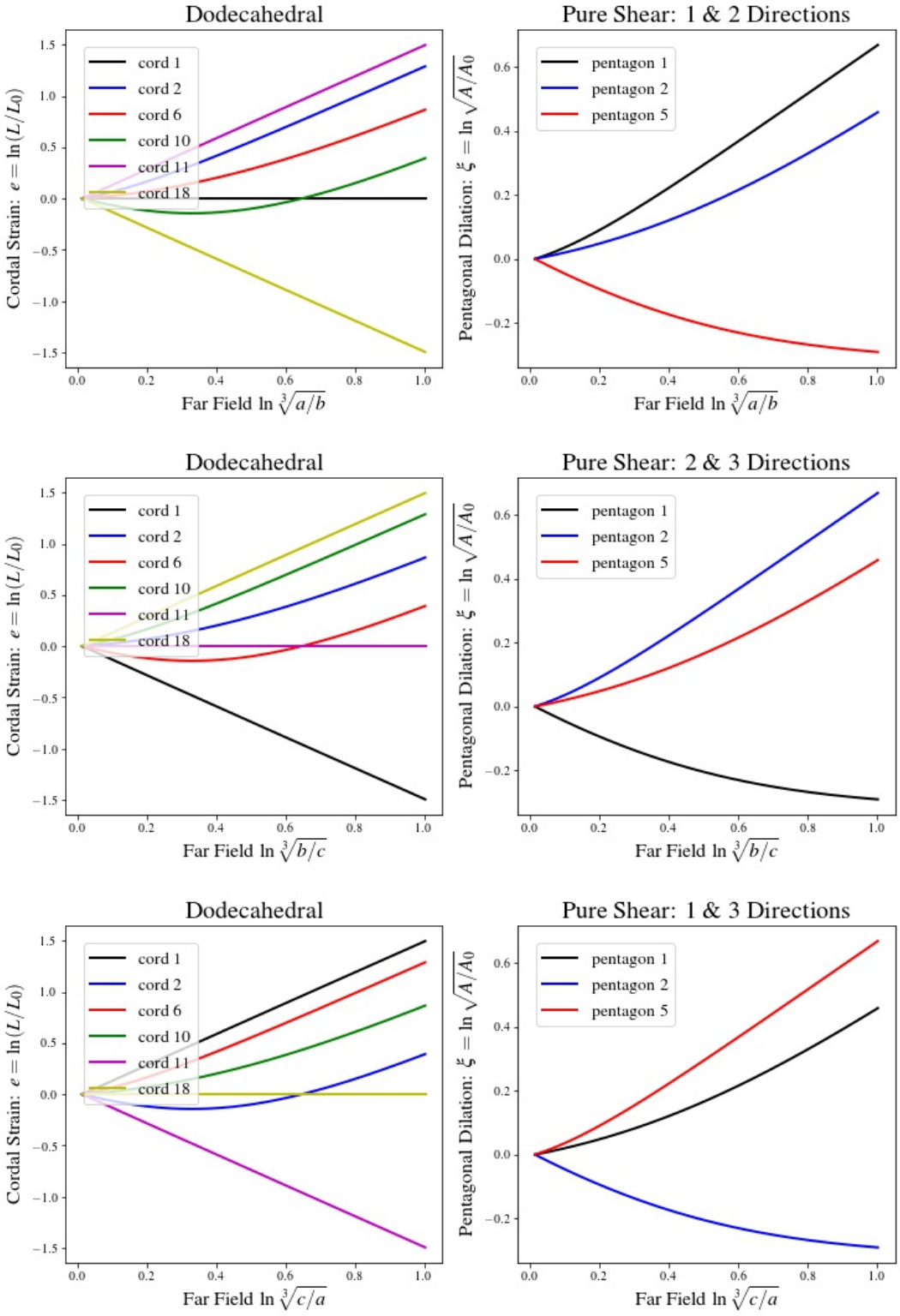

Figure 5.9: Response of a dodecahedron exposed to far-field pure-shear motions in the sense of Treloar [9]: $a = \ell$, $b = 1/\ell$ and $c = 1$ in the top images; $a = 1$, $b = \ell$ and $c = 1/\ell$ in the middle images; and $a = 1/\ell$, $b = 1$ and $c = \ell$ in the bottom images, with ℓ denoting an elongation of extrusion.

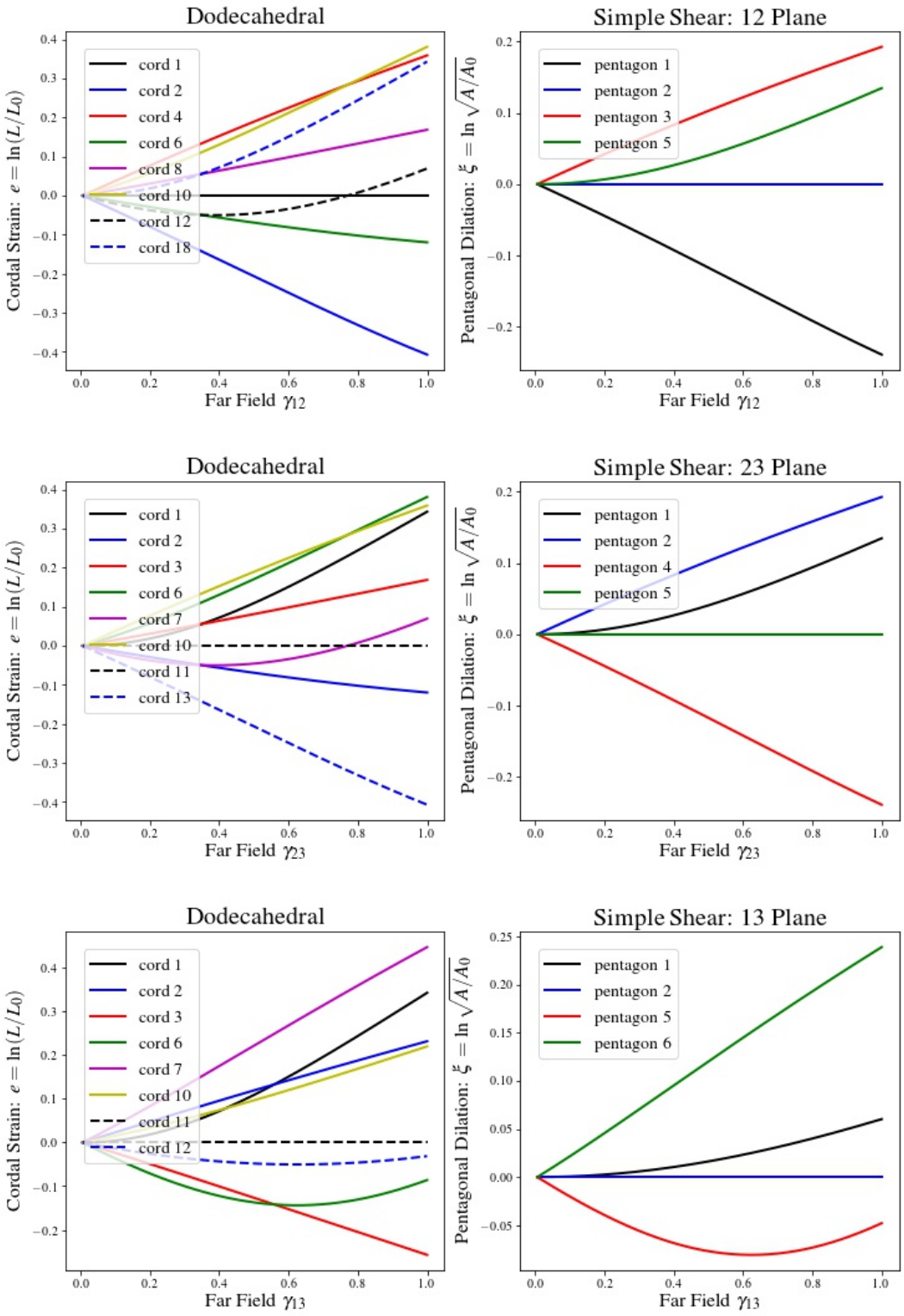

Figure 5.10: Response of a dodecahedron exposed to far-field simple-shear motions.

The curves in Figs. 5.9 & 5.10 were obtained from geometric measures for chordal strain $\ln(L/L_0)$ and areal dilation $\ln\sqrt{A/A_0}$. They were computed under separate far-field conditions of pure and simple shears. The curves in Figs. 5.11 & 5.12 were obtained from thermodynamic measures for membrane strain under the same far-field deformations.

Figures 5.9–5.12 allow us to conclude that if septal dilation were the only mode of planar deformation thought to cause a mechanical response, then knowledge of the geometric strain $\xi = \ln\sqrt{A/A_0}$ would be adequate; there would be no need to introduce a separate finite element discretization of the septal planes for acquiring their deformation gradients. However, if the non-uniform responses of squeeze ε and shear γ are thought to contribute to the overall mechanical response of these membranes, then the shape functions of Wachspress [42, 43] ought to be used for acquiring the deformation gradient within a septal plane.

5.3 Constitutive Theory

We recall from our kinematic study of a dodecahedron that the geometric strains (i.e., $e := \ln(L/L_0)$ for the elongation of septal chords, $\xi := \ln\sqrt{A/A_0}$ for the dilation of septal membranes, and $\Xi := \ln\sqrt[3]{V/V_0}$ for the dilatation of alveolar volume) are equivalent to one another under motions of uniform expansion/compression.

5.3.1 Green Thermoelastic Solids: Uniform Motions in 1D, 2D, and 3D

Combining the First and Second Laws of Thermodynamics governing uniform, reversible, adiabatic processes results in the following three formulæ, one per dimension; they are

$$\text{In 1D:} \qquad \mathrm{d}U = \theta\,\mathrm{d}\eta + \tfrac{1}{\rho_{1D}}\,F\,\mathrm{d}L/L \tag{5.26a}$$

$$\text{In 2D:} \qquad \mathrm{d}U = \theta\,\mathrm{d}\eta + \tfrac{1}{\rho_{2D}}\,T\,\mathrm{d}A/A \tag{5.26b}$$

$$\text{In 3D:} \qquad \mathrm{d}U = \theta\,\mathrm{d}\eta - \tfrac{1}{\rho_{3D}}\,P\,\mathrm{d}V/V \tag{5.26c}$$

wherein U is an internal energy density (erg/g = dyne.cm/g), which is a function of state, θ is a temperature in Kelvin ($273 + {}^\circ$C), η is an entropy density (erg/g.K), L is a length of

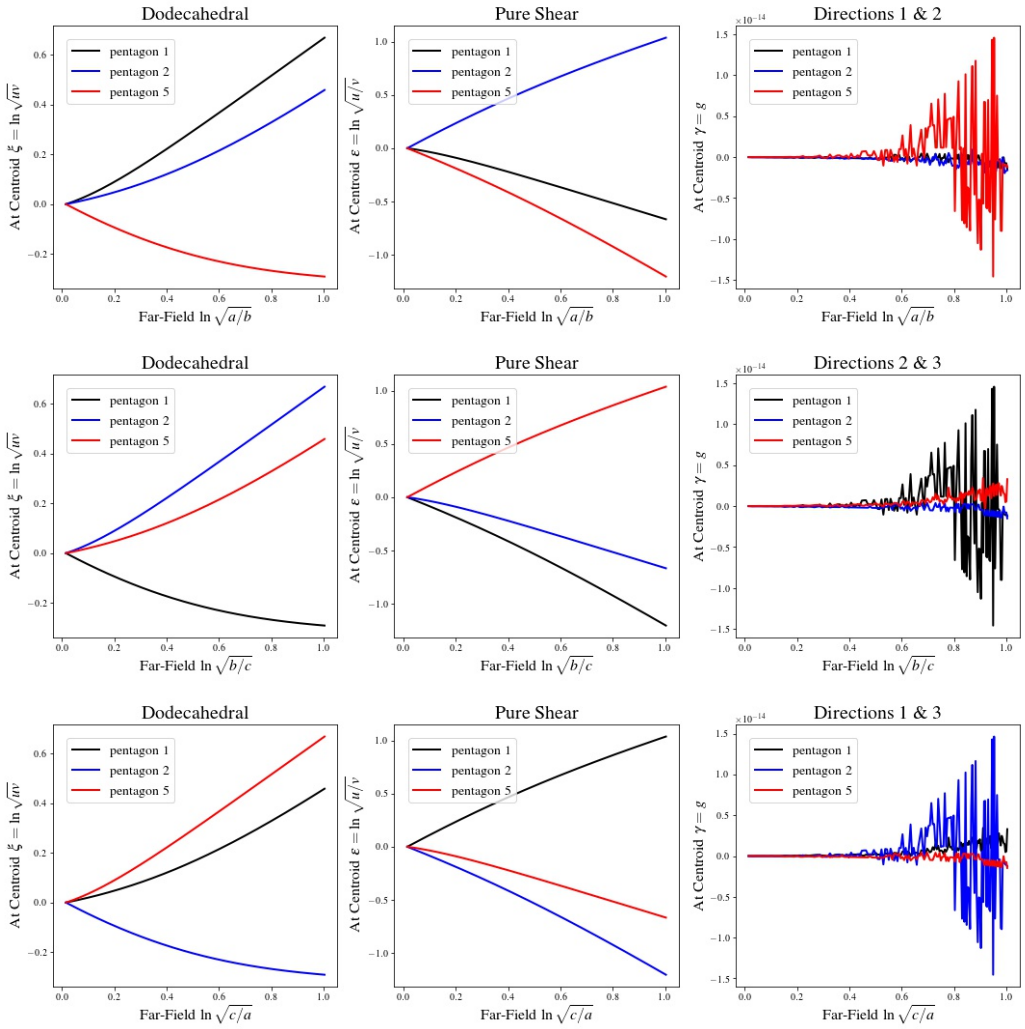

Figure 5.11: Same boundary conditions as in Fig. 5.9. Pentagonal areas were used to compute dilation in Fig. 5.9. The shape functions of Wachspress were used to compute dilation here. The uniform response in the right column of Fig. 5.9 and in the left column above are the same, providing additional assurance that the code has been correctly implemented. The squeeze response shown in the center column is the same for all three orientations of far-field pure shear, i.e., this response is isotropic.

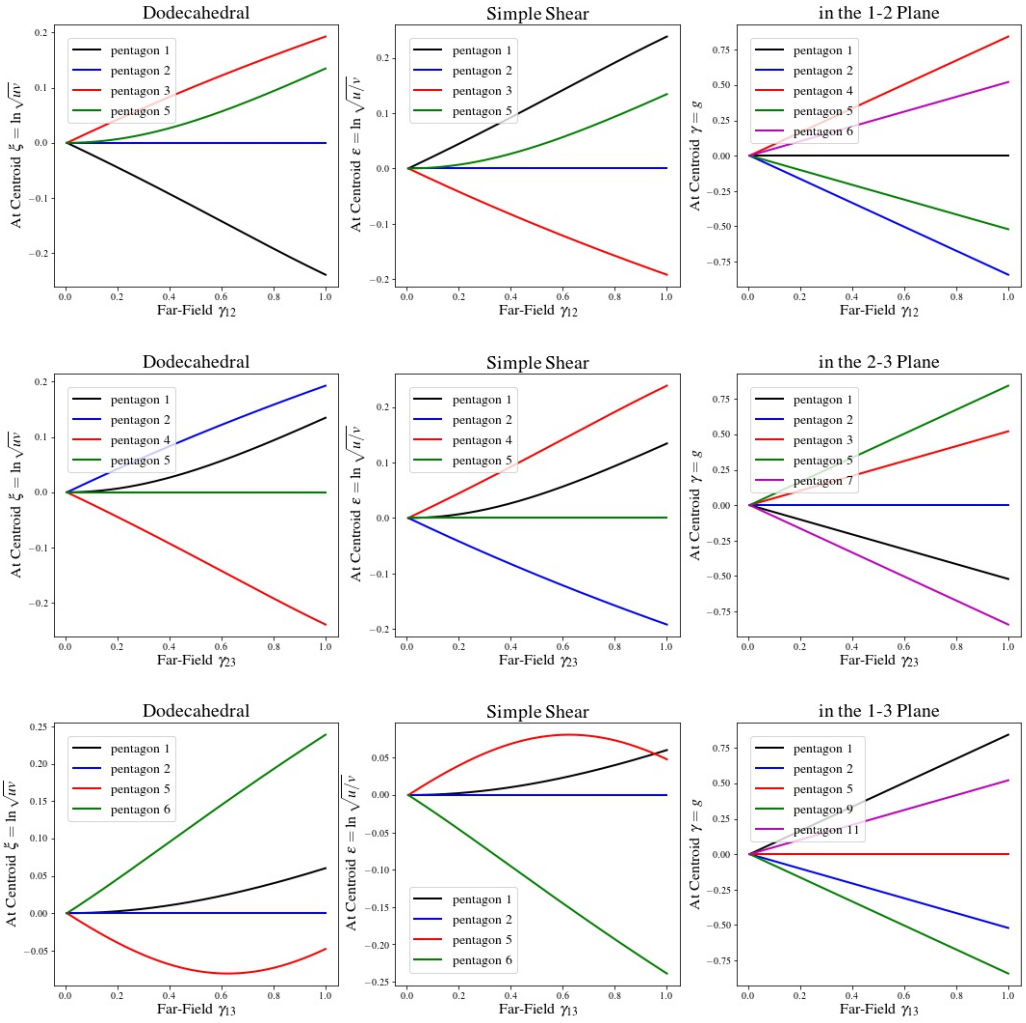

Figure 5.12: Same boundary conditions as in Fig. 5.10. Pentagonal areas were used to compute dilation in Fig. 5.10. The shape functions of Wachspress were used to compute dilation here. The uniform response in the right column of Fig. 5.10 and in the left column above are the same, providing additional assurance that the code has been correctly implemented.

line (cm), A is an area of surface (cm^2), V is a volume of space (cm^3), F is a force (dyne), T is a surface tension (dyne/cm), and P is a pressure ($dyne/cm^2$ = barye), whereas the mass densities ρ_{1D} (g/cm), ρ_{2D} (g/cm^2) and ρ_{3D} (g/cm^3) associate with a reference state of per unit length, or per unit area, or per unit volume, as appropriate.

5.3.1.1 Constitutive Equations

Because the internal energy density U is a state function, its differential rate of change describes a Pfaffian form [33] out of which the following constitutive formulæ are readily obtained

$$\text{In 1D:} \qquad \theta = \partial_\eta U(\eta, e) \qquad F = \rho_{1D}\, \partial_e U(\eta, e) \tag{5.27a}$$

$$\text{In 2D:} \qquad \theta = \partial_\eta U(\eta, \xi) \qquad \pi = \rho_{2D}\, \partial_\xi U(\eta, \xi) \tag{5.27b}$$

$$\text{In 3D:} \qquad \theta = \partial_\eta U(\eta, \Xi) \qquad \Pi = \rho_{3D}\, \partial_\Xi U(\eta, \Xi) \tag{5.27c}$$

where strains are logarithms of dimension-appropriate stretches. As a matter of convenience, we adopt the notation $\partial_\eta U := \partial U/\partial\eta$, etc. Here, $\pi := 2T$ and $\Pi := -3P$ are the measures for surface tension and pressure that we use in this work. We find it useful to use this negative measure for pressure because the transpulmonary pressure in lung, under normal physiologic conditions, is typically negative; hence, Π would be positive in its specification of transpulmonary pressure.

We consider response variables for temperature and force/surface-tension/pressure to be C^1 functions of state; therefore, the internal energy U is a C^2 function of state in a Green thermoelastic solid undergoing uniform adiabatic motions (cf. Weinhold [47] and Gilmore [48]). Under these conditions of smoothness, one can differentiate Eqn. (5.27), thereby producing the following collection of coupled, partial, differential equations with exchanging

cause and effect between entropy and temperature In 1D:

$$\begin{Bmatrix} \mathrm{d}\eta \\ \mathrm{d}F \end{Bmatrix} = \begin{bmatrix} \theta/\partial_{\eta\eta}U & -\partial_{\eta e}U/\partial_{\eta\eta}U \\ \rho_{1D}\theta\,\partial_{e\eta}U/\partial_{\eta\eta}U & \rho_{1D}(\partial_{ee}U - \partial_{e\eta}U\cdot\partial_{\eta e}U/\partial_{\eta\eta}U) \end{bmatrix} \begin{Bmatrix} \theta^{-1}\,\mathrm{d}\theta \\ \mathrm{d}e \end{Bmatrix} \tag{5.28a}$$

In 2D:

$$\begin{Bmatrix} \mathrm{d}\eta \\ \mathrm{d}\pi \end{Bmatrix} = \begin{bmatrix} \theta/\partial_{\eta\eta}U & -\partial_{\eta\xi}U/\partial_{\eta\eta}U \\ \rho_{2D}\theta\,\partial_{\xi\eta}U/\partial_{\eta\eta}U & \rho_{2D}(\partial_{\xi\xi}U - \partial_{\xi\eta}U\cdot\partial_{\eta\xi}U/\partial_{\eta\eta}U) \end{bmatrix} \begin{Bmatrix} \theta^{-1}\,\mathrm{d}\theta \\ \mathrm{d}\xi \end{Bmatrix} \tag{5.28b}$$

In 3D:

$$\begin{Bmatrix} \mathrm{d}\eta \\ \mathrm{d}\Pi \end{Bmatrix} = \begin{bmatrix} \theta/\partial_{\eta\eta}U & -\partial_{\eta\Xi}U/\partial_{\eta\eta}U \\ \rho_{3D}\theta\,\partial_{\Xi\eta}U/\partial_{\eta\eta}U & \rho_{3D}(\partial_{\Xi\Xi}U - \partial_{\Xi\eta}U\cdot\partial_{\eta\Xi}U/\partial_{\eta\eta}U) \end{bmatrix} \begin{Bmatrix} \theta^{-1}\,\mathrm{d}\theta \\ \mathrm{d}\Xi \end{Bmatrix} \tag{5.28c}$$

where we recall that $\mathrm{d}e = L^{-1}\,\mathrm{d}L$, $\mathrm{d}\xi = \frac{1}{2}A^{-1}\,\mathrm{d}A$ and $\mathrm{d}\Xi = \frac{1}{3}V^{-1}\,\mathrm{d}V$.

5.3.1.2 Material Response Functions

Experiments are typically done to quantify the following material properties, defined here as tangents to response curves, and selected per a material's physical dimension.

In 1D:

$$C_F := \left.\frac{\mathrm{d}\eta}{\theta^{-1}\,\mathrm{d}\theta}\right|_{\mathrm{d}F=0} \qquad \alpha_F := \left.\frac{L^{-1}\,\mathrm{d}L}{\theta^{-1}\,\mathrm{d}\theta}\right|_{\mathrm{d}F=0} \qquad E_\theta := \left.\frac{\mathrm{d}F}{L^{-1}\,\mathrm{d}L}\right|_{\mathrm{d}\theta=0} \tag{5.29a}$$

In 2D:

$$C_T := \left.\frac{\mathrm{d}\eta}{\theta^{-1}\,\mathrm{d}\theta}\right|_{\mathrm{d}T=0} \qquad \alpha_T := \left.\frac{A^{-1}\,\mathrm{d}A}{\theta^{-1}\,\mathrm{d}\theta}\right|_{\mathrm{d}T=0} = 2\alpha_F \qquad M_\theta := \left.\frac{\mathrm{d}T}{A^{-1}\,\mathrm{d}A}\right|_{\mathrm{d}\theta=0} \tag{5.29b}$$

In 3D:

$$C_P := \left.\frac{\mathrm{d}\eta}{\theta^{-1}\,\mathrm{d}\theta}\right|_{\mathrm{d}P=0} \qquad \alpha_P := \left.\frac{V^{-1}\,\mathrm{d}V}{\theta^{-1}\,\mathrm{d}\theta}\right|_{\mathrm{d}P=0} = 3\alpha_F \qquad K_\theta := \left.\frac{-\mathrm{d}P}{V^{-1}\,\mathrm{d}V}\right|_{\mathrm{d}\theta=0} \tag{5.29c}$$

whose analogs as secant functions are defined in Appendix D.

The various thermal strain coefficients α_F, α_T, α_P are, however, distinct from one another. Even though each is dimensionless, each is defined with respect to its own physical dimension. Nevertheless, because $\ln(L/L_0) = \frac{1}{2}\ln(A/A_0) = \frac{1}{3}\ln(V/V_0)$, it follows that $\alpha_T = 2\alpha_F$ and $\alpha_P = 3\alpha_F$, so there is really just one thermal strain coefficient, i.e., α_F, that, hereafter, is denoted as α_t where the subscript 't' denotes *tangent*.

The various specific heats C_F, C_T, C_P (erg/g.K) are distinct, yet essentially, they are equivalent as each is defined per unit mass, insensitive to dimension. They are evaluated at a fixed thermodynamic force, which does depend upon dimension. Hereafter, we will denote the tangent response to specific heat as C_t that, in Appendix D, is shown to relate to the secant version of specific heat C_s via

$$\text{1D:} \qquad C_t = C_s - \alpha_s \frac{F - F_0}{\rho_{1D}\theta} \tag{5.30a}$$

$$\text{2D:} \qquad C_t = C_s - \alpha_s \frac{\pi - \pi_0}{\rho_{2D}\theta} \tag{5.30b}$$

$$\text{3D:} \qquad C_t = C_s - \alpha_s \frac{\Pi - \Pi_0}{\rho_{3D}\theta} \tag{5.30c}$$

where C_s is the density of specific heat at constant pressure that one typically finds tabulated in the literature. Usually, the secant and tangent versions for the thermal strain coefficient are equivalent, i.e., $\alpha_s \equiv \alpha_t$. Here F_0, π_0 and Π_0 are the force, surface tension, and pressure associated with some specified reference state.

The various tangent moduli E_θ, M_θ and K_θ are also distinct. They have different dimensions. Material property E_θ is a modulus of extension (dyne); material property M_θ is a modulus of dilation (dyne/cm); and material property K_θ is a modulus of dilatation (dyne/cm^2), a.k.a. the bulk modulus, with each modulus being measured at a fixed temperature. The above material properties are gradients. They constitute tangents to their associated physical response curves, and as such, are denoted hereafter as E_t, M_t and K_t. Consequently, they need not be of constant value throughout state space, like a Hookean

material would suppose them to be. In other words, the secant and tangent moduli need not be the same at any given state.

In terms of the material properties, Eqn. (5.29), of which there are three per dimension, the internal energy density has three curvatures that associate with it. For 1D materials:

$$\partial_{\eta\eta}U = \frac{\rho_{1D}\theta^2}{\rho_{1D}C_t\theta - \alpha_t^2 E_t}, \quad \partial_{ee}U = \frac{C_t E_t \theta}{\rho_{1D}C_t\theta - \alpha_t^2 E_t}, \quad \partial_{\eta e}U \equiv \partial_{e\eta}U = \frac{-\alpha_t E_t \theta}{\rho_{1D}C_t\theta - \alpha_t^2 E_t} \tag{5.31a}$$

For 2D materials:

$$\partial_{\eta\eta}U = \frac{\rho_{2D}\theta^2}{\rho_{2D}C_t\theta - 4\alpha_t^2 M_t}, \quad \partial_{\xi\xi}U = \frac{4C_t M_t \theta}{\rho_{2D}C_t\theta - 4\alpha_t^2 M_t}, \quad \partial_{\eta\xi}U \equiv \partial_{\xi\eta}U = \frac{-4\alpha_t M_t \theta}{\rho_{2D}C_t\theta - 4\alpha_t^2 M_t} \tag{5.31b}$$

For 3D materials (cf. Weinhold [47] and Gilmore [48]):

$$\partial_{\eta\eta}U = \frac{\rho_{3D}\theta^2}{\rho_{3D}C_t\theta - 9\alpha_t^2 K_t}, \quad \partial_{\Xi\Xi}U = \frac{9C_t K_t \theta}{\rho_{3D}C_t\theta - 9\alpha_t^2 K_t}, \quad \partial_{\eta\Xi}U \equiv \partial_{\Xi\eta}U = \frac{-9\alpha_t K_t \theta}{\rho_{3D}C_t\theta - 9\alpha_t^2 K_t} \tag{5.31c}$$

These materials constants are constrained by thermodynamics in that

$$0 < E_t < \frac{\rho_{1D}C_t\theta}{\alpha_t^2}, \quad 0 < M_t < \frac{\rho_{2D}C_t\theta}{4\alpha_t^2}, \quad 0 < K_t < \frac{\rho_{3D}C_t\theta}{9\alpha_t^2} \tag{5.32}$$

which ensure that their respective thermodynamic Jacobians cannot become singular.

5.3.1.3 Thermoelastic Models for Modeling Alveoli: Uniform Motions

We now write down our constitutive formulæ for quantifying uniform responses in thermoelastic solids of 1, 2 and 3 dimensions. They are thermoelastic constitutive equations (5.28) with Helmholtz variables expressed in terms of the material properties defined in Eqn. (5.29)

assigned to the internal energy density U according to Eqn. (5.31), with outcomes of:

$$\text{For 1D:} \qquad \begin{Bmatrix} \mathrm{d}\eta \\ \mathrm{d}F \end{Bmatrix} = \begin{bmatrix} C_t - \alpha_t^2 E_t/\rho\theta & \alpha_t E_t/\rho\theta \\ -\alpha_t E_t & E_t \end{bmatrix} \begin{Bmatrix} \theta^{-1}\,\mathrm{d}\theta \\ \mathrm{d}e \end{Bmatrix} \tag{5.33a}$$

$$\text{For 2D:} \qquad \begin{Bmatrix} \mathrm{d}\eta \\ \mathrm{d}\pi \end{Bmatrix} = \begin{bmatrix} C_t - 4\alpha_t^2 M_t/\rho\theta & 4\alpha_t M_t/\rho\theta \\ -4\alpha_t M_t & 4M_t \end{bmatrix} \begin{Bmatrix} \theta^{-1}\,\mathrm{d}\theta \\ \mathrm{d}\xi \end{Bmatrix} \tag{5.33b}$$

$$\text{For 3D:} \qquad \begin{Bmatrix} \mathrm{d}\eta \\ \mathrm{d}\Pi \end{Bmatrix} = \begin{bmatrix} C_t - 9\alpha_t^2 K_t/\rho\theta & 9\alpha_t K_t/\rho\theta \\ -9\alpha_t K_t & 9K_t \end{bmatrix} \begin{Bmatrix} \theta^{-1}\,\mathrm{d}\theta \\ \mathrm{d}\Xi \end{Bmatrix} \tag{5.33c}$$

We simplify our expressions by suppressing the dimension for which mass density applies.

Equation (5.33) has cause and effect variables that are appropriate for our multiscale application. In this process, a localization procedure pulls the temperature and deformation gradient taken from the parenchyma scale down to the level of an alveolar scale. Differential strain rates $\mathrm{d}\boldsymbol{\mathcal{U}} \cdot \boldsymbol{\mathcal{U}}^{-1}$ are then constructed through appropriate finite difference formulæ, where $\boldsymbol{\mathcal{U}}$ denotes the Laplace stretch. These continuum rates are then mapped into our local thermodynamic rates, with alveolar entropy and stress following from a numerical integration of the above constitutive equations. These constitutive equations apply to the various facets of our dodecahedral model for an alveolar sac through a finite element discretization.

5.3.2 Green Thermoelastic Membranes: Non-Uniform Motions

The First and Second Laws of Thermodynamics governing a reversible adiabatic process are described by the formula $\mathrm{d}U = \theta\,\mathrm{d}\eta + \frac{1}{\rho}\,\mathrm{d}W$, where $\mathrm{d}W$ is the mechanical power expended by stressing a material element of mass density ρ. For the case of a 2D planar membrane, a mass density of $\rho \Leftarrow \rho_{2D}$ applies, with its change in mechanical work being expressed as

$$\mathrm{d}W = \mathrm{tr}\left(\begin{bmatrix} \mathcal{S}_{11} & \mathcal{S}_{12} \\ \mathcal{S}_{21} & \mathcal{S}_{22} \end{bmatrix} \begin{bmatrix} a^{-1}\,\mathrm{d}a & (a/b)\,\mathrm{d}g \\ 0 & b^{-1}\,\mathrm{d}b \end{bmatrix} \right) = \pi\,\mathrm{d}\xi + \sigma\,\mathrm{d}\varepsilon + \tau\,\mathrm{d}\gamma \tag{5.34a}$$

wherein $\mathcal{S}_{ij}$ are the components of a surface tension in the co-ordinate frame of a membrane. Equation (5.34a) conjectures that the First and Second Laws of Thermodynamics can be expressed as a differential equation known as a Pfaffian form that, in this case, looks like

$$\mathrm{d}U = \theta\,\mathrm{d}\eta + \tfrac{1}{\rho}\big(\pi\,\mathrm{d}\xi + \sigma\,\mathrm{d}\varepsilon + \tau\,\mathrm{d}\gamma\big) \tag{5.34b}$$

Conjugate pair (ξ, π) describes a dilation $2\,\mathrm{d}\xi \Leftarrow A^{-1}\,\mathrm{d}A$ caused by a surface tension $\pi \Leftarrow 2T$. Pair (ε, σ) describes a squeeze ε (or pure shear) caused by a normal-stress difference. And pair (γ, τ) describes an in-plane shear γ caused by a shear stress τ.

5.3.2.1 General Constitutive Equations

Because a change in the internal energy $\mathrm{d}U$ governing a reversible adiabatic process is described by an exact differential [33], with $U(\eta, \xi, \varepsilon, \gamma)$ in the case of a planar membrane, it follows that a constitutive response for a Green thermoelastic membrane is described by

$$\theta = \partial_\eta U(\eta,\xi,\varepsilon,\gamma) \quad \pi = \rho\,\partial_\xi U(\eta,\xi,\varepsilon,\gamma) \quad \sigma = \rho\,\partial_\varepsilon U(\eta,\xi,\varepsilon,\gamma) \quad \tau = \rho\,\partial_\gamma U(\eta,\xi,\varepsilon,\gamma) \tag{5.35}$$

The constitutive expressions can be recast into the following system of differential equations

$$\begin{Bmatrix} \mathrm{d}\theta \\ \mathrm{d}\pi \\ \mathrm{d}\sigma \\ \mathrm{d}\tau \end{Bmatrix} = \begin{bmatrix} \partial_{\eta\eta}U & \partial_{\eta\xi}U & \partial_{\eta\varepsilon}U & \partial_{\eta\gamma}U \\ \rho\,\partial_{\xi\eta}U & \rho\,\partial_{\xi\xi}U & \rho\,\partial_{\xi\varepsilon}U & \rho\,\partial_{\xi\gamma}U \\ \rho\,\partial_{\varepsilon\eta}U & \rho\,\partial_{\varepsilon\xi}U & \rho\,\partial_{\varepsilon\varepsilon}U & \rho\,\partial_{\varepsilon\gamma}U \\ \rho\,\partial_{\gamma\eta}U & \rho\,\partial_{\gamma\xi}U & \rho\,\partial_{\gamma\varepsilon}U & \rho\,\partial_{\gamma\gamma}U \end{bmatrix} \begin{Bmatrix} \mathrm{d}\eta \\ \mathrm{d}\xi \\ \mathrm{d}\varepsilon \\ \mathrm{d}\gamma \end{Bmatrix} \tag{5.36}$$

The above 4×4 matrix describes the full non-uniform response permissible by a Green thermoelastic membrane undergoing an adiabatic process. For our application, it is reasonable to assume that the presence of a non-uniform planar motion will not cause an uniform planar response. As such, $\partial_{\eta\varepsilon}U = \partial_{\eta\gamma}U = \partial_{\xi\varepsilon}U = \partial_{\xi\gamma}U = 0$. It is also considered that the pure and simple shear responses act independently, too, so that $\partial_{\gamma\varepsilon}U = \partial_{\varepsilon\gamma}U = 0$.

Converting the above internal energy formulation into its Helmholtz equivalent produces

$$\begin{Bmatrix} \mathrm{d}\eta \\ \mathrm{d}\pi \end{Bmatrix} = \begin{bmatrix} \theta/\partial_{\eta\eta}U & -\partial_{\eta\xi}U/\partial_{\eta\eta}U \\ \rho\theta\,\partial_{\xi\eta}U/\partial_{\eta\eta}U & \rho\big(\partial_{\xi\xi}U - \partial_{\xi\eta}U\cdot\partial_{\eta\xi}U/\partial_{\eta\eta}U\big) \end{bmatrix} \begin{Bmatrix} \theta^{-1}\,\mathrm{d}\theta \\ \mathrm{d}\xi \end{Bmatrix} \tag{5.37a}$$

where both $\theta^{-1}\,\mathrm{d}\theta$ and $\mathrm{d}\xi = \frac{1}{2}A^{-1}\,\mathrm{d}A$ are logarithmic rates, and

$$\begin{Bmatrix} \mathrm{d}\sigma \\ \mathrm{d}\tau \end{Bmatrix} = \rho \begin{bmatrix} \partial_{\varepsilon\varepsilon}U & 0 \\ 0 & \partial_{\gamma\gamma}U \end{bmatrix} \begin{Bmatrix} \mathrm{d}\varepsilon \\ \mathrm{d}\gamma \end{Bmatrix} \tag{5.37b}$$

where $\mathrm{d}\varepsilon = \Gamma^{-1}\,\mathrm{d}\Gamma$ is logarithmic in structure, while $\mathrm{d}\gamma = \mathrm{d}g$ is linear in deformation field.

5.3.2.2 Constitutive Equations Governing a Thermoelastic Membrane

It is the Gibbs free-energy potential (viz., $\mathcal{G}(\theta,\pi,\sigma,\tau) = U - \theta\eta - \pi\xi - \sigma\varepsilon - \tau\gamma$, which exchanges cause and effect with that of the internal energy $U(\eta,\xi,\varepsilon,\gamma)$), that is most easily expressed in terms of our material properties. The upper-left 2×2 sub-matrix, which describes the uniform response, can be rearranged to read as

$$\begin{Bmatrix} \mathrm{d}\eta \\ \mathrm{d}\pi \end{Bmatrix} = \begin{bmatrix} C_t - 4\alpha_t^2 M/\rho\theta & 4\alpha_t M/\rho\theta \\ -4\alpha_t M & 4M \end{bmatrix} \begin{Bmatrix} \theta^{-1}\,\mathrm{d}\theta \\ \mathrm{d}\xi \end{Bmatrix} \tag{5.38a}$$

where $M = M_t(\theta,\xi,\pi)$, while the non-uniform or shear response is given quite simply by

$$\begin{Bmatrix} \mathrm{d}\sigma \\ \mathrm{d}\tau \end{Bmatrix} = \begin{bmatrix} 2N & 0 \\ 0 & G \end{bmatrix} \begin{Bmatrix} \mathrm{d}\varepsilon \\ \mathrm{d}\gamma \end{Bmatrix} \tag{5.38b}$$

where $N = N_t(\varepsilon,\sigma)$ and $G = G_t(\gamma,\tau)$. Collectively, moduli M_t, N_t, and G_t describe the tangent mechanical response of a thermoelastic membrane.

5.3.3 Green Thermoelastic Solids: Non-Uniform Motions

The First and Second Laws of Thermodynamics governing a reversible adiabatic process done on a 3D body result in the formula $\mathrm{d}U = \theta\,\mathrm{d}\eta + \frac{1}{\rho}\,\mathrm{d}W$, where $\mathrm{d}W$ is the mechanical power expended by stressing a body with a mass density of ρ; specifically, [28, 5, 6, 49]

$$\begin{aligned}\mathrm{d}W &= \mathrm{tr}\left(\begin{bmatrix}\mathcal{S}_{11} & \mathcal{S}_{12} & \mathcal{S}_{13}\\ \mathcal{S}_{21} & \mathcal{S}_{22} & \mathcal{S}_{23}\\ \mathcal{S}_{31} & \mathcal{S}_{32} & \mathcal{S}_{33}\end{bmatrix}\begin{bmatrix}a^{-1}\,\mathrm{d}a & (a/b)\,\mathrm{d}\gamma & (a/c)(\mathrm{d}\beta-\alpha\,\mathrm{d}\gamma)\\ 0 & b^{-1}\,\mathrm{d}b & (b/c)\,\mathrm{d}\alpha\\ 0 & 0 & c^{-1}\,\mathrm{d}c\end{bmatrix}\right)\\ &= \Pi\,\mathrm{d}\Xi + \sum_{i=1}^{3}(\sigma_i\,\mathrm{d}\varepsilon_i + \tau_i\,\mathrm{d}\gamma_i)\end{aligned} \tag{5.39a}$$

which is subject to constraints $\sigma_3 = -(\sigma_1+\sigma_2)$ and $\mathrm{d}\varepsilon_3 = -(\mathrm{d}\varepsilon_1+\mathrm{d}\varepsilon_2)$.

The above expression conjectures that the thermodynamics of a 3D elastic solid contained within the confines of an adiabatic enclosure can be described by the Pfaffian equation

$$\mathrm{d}U = \theta\,\mathrm{d}\eta + \frac{1}{\rho}\left(\Pi\,\mathrm{d}\Xi + \sum_{i=1}^{2}\sigma_i\,\mathrm{d}\varepsilon_i + (\sigma_1+\sigma_2)(\mathrm{d}\varepsilon_1+\mathrm{d}\varepsilon_2) + \sum_{i=1}^{3}\tau_i\,\mathrm{d}\gamma_i\right). \tag{5.39b}$$

5.3.3.1 Constitutive Equations

Because a change in the internal energy $\mathrm{d}U$ governing a reversible adiabatic process is described by an exact differential [33], with $U(\eta,\Xi,\varepsilon_1,\varepsilon_2,\gamma_1,\gamma_2,\gamma_3)$ in three space, it necessarily follows that a constitutive response for a Green thermoelastic solid is governed by two constitutive equations for temperature and pressure [32]

$$\theta = \partial_\eta U(\eta,\Xi,\varepsilon_1,\varepsilon_2,\gamma_1,\gamma_2,\gamma_3), \quad \Pi = \rho\,\partial_\Xi U(\eta,\Xi,\varepsilon_1,\varepsilon_2,\gamma_1,\gamma_2,\gamma_3) \tag{5.40a}$$

two constitutive equations for the normal-stress differences

$$\begin{Bmatrix} \sigma_1 \\ \sigma_2 \end{Bmatrix} = \frac{1}{3} \begin{bmatrix} 2 & -1 \\ -1 & 2 \end{bmatrix} \begin{Bmatrix} \rho\, \partial_{\varepsilon_1} U(\eta, \Xi, \varepsilon_1, \varepsilon_2, \gamma_1, \gamma_2, \gamma_3) \\ \rho\, \partial_{\varepsilon_2} U(\eta, \Xi, \varepsilon_1, \varepsilon_2, \gamma_1, \gamma_2, \gamma_3) \end{Bmatrix} \tag{5.40b}$$

and three constitutive equations for the shear stresses

$$\begin{aligned} \tau_1 &= \rho\, \partial_{\gamma_1} U(\eta, \Xi, \varepsilon_1, \varepsilon_2, \gamma_1, \gamma_2, \gamma_3), \quad \tau_2 = \rho\, \partial_{\gamma_2} U(\eta, \Xi, \varepsilon_1, \varepsilon_2, \gamma_1, \gamma_2, \gamma_3) \\ \tau_3 &= \rho\, \partial_{\gamma_3} U(\eta, \Xi, \varepsilon_1, \varepsilon_2, \gamma_1, \gamma_2, \gamma_3) \end{aligned} \tag{5.40c}$$

Considering each, independent, intensive variable, to be a C^1 function of each, independent, extensive variable, then the internal energy U will be at least a C^2 function of state, and therefore the constitutive expressions can be recast into the following system of equations

$$\begin{Bmatrix} \mathrm{d}\theta \\ \mathrm{d}\Pi \\ \mathrm{d}\sigma_1 \\ \mathrm{d}\sigma_2 \\ \mathrm{d}\tau_1 \\ \mathrm{d}\tau_2 \\ \mathrm{d}\tau_3 \end{Bmatrix} = \begin{bmatrix} \partial_{\eta\eta} U & \partial_{\eta\Xi} U & \partial_{\eta\varepsilon_1} U & \partial_{\eta\varepsilon_2} U & \partial_{\eta\gamma_1} U & \partial_{\eta\gamma_2} U & \partial_{\eta\gamma_3} U \\ \rho\, \partial_{\Xi\eta} U & \rho\, \partial_{\Xi\Xi} U & \rho\, \partial_{\Xi\varepsilon 1} U & \rho\, \partial_{\Xi\varepsilon 2} U & \rho\, \partial_{\Xi\gamma_1} U & \rho\, \partial_{\Xi\gamma_2} U & \rho\, \partial_{\Xi\gamma_3} U \\ \rho\, M_{1\eta} & \rho\, M_{1\Xi} & \rho\, M_{1\varepsilon_1} & \rho\, M_{1\varepsilon_2} & \rho\, M_{1\gamma_1} & \rho\, M_{1\gamma_2} & \rho\, M_{1\gamma_3} \\ \rho\, M_{2\eta} & \rho\, M_{2\Xi} & \rho\, M_{2\varepsilon_1} & \rho\, M_{2\varepsilon_2} & \rho\, M_{2\gamma_1} & \rho\, M_{2\gamma_2} & \rho\, M_{2\gamma_3} \\ \rho\, \partial_{\gamma_1\eta} U & \rho\, \partial_{\gamma_1\Xi} U & \rho\, \partial_{\gamma_1\varepsilon_1} U & \rho\, \partial_{\gamma_1\varepsilon_2} U & \rho\, \partial_{\gamma_1\gamma_1} U & \rho\, \partial_{\gamma_1\gamma_2} U & \rho\, \partial_{\gamma_1\gamma_3} U \\ \rho\, \partial_{\gamma_2\eta} U & \rho\, \partial_{\gamma_2\Xi} U & \rho\, \partial_{\gamma_2\varepsilon_1} U & \rho\, \partial_{\gamma_2\varepsilon_2} U & \rho\, \partial_{\gamma_2\gamma_1} U & \rho\, \partial_{\gamma_2\gamma_2} U & \rho\, \partial_{\gamma_2\gamma_3} U \\ \rho\, \partial_{\gamma_3\eta} U & \rho\, \partial_{\gamma_3\Xi} U & \rho\, \partial_{\gamma_3\varepsilon_1} U & \rho\, \partial_{\gamma_3\varepsilon_2} U & \rho\, \partial_{\gamma_3\gamma_1} U & \rho\, \partial_{\gamma_3\gamma_2} U & \rho\, \partial_{\gamma_3\gamma_3} U \end{bmatrix} \begin{Bmatrix} \mathrm{d}\eta \\ \mathrm{d}\Xi \\ \mathrm{d}\varepsilon_1 \\ \mathrm{d}\varepsilon_2 \\ \mathrm{d}\gamma_1 \\ \mathrm{d}\gamma_2 \\ \mathrm{d}\gamma_3 \end{Bmatrix} \tag{5.41}$$

The squeeze response associates with tangent moduli that are defined accordingly

$$M_{1\eta} = \tfrac{1}{3}\big(2\partial_{\varepsilon_1\eta} U - \partial_{\varepsilon_2\eta} U\big) \qquad M_{2\eta} = \tfrac{1}{3}\big(2\partial_{\varepsilon_2\eta} U - \partial_{\varepsilon_1\eta} U\big) \tag{5.42a}$$

$$M_{1\Xi} = \tfrac{1}{3}\big(2\partial_{\varepsilon_1\Xi} U - \partial_{\varepsilon_2\Xi} U\big) \qquad M_{2\Xi} = \tfrac{1}{3}\big(2\partial_{\varepsilon_2\Xi} U - \partial_{\varepsilon_1\Xi} U\big) \tag{5.42b}$$

$$M_{1\varepsilon_1} = \tfrac{1}{3}\big(2\partial_{\varepsilon_1\varepsilon_1} U - \partial_{\varepsilon_2\varepsilon_1} U\big) \qquad M_{2\varepsilon_1} = \tfrac{1}{3}\big(2\partial_{\varepsilon_2\varepsilon_1} U - \partial_{\varepsilon_1\varepsilon_1} U\big) \tag{5.42c}$$

$$M_{1\varepsilon_2} = \tfrac{1}{3}\big(2\partial_{\varepsilon_1\varepsilon_2} U - \partial_{\varepsilon_2\varepsilon_2} U\big) \qquad M_{2\varepsilon_2} = \tfrac{1}{3}\big(2\partial_{\varepsilon_2\varepsilon_2} U - \partial_{\varepsilon_1\varepsilon_2} U\big) \tag{5.42d}$$

$$M_{1\gamma_1} = \tfrac{1}{3}\big(2\partial_{\varepsilon_1\gamma_1} U - \partial_{\varepsilon_2\gamma_1} U\big) \qquad M_{2\gamma_1} = \tfrac{1}{3}\big(2\partial_{\varepsilon_2\gamma_1} U - \partial_{\varepsilon_1\gamma_1} U\big) \tag{5.42e}$$

$$M_{1\gamma_2} = \tfrac{1}{3}\big(2\partial_{\varepsilon_1\gamma_2} U - \partial_{\varepsilon_2\gamma_2} U\big) \qquad M_{2\gamma_2} = \tfrac{1}{3}\big(2\partial_{\varepsilon_2\gamma_2} U - \partial_{\varepsilon_1\gamma_2} U\big) \tag{5.42f}$$

$$M_{1\gamma_3} = \tfrac{1}{3}\big(2\partial_{\varepsilon_1\gamma_3} U - \partial_{\varepsilon_2\gamma_3} U\big) \qquad M_{2\gamma_3} = \tfrac{1}{3}\big(2\partial_{\varepsilon_2\gamma_3} U - \partial_{\varepsilon_1\gamma_3} U\big) \tag{5.42g}$$

Collectively, Eqns.(5.41 & 5.42) describe the full non-uniform response permissible by a Green thermoelastic solid expressed as a hypo-elastic material undergoing an adiabatic process.

As in the case of membranes, it is reasonable to assume that the presence of a non-uniform motion will not cause an uniform response. For our application, it is also reasonable to assume that there is no coupling between the modes of squeeze and shear. Furthermore, it is assumed that there is no coupling betwixt the two independent squeeze modes, nor between the three independent shear modes. Consequently, all mixed partial derivatives that associate with a non-uniform response are taken to be zero.

Therefore the above system of equations can be rewritten as three independent systems of differential equations; specifically, the first differential matrix equation when written in terms of Helmholz state variables is

$$\begin{Bmatrix} \mathrm{d}\eta \\ \mathrm{d}\Pi \end{Bmatrix} = \begin{bmatrix} \theta/\partial_{\eta\eta}U & -\partial_{\eta\Xi}U/\partial_{\eta\eta}U \\ \rho\theta\,\partial_{\Xi\eta}U/\partial_{\eta\eta}U & \rho\big(\partial_{\Xi\Xi}U - \partial_{\Xi\eta}U\cdot\partial_{\eta\Xi}U/\partial_{\eta\eta}U\big) \end{bmatrix} \begin{Bmatrix} \theta^{-1}\,\mathrm{d}\theta \\ \mathrm{d}\Xi \end{Bmatrix} \tag{5.43a}$$

recalling that $\mathrm{d}\Xi = \frac{1}{3}V^{-1}\,\mathrm{d}V$, plus a full matrix equation that governs the squeeze response

$$\begin{Bmatrix} \mathrm{d}\sigma_1 \\ \mathrm{d}\sigma_2 \end{Bmatrix} = \frac{\rho}{3}\begin{bmatrix} 2\,\partial_{\varepsilon_1\varepsilon_1}U & -\partial_{\varepsilon_2\varepsilon_2}U \\ -\partial_{\varepsilon_1\varepsilon_1}U & 2\,\partial_{\varepsilon_2\varepsilon_2}U \end{bmatrix} \begin{Bmatrix} \mathrm{d}\varepsilon_1 \\ \mathrm{d}\varepsilon_2 \end{Bmatrix} \tag{5.43b}$$

and a diagonal matrix equation that governs the shear response

$$\begin{Bmatrix} \mathrm{d}\tau_1 \\ \mathrm{d}\tau_2 \\ \mathrm{d}\tau_3 \end{Bmatrix} = \rho\begin{bmatrix} \partial_{\gamma_1\gamma_1}U & 0 & 0 \\ 0 & \partial_{\gamma_2\gamma_2}U & 0 \\ 0 & 0 & \partial_{\gamma_3\gamma_3}U \end{bmatrix} \begin{Bmatrix} \mathrm{d}\gamma_1 \\ \mathrm{d}\gamma_2 \\ \mathrm{d}\gamma_3 \end{Bmatrix} \tag{5.43c}$$

5.3.3.2 Constitutive Equations Governing a Thermoelastic Solid

In terms of the material properties, the uniform response of the thermoelastic solid given in Eqn. (5.43a) takes on the form of

$$\begin{Bmatrix} \mathrm{d}\eta \\ \mathrm{d}\Pi \end{Bmatrix} = \begin{bmatrix} C_t - 9\alpha^2 K/\rho\theta & 9\alpha K/\rho\theta \\ -9\alpha K & 9K \end{bmatrix} \begin{Bmatrix} \theta^{-1}\mathrm{d}\theta \\ \mathrm{d}\Xi \end{Bmatrix}, \qquad \begin{matrix} \alpha = \alpha_t \\ K = K_t(\theta, \Pi, \Xi) \end{matrix} \tag{5.44a}$$

while the non-uniform squeeze response is described by

$$\begin{Bmatrix} \mathrm{d}\sigma_1 \\ \mathrm{d}\sigma_2 \end{Bmatrix} = \frac{3}{2} \begin{bmatrix} 2N_1 & -N_2 \\ -N_1 & 2N_2 \end{bmatrix} \begin{Bmatrix} \mathrm{d}\varepsilon_1 \\ \mathrm{d}\varepsilon_2 \end{Bmatrix}, \qquad \begin{matrix} N_1 = N_t(\sigma_1, \varepsilon_1) \\ N_2 = N_t(\sigma_2, \varepsilon_2) \end{matrix} \tag{5.44b}$$

and the non-uniform shear response is described by

$$\begin{Bmatrix} \mathrm{d}\tau_1 \\ \mathrm{d}\tau_2 \\ \mathrm{d}\tau_3 \end{Bmatrix} = \begin{bmatrix} G_1 & 0 & 0 \\ 0 & G_2 & 0 \\ 0 & 0 & G_3 \end{bmatrix} \begin{Bmatrix} \mathrm{d}\gamma_1 \\ \mathrm{d}\gamma_2 \\ \mathrm{d}\gamma_3 \end{Bmatrix}, \qquad \begin{matrix} G_1 = G_t(\tau_1, \gamma_1) \\ G_2 = G_t(\tau_2, \gamma_2) \\ G_3 = G_t(\tau_3, \gamma_3) \end{matrix} \tag{5.44c}$$

which is the general form for a thermoelastic solid that we shall use going forward.

5.3.4 Modeling an Alveolus

To facilitate the numeric implementation of our models, and to facilitate interpretations of their results by engineers and scientists whom will use our framework, this section converts all fields defined in 1D and 2D into their 3D analogs; specifically, forces and surface tensions are converted into stresses, all moduli will now have units of stress, all thermal strain coefficients associate with linear expansions, and all mass densities relate mass to volume.

5.3.4.1 Constraints/Assumptions for Alveoli Subjected to Shock Waves

Because the primary purpose for the alveolar model being constructed here is to better understand alveolar behavior as a shock wave passes over it, there are certain assumptions

that we impose upon our model that under normal or different physiologic conditions might otherwise not apply.

First: An alveolus is considered to be an adiabatic pressure vessel in which air and heat cannot move into or out of as a shock wave passes over it, simply because the wave speed is too fast. There is insufficient time for t hese transport phenomena to occur.

Second: Whenever a lung is subjected to a shock wave there is insufficient time for the viscous characteristics in a viscoelastic response to manifest themselves; therefore, the overall response is modeled as glassy elastic.

Third: Even though one could construct a mixture theory for the modeling of alveolar membranes, it would be challenging to establish their boundary conditions, nor would we be able to construct the necessary experiments to parameterize it. Consequently, an isotropic, elastic, homogeneous continuum is assumed for modeling the planar septa.

Fourth: Temperature remains continuous in a jump across the kinematic discontinuity caused by a shock wave traveling through a compressible gas. [50] As such, temperature is expected to be continuous across the spatial discontinuity of a shock wave traveling through parenchyma, too. Nevertheless, temperature is expected to change both in front of and behind a traveling wave, where the alveolar sac first compresses and then exapnds. Throughout this excursion, the overall process is considered to be adiabatic. Furthermore, because temperature changes are expected to be small, and wave speeds are fast, the finite element models being developed here assume temperatures will remain constant.

Fifth: Alveolar surfaces are modeled as membranes, not plates, and therefore are assumed to have no out-of-plane bending stiffness. This is in concert with our assumption that the septal chords are modeled as rods, not beams, because of their slenderness ratio. Furthermore, these septa tend to be flat because there are roughly equal pressures acting on both sides of these membranes, thereby eliminating any curvature, which is the driving force behind out-of-plane bending [40] and, we surmise, also helps to suppress wrinkling.

transpulmonary pressure	$4\,\mathrm{cm\,H_2O}$		
Age	15–35	36–45	> 65
collagen: $\sqrt{D}$, $(\mu\mathrm{m})^{1/2}$	0.952 ± 0.242	0.958 ± 0.255	1.045 ± 0.270
elastin: $\sqrt{D}$, $(\mu\mathrm{m})^{1/2}$	0.957 ± 0.239	0.970 ± 0.213	1.093 ± 0.274
transpulmonary pressure	$14\,\mathrm{cm\,H_2O}$		
Age	15–35	36–45	> 65
collagen: $\sqrt{D}$, $(\mu\mathrm{m})^{1/2}$	0.955 ± 0.246	0.994 ± 0.237	1.054 ± 0.279
elastin: $\sqrt{D}$, $(\mu\mathrm{m})^{1/2}$	0.956 ± 0.237	0.988 ± 0.263	1.079 ± 0.281

Table 5.4: Mean and standard deviations in variance for the square root of septal chord diameters $\sqrt{D}$ reported by Sobin *et al.* [51].

5.3.4.2 Modeling Septal Chords Subjected to Shock Waves

The extent of elastic energy stored within a chord will depend upon the diameters D^c and D^e and length L of these individual fibers. Let superscript '^{c}' denote collagen, and superscript '^{e}' denote elastin. Sobin *et al.* [51] determined that the square root of their diameters $\sqrt{D}$ distribute normally, with a mean $\bar{D}^{1/2}$ and standard deviation $\sigma_{\sqrt{D}}$ that also depend upon age and transpulmonary pressure, as presented in Table 5.4.

The collagen and elastin fibers that make up a septal chord have the same length L, they experience the same strain e, and they exist at the same temperature θ; therefore, we employ Eqn. (5.33a) as the governing constitutive equation to describe their mechanical behaviors; specifically, for the collagen fiber in an alveolar chord

$$\begin{Bmatrix} \mathrm{d}\eta^c \\ \mathrm{d}s^c \end{Bmatrix} = \begin{bmatrix} C_t^c - (\alpha_t^c)^2 E^c/\rho^c\theta & \alpha_t^c E^c/\rho^c\theta \\ -\alpha_t^c E^c & E^c \end{bmatrix} \begin{Bmatrix} \theta^{-1}\,\mathrm{d}\theta \\ L^{-1}\,\mathrm{d}L \end{Bmatrix} \tag{5.45a}$$

where $E^c = E_t^c(\theta, e, s^c)$, and for the elastin fiber in an alveolar chord

$$\begin{Bmatrix} \mathrm{d}\eta^e \\ \mathrm{d}s^e \end{Bmatrix} = \begin{bmatrix} C_t^e - (\alpha_t^e)^2 E^e/\rho^e\theta & \alpha_t^e E^e/\rho^e\theta \\ -\alpha_t^e E^e & E^e \end{bmatrix} \begin{Bmatrix} \theta^{-1}\,\mathrm{d}\theta \\ L^{-1}\,\mathrm{d}L \end{Bmatrix} \tag{5.45b}$$

where $E^e = E^e_t(\theta, e, s^e)$, and where η^c and η^e are the entropy densities (erg/g.K) for collagen and elastin; $s^c := \lambda F^c/A^c_0$ and $s^e := \lambda F^e/A^e_0$ are the chordal stresses (barye = dyne/cm^2) carried by the collagen and elastin fibers, wherein $\lambda = L/L_0$ is the fiber stretch, A^c_0 and A^e_0 are their traction-free cross-sectional areas (cm^2), and F^c and F^e are the forces (dyne) they transmit. Parameters C^c_t and C^e_t are their specific heats at constant pressure (erg/g.K), α^c_t and α^e_t are their lineal thermal strain coefficients, E^c and E^e are their elastic moduli (dyne/cm^2 = erg/cm^3), and ρ^c and ρ^e are their mass densities (g/cm^3). These differential equations are subject to initial conditions considered to be $s^c_0 = s^c|_{L=L_0}$, $s^e_0 = s^e|_{L=L_0}$, $\eta^c = \eta^c_0$ and $\eta^e = \eta^e_0$, where η^c_0 and η^e_0 are their respective entropy densities at rest. *In vivo*, s^c_0 and s^e_0 are positive valued, cf. Appendix D; whereas, *ex vivo*, s^c_0 and s^e_0 would be zero valued.

The actual force and entropy of an individual septal chord in our alveolar model is taken to be one third of a fiber's calculated values, as determined by Eqn. (5.45), because each alveolar chord is typically shared between three adjoining alveoli; consequently,

$$F^f = (A^c_0 s^c + A^e_0 s^e)/3\lambda \quad \text{and} \quad S^f = (\rho^c V^c_0 \eta^c + \rho^e V^e_0 \eta^e)/3 \tag{5.46}$$

where F^f (dyne) is a third of the fiber's force carried by a septal chord, and S^f (erg/K) is a third of the fiber's entropy.

Both collagen and elastin are modeled as Freed–Rajagopal biologic fibers, which are described in terms of two such internal energies. Their model is derived from the theory of implicit elasticity, cf. Appendix D. According to their model, Eqn. (D.7), tangent compliances for collagen and elastin, pertinent to the hypo-elastic constitutive formulation of Eqn. (5.45), are described by

$$\frac{1}{E^c_t(\theta, s^c, e)} = \frac{e^c_{1_{\max}} - e^c_1}{E^c_1 e^c_{1_{\max}} + 2(s^c - s^c_0)} + \frac{1}{E^c_2} \tag{5.47a}$$

$$\frac{1}{E^e_t(\theta, s^e, e)} = \frac{e^e_t - e^e_1}{E^e_1 e^e_t + 2(s^e - s^e_0)} + \frac{1}{E^e_2} \tag{5.47b}$$

whose internal strains are established from

$$e_1^c = e - \alpha_t^c \ln\left(\frac{\theta}{\theta_0}\right) - \frac{s^c - s_0^c}{E_2^c}, \quad e_1^e = e - \alpha_t^e \ln\left(\frac{\theta}{\theta_0}\right) - \frac{s^e - s_0^e}{E_2^e} \tag{5.47c}$$

with θ_0 being body temperature, i.e., 310 K. Material constants E_1^c and E_2^c are the two asymptotic moduli for collagen that bound its response, i.e., $E_1^c \leqslant E_t^c \leqslant E_2^c$, while E_1^e and E_2^e are the two asymptotic moduli for elastin that bound its response, viz., $E_1^e \leqslant E_t^e \leqslant E_2^e$, both having units of stress (barye = dyne/cm^2), with $e_{1_{\max}}^c$ and $e_{2_{\max}}^e$ being their respective transition strains (see their derivation in Appendix D). Collagen fibers are considered to fracture whenever the strain of stretching molecular bonds exceeds $e_f^c := s_f^c/E_2^c$, where s_f^c is the fracture stress. In contrast, elastin fibers are assumed to remain intact.

Moduli $E_t^c = E_1^c E_2^c/(E_1^c + E_2^c)$ and $E_t^e = E_1^e E_2^e/(E_1^e + E_2^e)$ are considered to apply for stresses less than their respective reference stress, viz., for $s^c < s_0^c$ or $s^e < s_0^e$, to which we assign values of $s_0^c = \frac{1}{2}E_1^c e_{1_{\max}}^c$ and $s_0^e = \frac{1}{2}E_1^e e_{1_{\max}}^e$. At these reference stresses, L is set to L_0 and therefore strain $e = 0$. Material properties needed to model septal chords are listed in Tables 5.4 & 5.5. Collagen denatures at around 60°C [60], i.e., above this temperature collagen will shrink rapidly—an effect not modeled here. From Eqn. (5.32), these elastic moduli are bound from above by Eqn. (5.32) implying that $E_{\max}^c = 2.25 \times 10^{12}$ barye (dyne/cm^2) and $E_{\max}^e = 1.7 \times 10^{12}$ barye. We therefore observe that E_2^c and E_2^e are about 10^5 times smaller than $E_{\max}^c$ and $E_{\max}^e$, which seems reasonable for *in vivo* fibers.

5.3.4.3 Modeling Alveolar Septa Subjected to Shock Waves

The thermoelastic response of a planar membrane used to model alveolar septa, described in Eqn. (5.38), is used for modeling alveolar septa subjected to shock waves, where $s^\pi := \pi/h$ has units of stress (dyne/cm^2) with h denoting height or thickness of the spetal membrane. Assuming the volume of a septal membrane remains constant, thickness would obey $h = h_0 \exp(-2\xi)$ with h_0 being its reference thickness. $s^\sigma := \sigma/h$ and $s^\tau := \tau/h$ also have units of stress (dyne/cm^2).

Collagen		
ρ^c [g/cm^3]	1.34	Fels [52]
η_0^c [erg/g.K]	3.7×10^7	
C_p^c [erg/g.K]	1.7×10^7	Kanagy [53]
$\alpha_s^c = \alpha_t^c$	0.056	Weir [54]
$e^c_{1_{\max}}$	0.09 ± 0.018	estimated from TLC $\approx 30\%$
e_f^c	0.25 ± 0.025	
E_1^c [barye]	$5.0 \pm 1.0 \times 10^5$	
E_2^c [barye]	$5.0 \pm 0.5 \times 10^7$	
s_0^e [barye]	$E_1^c e^c_{1_{\max}}/2$	assumption
Elastin		
Parameter	Value	Reference
ρ^e [g/cm^3]	1.31	Lillie & Gosline [55]
η_0^e [erg/g.K]	3.4×10^7	Shadwick & Gosline [56]
C_p^e [erg/g.K]	4.2×10^7	Kakivaya & Hoeve [57]
$\alpha_s^e = \alpha_t^e$	0.1	Lillie & Gosline [55]
$e^e_{1_{\max}}$	0.4 ± 0.08	Shadwick & Gosline [56]
E_1^e [barye]	$2.3 \pm 0.3 \times 10^6$	Urry [58, Fig. 18]
E_2^e [barye]	$1.0 \pm 0.1 \times 10^7$	Lillie & Gosline [59, Fig. 5]
s_0^e [barye]	$E_1^e e^e_{1_{\max}}/2$	assumption

Table 5.5: Physical properties for hydrated collagen and elastin fibers.

Property	**Value**
ρ [g/cm^3]	1.1
η_0 [erg/g.K]	5.0×10^6
C_p [erg/g.K]	2.1×10^7
α_t	0.037
$\xi_{1_{\max}}$	0.24 ± 0.24
ξ_f	0.2
M_1 [barye]	$1.0 \pm 0.1 \times 10^4$
M_2 [barye]	$3.0 \pm 0.1 \times 10^6$
s_0^π [barye]	$M_1 \xi_{1_{\max}}/2$
$\gamma_{1_{\max}}$	$3\xi_{1_{\max}}/2$
G_1 [barye]	$M_1/25$
G_2 [barye]	$M_2/25$

Table 5.6: The elastic properties reported here are for visceral pleura taken from Freed *et al.* [28] and parenchyma taken from Saraf et al., [61].

By diminishing the moduli that are appropriate for describing a basement membrane with thickness $\sim$0.5 μm by a factor of 10, one gets an estimate for the effective septal moduli—an estimate applicable when modeling a whole septal membrane with thickness $\sim$5 μm. We employ the model parameters specified in Table 5.6, which are based upon this assumption. For our purposes, we model this collective ensemble of tissue and structure types as a homogeneous isotropic membrane modeled after the Freed–Rajagopal biologic fiber [62] that we have extended to membranes in App. D, specifically

$$\frac{1}{M_t(\theta,\xi,s^\pi)} = \frac{\xi_{1_{\max}} - \xi_1}{M_1\xi_{1_{\max}} + \frac{1}{2}(s^\pi - s_0^\pi)} + \frac{1}{M_2} \qquad \xi_1 = \xi - \alpha_t \ln\left(\frac{\theta}{\theta_0}\right) - \frac{s^\pi - s_0^\pi}{4M_2} \tag{5.48a}$$

and

$$\frac{1}{G_t(\gamma,s^\tau)} = \frac{\operatorname{sgn}(\gamma_1)\,\gamma_{1_{\max}} - \gamma_1}{G_1 \operatorname{sgn}(\gamma_1)\,\gamma_{1_{\max}} + 2s^\tau} + \frac{1}{G_2} \qquad \gamma_1 = \gamma - \frac{s^\tau}{G_2} \tag{5.48b}$$

where compliant, initial, tangent moduli M_1 and G_1 and stiff, terminal, tangent moduli M_2 and G_2 bound their respective responses so that $M_1 \leqslant M_t \leqslant M_2$ and $G_1 \leqslant G_t \leqslant G_2$, with

a gradual transition between their asymptotic bounds occurring around strains of $\xi_{1_{\max}}$ and $\gamma_{1_{\max}}$, with membrane failure or rupture being considered to only occur in the dilation mode whenever $\xi > \xi_f$.

Whenever $s^\pi < s_0^\pi$, modulus M_t is assigned a value of $M_t = M_1 M_2/(M_1 + M_2)$ that is the tangent modulus at reference stress s_0^π, which we take to be $\frac{1}{2} M_1 \xi_{1_{\max}}$. Negative surface tensions cause wrinkling of a membrane surface, which is not addressed here.

5.3.4.4 Modeling an Alveolar Volume Subjected to Shock Waves

Alveoli are connected to bronchial trees via alveolar ducts. Under normal conditions, air moves in and out of the alveoli via these ducts. However, when subjected to a stress wave passing over an alveolus, there is no time for the transport of air to take place. Hence, we can consider the air (and heat) within an alveolus to become "trapped", and the pressure to be uniform therein. The governing thermodynamic process is therefore adiabatic.

5.3.4.5 Alveoli Filled with Air

Considering the water saturated air within an alveolus to be an ideal gas, then [63]

$$PV = nR\theta \quad \text{or} \quad \frac{PV}{\theta} = \frac{P_0 V_0}{\theta_0} = nR = \text{constant} \tag{5.49}$$

where, in our case, P_0 is taken to be the atmospheric pressure at sea level (1 bar or 10^5 Pa or 10^6 barye), with V_0 being that alveolar volume whereat alveolar pressure and plural pressure are both atmospheric, while $\theta_0 = 37^\circ\text{C} = 310$ K is assigned as body temperature. Parameter n is the molar content of gas within an alveolus, and R is the universal gas constant.

The material properties associated with an ideal gas contained within an adiabatic enclosure are

$$\alpha_t := \frac{\theta}{L} \left.\frac{\partial L}{\partial \theta}\right|_P = \frac{\theta}{3V} \left.\frac{\partial V}{\partial \theta}\right|_P = \frac{1}{3\theta_0} \frac{P_0}{P} \frac{V_0}{V} \quad \text{and} \quad K_t := -V \left.\frac{\partial P}{\partial V}\right|_\theta = P_0 \frac{\theta}{\theta_0} \frac{V_0}{V} \tag{5.50a}$$

with the other two material properties pertaining to moist air at body temperature being

its mass density ρ of 1.125×10^{-3} g/cm^3 and its specific heat C_t of 1.007×10^7 erg/g.K at constant pressure, constrained by $K_t < K_{\max} = \rho C_t \theta / \alpha_t^2 \approx \rho C_t \theta_0 / 9 = 3.9 \times 10^5$ barye. An alveolar sac, when modeled as an adiabatic pressure vessel filled with an ideal gas, is described by

$$\begin{Bmatrix} \mathrm{d}\eta \\ -3\,\mathrm{d}P \end{Bmatrix} = \begin{bmatrix} C_t - 9\alpha_t^2 K_t/\rho\theta & 9\alpha_t K_t/\rho\theta \\ -9\alpha_t K_t & 9K_t \end{bmatrix} \begin{Bmatrix} \theta^{-1}\,\mathrm{d}\theta \\ \mathrm{d}\Xi \end{Bmatrix} \tag{5.33c}$$

where the entropy within an alveolar sac is given by $S^a = \rho V \eta$ whose initial condition is $S_0^a = \rho V_0 \eta_0$ with $\rho\eta_0$ being the entropy per unit volume of humid air at body temperature and atmospheric pressure, viz., $\rho\eta_0 = 7.770 \times 10^4$ erg/cm^3.K.

5.3.4.6 Alveoli Filled with Fluid

In lung tissues that are not healthy, fluids may fill alveolar volumes at various regions throughout a lung. In such localities the mechanical response of the local parenchyma will be vastly stiffer than that of healthy tissue, and as such, it will respond very differently to an imposed traveling shock wave.

In the presence of a passing shock wave, we suppose that an unhealthy alveolar sac, like a healthy one, can be modeled as an adiabatic enclosure, but now the fluid within such an alveolus is considered to behave, momentarily, like an elastic solid, viz., as the glassy, elastic, upper-bound response of a viscoelastic liquid, which blood is, for example.

5.3.5 Code Verification and Capabilities of the Constitutive Equations

Figure 5.13 presents realistic variability with what one should expect for chordal responses in the alveoli of lung for the deformation out to 10%, 20%, 30% and 40% strains. Both the chordal force and entropy (actual entropy, not entropy density) were calculated using the rule of mixtures based upon volume fractions of collagen vs. elastin. The change in chordal entropy was so small that variability caused by variation in volume fraction dominates this response; hence, relative changes in entropy ($S - S_0$) had to be plotted to visualize the effect.

The three conjugate pairs that describe a membrane's response are presented as rows in

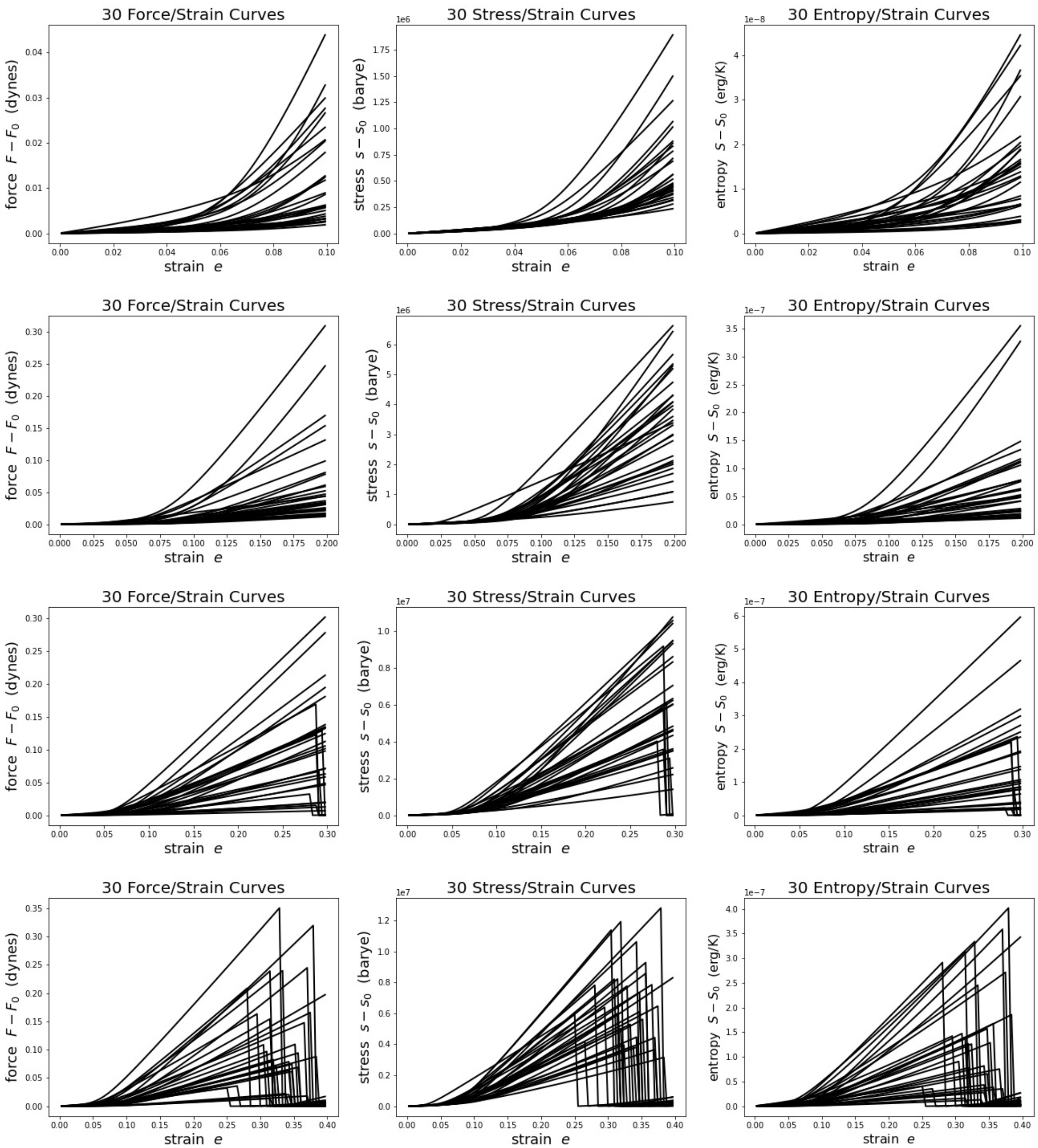

Figure 5.13: Relative force/strain (left column), relative nominal stress/strain (center column), and relative entropy/strain (right column) curves for septal chords comprised of individual collagen and elastin fibers whose material parameters are listed in Table 5.5, which are described in terms of probability distributions.

Fig. 5.14—one row per experiment, with there being 30 curves per plot. These conjugate pairs describe: uniform dilation (s^π, ξ), non-uniform squeeze (s^σ, ε), and non-uniform (simple) shear (s^τ, γ). The three motions that we consider include:
dilation

$$a = \lambda \qquad b = \lambda \qquad g - g_0 = 0 \tag{5.51a}$$

pure shear [27]

$$a = \frac{\sqrt{\lambda^2 + \lambda^{-2}}}{\sqrt{2}} \qquad b = \frac{\sqrt{2}}{\sqrt{\lambda^2 + \lambda^{-2}}} \qquad g - g_0 = \frac{\lambda^2 - \lambda^{-2}}{\lambda^2 + \lambda^{-2}} \tag{5.51b}$$

and simple shear

$$a = 1 \qquad b = 1 \qquad g - g_0 \neq 0 \tag{5.51c}$$

where λ denotes a stretch with $\lambda_0 = 1$. For dilation: $\xi = \ln \lambda$, $\varepsilon = 0$ & $\gamma = 0$; for pure shear: $\xi = 0$, $\varepsilon = \ln\left(\frac{1}{2}(\lambda^2 + \lambda^{-2})\right)$ & $\gamma = (\lambda^2 - \lambda^{-2})/(\lambda^2 + \lambda^{-2})$; and for simple shear: $\xi = 0$, $\varepsilon = 0$ & $\gamma = g - g_0$. The constitutive model is that of Eqns. (5.38 & 5.48), applying material parameters (and their variability) given in Table 5.6. In the dilation experiment (top row) there is only uniform (s^π, ξ) response. There are no non-uniform responses, neither (s^σ, ε) nor (s^τ, γ) in an uniform dilation, either theoretical or numerical. The pure shear experiment (middle row) is dominated by both a squeeze (s^σ, ε) and a shear (s^τ, γ) response, with there being a small, systematic, dilational coupling through pair (s^π, ξ) that is on the order of 1 part in 10^6.

Observation: The change in entropy caused by deformation has been shown to be negligible when compared with the entropy present in its reference state. As such, entropy and its conjugate, i.e., temperature, will not be modeled in our finite element representations of alveoli being exposed to traveling shock waves.

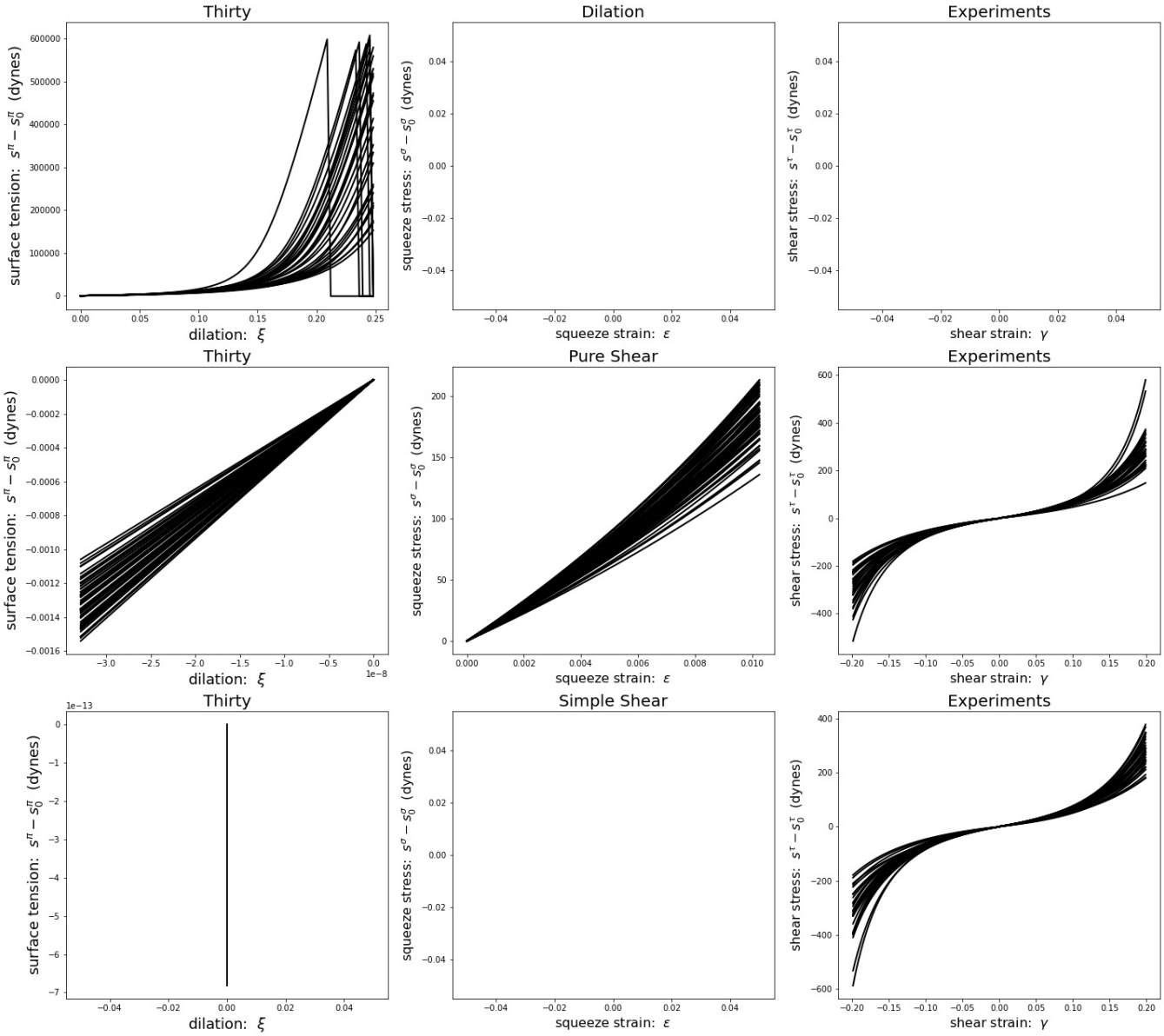

Figure 5.14: Membrane response from 30 numerical experiments whose constitutive behavior is described by Eqns. (5.38 & 5.48) using the parameters listed in Table 5.6. During these numerical experiments, eight membranes ruptured under dialation, while none ruptured during these pure and simple shear experiments.

6.1 Quadrature Rules for Spatial Integration

Particular to our application, a suite of nodes is common betwixt three, separate, finite-element models that share 20 common vertices. These vertices establish the geometry of a dodecahedron used as the model for a microscopic alveolus. The resultant microscopic force at each vertex arises from: *i*) a finite element model of 30 1D rods representing the alveolar chords, *ii*) a finite element model of 12 2D pentagons representing the alveolar membranes, and *iii*) a finite element model of 60 3D tetrahedra representing the alveolar sac. The microscopic forces coming from these three geometric models are summed at their twenty common vertices.

Shape functions are introduced for interpolating within an element; specifically, consider an arbitrary field, say f, whose values are known at the nodes, then

$$f(\boldsymbol{\xi}_k) = \sum_{i=1}^{n} N_i(\boldsymbol{\xi}_k) f(\boldsymbol{x}_i) \qquad\qquad k = 1, 2, \ldots, m \tag{6.1a}$$

where the $\boldsymbol{x}_i$ are co-ordinates that locate one of the n nodes in an element of interest, and where the $\boldsymbol{\xi}_i$ are co-ordinates that locate one of its m Gauss points, both being evaluated in the natural co-ordinate system of the element. Functions N_i are the so-called shape functions. They obey $\sum_{i=1}^{n} N_i(\boldsymbol{\xi}) = 1 \;\forall\; \boldsymbol{\xi}$.

6.1.1 Self-Consistent Interpolation Procedures for Rods

Considering a rod with two Gauss points, the interpolation of an arbitrary field (say f, whose values are known at nodal points x_i, $i = 1, 2$) into approximated values located at Gauss points ξ_i, assigned according to Table 6.1 which approximates $\int_{-1}^{1} f(\xi)\,\mathrm{d}\xi$ using two Gauss points, i.e., $\int_{-1}^{1} f(\xi)\,\mathrm{d}\xi \approx \sum_{i=1}^{2} w_i f(\xi_i)$. The weights of quadrature w_i sum to its length, because $L = \int_{-1}^{1} \mathrm{d}\xi = 2$. Selecting shape (interpolation) functions $N_1 = \frac{1}{2}(1 - \xi)$ and

node	$\boldsymbol{\xi}$ co-ordinate	weight
1	$-\sqrt{3}/3$	1
2	$\sqrt{3}/3$	1

Table 6.1: A quadrature rule for integrating functions over a length of line.

$N_2 = \frac{1}{2}(1+\xi)$, where $-1 \leqslant \xi \leqslant 1$, results in an interpolation map that sends values for a field known at the element nodes down to its Gauss points via

$$\begin{Bmatrix} f(-\sqrt{3}/3) \\ f(\sqrt{3}/3) \end{Bmatrix} = \frac{1}{6}\begin{bmatrix} 3+\sqrt{3} & 3-\sqrt{3} \\ 3-\sqrt{3} & 3+\sqrt{3} \end{bmatrix}\begin{Bmatrix} f(-1) \\ f(1) \end{Bmatrix}. \tag{6.2a}$$

6.1.2 Self-Consistent Interpolation Procedures for Triangles

Now, considering a triangle with three Gauss points, the interpolation of an arbitrary field f whose values are known at nodal points $\boldsymbol{x}_i$, $i = 1, 2, 3$, into approximated values located at Gauss points $\boldsymbol{\xi}$, assigned according to Table 6.2 that approximates $\int_0^1 \int_0^{1-\xi} f(\xi,\eta)\,\mathrm{d}\eta\,\mathrm{d}\xi$ using three Gauss points, i.e., $\int_0^1 \int_0^{1-\xi} f(\xi,\eta)\,\mathrm{d}\eta\,\mathrm{d}\xi \approx \sum_{i=1}^{3} w_i f(\xi_i,\eta_i)$. The weights of quadrature w_i sum to its area, because $A = \int_0^1 \int_0^{1-\xi} \mathrm{d}\eta\,\mathrm{d}\xi = 1/2$. Selecting shape (interpolation) functions $N_1 = 1-\xi-\eta$, $N_2 = \xi$, and $N_3 = \eta$, where $0 \leqslant \xi \leqslant 1$ and $0 \leqslant \eta \leqslant 1-\xi$, results in an interpolation that maps according to

$$\begin{Bmatrix} f(1/6,\,1/6) \\ f(2/3,\,1/6) \\ f(1/6,\,2/3) \end{Bmatrix} = \frac{1}{6}\begin{bmatrix} 4 & 1 & 1 \\ 1 & 4 & 1 \\ 1 & 1 & 4 \end{bmatrix}\begin{Bmatrix} f(0,0) \\ f(1,0) \\ f(0,1) \end{Bmatrix}. \tag{6.3a}$$

6.1.3 Self-Consistent Interpolation Procedures for Pentagons

Because we seek a quadrature rule for regular pentagons that employs five Gauss points, and pentagons posses five radial lines of symmetry, it is reasonable to consider that the five

node	ξ co-ordinate	η co-ordinate	weight
1	1/6	1/6	1/6
2	2/3	1/6	1/6
3	1/6	2/3	1/6

Table 6.2: A simple quadrature rule for integrating functions over the area of a triangle.

nodes of quadrature that we seek lie along these five radial lines. Specifically, we seek a quadrature rule for a pentagon whose nodes are located at $\boldsymbol{x}_i$, $i = 1, 2, \ldots, 5$, and whose Gauss points are located at $\boldsymbol{\xi}_i$, $i = 1, 2, \ldots, 5$, with

$$\boldsymbol{x}_1 = \big(\cos(\pi/2), \sin(\pi/2)\big) \qquad \boldsymbol{\xi}_1 = \ell \boldsymbol{x}_1 \tag{6.4a}$$

$$\boldsymbol{x}_2 = \big(\cos(9\pi/10), \sin(9\pi/10)\big) \qquad \boldsymbol{\xi}_2 = \ell \boldsymbol{x}_2 \tag{6.4b}$$

$$\boldsymbol{x}_3 = \big(\cos(13\pi/10), \sin(13\pi/10)\big) \qquad \boldsymbol{\xi}_3 = \ell \boldsymbol{x}_3 \tag{6.4c}$$

$$\boldsymbol{x}_4 = \big(\cos(17\pi/10), \sin(17\pi/10)\big) \qquad \boldsymbol{\xi}_4 = \ell \boldsymbol{x}_4 \tag{6.4d}$$

$$\boldsymbol{x}_5 = \big(\cos(\pi/10), \sin(\pi/10)\big) \qquad \boldsymbol{\xi}_5 = \ell \boldsymbol{x}_5 \tag{6.4e}$$

where lines radiating from the origin out to each vertex $\boldsymbol{x}_i$ have unit length, while the lines that radiate out to the Gauss points $\boldsymbol{\xi}_i$ each have a shorter length of ℓ.

Implementing the strategies that underlie Gauss quadrature, length ℓ represents a distance from the pentagon's centroid out to the centroid of a quadrilateral. In our case, this area (one of five equivalent areas) is a four-sided polygon whose apex has an inside angle of 108°, whose two shoulders have right angles, while the inside angle is 72° at the origin. A little bit of algebra and geometry leads to the result

$$\ell = \frac{1 + \sin(3\pi/10)}{3 \sin(3\pi/10)} \approx 0.7454 \tag{6.5a}$$

whose area becomes the associated weight of quadrature, it being

$$w = \sin(3\pi/10)\cos(3\pi/10) \approx 0.4755 \tag{6.5b}$$

which is one-fifth the area of a regular pentagon, cf. Eqn. (5.3). To the best of our knowledge, the quadrature rule put forward in Eqns. (6.4 & 6.5) for pentagons is new to the literature.

Adopting the shape functions of Wachspress, while using the quadrature rule of Eqns. (6.4 & 6.5), results in a symmetric interpolation map of

$$\begin{Bmatrix} f(\boldsymbol{\xi}_1) \\ f(\boldsymbol{\xi}_2) \\ f(\boldsymbol{\xi}_3) \\ f(\boldsymbol{\xi}_4) \\ f(\boldsymbol{\xi}_5) \end{Bmatrix} = \begin{bmatrix} a & b & c & c & b \\ b & a & b & c & c \\ c & b & a & b & c \\ c & c & b & a & b \\ b & c & c & b & a \end{bmatrix} \begin{Bmatrix} f(\boldsymbol{x}_1) \\ f(\boldsymbol{x}_2) \\ f(\boldsymbol{x}_3) \\ f(\boldsymbol{x}_4) \\ f(\boldsymbol{x}_5) \end{Bmatrix} \tag{6.6a}$$

whose matrix elements are $a = 0.6901471673508344$, $b = 0.1367959452017669$ and $c = 0.0181304711228159$.

6.1.4 Self-Consistent Interpolation Procedures for Tetrahedra

We now consider a tetrahedron with four Gauss points. Here the interpolation of an arbitrary field f whose values are known at nodal points $\boldsymbol{x}_i$, $i = 1, 2, 3, 4$, into approximated values located at Gauss points $\boldsymbol{\xi}_i$, assigned according to Table 6.3 that approximates $\int_0^1 \int_0^{1-\xi} \int_0^{1-\xi-\eta} f(\xi, \eta, \zeta)\, \mathrm{d}\zeta\, \mathrm{d}\eta\, \mathrm{d}\xi$ using four Gauss points, i.e., $\int_0^1 \int_0^{1-\xi} \int_0^{1-\xi-\eta} f(\xi, \eta, \zeta)\, \mathrm{d}\zeta\, \mathrm{d}\eta\, \mathrm{d}\xi \approx \sum_{i=1}^{4} w_i f(\xi_i, \eta_i, \zeta_i)$. Selecting shape functions $N_1 = 1-\xi-\eta-\zeta$, $N_2 = \xi$, $N_3 = \eta$, and $N_4 = \zeta$, bounded by $0 \leqslant \xi \leqslant 1$, $0 \leqslant \eta \leqslant 1-\xi$ and $0 \leqslant \zeta \leqslant 1-\xi-\eta$, leads to the following interpolation

node	ξ co-ordinate	η co-ordinate	ζ co-ordinate	weight
1	0.1381966011250105	0.1381966011250105	0.1381966011250105	1/24
2	0.5854101966249685	0.1381966011250105	0.1381966011250105	1/24
3	0.1381966011250105	0.5854101966249685	0.1381966011250105	1/24
4	0.1381966011250105	0.1381966011250105	0.5854101966249685	1/24

Table 6.3: A quadrature rule for integrating functions over the volume of a tetrahedron.

formula

$$\begin{Bmatrix} f(a,a,a) \\ f(b,a,a) \\ f(a,b,a) \\ f(a,a,b) \end{Bmatrix} = \begin{bmatrix} 1-3a & a & a & a \\ 1-2a-b & b & a & a \\ 1-2a-b & a & b & a \\ 1-2a-b & a & a & b \end{bmatrix} \begin{Bmatrix} f(0,0,0) \\ f(1,0,0) \\ f(0,1,0) \\ f(0,0,1) \end{Bmatrix} \tag{6.7a}$$

where $a = 0.1381966011250105$ and $b = 0.5854101966249685$ from Table 6.3.

6.2 Finite Element Analysis

The problem that we have set up to solve is cast in a Lagrangian setting and takes on the general form of a second-order, ODE; specifically,

$$\boldsymbol{F} = \mathbf{K}\,\boldsymbol{\Delta} + \mathbf{C}\,\dot{\boldsymbol{\Delta}} + \mathbf{M}\,\ddot{\boldsymbol{\Delta}} \tag{6.8a}$$

that under conditions of equilibrium (i.e., whenever $\ddot{\boldsymbol{\Delta}} = \dot{\boldsymbol{\Delta}} = \mathbf{0}$) reduces to

$$\boldsymbol{F} = \mathbf{K}\,\boldsymbol{\Delta} \tag{6.8b}$$

where $\mathbf{K}$ is a secant stiffness matrix, $\mathbf{C}$ is a tangent stiffness matrix[1], $\mathbf{M}$ is a mass matrix, and $\boldsymbol{F}$ is a force vector, while vector $\boldsymbol{\Delta}$ contains the assembled nodal displacements with $\dot{\boldsymbol{\Delta}}$ and $\ddot{\boldsymbol{\Delta}}$ denoting their velocities and accelerations.

[1]In the literature, matrix $\mathbf{C}$ is typically utilized as a damping matrix; however, there are presently no damping mechanisms in our alveolar model.

Our problem of interest is the dynamic mechanical response of an alveolus, whose geometry is modeled as a dodecahedron. The shape of an irregular dodecahedron is described by a set of 20 vertices, each experiencing displacements of

$$\mathbf{u}_i^{(v)} = \left\{ u_i^{(v)} \quad v_i^{(v)} \quad w_i^{(v)} \right\}^{\mathsf{T}} \tag{6.9a}$$

where at the beginning of a solution step $u_i^{(v)} := x_i^{(v)} - x_0^{(v)}$, $v_i^{(v)} := y_i^{(v)} - y_0^{(v)}$, and $w_i^{(v)} := z_i^{(v)} - z_0^{(v)}$, while at the end of that solution step $u_{i+1}^{(v)} = x_{i+1}^{(v)} - x_0^{(v)}$, $v_{i+1}^{(v)} = y_{i+1}^{(v)} - y_0^{(v)}$, and $w_{i+1}^{(v)} = z_{i+1}^{(v)} - z_0^{(v)}$, with $(x^{(v)}, y^{(v)}, z^{(v)})$ denoting co-ordinates for vertex v in the co-ordinate frame $(\vec{\boldsymbol{E}}_1, \vec{\boldsymbol{E}}_2, \vec{\boldsymbol{E}}_3)$ of a dodecahedron. The velocities at these vertices are

$$\dot{\mathbf{u}}_i^{(v)} = \left\{ \dot{u}_i^{(v)} \quad \dot{v}_i^{(v)} \quad \dot{w}_i^{(v)} \right\}^{\mathsf{T}} \tag{6.9b}$$

where at the beginning of a solution step $\dot{\delta}_i = \frac{1}{2\mathrm{d}t}(\delta_{i+1} - \delta_{i-1})$, while at the end of that solution step $\dot{\delta}_{i+1} = \frac{1}{2\mathrm{d}t}(3\delta_{i+1} - 4\delta_i + \delta_{i-1})$, with $\delta \in \{u^{(v)}, v^{(v)}, w^{(v)}\}$. Likewise, their accelerations are

$$\ddot{\mathbf{u}}_i^{(v)} = \left\{ \ddot{u}_i^{(v)} \quad \ddot{v}_i^{(v)} \quad \ddot{w}_i^{(v)} \right\}^{\mathsf{T}} \tag{6.9c}$$

where at the beginning of a solution step $\ddot{\delta}_i = \frac{1}{(\mathrm{d}t)^2}(\delta_{i+1} - 2\delta_i + \delta_{i-1})$, while at the end of that solution step $\ddot{\delta}_{i+1} = \frac{1}{(\mathrm{d}t)^2}(2\delta_{i+1} - 5\delta_i + 4\delta_{i-1} - \delta_{i-2})$. An evaluation of these nodal fields requires knowledge of the co-ordinates for each vertex at states $i+1$, i, $i-1$, and $i-2$. All finite difference equations listed above are second-order formulæ.

Symbol $\boldsymbol{\Delta}$ is used to denote an assemblage of all nodal displacements, while symbol $\mathbf{u}^{(v)}$ is used to denote the nodal displacement of an individual vertex (node) v located within this model, of which there are 20 in our dodecahedral model.

Our problem is not cast as a typical finite element solution, in the sense that we know the nodal displacements $\boldsymbol{\Delta}$, velocities $\dot{\boldsymbol{\Delta}}$, and accelerations $\ddot{\boldsymbol{\Delta}}$ *a priori*, for which nodal forces $\boldsymbol{F}$ are to be found. Typically, boundary conditions are known for which displacements are

determined in a weak sense, which is the opposite of our situation. Inputs for our model are considered to come from a finite element model of a torso subjected to an impact caused by either a ballistic projectile or a blast wave.

The assembled nodal forces $\boldsymbol{F}(\boldsymbol{T})$, depend upon stresses $\boldsymbol{T}$ evaluated at the Gauss points, as do the tangent and secant stiffness matrices, i.e., $\mathbf{C}(\boldsymbol{T})$ and $\mathbf{K}(\boldsymbol{T})$, which thereby couples the system of equations that are to be solved. As such, an iterative solver is proposed. The mass matrix $\mathbf{M}$ will vary between solution steps, too, but not because the mass matrix of a particular element changes, but rather, because rotations of the local co-ordinate systems for the elements about the global reference frame for the dodecahedron can become large, and as such, effect change in the assembled mass matrix.

The stress that arises from $\mathbf{K}\boldsymbol{\Delta}$ is due to an elastic deformation that begins in some reference state (at an initial time t_0) and ends at the current state (at present time t_i). The stress that arises from $\mathbf{C}\dot{\boldsymbol{\Delta}}$ is due to an additional elastic deformation that begins in this current state (at time t_i) and ends at some nearby state (at a future time $t_{i+1} = t_i + \mathrm{d}t$). While an inertial contribution to stress results from $\mathbf{M}\ddot{\boldsymbol{\Delta}}$.

The solution strategy adopted here mimics that of a predictor/corrector method used for solving ODEs. At the beginning of a current solution step, the solution at the end of its previous step takes on the form of

$$\boldsymbol{F}_i = \mathbf{K}_i\boldsymbol{\Delta}_i + \mathbf{M}_i\ddot{\boldsymbol{\Delta}}_i \tag{6.10a}$$

where $\boldsymbol{F}_i = \boldsymbol{F}(\boldsymbol{T}_i)$ and $\mathbf{K}_i = \mathbf{K}(\boldsymbol{T}_i)$. Recall that there is no damping in our model, so there is no $\dot{\boldsymbol{\Delta}}_i$ contribution entering here. At the beginning of a step the stiffness response arises singularly from a secant modulus. Meanwhile, the response at the end of the time step is considered to be described by a predictor of the form

$$\boldsymbol{F}^p_{i+1} = \mathbf{K}_i\boldsymbol{\Delta}_i + \mathbf{C}_i\dot{\boldsymbol{\Delta}}_i + \mathbf{M}_i\ddot{\boldsymbol{\Delta}}_i$$

where $\boldsymbol{F}_{i+1}^{p} = \boldsymbol{F}(\boldsymbol{T}_{i+1}^{p})$. Subtracting Eqn. (6.10a) from the above equation produces

$$\boldsymbol{F}_{i+1}^{p} = \boldsymbol{F}_{i} + \mathbf{C}_{i}\dot{\boldsymbol{\Delta}}_{i} \tag{6.10b}$$

At this point in the solution process, one evaluates the mass and secant stiffness matrices according to $\mathbf{M}_{i+1}$ and $\mathbf{K}_{i+1} = \mathbf{K}(\boldsymbol{T}_{i+1}^{p})$ and then corrects the solution via

$$\boldsymbol{F}_{i+1} = \mathbf{K}_{i+1}\boldsymbol{\Delta}_{i+1} + \mathbf{M}_{i+1}\ddot{\boldsymbol{\Delta}}_{i+1} \tag{6.10c}$$

where $\dot{\boldsymbol{\Delta}}_{i+1}$ and $\ddot{\boldsymbol{\Delta}}_{i+1}$ are approximated using backward difference formulæ. A reevaluation of $\mathbf{K}_{i+1} = \mathbf{K}(\boldsymbol{T}_{i+1})$ now takes place, and Eqn. (6.10c) is iterated on until convergence. In preparation to the next step, one evaluates the tangent stiffness matrix $\mathbf{C}_{i+1} = \mathbf{C}(\boldsymbol{T}_{i+1})$. Equation (6.10) is not self starting. To start, because $\ddot{\boldsymbol{\Delta}}_{0} = \boldsymbol{\Delta}_{0} = \mathbf{0}$, it follows that

$$\boldsymbol{F}_{1}^{p} = \boldsymbol{F}_{0} + \mathbf{C}_{0}\dot{\boldsymbol{\Delta}}_{0} \tag{6.11a}$$

where $\boldsymbol{F}_{0} = \boldsymbol{F}(\boldsymbol{T}_{0})$ denotes a residual force or prestress that must exist in biologic tissues, while $\mathbf{C}_{0} = \mathbf{C}(\boldsymbol{T}_{0})$ and $\boldsymbol{F}_{1}^{p} = \boldsymbol{F}(\boldsymbol{T}_{1}^{p})$. Here $\dot{\boldsymbol{\Delta}}_{0}$ is to be approximated using an Euler forward step. After evaluating $\mathbf{K}_{1} = \mathbf{K}(\boldsymbol{T}_{1}^{p})$, a correction is computed

$$\boldsymbol{F}_{1} = \mathbf{K}_{1}\boldsymbol{\Delta}_{1} \tag{6.11b}$$

where $\boldsymbol{F}_{1} = \boldsymbol{F}(\boldsymbol{T}_{1})$. Upon convergence, one determines the mass matrix $\mathbf{M}_{1}$ and the tangent stiffness matrix $\mathbf{C}_{1} = \mathbf{C}(\boldsymbol{T}_{1})$ in preparation for advancing to solution step 2. It is during the second solution interval whereat nodal accelerations can first be computed, so that with Eqn. (6.11b) appling at the start of this interval, and with the following predictor considered to apply at the end of the interval

$$\boldsymbol{F}_{2}^{p} = \mathbf{K}_{1}\boldsymbol{\Delta}_{1} + \mathbf{C}_{1}\dot{\boldsymbol{\Delta}}_{1} + \mathbf{M}_{1}\ddot{\boldsymbol{\Delta}}_{1}$$

then subtracting Eqn. (6.11b) from this equation finds the solution advances via

$$\boldsymbol{F}_2^p = \boldsymbol{F}_1 + \mathbf{C}_1\dot{\boldsymbol{\Delta}}_1 + \mathbf{M}_1\ddot{\boldsymbol{\Delta}}_1 \tag{6.11c}$$

where $\boldsymbol{F}_2^p = \boldsymbol{F}(\boldsymbol{T}_2^p)$. At this point there is enough information to estimate the nodal accelerations $\ddot{\boldsymbol{\Delta}}_1$, as displacement data are available for $i+1=2$. Both $\dot{\boldsymbol{\Delta}}_1$ and $\ddot{\boldsymbol{\Delta}}_1$ are approximated using central difference formulæ. Upon evaluating the mass matrix $\mathbf{M}_2$ and the secant stiffness matrix $\mathbf{K}_2 = \mathbf{K}(\boldsymbol{T}_2^p)$, a corrected solution at the end of the step is computed via

$$\boldsymbol{F}_2 = \mathbf{K}_2\boldsymbol{\Delta}_2 + \mathbf{M}_2\ddot{\boldsymbol{\Delta}}_2 \tag{6.11d}$$

where $\ddot{\boldsymbol{\Delta}}_2 \leftarrow \ddot{\boldsymbol{\Delta}}_1$, because at this juncture there is not enough nodal displacement information to estimate acceleration at the end of this step, while $\dot{\boldsymbol{\Delta}}_2$ is approximated using a backward difference formula. Equation (6.11d) allows for an improvement for $\mathbf{K}_2 = \mathbf{K}(\boldsymbol{T}_2)$ that can be inserted back into itself, iterating until convergence. Upon convergence, one determines the tangent stiffness matrix $\mathbf{C}_2 = \mathbf{C}(\boldsymbol{T}_1)$ in preparation for advancing to solution step 3.

We construct three, individual, finite-element models governed by the following three systems of differential equations

$$\boldsymbol{F}_{1\mathrm{D}} = \mathbf{K}_{1\mathrm{D}}\,\boldsymbol{\Delta} + \mathbf{C}_{1\mathrm{D}}\,\dot{\boldsymbol{\Delta}} + \mathbf{M}_{1\mathrm{D}}\,\ddot{\boldsymbol{\Delta}} \tag{6.12a}$$

$$\boldsymbol{F}_{2\mathrm{D}} = \mathbf{K}_{2\mathrm{D}}\,\boldsymbol{\Delta} + \mathbf{C}_{2\mathrm{D}}\,\dot{\boldsymbol{\Delta}} + \mathbf{M}_{2\mathrm{D}}\,\ddot{\boldsymbol{\Delta}} \tag{6.12b}$$

$$\boldsymbol{F}_{3\mathrm{D}} = \mathbf{K}_{3\mathrm{D}}\,\boldsymbol{\Delta} + \mathbf{C}_{3\mathrm{D}}\,\dot{\boldsymbol{\Delta}} + \mathbf{M}_{3\mathrm{D}}\,\ddot{\boldsymbol{\Delta}} \tag{6.12c}$$

wherein subscript '$_{1\mathrm{D}}$' associates with alveolar chords that assemble into a 3D space truss, subscript '$_{2\mathrm{D}}$' associates with alveolar membranes that assemble into a 3D tiled balloon-like structure, and subscript '$_{3\mathrm{D}}$' associates with an alveolar sac.

When assembled, vectors $\boldsymbol{F}$, $\boldsymbol{\Delta}$, $\dot{\boldsymbol{\Delta}}$ and $\ddot{\boldsymbol{\Delta}}$ have lengths of 60 for the alveolar chord and

alveolar membrane models, and a length of 63 for the alveolar sac model, while matrices $\mathbf{K}$, $\mathbf{C}$ and $\mathbf{M}$ have dimensions of 60×60 for the alveolar chord and alveolar membrane models, and dimensions of 63×63 for the alveolar sac model. The model for alveolar volume has an extra node located at the centroid of the dodecahedron.

6.2.1 Mass Matrices

The consistent mass matrix of an element, [64] when quantified in the element's coordinate frame $(\vec{\boldsymbol{e}}_1, \vec{\boldsymbol{e}}_2, \vec{\boldsymbol{e}}_3)$, is defined as follows: For 1D elements

$$\mathbf{M}_{\mathrm{C1D}} = \int_L \rho\, \mathbf{N}^{\mathsf{T}}\mathbf{N}\, A\, \mathrm{d}L \qquad\qquad M_{ij}^{\mathrm{C1D}} = \int_L \rho\, N_{1i}N_{1j}\, A\, \mathrm{d}L \tag{6.13a}$$

with $i, j = 1, 2, \ldots, n$ where n is the number of nodal points. For 2D elements

$$\mathbf{M}_{\mathrm{C2D}} = \int_A \rho\, \mathbf{N}^{\mathsf{T}}\mathbf{N}\, H\, \mathrm{d}A \qquad\qquad M_{ij}^{\mathrm{C2D}} = \int_A \rho \sum_{k=1}^{2} N_{ki}N_{kj}\, H\, \mathrm{d}A \tag{6.13b}$$

with $i, j = 1, 2, \ldots, 2n$ where n is the number of nodal points. And for 3D elements

$$\mathbf{M}_{\mathrm{C3D}} = \int_V \rho\, \mathbf{N}^{\mathsf{T}}\mathbf{N}\, \mathrm{d}V \qquad\qquad M_{ij}^{\mathrm{C3D}} = \int_V \rho \sum_{k=1}^{3} N_{ki}N_{kj}\, \mathrm{d}V \tag{6.13c}$$

with $i, j = 1, 2, \ldots, 3n$ where n is the number of nodal points. For a rod, $\mathbf{M}_{\mathrm{C1D}}$ is a 2×2 matrix; for a pentagon, $\mathbf{M}_{\mathrm{C2D}}$ is a 10×10 matrix; and for a tetrahedron, $\mathbf{M}_{\mathrm{C3D}}$ is a 12×12 matrix. In each expression, ρ is mass per unit volume, $\mathbf{N}$ is a matrix of shape functions for the element of interest, L is length, H is height, A is area, and V is volume.

One form of a lumped mass matrix is where the entries from each row of a consistent mass matrix are summed and placed in their respective diagonal entries; specifically: [65] For 1D elements

$$M_{ii}^{\mathrm{L1D}} = \sum_{j=1}^{n} M_{ij}^{\mathrm{C1D}} = \int_L \rho N_{1i} \sum_{j=1}^{n} N_{1j}\, A\, \mathrm{d}L, \qquad\qquad M_{ij}^{\mathrm{L1D}} = 0 \quad i \neq j \tag{6.14a}$$

with $i = 1, 2, \ldots, n$ where n is the number of nodal points. For 2D elements

$$M_{ii}^{\mathrm{L2D}} = \sum_{j=1}^{2n} M_{ij}^{\mathrm{C2D}} = \int_A \rho \sum_{k=1}^{2} N_{ki} \sum_{j=1}^{2n} N_{kj}\, H \,\mathrm{d}A, \qquad M_{ij}^{\mathrm{L2D}} = 0 \quad i \neq j \tag{6.14b}$$

with $i = 1, 2, \ldots, 2n$ where n is the number of nodal points. And for 3D elements

$$M_{ii}^{\mathrm{L3D}} = \sum_{j=1}^{3n} M_{ij}^{\mathrm{C3D}} = \int_V \rho \sum_{k=1}^{3} N_{ki} \sum_{j=1}^{3n} N_{kj} \,\mathrm{d}V, \qquad M_{ij}^{\mathrm{L3D}} = 0 \quad i \neq j \tag{6.14c}$$

with $i = 1, 2, \ldots, 3n$ where n is the number of nodal points.

A lumped-consistent (or weighted) mass matrix $\mathbf{M}_{\mathrm{W}}$ can then be created as follows

$$\mathbf{M}_{\mathrm{W}} = (1 - \mu)\, \mathbf{M}_{\mathrm{C}} + \mu\, \mathbf{M}_{\mathrm{L}}$$

wherein μ is a free scalar parameter for weighting between the consistent and lumped mass matrices. The reason for mixing $\mathbf{M}_{\mathrm{C}}$ and $\mathbf{M}_{\mathrm{L}}$ is to achieve a non-singular mass matrix by making the resulting matrix diagonally dominant. In this work, μ is taken to be a half, i.e., an averaged mass matrix is adopted, which has a nice property of minimizing low frequency dispersion. Specifically, we select

$$\mathbf{M}_{\mathrm{1D}} := \tfrac{1}{2}(\mathbf{M}_{\mathrm{C1D}} + \mathbf{M}_{\mathrm{L1D}}) \tag{6.15a}$$

$$\mathbf{M}_{\mathrm{2D}} := \tfrac{1}{2}(\mathbf{M}_{\mathrm{C2D}} + \mathbf{M}_{\mathrm{L2D}}) \tag{6.15b}$$

$$\mathbf{M}_{\mathrm{3D}} := \tfrac{1}{2}(\mathbf{M}_{\mathrm{C3D}} + \mathbf{M}_{\mathrm{L3D}}) \tag{6.15c}$$

as our means for constructing mass matrices. Each of these mass matrices is invertible that, for example, is a requirement of the numerical solution strategy.

6.2.1.1 Mass Matrix for a Chord

A two-noded alveolar chord (a pinned beam in finite element terminology) has shape functions N_i that aggregate into a 1×2 matrix of shape functions when evaluated in their

natural co-ordinate system wherein $-1 \leqslant \xi \leqslant 1$, viz.,

$$\mathbf{N}(\xi) = \begin{bmatrix} N_1 & N_2 \end{bmatrix} = \begin{bmatrix} \frac{1}{2}(1-\xi) & \frac{1}{2}(1+\xi) \end{bmatrix} \tag{6.16a}$$

from which a symmetric matrix arises to become the backbone for this mass matrix (which happens to be singular), its components being

$$\mathbf{N}^{\mathsf{T}}\mathbf{N}(\xi_i) = \frac{1}{4}\begin{bmatrix} 1-2\xi_i+\xi_i^2 & 1-\xi_i^2 \\ 1-\xi_i^2 & 1+2\xi_i+\xi_i^2 \end{bmatrix} \tag{6.16b}$$

where ξ_i designates a co-ordinate for the i^{th} Gauss point associated with a specific Gauss quadrature rule for integration, which in our case comes from Table 6.1.

The determinant $|\mathbf{J}|$ of Jacobian matrix $\mathbf{J}$ is used to transform the integrals in Eqns. (6.13 & 6.14) from their natural co-ordinates into the co-ordinate system $(\vec{\boldsymbol{e}}_1, \vec{\boldsymbol{e}}_2, \vec{\boldsymbol{e}}_3)$ of a chord, cf. Fig. 5.3. Its value is

$$\mathbf{J} \equiv |\mathbf{J}| = \sum\nolimits_{i=1}^{2} N_{i,\xi}(\xi)\, x_i = -\tfrac{1}{2} \cdot -\tfrac{1}{2}L + \tfrac{1}{2} \cdot \tfrac{1}{2}L = \tfrac{1}{2}L \tag{6.17}$$

given nodal co-ordinates of $x_1 = -\frac{1}{2}L$ and $x_2 = \frac{1}{2}L$, where L is the length of our alveolar chord. The Jacobian matrix $\mathbf{J}$ and its determinant $|\mathbf{J}|$ are equivalent in the case of a rod, because this geometric space is one dimensional.

The consistent mass matrix for a 1D alveolar chord modeled as a two-noded rod, when evaluated in the co-ordinate system of the chord, becomes

$$\begin{aligned} \mathbf{M}_{\text{C1D}} &= \int_0^L \rho\, \mathbf{N}^{\mathsf{T}}\mathbf{N}\, A \,\mathrm{d}x = \int_{-1}^{1} \rho\, \mathbf{N}^{\mathsf{T}}\mathbf{N}\, A\, |\mathbf{J}| \,\mathrm{d}\xi = |\mathbf{J}| \sum_{i=1}^{m} \rho_i A_i\, \mathbf{N}^{\mathsf{T}}\mathbf{N}(\xi_i)\, w_i \\ &= \frac{L}{2} \sum_{i=1}^{m} \frac{\rho_i A_i w_i}{4} \begin{bmatrix} 1-2\xi_i+\xi_i^2 & 1-\xi_i^2 \\ 1-\xi_i^2 & 1+2\xi_i+\xi_i^2 \end{bmatrix} \end{aligned} \tag{6.18}$$

where $\mathbf{N}(\xi_i)$ is a matrix of shape functions evaluated at a node of quadrature ξ_i whose

associated weight of quadrature is w_i, both evaluated at Gauss point i for a selected Gauss integration rule comprising m Gauss points. Table 6.1 presents values for the co-ordinates ξ_i and weights w_i of quadrature where two Gauss points of integration ($m = 2$) are employed for integrating over a length of chord.

A lumped mass matrix for a 1D alveolar chord, when evaluated in the co-ordinate system of a chord is

$$\mathbf{M}_{\mathrm{L1D}} = \sum_{\text{rows}} \frac{L}{2} \sum_{i=1}^{m} \frac{\rho_i A_i w_i}{4} \begin{bmatrix} 1 - 2\xi_i + \xi_i^2 & 1 - \xi_i^2 \\ 1 - \xi_i^2 & 1 + 2\xi_i + \xi_i^2 \end{bmatrix} = \frac{L}{2} \sum_{i=1}^{m} \frac{\rho_i A_i w_i}{2} \begin{bmatrix} 1 - \xi_i & 0 \\ 0 & 1 + \xi_i \end{bmatrix}. \tag{6.19}$$

It is seen that the mass matrix in Eqn. (6.18) is singular at any given Gauss point, whereas the mass matrix in Eqn. (6.19) has a reciprocal, except whenever $\xi = \pm 1$, which are points not realized in Gaussian quadrature rules.

A chordal mass matrix that is appropriate for biologic fibers, and that associates with the Gauss quadrature rule listed in Table 6.1, has a consistent and lumped mass matrix that when averaged become

$$\mathbf{M}_{\mathrm{1D}} = \frac{\rho_1 A_1 L}{24} \begin{bmatrix} 5 + 2\sqrt{3} & 1 \\ 1 & 5 - 2\sqrt{3} \end{bmatrix} + \frac{\rho_2 A_2 L}{24} \begin{bmatrix} 5 - 2\sqrt{3} & 1 \\ 1 & 5 + 2\sqrt{3} \end{bmatrix} \tag{6.20}$$

with $\mathbf{M}_{\mathrm{1D}}$ being the 1D mass matrix that we implement. Because the mass of an alveolar chord does not change when exposed to a traveling shock wave, it follows that $\rho AL = \rho_0 A_0 L_0$, and as such, this mass matrix only needs to be evaluated once.

6.2.1.2 Assembly of Chordal Mass Matrices

In our alevolar model comprising septal chords, there are 20 nodes (vertices) whose numbering scheme and natural co-ordinates (those of a regular dodecahedron) are specified in Table 5.1. Connecting these 20 nodes are 30 line segments (septal chords) whose numbering scheme and associated nodal numbers are specified in Table 5.2.

In 3D analyses, the components M_{ij}^{1D} of mass matrix $\mathbf{M}_{\mathrm{1D}}$ from Eqn. (6.20) populate a mass matrix $\boldsymbol{M}_{\mathrm{1D}}^{(e)}$ for element e, $e \in \{1, 2, \ldots, 30\}$, accordingly

$$\boldsymbol{M}_{\mathrm{1D}}^{(e)} = \left[\begin{array}{ccc|ccc} M_{11}^{\mathrm{1D}} & 0 & 0 & M_{12}^{\mathrm{1D}} & 0 & 0 \\ 0 & 0 & 0 & 0 & 0 & 0 \\ 0 & 0 & 0 & 0 & 0 & 0 \\ \hline M_{21}^{\mathrm{1D}} & 0 & 0 & M_{22}^{\mathrm{1D}} & 0 & 0 \\ 0 & 0 & 0 & 0 & 0 & 0 \\ 0 & 0 & 0 & 0 & 0 & 0 \end{array}\right] \tag{6.21}$$

To rotate this mass matrix for an element from its co-ordinate system for a chord $(\vec{\boldsymbol{e}}_1, \vec{\boldsymbol{e}}_2, \vec{\boldsymbol{e}}_3)^{(e)}$ into the fixed co-ordinate system for a dodecahedron $(\vec{\boldsymbol{E}}_1, \vec{\boldsymbol{E}}_2, \vec{\boldsymbol{E}}_3)$, where it can be assembled with the mass matrices from the other 29 chordal elements, one must first apply the orthogonal transformation

$$\mathbf{R}_{\mathrm{1D}}^{(e)} = \left[\begin{array}{ccc|ccc} Q_{11}^{(e)} & Q_{12}^{(e)} & Q_{13}^{(e)} & 0 & 0 & 0 \\ Q_{21}^{(e)} & Q_{22}^{(e)} & Q_{23}^{(e)} & 0 & 0 & 0 \\ Q_{31}^{(e)} & Q_{32}^{(e)} & Q_{33}^{(e)} & 0 & 0 & 0 \\ \hline 0 & 0 & 0 & Q_{11}^{(e)} & Q_{12}^{(e)} & Q_{13}^{(e)} \\ 0 & 0 & 0 & Q_{21}^{(e)} & Q_{22}^{(e)} & Q_{23}^{(e)} \\ 0 & 0 & 0 & Q_{31}^{(e)} & Q_{32}^{(e)} & Q_{33}^{(e)} \end{array}\right] \tag{6.22}$$

so that, accordingly,

$$\mathbf{M}_{\mathrm{1D}}^{(e)} = \left(\mathbf{R}_{\mathrm{1D}}^{(e)}\right)^{\mathsf{T}} \boldsymbol{M}_{\mathrm{1D}}^{(e)} \mathbf{R}_{\mathrm{1D}}^{(e)} \tag{6.23}$$

where $\mathbf{M}_{\mathrm{1D}}^{(e)}$ becomes this mass matrix, transformed into a dodecahedral co-ordinate system $(\vec{\boldsymbol{E}}_1, \vec{\boldsymbol{E}}_2, \vec{\boldsymbol{E}}_3)$ with $\left[\{\vec{\boldsymbol{e}}_1\}\{\vec{\boldsymbol{e}}_2\}\{\vec{\boldsymbol{e}}_3\}\right]^{(e)} = \left[\{\vec{\boldsymbol{E}}_1\}\{\vec{\boldsymbol{E}}_2\}\{\vec{\boldsymbol{E}}_3\}\right]\left[\mathbf{Q}^{(e)}\right]$, cf. Fig. 5.3. Even though $\boldsymbol{M}_{\mathrm{1D}}^{(e)}$ is a constant mass matrix, $\mathbf{M}_{\mathrm{1D}}^{(e)}$ need not be, because $\mathbf{R}_{\mathrm{1D}}^{(e)}$ will typically vary over time in our analysis of alveoli subjected to shock waves.

We can now re-write our example equation for $\boldsymbol{f} = \mathbf{M}\ddot{\boldsymbol{u}}$ as a block matrix equation

$$\begin{Bmatrix} \boldsymbol{f}_i \\ \boldsymbol{f}_j \end{Bmatrix} = \begin{bmatrix} \mathbf{M}^{(e)}_{\text{1D:}ii} & \mathbf{M}^{(e)}_{\text{1D:}ij} \\ \mathbf{M}^{(e)}_{\text{1D:}ji} & \mathbf{M}^{(e)}_{\text{1D:}jj} \end{bmatrix} \begin{Bmatrix} \ddot{\boldsymbol{u}}_i \\ \ddot{\boldsymbol{u}}_j \end{Bmatrix}$$

wherein $\boldsymbol{f}_i = f_1^{(i)}\vec{\boldsymbol{E}}_1 + f_2^{(i)}\vec{\boldsymbol{E}}_2 + f_3^{(i)}\vec{\boldsymbol{E}}_3$, etc., where i and j are the nodal numbers for the two nodes that establish this chord.

6.2.1.3 Mass Matrix for a Pentagon

The surface of a dodecahedron is tiled with 12 pentagons, and as such, an analysis to establish a mass matrix for a pentagon becomes the building block needed to be able to assemble a 2D mass matrix $\mathbf{M}_{\text{2D}}$ representing the alveolar membranes that envelope an alveolar sac.

For an alveolar membrane, represented here as an irregular pentagon, the matrix of shape functions $\mathbf{N}(\xi, \eta)$ takes on the general form of

$$\mathbf{N} = \begin{bmatrix} N_1 & 0 & N_2 & 0 & N_3 & 0 & N_4 & 0 & N_5 & 0 \\ 0 & N_1 & 0 & N_2 & 0 & N_3 & 0 & N_4 & 0 & N_5 \end{bmatrix} \tag{6.24}$$

wherein N_i, $i = 1, \ldots, 5$, are the five shape functions that correspond with the five vertices of a pentagon. These shape functions are nonlinear functions of their co-ordinates (ξ, η), which is readily apparent in Fig. 5.6.

A consistent mass matrix $\mathbf{M}_{\text{C2D}}$ is constructed by substituting the above matrix of shape functions into the following expression

$$\mathbf{M}_{\text{C2D}} = \int_{\pentagon} \rho\, \mathbf{N}^{\mathsf{T}}\mathbf{N}\, |\mathbf{J}|\, H\, \mathrm{d}\xi\, \mathrm{d}\eta = |\mathbf{J}| \sum_{i=1}^{m} \rho_i H_i\, \mathbf{N}^{\mathsf{T}}\mathbf{N}(\xi_i, \eta_i)\, w_i \tag{6.25}$$

where m is the number of Gauss points with (ξ_i, η_i) and w_i being their respective co-ordinates and weights of quadrature that, in our implementation, are provided by Eqns. (6.4 & 6.5). As

with alveolar chords, alveolar membranes have mass densities ρ_i and heights H_i (thicknesses) that are not uniform across a membrane.

Here $|\mathbf{J}|$ is the Jacobian determinant of a 2×2 Jacobian matrix $\mathbf{J}$. In areal derivations, the Jacobian of a 2D transformation connects the physical x, y to the natural ξ, η co-ordinate systems involved. Components of this Jacobian matrix are calculated using derivatives of shape functions taken with respect to the local co-ordinates [65, pg. 424], with

$$|\mathbf{J}| = \frac{\partial x}{\partial \xi}\frac{\partial y}{\partial \eta} - \frac{\partial x}{\partial \eta}\frac{\partial y}{\partial \xi} \tag{6.26}$$

establishing the Jacobian determinant. It is proportional to the area of the pentagon $A_{\pentagon}$ because $A_{\pentagon} = \int_{\pentagon} \mathrm{d}x\,\mathrm{d}y = \int_{\pentagon} |\mathbf{J}|\,\mathrm{d}\xi\,\mathrm{d}\eta = |\mathbf{J}| \sum_{i=1}^{5} w_i = 2.378|\mathbf{J}|$ using the quadrature rule for pentagons given in Eqn. (6.5), cf. Eqn. (5.3).

6.2.1.4 Assembly of Pentagonal Mass Matrices

In the co-ordinate system of a pentagon $(\vec{\boldsymbol{e}}_1, \vec{\boldsymbol{e}}_2, \vec{\boldsymbol{e}}_3)^{(e)}$, $e \in \{1, 2, \ldots, 12\}$, a pentagon has a mass matrix with a symmetric block structure of

$$\boldsymbol{M}_{\mathrm{2D}}^{(e)} = \begin{bmatrix} \boldsymbol{M}_{11}^{\mathrm{2D}} & \boldsymbol{M}_{12}^{\mathrm{2D}} & \boldsymbol{M}_{13}^{\mathrm{2D}} & \boldsymbol{M}_{14}^{\mathrm{2D}} & \boldsymbol{M}_{15}^{\mathrm{2D}} \\ \boldsymbol{M}_{21}^{\mathrm{2D}} & \boldsymbol{M}_{22}^{\mathrm{2D}} & \boldsymbol{M}_{23}^{\mathrm{2D}} & \boldsymbol{M}_{24}^{\mathrm{2D}} & \boldsymbol{M}_{25}^{\mathrm{2D}} \\ \boldsymbol{M}_{31}^{\mathrm{2D}} & \boldsymbol{M}_{32}^{\mathrm{2D}} & \boldsymbol{M}_{33}^{\mathrm{2D}} & \boldsymbol{M}_{34}^{\mathrm{2D}} & \boldsymbol{M}_{35}^{\mathrm{2D}} \\ \boldsymbol{M}_{41}^{\mathrm{2D}} & \boldsymbol{M}_{42}^{\mathrm{2D}} & \boldsymbol{M}_{43}^{\mathrm{2D}} & \boldsymbol{M}_{44}^{\mathrm{2D}} & \boldsymbol{M}_{45}^{\mathrm{2D}} \\ \boldsymbol{M}_{51}^{\mathrm{2D}} & \boldsymbol{M}_{52}^{\mathrm{2D}} & \boldsymbol{M}_{53}^{\mathrm{2D}} & \boldsymbol{M}_{54}^{\mathrm{2D}} & \boldsymbol{M}_{55}^{\mathrm{2D}} \end{bmatrix} \tag{6.27a}$$

with each element in this matrix being a 3×3 matrix with diagonal entries of

$$\boldsymbol{M}_{ij}^{\mathrm{2D}} = \begin{bmatrix} M_{ij}^{\mathrm{2D}} & 0 & 0 \\ 0 & M_{ij}^{\mathrm{2D}} & 0 \\ 0 & 0 & 0 \end{bmatrix} \tag{6.27b}$$

whose components have values of

$$M_{ii}^{\mathrm{2D}} = \frac{|\mathbf{J}_0|}{2} \sum_{k=1}^{5} \rho_{0k} H_{0k} N_i (1 + N_i)(\xi_k, \eta_k)\, w_k \qquad i = 1, 2, \ldots, 5 \tag{6.28a}$$

$$M_{ij}^{\mathrm{2D}} = M_{ji}^{\mathrm{2D}} = \frac{|\mathbf{J}_0|}{2} \sum_{k=1}^{5} \rho_{0k} H_{0k} N_i N_j (\xi_k, \eta_k)\, w_k \qquad i \neq j \tag{6.28b}$$

with co-ordinates (ξ_i, η_i) and weights w_i of quadrature being given in Eqns. (6.4 & 6.5), and whose shape functions are defined according to Eqn. (5.16). Because the mass of an alveolar membrane is conserved when exposed to a traveling shock wave, it follows that $\rho H|\mathbf{J}| = \rho_0 H_0 |\mathbf{J}_0|$, and as such, like the mass matrices $\boldsymbol{M}_{\mathrm{1D}}^{(e)}$ and $\boldsymbol{M}_{\mathrm{3D}}^{(e)}$ for chords and tetrahedra, the mass matrix $\boldsymbol{M}_{\mathrm{2D}}^{(e)}$ for each pentagon only needs to be evaluated once.

To rotate this mass matrix for element e, $e \in \{1, 2, \ldots, 12\}$, from its elemental co-ordinate system for the pentagon $(\vec{\boldsymbol{e}}_1, \vec{\boldsymbol{e}}_2, \vec{\boldsymbol{e}}_3)^{(e)}$ into a fixed co-ordinate system for the dodecahedron $(\vec{\boldsymbol{E}}_1, \vec{\boldsymbol{E}}_2, \vec{\boldsymbol{E}}_3)$, where it can be assembled with mass matrices from the other 11 elements, one must apply the orthogonal transformation

$$\mathbf{R}_{\mathrm{2D}}^{(e)} = \begin{bmatrix} \mathbf{Q}^{(e)} & \mathbf{0} & \mathbf{0} & \mathbf{0} & \mathbf{0} \\ \mathbf{0} & \mathbf{Q}^{(e)} & \mathbf{0} & \mathbf{0} & \mathbf{0} \\ \mathbf{0} & \mathbf{0} & \mathbf{Q}^{(e)} & \mathbf{0} & \mathbf{0} \\ \mathbf{0} & \mathbf{0} & \mathbf{0} & \mathbf{Q}^{(e)} & \mathbf{0} \\ \mathbf{0} & \mathbf{0} & \mathbf{0} & \mathbf{0} & \mathbf{Q}^{(e)} \end{bmatrix} \tag{6.29a}$$

whose diagonal entries are themselves orthogonal matrices with components

$$\mathbf{Q}^{(e)} = \begin{bmatrix} Q_{11}^{(e)} & Q_{12}^{(e)} & Q_{13}^{(e)} \\ Q_{21}^{(e)} & Q_{22}^{(e)} & Q_{23}^{(e)} \\ Q_{31}^{(e)} & Q_{32}^{(e)} & Q_{33}^{(e)} \end{bmatrix} \tag{6.29b}$$

so that, accordingly,

$$\mathbf{M}_{\mathrm{2D}}^{(e)} = \left(\mathbf{R}_{\mathrm{2D}}^{(e)}\right)^{\mathsf{T}} \boldsymbol{M}_{\mathrm{2D}}^{(e)} \mathbf{R}_{\mathrm{2D}}^{(e)} \tag{6.29c}$$

where $\mathbf{M}_{\mathrm{2D}}^{(e)}$ is its mass matrix transformed into the dodecahedral co-ordinate system $(\vec{\boldsymbol{E}}_1, \vec{\boldsymbol{E}}_2, \vec{\boldsymbol{E}}_3)$ according to the map $[\{\vec{\boldsymbol{e}}_1\}\{\vec{\boldsymbol{e}}_2\}\{\vec{\boldsymbol{e}}_3\}]^{(e)} = \big[\{\vec{\boldsymbol{E}}_1\}\{\vec{\boldsymbol{E}}_2\}\{\vec{\boldsymbol{E}}_3\}\big]\big[\mathbf{Q}^{(e)}\big]$, cf. Fig. 5.4.

6.2.1.5 Mass Matrix for a Tetrahedron

The volume of a dodecahedron is filled with 60 tetrahedra, whose centroid (the origin in its natural co-ordinate system) is a common vertex among these 60 tetrahedra.

The matrix of shape functions $\mathbf{N}(\xi, \eta, \zeta)$ for a tetrahedron has a general form of

$$\mathbf{N} = \begin{bmatrix} N_1 & 0 & 0 & N_2 & 0 & 0 & N_3 & 0 & 0 & N_4 & 0 & 0 \\ 0 & N_1 & 0 & 0 & N_2 & 0 & 0 & N_3 & 0 & 0 & N_4 & 0 \\ 0 & 0 & N_1 & 0 & 0 & N_2 & 0 & 0 & N_3 & 0 & 0 & N_4 \end{bmatrix} \tag{6.30}$$

in which the N_i, $i = 1, 2, 3, 4$, are the four shape functions corresponding to the four vertices of a tetrahedron. Numerical integration is used to obtain a consistent mass matrix for a tetrahedron

$$\mathbf{M}_{\mathrm{C3D}} = \int_V \rho\, \mathbf{N}^{\mathsf{T}}\mathbf{N}\, \mathrm{d}\mathbf{z}\, \mathrm{d}\mathbf{y}\, \mathrm{d}\mathbf{x} = \int_0^1 \int_0^{1-\xi} \int_0^{1-\xi-\eta} \rho\, \mathbf{N}^{\mathsf{T}}\mathbf{N}\, |\mathbf{J}|\, \mathrm{d}\zeta\, \mathrm{d}\eta\, \mathrm{d}\xi = \rho\, |\mathbf{J}| \sum_{i=1}^{m} \mathbf{N}^{\mathsf{T}}\mathbf{N}(\xi_i, \eta_i, \zeta_i)\, w_i \tag{6.31}$$

where $|\mathbf{J}|$ is the determinant of the Jacobian matrix $\mathbf{J}$, with m being the number of Gauss points used for spatial integration, which in our case is four. The co-ordinates (ξ_i, η_i, ζ_i) and weights w_i of quadrature used for integrating over the volume of a tetrahedron are found in Table 6.3. The Jacobian is calculated from taking derivatives of the shape functions with respect to their local co-ordinates (ξ, η, ζ), cf. Ref. [65, pg. 424], whose determinant $|\mathbf{J}|$ is proportional to the volume of this element when evaluated in the physical co-ordinate system $(\vec{\boldsymbol{E}}_1, \vec{\boldsymbol{E}}_2, \vec{\boldsymbol{E}}_3)$. Specifically, $|\mathbf{J}| = 6V_{tet}$ because $V_{tet} = \int_{V_{tet}} \mathrm{d}z\, \mathrm{d}y\, \mathrm{d}x = \int_0^1 \int_0^{1-\xi} \int_0^{1-\xi-\eta} |\mathbf{J}|\, \mathrm{d}\zeta\, \mathrm{d}\eta\, \mathrm{d}\xi = |\mathbf{J}| \sum_{i=1}^{m} w_i = \frac{1}{6}|\mathbf{J}|$.

6.2.1.6 Assembly of Tetrahedral Mass Matrices

In our finite element model for an alveolar sac, there are 21 nodes (20 vertices and the origin) whose numbering scheme and natural co-ordinates are given in Table 5.1. Filling

this volume are 60 tetrahedra whose numbering scheme and associated nodal numbers are specified according to the following strategy. Associated with any given pentagon are 5 tetrahedra. Nodes 1 and 4 of these five tetrahedra are the same. Node 1 is at the centroid of the pentagon, and node 4 is at the origin of the dodecahedron. Nodes 2 and 3 of the tetrahedron are also nodes of this pentagon, and are sequenced such that when traversing nodes $1 \rightarrow 2 \rightarrow 3$ of a tetrahedron one undergoes a counterclockwise path when viewed looking inward from outside of the dodecahedron. In the co-ordinate system of a tetrahedron $(\vec{\boldsymbol{e}}_1, \vec{\boldsymbol{e}}_2, \vec{\boldsymbol{e}}_3)^{(e)}$, a tetrahedron has a mass matrix with a symmetric block structure of

$$\boldsymbol{M}_{3\mathrm{D}}^{(e)} = \begin{bmatrix} \boldsymbol{M}_{11}^{3\mathrm{D}} & \boldsymbol{M}_{12}^{3\mathrm{D}} & \boldsymbol{M}_{13}^{3\mathrm{D}} & \boldsymbol{M}_{14}^{3\mathrm{D}} \\ \boldsymbol{M}_{21}^{3\mathrm{D}} & \boldsymbol{M}_{22}^{3\mathrm{D}} & \boldsymbol{M}_{23}^{3\mathrm{D}} & \boldsymbol{M}_{24}^{3\mathrm{D}} \\ \boldsymbol{M}_{31}^{3\mathrm{D}} & \boldsymbol{M}_{32}^{3\mathrm{D}} & \boldsymbol{M}_{33}^{3\mathrm{D}} & \boldsymbol{M}_{34}^{3\mathrm{D}} \\ \boldsymbol{M}_{41}^{3\mathrm{D}} & \boldsymbol{M}_{42}^{3\mathrm{D}} & \boldsymbol{M}_{43}^{3\mathrm{D}} & \boldsymbol{M}_{44}^{3\mathrm{D}} \end{bmatrix} \tag{6.32a}$$

with each element in this matrix being a 3×3 matrix with diagonal entries of

$$\boldsymbol{M}_{ij}^{3\mathrm{D}} = \begin{bmatrix} M_{ij}^{3\mathrm{D}} & 0 & 0 \\ 0 & M_{ij}^{3\mathrm{D}} & 0 \\ 0 & 0 & M_{ij}^{3\mathrm{D}} \end{bmatrix} \tag{6.32b}$$

whose components have values of

$$M_{ii}^{3\mathrm{D}} = \frac{\rho_0 |\mathbf{J}_0|}{2} \sum_{k=1}^{4} N_i(1 + N_i)(\xi_k, \eta_k, \zeta_k)\, w_k \qquad i = 1, 2, 3, 4 \tag{6.33a}$$

$$M_{ij}^{3\mathrm{D}} = M_{ji}^{3\mathrm{D}} = \frac{\rho_0 |\mathbf{J}_0|}{2} \sum_{k=1}^{4} N_i N_j(\xi_k, \eta_k, \zeta_k)\, w_k \qquad i \neq j \tag{6.33b}$$

with co-ordinates (ξ_i, η_i, ζ_i) and weights w_i of quadrature being given in Table 6.3. Here we consider that mass is conserved over the volume of each element, and as such, $\rho|\mathbf{J}| = \rho_0|\mathbf{J}_0|$.

To rotate this mass matrix for element e, $e \in \{1, 2, \ldots, 60\}$, from its elemental co-ordinate

system for the tetrahedron $(\vec{\boldsymbol{e}}_1, \vec{\boldsymbol{e}}_2, \vec{\boldsymbol{e}}_3)^{(e)}$ into a fixed co-ordinate system for the dodecahedron $(\vec{\boldsymbol{E}}_1, \vec{\boldsymbol{E}}_2, \vec{\boldsymbol{E}}_3)$, where it can be assembled with mass matrices from the other 59 elements, one must apply the orthogonal transformation

$$\mathbf{R}_{3\mathrm{D}}^{(e)} = \begin{bmatrix} \mathbf{Q}^{(e)} & \mathbf{0} & \mathbf{0} & \mathbf{0} \\ \mathbf{0} & \mathbf{Q}^{(e)} & \mathbf{0} & \mathbf{0} \\ \mathbf{0} & \mathbf{0} & \mathbf{Q}^{(e)} & \mathbf{0} \\ \mathbf{0} & \mathbf{0} & \mathbf{0} & \mathbf{Q}^{(e)} \end{bmatrix} \tag{6.34a}$$

whose diagonal entries are themselves orthogonal matrices with components

$$\mathbf{Q}^{(e)} = \begin{bmatrix} Q_{11}^{(e)} & Q_{12}^{(e)} & Q_{13}^{(e)} \\ Q_{21}^{(e)} & Q_{22}^{(e)} & Q_{23}^{(e)} \\ Q_{31}^{(e)} & Q_{32}^{(e)} & Q_{33}^{(e)} \end{bmatrix} \tag{6.34b}$$

so that, accordingly,

$$\mathbf{M}_{3\mathrm{D}}^{(e)} = \left(\mathbf{R}_{3\mathrm{D}}^{(e)}\right)^{\mathsf{T}} \boldsymbol{M}_{3\mathrm{D}}^{(e)} \mathbf{R}_{3\mathrm{D}}^{(e)} \tag{6.34c}$$

where $\mathbf{M}_{3\mathrm{D}}^{(e)}$ is its mass matrix transformed into the dodecahedral co-ordinate system $(\vec{\boldsymbol{E}}_1, \vec{\boldsymbol{E}}_2, \vec{\boldsymbol{E}}_3)$ according to the map $[\{\vec{\boldsymbol{e}}_1\}\{\vec{\boldsymbol{e}}_2\}\{\vec{\boldsymbol{e}}_3\}]^{(e)} = \big[\{\vec{\boldsymbol{E}}_1\}\{\vec{\boldsymbol{E}}_2\}\{\vec{\boldsymbol{E}}_3\}\big]\big[\mathbf{Q}^{(e)}\big]$. Even though $\boldsymbol{M}_{3\mathrm{D}}^{(e)}$ is a constant mass matrix, $\mathbf{M}_{3\mathrm{D}}^{(e)}$ need not be, because $\mathbf{R}_{3\mathrm{D}}^{(e)}$ will typically vary over time in our analysis of alveoli subjected to shock waves.

6.2.2 Constitutive Models for Finite Elements

In this study, we implement implicit, elastic, material models. Consequently, their elastic compliance $\boldsymbol{\mathcal{C}}$ and modulus $\boldsymbol{\mathcal{M}}$, where $\boldsymbol{\mathcal{M}} := \boldsymbol{\mathcal{C}}^{-1}$, are taken to be functions of both strain *and* stress in a manner that is consistent with thermodynamics. Furthermore, the conjugate response between temperature and entropy is not incorporated into our finite element solution strategy, because changes in entropy caused by elastic deformations have been shown

to be negligible in our application. As such, one can write down the governing constitutive equations for use in finite elements as

$$\boldsymbol{E} = \boldsymbol{\mathcal{C}}^s(\boldsymbol{E},\boldsymbol{T}) \cdot (\boldsymbol{T} - \boldsymbol{T}_0) \tag{6.35a}$$

$$\boldsymbol{T} = \boldsymbol{T}_0 + \boldsymbol{\mathcal{M}}^s(\boldsymbol{E},\boldsymbol{T}) \cdot \boldsymbol{E} \tag{6.35b}$$

where $\boldsymbol{T}_0$ is an initial (residual) stress at zero strain, and where $\boldsymbol{\mathcal{C}}^s$ and $\boldsymbol{\mathcal{M}}^s$ are the secant compliance and secant modulus, respectively, obeying $\boldsymbol{\mathcal{M}}^s = (\boldsymbol{\mathcal{C}}^s)^{-1}$. Written symbolically, $\boldsymbol{\mathcal{C}}^s = \boldsymbol{E}/(\boldsymbol{T} - \boldsymbol{T}_0)$ and $\boldsymbol{\mathcal{M}}^s = (\boldsymbol{T} - \boldsymbol{T}_0)/\boldsymbol{E}$.

Expressing these constitutive equations in differential form, one can write

$$\mathrm{d}\boldsymbol{E} = \boldsymbol{\mathcal{C}}^t(\boldsymbol{E},\boldsymbol{T}) \cdot \mathrm{d}\boldsymbol{T} \tag{6.35c}$$

$$\mathrm{d}\boldsymbol{T} = \boldsymbol{\mathcal{M}}^t(\boldsymbol{E},\boldsymbol{T}) \cdot \mathrm{d}\boldsymbol{E} \tag{6.35d}$$

where $\boldsymbol{\mathcal{C}}^t$ and $\boldsymbol{\mathcal{M}}^t$ are the tangent compliance and tangent modulus, respectively, obeying $\boldsymbol{\mathcal{M}}^t = (\boldsymbol{\mathcal{C}}^t)^{-1}$. Written symbolically, $\boldsymbol{\mathcal{C}}^t = \mathrm{d}\boldsymbol{E}/\mathrm{d}\boldsymbol{T}$ and $\boldsymbol{\mathcal{M}}^t = \mathrm{d}\boldsymbol{T}/\mathrm{d}\boldsymbol{E}$. The components from these elastic compliance and moduli relate to one another via

$$\mathcal{C}^t_{ij} = \left(I_{ik} - \frac{\partial \mathcal{C}^s_{i\ell}}{\partial E_k}\,(T_\ell - T_{0\,\ell})\right)^{-1} \left(\mathcal{C}^s_{kj} + \frac{\partial \mathcal{C}^s_{k\ell}}{\partial T_j}(T_\ell - T_{0\,\ell})\right) \tag{6.35e}$$

$$\mathcal{M}^t_{ij} = \left(I_{ik} - \frac{\partial \mathcal{M}^s_{i\ell}}{\partial T_k}\,E_\ell\right)^{-1} \left(\mathcal{M}^s_{kj} + \frac{\partial \mathcal{M}^s_{k\ell}}{\partial E_j}\,E_\ell\right) \tag{6.35f}$$

that, because $\boldsymbol{\mathcal{M}}^t = (\boldsymbol{\mathcal{C}}^t)^{-1}$, enables one to write

$$\mathcal{M}^t_{ij} = \left(\mathcal{C}^s_{ik} + \frac{\partial \mathcal{C}^s_{i\ell}}{\partial T_k}\,(T_\ell - T_{0\,\ell})\right)^{-1} \left(I_{kj} - \frac{\partial \mathcal{C}^s_{k\ell}}{\partial E_j}\,(T_\ell - T_{0\,\ell})\right) \tag{6.35g}$$

and therefore we observe that if $\boldsymbol{\mathcal{C}}^s(\boldsymbol{E},\boldsymbol{T})$ and $\boldsymbol{T}_0$ are known, then $\boldsymbol{\mathcal{M}}^s$, $\boldsymbol{\mathcal{C}}^t$ and $\boldsymbol{\mathcal{M}}^t$ can all be determined in terms of this secant compliance and initial stress. It is the moduli $\boldsymbol{\mathcal{M}}^s$ and $\boldsymbol{\mathcal{M}}^t$ that appear later in our finite element equations (6.52).

In finite element implementations, strain $\boldsymbol{E}$ and stress $\boldsymbol{T}$ are treated as vectors of size $\ell\times 1$, while the compliance $\boldsymbol{\mathcal{C}}^s$ and $\boldsymbol{\mathcal{C}}^t$ and the moduli $\boldsymbol{\mathcal{M}}^s$ and $\boldsymbol{\mathcal{M}}^t$ are each matrices of size $\ell\times\ell$, where ℓ denotes the number of independent stress/strain attribute pairs that there are.

6.2.2.1 Moduli for a Chord

Alveolar chords comprising collagen and elastin fibers are loaded in parallel. Consequently, they are exposed to the same axial strain of $e = \ln(L/L_0)$ but carry different stresses s^c and s^e, where ^{c} is for collagen and ^{e} is for elastin. The rule of mixtures is used to average their individual responses into a collective chordal response. Specifically, the chordal, elastic, secant modulus is described by the averaged response

$$E^s := \phi\, E^c_s + (1-\phi)E^e_s \tag{6.36a}$$

while the chordal, elastic, secant compliance is described by the averaged response

$$C^s = \frac{C^c_s\, C^e_s}{\phi\, C^e_s + (1-\phi)C^c_s}. \tag{6.36b}$$

Consequently, the chordal, elastic, secant modulus $\boldsymbol{\mathcal{M}}^s$ becomes

$$\mathcal{M}^s = \phi/C^c_s + (1-\phi)/C^e_s. \tag{6.36c}$$

Given the constitutive equation $s = s_0 + E^s e$, it follows that the stresses average as

$$s_0 := \phi\, s^c_0 + (1-\phi)s^e_0 \quad \text{and} \quad s := \phi\, s^c + (1-\phi)s^e \tag{6.36d}$$

because these fibers experience the same strain. The collagen, fiber, volume fraction ϕ that does this partitioning is established by

$$\phi := A^c_0/(A^c_0 + A^e_0) \tag{6.36e}$$

where the cross-sectional area of a chord is the sum of cross-sectional areas for its collagen A_0^c and elastin A_0^e fibers, here evaluated in a reference state.

The secant compliance C^s that we apply to the collagen and elastin fibers in an alveolar chord are derived in Appendix D, cf. Eqn. (D.9). This model, under isothermal conditions, describes an elastic secant compliance for collagen of

$$C_s^c(s^c) = \frac{e^c_{1_{\max}}}{s^c - s_0^c}\left(1 - \frac{\sqrt{E_1^c e^c_{1_{\max}}}}{\sqrt{E_1^c e^c_{1_{\max}} + 2(s^c - s_0^c)}}\right) + \frac{1}{E_2^c} \tag{6.37a}$$

and an elastic secant compliance for elastin of

$$C_s^e(s^e) = \frac{e^e_{1_{\max}}}{s^e - s_0^e}\left(1 - \frac{\sqrt{E_1^e e^e_{1_{\max}}}}{\sqrt{E_1^e e^e_{1_{\max}} + 2(s^e - s_0^e)}}\right) + \frac{1}{E_2^e} \tag{6.37b}$$

whose inverses, viz., $E_s^c := 1/C_s^c$ and $E_s^e := 1/C_s^e$, are their secant moduli, which are defined in accordance with Eqns. (6.35a & 6.35b), and as such, $s^c = s_0^c + E_s^c e$ and $s^e = s_0^e + E_s^e e$. The material properties associated with collagen fibers are: a soft initial modulus E_1^c, a stiff terminal modulus E_2^c, and their strain of transition $e^c_{1_{\max}}$, with like material properties describing an elastin fiber. Whenever $s^c < s_0^c$, the elastic modulus for collagen is taken to be its modulus at zero strain, i.e., $E_s^c = E_1^c E_2^c/(E_1^c + E_2^c)$ so that $C_s^c = (E_1^c + E_2^c)/E_1^c E_2^c$. The elastic fiber compliance in Eqn. (6.37) depend only upon stress, not upon strain, and as such the elastic tangent modulus $\boldsymbol{\mathcal{M}}^t$ of Eqn. (6.35g), which is one of two moduli we use in our finite element implementation, reduces in this 1D case to

$$\mathcal{M}^t = \left(\mathcal{C}^s + \frac{\partial\, \mathcal{C}^s}{\partial s}\,(s - s_0)\right)^{-1} \tag{6.38a}$$

where C^s is given by Eqn. (6.36b), whose individual compliance C_s^c and C_s^e are described by Eqn. (6.37), and whose derivatives are determined to be

$$\frac{\partial\, \mathcal{C}^s}{\partial s} = \frac{\partial}{\partial s^c}\frac{\mathcal{C}_s^c(s^c)\,\mathcal{C}_s^e(s^e)}{\phi\,\mathcal{C}_s^e(s^e) + (1-\phi)\,\mathcal{C}_s^c(s^c)}\left(\frac{\partial s}{\partial s^c}\right)^{-1} + \frac{\partial}{\partial s^e}\frac{\mathcal{C}_s^c(s^c)\,\mathcal{C}_s^e(s^e)}{\phi\,\mathcal{C}_s^e(s^e) + (1-\phi)\,\mathcal{C}_s^c(s^c)}\left(\frac{\partial s}{\partial s^e}\right)^{-1} \tag{6.38b}$$

which follow from Eqn. (6.37).

6.2.2.2 Moduli for a Pentagon

The secant response of an isothermal, isochoric, elastic pentagon can be written in terms of Eqn. (6.35a),whose constitutive behavior is established through an elastic modulus $\boldsymbol{\mathcal{M}}^s$ such that

$$\underbrace{\begin{Bmatrix} s^\pi \\ s^\sigma \\ s^\tau \end{Bmatrix}}_{\boldsymbol{T}} = \underbrace{\begin{Bmatrix} s_0^\pi \\ 0 \\ 0 \end{Bmatrix}}_{\boldsymbol{T}_0} + \underbrace{\begin{bmatrix} 4M^s & 0 & 0 \\ 0 & 4M^s/3 & 0 \\ 0 & 0 & G^s \end{bmatrix}}_{\boldsymbol{\mathcal{M}}^s} \underbrace{\begin{Bmatrix} \xi \\ \varepsilon \\ \gamma \end{Bmatrix}}_{\boldsymbol{E}} \tag{6.39}$$

which is used in our finite element implementation. This strain vector $\boldsymbol{E}$ has elements denoting a dilation $\xi = \ln\sqrt{ab/a_0b_0}$, a squeeze (pure shear) $\varepsilon = \ln\sqrt{ab_0/a_0b}$, and a (simple) shear $\gamma = g - g_0$, which in turn are described in terms of two elongations a and b plus an in-plane shear g, with their reference values being a_0, b_0 and g_0.

The stress vector $\boldsymbol{T} = \{s^\pi, s^\sigma, s^\tau\}^\mathsf{T}$ conjugate to strain vector $\boldsymbol{E} = \{\xi, \varepsilon, \gamma\}^\mathsf{T}$ has elements of a surface tension $s^\pi = \mathcal{S}_{11} + \mathcal{S}_{22}$, a normal-stress difference $s^\sigma = \mathcal{S}_{11} - \mathcal{S}_{22}$, and a shear stress $s^\tau = \frac{a}{b}\,\mathcal{S}_{12}$. Only surface tension is considered to have a residual state of stress s_0^π, which is necessary for alveolar stability, and is caused, in part, by the presence of surfactant. In a reciprocal sense, the stress components are assigned via $\mathcal{S}_{11} = \frac{1}{2}(s^\pi + s^\sigma)$, $\mathcal{S}_{22} = \frac{1}{2}(s^\pi - s^\sigma)$ and $\mathcal{S}_{12} = \mathcal{S}_{21} = \frac{b}{a}s^\tau$ such that $\mathbf{S} = \mathbf{P}\boldsymbol{\mathcal{U}}^{-1}\boldsymbol{\mathcal{S}}\boldsymbol{\mathcal{U}}^{-\mathsf{T}}\mathbf{P}^\mathsf{T}$ with $\mathbf{S}$ being the second Piola–Kirchhoff stress evaluated in the co-ordinate system of a pentagon, while $\boldsymbol{\mathcal{U}}$ is the Laplace stretch, and $\mathbf{P}$ is a re-indexer of co-ordinate labeling needed to ensure invariance under a transformation of Laplace stretch.

The elastic compliance governing an isothermal dilation response is

$$\frac{1}{4M^s(s^\pi)} = \frac{\xi_{1_{\max}}}{s^\pi - s_0^\pi}\left(1 - \frac{\sqrt{M_1\xi_{1_{\max}}}}{\sqrt{M_1\xi_{1_{\max}} + \frac{1}{2}(s^\pi - s_0^\pi)}}\right) + \frac{1}{4M_2} \tag{6.40a}$$

where $M^s(s^\pi \leqslant s_0^\pi) = M_1 M_2/(M_1 + M_2)$. The elastic compliance governing shear response is

$$\frac{1}{G^s(s^\tau)} = \frac{\gamma_{1_{\max}}}{|s^\tau|}\left(1 - \frac{\sqrt{G_1\gamma_{1_{\max}}}}{\sqrt{G_1\gamma_{1_{\max}} + 2|s^\tau|}}\right) + \frac{1}{G_2} \tag{6.40b}$$

where $G^s(s^\tau = 0) = G_1 G_2/(G_1 + G_2)$. Like the fiber compliance used to model an alveolar chord, the membrane compliance used to model an alveolar septa has components that depend upon stress, but not upon strain. Consequently, the tangent modulus is

$$\boldsymbol{\mathcal{M}}^t = \begin{bmatrix} \frac{1}{4M^s} + (s^\pi - s_0^\pi)\frac{\mathrm{d}(1/4M^s)}{\mathrm{d}s^\pi} & 0 & 0 \\ 0 & \frac{3}{4M^s} + (s^\pi - s_0^\pi)\frac{\mathrm{d}(3/4M^s)}{\mathrm{d}s^\pi} & 0 \\ 0 & 0 & \frac{1}{G^s} + s^\tau\frac{\mathrm{d}(1/G^s)}{\mathrm{d}s^\tau} \end{bmatrix}^{-1} \tag{6.41}$$

whose entries, taking into account Eqn. (6.40), are determined to be

$$\frac{1}{4M^s} + (s^\pi - s_0^\pi)\frac{\mathrm{d}(1/4M^s)}{\mathrm{d}s^\pi} = \frac{\xi_{1_{\max}}\sqrt{M_1\xi_{1_{\max}}}}{4\big(M_1\xi_{1_{\max}} + \frac{1}{2}(s^\pi + s_0^\pi)\big)^{3/2}} + \frac{1}{4M_2} \tag{6.42a}$$

$$\frac{1}{G^s} + s^\tau\frac{\mathrm{d}(1/G^s)}{\mathrm{d}s^\tau} = \frac{\gamma_{1_{\max}}\sqrt{G_1\gamma_{1_{\max}}}}{(G_1\gamma_{1_{\max}} + 2|s^\tau|)^{3/2}} + \frac{1}{G_2} \tag{6.42b}$$

and as such, our implementation becomes quite straightforward.

6.2.2.3 Moduli for a Tetrahedron

The isothermal response of a volume element located within an alveolar sac will have a secant response governed by

$$\underbrace{\begin{Bmatrix} \Pi \\ \sigma_1 \\ \sigma_2 \\ \tau_1 \\ \tau_2 \\ \tau_3 \end{Bmatrix}}_{\boldsymbol{T}} = \underbrace{\begin{Bmatrix} \Pi_0 \\ 0 \\ 0 \\ 0 \\ 0 \\ 0 \end{Bmatrix}}_{\boldsymbol{T}_0} + \underbrace{\begin{bmatrix} 9K & 0 & 0 & 0 & 0 & 0 \\ 0 & 3N & -\frac{3}{2}N & 0 & 0 & 0 \\ 0 & -\frac{3}{2}N & 3N & 0 & 0 & 0 \\ 0 & 0 & 0 & G & 0 & 0 \\ 0 & 0 & 0 & 0 & G & 0 \\ 0 & 0 & 0 & 0 & 0 & G \end{bmatrix}}_{\boldsymbol{\mathcal{M}}^s} \underbrace{\begin{Bmatrix} \Xi \\ \varepsilon_1 \\ \varepsilon_2 \\ \gamma_1 \\ \gamma_2 \\ \gamma_3 \end{Bmatrix}}_{\boldsymbol{E}} \tag{6.43}$$

where, for air, only the bulk modulus K is non-zero. The strain vector $\boldsymbol{E} = \{\Xi, \varepsilon_1, \varepsilon_2, \gamma_1, \gamma_2, \gamma_3\}^{\mathsf{T}}$ has elements that denote a dilatation $\Xi = \ln \sqrt[3]{abc/a_0b_0c_0}$, two separate squeezes (pure shears) $\varepsilon_1 = \ln \sqrt[3]{ab_0/a_0b}$ and $\varepsilon_2 = \ln \sqrt[3]{bc_0/b_0c}$, and three separate (simple) shears $\gamma_1 = \alpha - \alpha_0$, $\gamma_2 = \beta - \beta_0$, and $\gamma_3 = \gamma - \gamma_0$. The stress vector $\boldsymbol{T} = \{\Pi, \sigma_1, \sigma_2, \tau_1, \tau_2, \tau_3\}^{\mathsf{T}}$ conjugate to strain $\boldsymbol{E}$ has elements that comprise a pressure $\Pi = \mathcal{S}_{11} + \mathcal{S}_{22} + \mathcal{S}_{33} = -3P$ where P denotes the common definition for pressure, two separate normal-stress differences $\sigma_1 = \mathcal{S}_{11} - \mathcal{S}_{22}$ and $\sigma_2 = \mathcal{S}_{22} - \mathcal{S}_{33}$, and three separate shear stresses $\tau_1 = \frac{b}{c}\mathcal{S}_{32}$, $\tau_2 = \frac{a}{c}\mathcal{S}_{31}$ and $\tau_3 = \frac{a}{b}\mathcal{S}_{21} - \alpha\tau_2$. Of these, only pressure has an initial value, viz., Π_0, which represents atmospheric pressure. Moduli K, N, and G are considered to be constants in our modeling of an alveolar sac; therefore, $\boldsymbol{\mathcal{M}}^t = \boldsymbol{\mathcal{M}}^s$ when modeling alveolar volumes.

6.2.3 Stiffness Matrices

6.2.3.1 Strain-Displacement Matrices

Finite element techniques introduce a matrix $\mathbf{B}$ that transforms nodal displacements $\boldsymbol{u}^{(e)}$ for an element e into a vector of thermodynamic strains $\boldsymbol{E}$ located at a Gauss point via

$$\boldsymbol{E} = \mathbf{B}\,\boldsymbol{u}^{(e)} \tag{6.44}$$

where $\boldsymbol{E}$ has size $\ell \times 1$, $\mathbf{B}$ has size $\ell \times nd$, and $\boldsymbol{u}^{(e)}$ has size $nd \times 1$. Here: d is the spatial dimension of an element (viz., $d = 1, 2$ or 3 that, in our case, associate with a chord, a pentagon, and a tetrahedron, respectively); ℓ is the number of conjugate pairs appropriate for an element (viz., $\ell = 1, 3$ or 6 that, in our case, associate with a chord, a pentagon, and a tetrahedron, respectively); while n is the number of nodes in an element (viz., $n = 2, 5$ or 4 that, in our case, associate with a chord, a pentagon, and a tetrahedron, respectively).

In order to make our computation more systematic, the strain-displacement matrix $\mathbf{B}$ is taken to additively decompose into linear and nonlinear constituents such that

$$\mathbf{B} = \mathbf{B}_L + \mathbf{B}_N \tag{6.45a}$$

where the entries in $\mathbf{B}_L$ are constants, while the entries in $\mathbf{B}_N$ are functions of displacement. Hence, this decomposition allows linear and nonlinear strain constituents to be

$$\boldsymbol{E}_L := \mathbf{B}_L\,\boldsymbol{u}^{(e)} \quad \text{and} \quad \boldsymbol{E}_N := \mathbf{B}_N\,\boldsymbol{u}^{(e)} \tag{6.45b}$$

which $\boldsymbol{E} = \boldsymbol{E}_L + \boldsymbol{E}_N$. Their associated derivatives, taken with respect to displacement, produce the formulæ

$$\mathrm{d}\boldsymbol{E}_L = \mathbf{B}_L\,\mathrm{d}\boldsymbol{u}^{(e)} \quad \because \quad \mathrm{d}\mathbf{B}_L = \mathbf{0} \tag{6.45c}$$

$$\mathrm{d}\boldsymbol{E}_N = \mathbf{B}_N\,\mathrm{d}\boldsymbol{u}^{(e)} + \mathrm{d}\mathbf{B}_N\,\boldsymbol{u}^{(e)} \tag{6.45d}$$

which obey $\mathrm{d}\boldsymbol{E} = \mathrm{d}\boldsymbol{E}_L + \mathrm{d}\boldsymbol{E}_N$ and $\mathrm{d}\mathbf{B} = \mathrm{d}\mathbf{B}_N$ so that $\mathrm{d}\boldsymbol{E} = \mathbf{B}\,\mathrm{d}\boldsymbol{u}^{(e)} + \mathrm{d}\mathbf{B}\,\boldsymbol{u}^{(e)}$. This differential equation reduces to the classic result $\mathrm{d}\boldsymbol{E} = \mathbf{B}\,\mathrm{d}\boldsymbol{u}^{(e)}$ found in the finite element literature whenever the total displacements are infinitesimal in extent, under which conditions $\mathbf{B}_N \approx \mathbf{0}$ and $\mathbf{dB}_N \approx \mathbf{0}$. It is advantageous for us to re-write this nonlinear strain-displacement relation $\mathbf{B}_N$ as a product between two matrices such that

$$\mathbf{B}_N = \mathbf{A}\,\mathbf{H} \tag{6.46a}$$

where matrix $\mathbf{A}$ has size $\ell \times d$, while matrix $\mathbf{H}$ has size $d \times nd$, with $\mathbf{A}$ being comprised of various displacement gradients, and $\mathbf{H}$ being comprised of derivatives of shape functions taken in the element's co-ordinate system, and as such

$$\mathrm{d}\mathbf{B}_N = \mathrm{d}\mathbf{A} \cdot \mathbf{H} \quad \because \quad \mathrm{d}\mathbf{H} = \mathbf{0}. \tag{6.46b}$$

As a consequence of this definition, at least for the elements of interest to us, it turns out that one can establish another useful relationship, specifically

$$\mathrm{d}\mathbf{A}^{\mathsf{T}}\,\boldsymbol{T} = \mathbf{S}\,\mathbf{H}\,\mathrm{d}\boldsymbol{u}^{(e)} \tag{6.46c}$$

wherein $\mathbf{S}$ is a symmetric matrix of size $d \times d$ whose components come from those of its conjugate stress vector $\boldsymbol{T}$ of size $\ell \times 1$.

6.2.3.2 Secant Stiffness Matrix

For nonlinear elastic materials, like soft tissues, their stress/strain response curves generally become stiffer with increasing deformation. Consequently, the slope of a line segment connecting the origin with its current stress/strain state, located somewhere along its response curve, will change with a change in stress and strain, and therefore, its secant modulus will necessarily be a function of stress and/or strain.

A variation in the residual energy R of a deformed elastic body is the difference between variations from two energy sources, assuming a simply connected body whose motion maps have sufficient smoothness, etc. These energies are: a potential energy U that stores an internal strain energy, and a work done W that expends energy through an external loading, specifically

$$\delta R = \delta U - \delta W \tag{6.47a}$$

such that for an element e one has [66]

$$\delta W = \sum\nolimits_e \boldsymbol{F} \cdot \delta \boldsymbol{u}^{(e)} \tag{6.47b}$$

$$\delta U = \sum\nolimits_e \int_V \mathbf{B}^{\mathsf{T}} \boldsymbol{T} \, \mathrm{d}V \cdot \delta \boldsymbol{u}^{(e)} \tag{6.47c}$$

or alternatively

$$\delta R = \sum\nolimits_e \boldsymbol{R} \cdot \delta \boldsymbol{u}^{(e)} = \sum\nolimits_e \left(\int_V \mathbf{B}^{\mathsf{T}} \boldsymbol{T} \, \mathrm{d}V - \boldsymbol{F} \right) \cdot \delta \boldsymbol{u}^{(e)} \tag{6.47d}$$

where $\boldsymbol{F}$ and $\boldsymbol{R}$ are vectors denoting the external and residual forces, respectively, while $\boldsymbol{T}$ is a stress conjugate to strain $\boldsymbol{E}$, which are represented here as vector fields, with $\mathbf{B}$ being the well-known strain-displacement matrix found in Eqn. (6.44).

In order to satisfy equilibrium, the internal and external forces of Eqn. (6.47) must be in balance, and therefore, for each element [67]

$$\boldsymbol{R} = \int_V \mathbf{B}^\mathsf{T}\,\boldsymbol{T}\,\mathrm{d}V - \boldsymbol{F} = \mathbf{0} \tag{6.48a}$$

whose solution is typically achieved through an iterative process. Substituting the secant constitutive equation Eqn. (6.35b) along with the strain-displacement relationship of Eqn. (6.44) into the above integral allows it to be re-written as

$$\int_V \mathbf{B}^\mathsf{T}\,\boldsymbol{T}\,\mathrm{d}V = \int_V \mathbf{B}^\mathsf{T}\,\boldsymbol{T}_0\,\mathrm{d}V + \int_V \mathbf{B}^\mathsf{T}\,\boldsymbol{\mathcal{M}}^s\,\boldsymbol{E}\,\mathrm{d}V = \underbrace{\int_V \mathbf{B}^\mathsf{T}\,\boldsymbol{T}_0\,\mathrm{d}V}_{\boldsymbol{F}_0} + \underbrace{\int_V \mathbf{B}^\mathsf{T}\,\boldsymbol{\mathcal{M}}^s\,\mathbf{B}\,\mathrm{d}V}_{\mathbf{K}^s}\,\boldsymbol{u}^{(e)} \tag{6.48b}$$

where $\mathbf{K}^s$ is a stiffness matrix built around the secant modulus $\boldsymbol{\mathcal{M}}^s$, and $\boldsymbol{F}_0$ is an internal force accounting for an initial residual stress of $\boldsymbol{T}_0$. Here $\mathbf{B}$ and $\boldsymbol{\mathcal{M}}^s$ are evaluated at current time t_i, i.e., at the beginning of an integration step.

6.2.3.3 Tangent Stiffness Matrix

Motivated by a definition for the tangent stiffness matrix being $\mathbf{C} := \mathrm{d}\boldsymbol{R}/\mathrm{d}\boldsymbol{u}$ that, e.g., would be appropriate for an updated-Lagrangian finite element formulation, [68] we differentiate Eqn. (6.47d) to get $\mathrm{d}\delta R = \delta \mathrm{d}R = \mathrm{d}\boldsymbol{R}\cdot\delta\boldsymbol{u}^{(e)}$ from which one gets

$$\mathrm{d}\boldsymbol{R} = \int_V \mathrm{d}\mathbf{B}^\mathsf{T}\,\boldsymbol{T}\,\mathrm{d}V + \int_V \mathbf{B}^\mathsf{T}\,\mathrm{d}\boldsymbol{T}\,\mathrm{d}V =: \mathbf{C}\,\mathrm{d}\boldsymbol{u}^{(e)} \tag{6.49}$$

which follows because the external force $\boldsymbol{F}$ is considered to be a fixed boundary condition during a variation in its displacements. This equation establishes that a change in residual force $\mathrm{d}\boldsymbol{R}$ is needed to further deform an elastic body from an equilibrium condition $\boldsymbol{R} = \mathbf{0}$ that exists at current time t_i into another equilibrium state associated with some future moment in time $t_{i+1} = t_i + \mathrm{d}t$. This differential force depends upon both the stress $\boldsymbol{T}$ at

time t_i and its change $\mathrm{d}\boldsymbol{T}$ that occurs when advancing from t_i to t_{i+1}.

Substituting constitutive equation (6.35b) for $\boldsymbol{T}$ into the first integral of Eqn. (6.49), while incorporating Eqn. (6.46), allows this integral to be re-written as

$$\int_V \mathrm{d}\mathbf{B}^\mathsf{T}\,\boldsymbol{T}\,\mathrm{d}V = \int_V \mathrm{d}\mathbf{B}^\mathsf{T}\big(\boldsymbol{T}_0 + \boldsymbol{\mathcal{M}}^s\boldsymbol{E}\big)\,\mathrm{d}V = \underbrace{\int_V \mathbf{H}^\mathsf{T}\,\mathbf{S}\,\mathbf{H}\,\mathrm{d}V}_{\mathbf{C}^s}\,\mathrm{d}\boldsymbol{u}^{(e)} \tag{6.50}$$

where $\boldsymbol{T}_0 + \boldsymbol{\mathcal{M}}^s\boldsymbol{E} \mapsto \mathbf{S}$, and as such, $\mathbf{C}^s$ is that contribution to the tangent stiffness matrix $\mathbf{C}$ attributed to the secant modulus $\boldsymbol{\mathcal{M}}^s$ appearing in Eqn. (6.35b), which is quadratic in $\mathbf{H}$. Now, substituting constitutive equation (6.35d) for $\mathrm{d}\boldsymbol{T}$ into the second integral in Eqn. (6.49), while employing Eqns. (6.45c & 6.45d) to describe strain rate $\mathrm{d}\boldsymbol{E}$, this integral becomes

$$\int_V \mathbf{B}^\mathsf{T}\,\mathrm{d}\boldsymbol{T}\,\mathrm{d}V = \int_V \mathbf{B}^\mathsf{T}\,\boldsymbol{\mathcal{M}}^t\,\mathrm{d}\boldsymbol{E}\,\mathrm{d}V = \underbrace{\int_V \mathbf{B}^\mathsf{T}\,\boldsymbol{\mathcal{M}}^t\,\mathbf{B}\,\mathrm{d}V}_{\mathbf{C}^t}\,\mathrm{d}\boldsymbol{u}^{(e)} + \underbrace{\int_V \mathbf{B}^\mathsf{T}\,\boldsymbol{\mathcal{M}}^t\,\mathrm{d}\mathbf{B}\,\mathrm{d}V}_{\mathbf{K}^t}\,\boldsymbol{u}^{(e)} \tag{6.51a}$$

where the contribution to the secant stiffness can be expressed alternatively as

$$\mathbf{K}^t = \int_V \mathbf{H}^\mathsf{T}\,\mathrm{d}\mathbf{S}\,\mathbf{H}\,\mathrm{d}V \quad \text{given} \quad \mathrm{d}\mathbf{S} := \mathbf{A}^\mathsf{T}\,\boldsymbol{\mathcal{M}}^t\,\mathrm{d}\mathbf{A}. \tag{6.51b}$$

6.2.3.4 Equations of Motion

Pulling everything together, the equations of motion Eqn. (6.8), when written for an element, are given by

$$\boldsymbol{F} = \mathbf{K}\,\boldsymbol{u}^{(e)} + \mathbf{C}\,\dot{\boldsymbol{u}}^{(e)} + \mathbf{M}\,\ddot{\boldsymbol{u}}^{(e)} \tag{6.52a}$$

which has a secant stiffness matrix of

$$\mathbf{K} = \mathbf{K}^s + \mathbf{K}^t \tag{6.52b}$$

a tangent stiffness matrix of

$$\mathbf{C} = \mathbf{C}^s + \mathbf{C}^t \tag{6.52c}$$

and a forcing function of

$$\boldsymbol{F} = \boldsymbol{F}_{BC} - \boldsymbol{F}_0 \tag{6.52d}$$

wherein

$$\mathbf{K}^s = \int_V \mathbf{B}^\mathsf{T}\, \boldsymbol{\mathcal{M}}^s\, \mathbf{B}\, \mathrm{d}V \tag{6.52e}$$

$$\mathbf{K}^t = \int_V \mathbf{H}^\mathsf{T}\, \mathrm{d}\mathbf{S}^t\, \mathbf{H}\, \mathrm{d}V \qquad \text{where} \qquad \mathrm{d}\mathbf{S}^t = \mathbf{A}^\mathsf{T}\, \boldsymbol{\mathcal{M}}^t\, \mathrm{d}\mathbf{A} \tag{6.52f}$$

$$\mathbf{C}^s = \int_V \mathbf{H}^\mathsf{T}\, \mathbf{S}^s\, \mathbf{H}\, \mathrm{d}V \qquad \text{where} \qquad \boldsymbol{T}_0 + \boldsymbol{\mathcal{M}}^s \boldsymbol{E} \mapsto \mathbf{S}^s \tag{6.52g}$$

$$\mathbf{C}^t = \int_V \mathbf{B}^\mathsf{T}\, \boldsymbol{\mathcal{M}}^t\, \mathbf{B}\, \mathrm{d}V \tag{6.52h}$$

$$\boldsymbol{F}_0 = \int_V \mathbf{B}^\mathsf{T}\, \boldsymbol{T}_0\, \mathrm{d}V \tag{6.52i}$$

with $\boldsymbol{F}_{BC}$ being an external force associated with the boundary conditions evaluated at the end of a solution step. All other fields are evaluated at the beginning of this solution step. Superscript '^{s}' implies that these matrices are evaluated using the secant modulus $\boldsymbol{\mathcal{M}}^s$, while superscript '^{t}' implies that these matrices are evaluated using the tangent modulus $\boldsymbol{\mathcal{M}}^t$. To minimize an accumulation of roundoff error, it is advantageous to compute $\mathbf{K}^s$ as four separate integrals, viz.,

$$\mathbf{K}^s \;=\; \int_V \mathbf{B}_L^\mathsf{T}\, \boldsymbol{\mathcal{M}}^s\, \mathbf{B}_L\, \mathrm{d}V \;+\; \int_V \mathbf{B}_L^\mathsf{T}\, \boldsymbol{\mathcal{M}}^s\, \mathbf{B}_N\, \mathrm{d}V \;+\; \int_V \mathbf{B}_N^\mathsf{T}\, \boldsymbol{\mathcal{M}}^s\, \mathbf{B}_L\, \mathrm{d}V \;+\; \int_V \mathbf{B}_N^\mathsf{T}\, \boldsymbol{\mathcal{M}}^s\, \mathbf{B}_N\, \mathrm{d}V$$

and to compute $\mathbf{C}^t$ as four separate integrals, too, viz.,

$$\mathbf{C}^t \;=\; \int_V \mathbf{B}_L^\mathsf{T}\, \boldsymbol{\mathcal{M}}^t\, \mathbf{B}_L\, \mathrm{d}V \;+\; \int_V \mathbf{B}_L^\mathsf{T}\, \boldsymbol{\mathcal{M}}^t\, \mathbf{B}_N\, \mathrm{d}V \;+\; \int_V \mathbf{B}_N^\mathsf{T}\, \boldsymbol{\mathcal{M}}^t\, \mathbf{B}_L\, \mathrm{d}V \;+\; \int_V \mathbf{B}_N^\mathsf{T}\, \boldsymbol{\mathcal{M}}^t\, \mathbf{B}_N\, \mathrm{d}V$$

while computing $\boldsymbol{F}_0$ as two separate integrals, viz.,

$$\boldsymbol{F}_0 = \int_V \mathbf{B}_L^{\mathsf{T}} \boldsymbol{T}_0 \, \mathrm{d}V + \int_V \mathbf{B}_N^{\mathsf{T}} \boldsymbol{T}_0 \, \mathrm{d}V$$

where the first integral will only need to be evaluated once, as its argument is constant valued.

6.2.4 Kinematic Matrices of Finite Elements

To implement our finite element discretization, it is necessary that we know the following matrices for a given element type: the linear strain-displacement matrix $\mathbf{B}_L$, the nonlinear strain-displacement matrix $\mathbf{B}_N$, and its decomposition $\mathbf{B}_N = \mathbf{AH}$, plus the differential rate $\mathrm{d}\mathbf{A}$. These matrices are acquired in the following sections for a chord, a pentagon, and a dodecahedron where **QR** kinematics have been adopted.

6.2.4.1 Kinematic Matrices for a Chord

The components of Laplace stretch $\boldsymbol{\mathcal{U}}$ can be obtained from a Cholesky factorization of the right, Cauchy–Green, deformation tensor $\mathbf{C} = \mathbf{F}^{\mathsf{T}}\mathbf{F} = \boldsymbol{\mathcal{U}}^{\mathsf{T}}\boldsymbol{\mathcal{U}}$, [26] which is a symmetric tensor. For a 1D chord, the only possible deformation is a stretch of the chord in its axial direction. Therefore, in this case, the deformation gradient, as well as the right Cauchy–Green tensor $\mathbf{C}$, have only one component. Consequently, the Laplace stretch $\boldsymbol{\mathcal{U}}$ also consists of only one component, which is denoted by a. If u is the axial displacement of a chord, then its axial elongation a becomes

$$a = \mathcal{U}_{11} = \sqrt{C_{11}} \quad \text{with} \quad \mathrm{C}_{11} = 1 + 2\,\frac{\partial \mathrm{u}}{\partial x} + \left(\frac{\partial \mathrm{u}}{\partial x}\right)^2 \quad \text{given} \quad F_{11} = 1 + \frac{\partial \mathrm{u}}{\partial x}. \tag{6.53a}$$

This chord is subjected to an axial strain defined as $e = \ln(a) = \ln(L/L_0)$, where L_0 and L are the initial and current lengths of the chord. Here we decompose the total strain into its

linear and nonlinear components as

$$e = e_L + e_N \tag{6.54}$$

as determined by a Taylor expansion of $e = \ln\sqrt{C_{11}}$, which gives

$$e_L = \frac{\partial \mathrm{u}}{\partial \mathrm{x}} \quad \text{and} \quad e_N = -\frac{1}{2}\frac{\partial \mathrm{u}}{\partial \mathrm{x}}\frac{\partial \mathrm{u}}{\partial \mathrm{x}} \tag{6.55}$$

The linear strain-displacement matrix $\mathbf{B}_L$ can now be obtained by expressing the linear strain e_L in terms of its nodal displacements, viz.,

$$e_L = \frac{\partial u}{\partial x} = \sum_{i=1}^{2} N_{i,x}\, u_i = \big[[\mathbf{b}_{L1}][\mathbf{b}_{L2}]\big]\big\{\mathbf{u}^{(e)}\big\} = \big[\mathbf{B}_L\big]\big\{\mathbf{u}^{(e)}\big\} \tag{6.56a}$$

wherein

$$[\mathbf{b}_{Li}] = [N_{i,x}] = [N_{i,\xi}][\mathbf{J}]^{-1} \quad \text{and} \quad \mathbf{u}^{(e)} = \begin{Bmatrix} u_1^{(e)} & u_2^{(e)} \end{Bmatrix}^{\mathsf{T}} \tag{6.56b}$$

where $N_{i,\xi}$ is the gradient of shape function N_i evaluated in element (e)'s natural co-ordinate system, which maps into gradient $N_{i,x}$ evaluated in the element's physical co-ordinate system via its Jacobian matrix $[\mathbf{J}]$, with $u_1^{(e)}$ and $u_2^{(e)}$ denoting the nodal displacements of the chord.

We introduce machinery that is excessive for chord, but becomes useful when constructing the nonlinear strain-displacement matrices for pentagon and tetrahedron. Let nonlinear strain e_N be written as a product between some matrix $\mathbf{A}$ and some vector $\boldsymbol{\theta}$; specifically,

$$e_N = \tfrac{1}{2}\,[-\partial u/\partial x]\{\partial u/\partial x\} = \tfrac{1}{2}\,\mathbf{A}\,\boldsymbol{\theta} \tag{6.57}$$

where $\mathbf{A} = [-\partial u/\partial x]$ whose differential is

$$\mathrm{d}\mathbf{A} = \big\{-\partial \mathrm{d}u/\partial x\big\} = \Big\{-\textstyle\sum_{i=1}^{2} N_{i,x}\,\mathrm{d}u_i\Big\} = \big[[\mathbf{l}_1][\mathbf{l}_2]\big]\big[[\mathbf{d}_1][\mathbf{d}_2]\big]^{\mathsf{T}} = \mathbf{L}\,\mathbf{D} \tag{6.58a}$$

wherein

$$[\mathbf{l}_i] = [-N_{i,x}] = [-N_{i,\xi}][\mathbf{J}]^{-1} \quad \text{and} \quad [\mathbf{d}_i] = [\mathrm{d}u_i]. \tag{6.58b}$$

Furthermore, we consider that $\boldsymbol{\theta}$ can be expressed in terms of the nodal displacements as

$$\boldsymbol{\theta} = \left\{\partial u/\partial x\right\} = \left\{\sum_{i=1}^{2} N_{i,x}\, u_i\right\} = \left[[\mathbf{h}_1][\mathbf{h}_2]\right]\left\{\mathbf{u}^{(e)}\right\} = \mathbf{H}\,\mathbf{u}^{(e)} \tag{6.59a}$$

wherein

$$\mathbf{H} = \left[[\mathbf{h}_1][\mathbf{h}_2]\right] \quad \text{with} \quad [\mathbf{h}_i] = [N_{i,x}] = [N_{i,\xi}][\mathbf{J}]^{-1} \tag{6.59b}$$

for the chord, there is no difference between $\mathbf{b}_{Li}$ and $\mathbf{h}_i$, which will not be the case in higher-dimensional spaces. Hence, the nonlinear strain-displacement matrix $\mathbf{B}_N$ becomes

$$\mathbf{B}_N = \mathbf{A}\,\mathbf{H} = \left[[\mathbf{b}_{N1}][\mathbf{b}_{N2}]\right] \tag{6.60}$$

where $\mathbf{b}_{Ni} = [-\partial u/\partial x][\mathbf{h}_i]$. The tangent stiffness matrix $\mathbf{C}^s$ associated with $\boldsymbol{T}_0 + \boldsymbol{\mathcal{M}}^s\boldsymbol{E} \mapsto \mathbf{S}^s = [s_0 + E^s e]$, which is defined in Eqn. (6.36), becomes

$$\mathbf{C}^s = \int_L \mathbf{H}^{\mathsf{T}}\,\mathbf{S}^s\,\mathbf{H}\,A\,\mathrm{d}L = |\mathbf{J}_0| \sum_{i=1}^{n} \mathbf{H}^{\mathsf{T}}\,\mathbf{S}^s(\xi_i)\,\mathbf{H}\,A_0(\xi_i)\,w_i \tag{6.61}$$

where an isochoric response is assumed in that $A_0|\mathbf{J}_0| = A|\mathbf{J}|$. Here ξ_i and w_i are the coordinates and weights of quadrature for Gauss point i, and A_0 and A are the initial and current cross-sectional areas of the chord with $A_0(\xi_i)$ being the initial cross-sectional area at Gauss point ξ_i.

The tangent stiffness matrix $\mathbf{C}^t$, as established in Eqn. (6.51), becomes

$$\mathbf{C}^t = \int_L \mathbf{B}^{\mathsf{T}}\,\boldsymbol{\mathcal{M}}^t\,\mathbf{B}\,A\,\mathrm{d}L = |\mathbf{J}_0| \sum_{i=1}^{n} \mathbf{B}^{\mathsf{T}}\,\boldsymbol{\mathcal{M}}^t(\xi_i)\,\mathbf{B}\,A_0(\xi_i)\,w_i \tag{6.62a}$$

where axial stress rate $\mathrm{d}s$ is described by a tangent modulus $\boldsymbol{\mathcal{M}}^t$ from Eqn. (6.38).

The secant stiffness matrix $\mathbf{K}^s$, as established in Eqn. (6.48b), becomes

$$\mathbf{K}^s = \int_L \mathbf{B}^\mathsf{T}\, \boldsymbol{\mathcal{M}}^s\, \mathbf{B}\, A\, \mathrm{d}L = |\mathbf{J}_0| \sum_{i=1}^{n} \mathbf{B}^\mathsf{T}\, \boldsymbol{\mathcal{M}}^s(\xi_i)\, \mathbf{B}\, A_0(\xi_i)\, w_i \tag{6.63a}$$

where axial stress s is described by a secant modulus $\boldsymbol{\mathcal{M}}^s$ from Eqn. (6.36).

Likewise, a secant stiffness matrix $\mathbf{K}^t$, also established in Eqn. (6.51), becomes

$$\mathbf{K}^t = \int_L \mathbf{H}^\mathsf{T}\, \mathrm{d}\mathbf{S}^t\, \mathbf{H}\, A\, \mathrm{d}L = |\mathbf{J}_0| \sum_{i=1}^{n} \mathbf{H}^\mathsf{T}\, \mathrm{d}\mathbf{S}^t(\xi_i)\, \mathbf{H}\, A_0(\xi_i)\, w_i \tag{6.64a}$$

where its stress rate is given by $\mathrm{d}\mathbf{S}^t := \mathbf{A}^\mathsf{T}\, \boldsymbol{\mathcal{M}}^t\, \mathrm{d}\mathbf{A}$.

6.2.4.2 Kinematic Matrices for a Pentagon

For a planar membrane, components of Laplace stretch $\boldsymbol{\mathcal{U}}$, obtained from a Cholesky factorization of the right Cauchy–Green tensor $\mathbf{C} := \mathbf{F}^\mathsf{T}\mathbf{F} = \boldsymbol{\mathcal{U}}^\mathsf{T}\boldsymbol{\mathcal{U}}$, cf. Eqn. (2.2), where C_{11}, $C_{12} = C_{21}$ and C_{22} are components of the right Cauchy–Green tensor $\mathbf{C}$ that can be expressed in terms of displacement gradients as

$$\mathrm{C}_{11} = 1 + 2\,\frac{\partial u}{\partial x} + \left(\frac{\partial u}{\partial x}\right)^2 + \left(\frac{\partial v}{\partial x}\right)^2 \tag{6.65a}$$

$$\mathrm{C}_{12} = \frac{\partial u}{\partial y} + \frac{\partial v}{\partial x} + \frac{\partial u}{\partial x} \cdot \frac{\partial u}{\partial y} + \frac{\partial v}{\partial x} \cdot \frac{\partial v}{\partial y} \tag{6.65b}$$

$$\mathrm{C}_{22} = 1 + 2\,\frac{\partial v}{\partial y} + \left(\frac{\partial u}{\partial y}\right)^2 + \left(\frac{\partial v}{\partial y}\right)^2 \tag{6.65c}$$

which arise from the deformation gradient

$$\mathbf{F} = \begin{bmatrix} 1 + \partial u/\partial x & \partial u/\partial y \\ \partial v/\partial x & 1 + \partial v/\partial y \end{bmatrix} \tag{6.65d}$$

where u and v are displacements associated with the deformation of a planar membrane.

Gradients of shape functions are used to construct the above spatial gradients, viz.,

$$\begin{Bmatrix} N_{i,\xi} \\ N_{i,\eta} \end{Bmatrix} = \begin{bmatrix} \partial x/\partial \xi & \partial y/\partial \xi \\ \partial x/\partial \eta & \partial y/\partial \eta \end{bmatrix} \begin{Bmatrix} N_{i,x} \\ N_{i,y} \end{Bmatrix}$$

whose matrix is the non-singular Jacobian, while $N_{i,\xi}$ and $N_{i,\eta}$ are gradients of the shape functions in their natural co-ordinates, as established in Eqn. (5.20) for pentagons. These are evaluated at i^{th} Gauss point for the quadrature rule used that, in our case, is found in Eqns.(6.4 & 6.5). It is necessary to invert this equation for it to become useful for us so that

$$\begin{Bmatrix} N_{i,x} \\ N_{i,y} \end{Bmatrix} = \begin{bmatrix} \partial x/\partial \xi & \partial y/\partial \xi \\ \partial x/\partial \eta & \partial y/\partial \eta \end{bmatrix}^{-1} \begin{Bmatrix} N_{i,\xi} \\ N_{i,\eta} \end{Bmatrix} \tag{6.66}$$

with $N_{i,x}$ and $N_{i,y}$ being employed below.

The thermodynamic strain attributes that we use are defined in Eqn. (2.10). Without loss of generality, we consider the membrane to be initially undeformed, which allows us to set a_0 and b_0 to one, while the initial shear g_0 is taken as zero. To gain computational advantage, we decompose these strain attributes into linear and nonlinear components; specifically, we consider

$$\xi = \xi_L + \xi_{N1} + \xi_{N2} + \xi_{N3} \tag{6.67a}$$

$$\varepsilon = \varepsilon_L + \varepsilon_{N1} + \varepsilon_{N2} + \varepsilon_{N3} \tag{6.67b}$$

$$\gamma = \gamma_L + \gamma_{N1} + \gamma_{N2} + \gamma_{N3}. \tag{6.67c}$$

Traditionally, finite element constructions decompose strain into a linear component and a nonlinear component. However, in our case, a further decomposition of the nonlinear strain component into three separate components makes our computation much easier.

Decomposition of strain attributes is achieved via Taylor expansions that retain terms through second-order. The linear and nonlinear components of these strain attributes, thus

obtained, are given as

$$\xi_L = \frac{1}{2}\left(\frac{\partial \mathrm{u}}{\partial \mathrm{x}} + \frac{\partial \mathrm{v}}{\partial \mathrm{y}}\right) \tag{6.68a}$$

$$\xi_N = \frac{1}{4}\left(-\frac{\partial \mathrm{v}}{\partial \mathrm{y}}\frac{\partial \mathrm{v}}{\partial \mathrm{y}} - \frac{\partial \mathrm{u}}{\partial \mathrm{x}}\frac{\partial \mathrm{u}}{\partial \mathrm{x}} - 2\,\frac{\partial \mathrm{u}}{\partial \mathrm{y}}\frac{\partial \mathrm{v}}{\partial \mathrm{x}}\right) \tag{6.68b}$$

$$\varepsilon_L = \frac{1}{2}\left(\frac{\partial \mathrm{u}}{\partial \mathrm{x}} - \frac{\partial \mathrm{v}}{\partial \mathrm{y}}\right) \tag{6.68c}$$

$$\varepsilon_N = \frac{1}{4}\left(2\,\frac{\partial \mathrm{v}}{\partial \mathrm{x}}\frac{\partial \mathrm{v}}{\partial \mathrm{x}} + \frac{\partial \mathrm{v}}{\partial \mathrm{y}}\frac{\partial \mathrm{v}}{\partial \mathrm{y}} - \frac{\partial \mathrm{u}}{\partial \mathrm{x}}\frac{\partial \mathrm{u}}{\partial \mathrm{x}} + 2\,\frac{\partial \mathrm{u}}{\partial \mathrm{y}}\frac{\partial \mathrm{v}}{\partial \mathrm{x}}\right) \tag{6.68d}$$

$$\gamma_L = \frac{\partial \mathrm{u}}{\partial \mathrm{y}} + \frac{\partial \mathrm{v}}{\partial \mathrm{x}} \tag{6.68e}$$

$$\gamma_N = \frac{\partial \mathrm{v}}{\partial \mathrm{x}}\frac{\partial \mathrm{v}}{\partial \mathrm{y}} - 2\,\frac{\partial \mathrm{u}}{\partial \mathrm{x}}\frac{\partial \mathrm{v}}{\partial \mathrm{x}} - \frac{\partial \mathrm{u}}{\partial \mathrm{x}}\frac{\partial \mathrm{u}}{\partial \mathrm{y}} \tag{6.68f}$$

where the linear components of these strain attributes consist only of first-order derivatives in the displacements, while the nonlinear components contain the second-order terms. In terms of the nodal displacements, the vector containing the linear strain attributes, i.e., $\boldsymbol{E}_L$, can be written as

$$\begin{aligned}\boldsymbol{E}_L &= \begin{Bmatrix}\xi_L\\ \varepsilon_L\\ \gamma_L\end{Bmatrix} = \begin{Bmatrix}\frac{1}{2}\,u_{,x} + \frac{1}{2}\,v_{,y}\\ \frac{1}{2}\,u_{,x} - \frac{1}{2}\,v_{,y}\\ u_{,y} + v_{,x}\end{Bmatrix} = \sum_{i=1}^{5}\begin{bmatrix}\frac{1}{2}\,N_{i,x} & \frac{1}{2}\,N_{i,y}\\ \frac{1}{2}\,N_{i,x} & -\frac{1}{2}\,N_{i,y}\\ N_{i,y} & N_{i,x}\end{bmatrix}\begin{Bmatrix}u_i\\ v_i\end{Bmatrix}\\ &= \big[[\mathbf{b}_{L1}][\mathbf{b}_{L2}][\mathbf{b}_{L3}][\mathbf{b}_{L4}][\mathbf{b}_{L5}]\big]\big\{\mathbf{u}^{(e)}\big\} = \mathbf{B}_L\,\mathbf{u}^{(e)}\end{aligned} \tag{6.69a}$$

where

$$[\mathbf{b}_{Li}] = \begin{bmatrix}\frac{1}{2}\,N_{i,x} & \frac{1}{2}\,N_{i,y}\\ \frac{1}{2}\,N_{i,x} & -\frac{1}{2}\,N_{i,y}\\ N_{i,y} & N_{i,x}\end{bmatrix}, \quad \mathbf{u}^{(e)} = \big\{u_1 \quad v_1 \quad u_2 \quad v_2 \quad u_3 \quad v_3 \quad u_4 \quad v_4 \quad u_5 \quad v_5\big\}^{\mathsf{T}} \tag{6.69b}$$

for element e, whose matrix entries come from Eqn. (6.66).

Now let nonlinear strain $\boldsymbol{E}_{N1}$ be written as a product between some matrix $\mathbf{A}_1$ and some

vector $\boldsymbol{\theta}_1$; specifically, let

$$\mathbf{E}_{N1} = \begin{Bmatrix} \xi_{N1} \\ \varepsilon_{N1} \\ \gamma_{N1} \end{Bmatrix} = \begin{Bmatrix} -\frac{1}{4}\, v_{,y}^2 \\ -\frac{1}{4}\, u_{,x}^2 + \frac{1}{4}\, v_{,y}^2 \\ v_{,x}\, v_{,y} \end{Bmatrix} = \frac{1}{2} \begin{bmatrix} 0 & -\frac{1}{2}\, \partial v/\partial y \\ -\frac{1}{2}\, \partial u/\partial x & \frac{1}{2}\, \partial v/\partial y \\ 0 & 2\, \partial v/\partial x \end{bmatrix} \begin{Bmatrix} \partial u/\partial x \\ \partial v/\partial y \end{Bmatrix} = \tfrac{1}{2}\, \mathbf{A}_1\, \boldsymbol{\theta}_1 \tag{6.70}$$

with

$$\begin{aligned} \mathrm{d}\mathbf{A}_1 &= \begin{bmatrix} 0 & -\frac{1}{2}\, \partial \mathrm{d}v/\partial y \\ -\frac{1}{2}\, \partial \mathrm{d}u/\partial x & \frac{1}{2}\, \partial \mathrm{d}v/\partial y \\ 0 & 2\, \partial \mathrm{d}v/\partial x \end{bmatrix} = \textstyle\sum_{i=1}^{5} \begin{bmatrix} 0 & -\frac{1}{2}\, N_{i,y}\, \mathrm{d}v_i \\ -\frac{1}{2}\, N_{i,x}\, \mathrm{d}u_i & \frac{1}{2}\, N_{i,y}\, \mathrm{d}v_i \\ 0 & 2\, N_{i,x}\, \mathrm{d}v_i \end{bmatrix} \\ &= \Big[[\mathbf{l}_1][\mathbf{l}_2][\mathbf{l}_3][\mathbf{l}_4][\mathbf{l}_5] \Big] \Big[[\mathbf{d}_1][\mathbf{d}_2][\mathbf{d}_3][\mathbf{d}_4][\mathbf{d}_5] \Big]^{\mathsf{T}} = \mathbf{L}_1 \mathbf{D}_1 \end{aligned} \tag{6.71a}$$

wherein

$$[\mathbf{l}_i] = \begin{bmatrix} 0 & -\frac{1}{2}\, N_{i,y} \\ -\frac{1}{2}\, N_{i,x} & \frac{1}{2}\, N_{i,y} \\ 0 & 2\, N_{i,x} \end{bmatrix} \quad \text{and} \quad [\mathbf{d}_i] = \begin{bmatrix} \mathrm{d}u_i & 0 \\ 0 & \mathrm{d}v_i \end{bmatrix}. \tag{6.71b}$$

To obtain the nonlinear strain–displacement matrix, we require the nonlinear strain to be expressed in terms of the nodal displacements. This is achieved by expressing the elements of displacement gradient in terms of the nodal displacements by using the shape functions, specifically, the vector $\boldsymbol{\theta}_1$ can be written as

$$\boldsymbol{\theta}_1 = \begin{Bmatrix} \partial u/\partial x \\ \partial v/\partial y \end{Bmatrix} = \textstyle\sum_{i=1}^{5} \begin{Bmatrix} N_{i,x}\, u_i \\ N_{i,y}\, v_i \end{Bmatrix} = \Big[[\mathbf{h}_1][\mathbf{h}_2][\mathbf{h}_3][\mathbf{h}_4][\mathbf{h}_5] \Big] \big\{ \mathbf{u}^{(e)} \big\} = \mathbf{H}_1 \mathbf{u}^{(e)} \tag{6.72a}$$

where the components of $\mathbf{H}_1$ contains the derivatives of shape functions with respect to spatial variables, i.e.,

$$[\mathbf{h}_i] = \begin{bmatrix} N_{i,x} & 0 \\ 0 & N_{i,y} \end{bmatrix}. \tag{6.72b}$$

Therefore, the first nonlinear strain–displacement matrix $\mathbf{B}_{N1}$ can be written as

$$\mathbf{B}_{N1} = \mathbf{A}_1\,\mathbf{H}_1 = \Big[\,[\mathbf{b}_{N1}][\mathbf{b}_{N2}][\mathbf{b}_{N3}][\mathbf{b}_{N4}][\mathbf{b}_{N5}]\,\Big] \tag{6.73a}$$

where the components of $\mathbf{B}_{N1}$ are given as

$$[\mathbf{b}_{Ni}] = \begin{bmatrix} 0 & -\frac{1}{2}\,\partial v/\partial y \\ -\frac{1}{2}\,\partial u/\partial x & \frac{1}{2}\,\partial v/\partial y \\ 0 & 2\,\partial v/\partial x \end{bmatrix} \begin{bmatrix} N_{i,x} & 0 \\ 0 & N_{i,y} \end{bmatrix}. \tag{6.73b}$$

In a similar manner, the second nonlinear strain terms can be written as

$$\mathbf{E}_{N2} \;=\; \begin{Bmatrix} \xi_{N2} \\ \varepsilon_{N2} \\ \gamma_{N2} \end{Bmatrix} \;=\; \begin{Bmatrix} -\frac{1}{2}\,u_{,y}\,v_{,x} \\ \frac{1}{2}\,u_{,y}\,v_{,x} \\ -2\,u_{,x}\,v_{,x} \end{Bmatrix} \;=\; \frac{1}{2} \begin{bmatrix} -\partial v/\partial x & 0 \\ \partial v/\partial x & 0 \\ 0 & -4\,\partial u/\partial x \end{bmatrix} \begin{Bmatrix} \partial u/\partial y \\ \partial v/\partial x \end{Bmatrix} \;=\; \tfrac{1}{2}\,\mathbf{A}_2\,\boldsymbol{\theta}_2 \tag{6.74}$$

with

$$\begin{aligned} \mathrm{d}\mathbf{A}_2 &= \begin{bmatrix} -\partial \mathrm{d}v/\partial x & 0 \\ \partial \mathrm{d}v/\partial x & 0 \\ 0 & -4\,\partial \mathrm{d}u/\partial x \end{bmatrix} = \sum\nolimits_{i=1}^{5} \begin{bmatrix} -N_{i,x}\,\mathrm{d}v_i & 0 \\ N_{i,x}\,\mathrm{d}v_i & 0 \\ 0 & -4\,N_{i,x}\,\mathrm{d}u_i \end{bmatrix} \\ &= \Big[\,[\mathbf{l}_1][\mathbf{l}_2][\mathbf{l}_3][\mathbf{l}_4][\mathbf{l}_5]\,\Big] \Big[\,[\mathbf{d}_1][\mathbf{d}_2][\mathbf{d}_3][\mathbf{d}_4][\mathbf{d}_5]\,\Big]^{\mathsf{T}} = \mathbf{L}_2\mathbf{D}_2 \end{aligned} \tag{6.75a}$$

wherein

$$[\mathbf{l}_i] = \begin{bmatrix} -N_{i,x} & 0 \\ N_{i,x} & 0 \\ 0 & -4\,N_{i,x} \end{bmatrix} \quad \text{and} \quad [\mathbf{d}_i] = \begin{bmatrix} \mathrm{d}v_i & 0 \\ 0 & \mathrm{d}u_i \end{bmatrix}. \tag{6.75b}$$

The vector $\boldsymbol{\theta}_2$ is expressed in terms of the nodal displacements with the use of shape functions

as

$$\boldsymbol{\theta}_2 = \begin{Bmatrix} \partial u/\partial y \\ \partial v/\partial x \end{Bmatrix} = \sum_{i=1}^{5} \begin{Bmatrix} N_{i,y}\, u_i \\ N_{i,x}\, v_i \end{Bmatrix} = \Big[[\mathbf{h}_1][\mathbf{h}_2][\mathbf{h}_3][\mathbf{h}_4][\mathbf{h}_5] \Big] \left\{ \mathbf{u}^{(e)} \right\} = \mathbf{H}_2 \mathbf{u}^{(e)} \tag{6.76a}$$

where the elements of $\mathbf{H}_2$ are given as

$$[\mathbf{h}_i] = \begin{bmatrix} N_{i,y} & 0 \\ 0 & N_{i,x} \end{bmatrix}. \tag{6.76b}$$

Hence, the second nonlinear strain–displacement matrix $\mathbf{B}_{N2}$ becomes

$$\mathbf{B}_{N2} = \mathbf{A}_2\, \mathbf{H}_2 = \Big[[\mathbf{b}_{N1}][\mathbf{b}_{N2}][\mathbf{b}_{N3}][\mathbf{b}_{N4}][\mathbf{b}_{N5}] \Big] \tag{6.77a}$$

where its elements are given as

$$[\mathbf{b}_{Ni}] = \begin{bmatrix} -\partial v/\partial x & 0 \\ \partial v/\partial x & 0 \\ 0 & -4\, \partial u/\partial x \end{bmatrix} \begin{bmatrix} N_{i,y} & 0 \\ 0 & N_{i,x} \end{bmatrix}. \tag{6.77b}$$

In like manner, the third nonlinear strain terms can be written as

$$\mathbf{E}_{N3} = \begin{Bmatrix} \xi_{N3} \\ \varepsilon_{N3} \\ \gamma_{N3} \end{Bmatrix} = \begin{Bmatrix} -\frac{1}{4}\, u_{,x}^2 \\ \frac{1}{2}\, v_{,x}^2 \\ -u_{,y}\, u_{,x} \end{Bmatrix} = \frac{1}{2} \begin{bmatrix} -\frac{1}{2}\, \partial u/\partial x & 0 \\ 0 & \partial v/\partial x \\ -2\, \partial u/\partial y & 0 \end{bmatrix} \begin{Bmatrix} \partial u/\partial x \\ \partial v/\partial x \end{Bmatrix} = \tfrac{1}{2}\, \mathbf{A}_3\, \boldsymbol{\theta}_3 \tag{6.78}$$

with

$$\begin{aligned} \mathrm{d}\mathbf{A}_3 &= \begin{bmatrix} -\frac{1}{2}\, \partial \mathrm{d}u/\partial x & 0 \\ 0 & \partial \mathrm{d}v/\partial x \\ -2\, \partial \mathrm{d}u/\partial y & 0 \end{bmatrix} = \sum_{i=1}^{5} \begin{bmatrix} -\frac{1}{2}\, N_{i,x}\, \mathrm{d}u_i & 0 \\ 0 & N_{i,x}\, \mathrm{d}v_i \\ -2\, N_{i,y}\, \mathrm{d}u_i & 0 \end{bmatrix} \\ &= \Big[[\mathbf{l}_1][\mathbf{l}_2][\mathbf{l}_3][\mathbf{l}_4][\mathbf{l}_5] \Big] \Big[[\mathbf{d}_1][\mathbf{d}_2][\mathbf{d}_3][\mathbf{d}_4][\mathbf{d}_5] \Big]^{\mathsf{T}} = \mathbf{L}_3 \mathbf{D}_3 \end{aligned} \tag{6.79a}$$

wherein

$$[\mathbf{l}_i] = \begin{bmatrix} -\frac{1}{2}\,N_{i,x} & 0 \\ 0 & N_{i,x} \\ -2\,N_{i,y} & 0 \end{bmatrix} \quad \text{and} \quad [\mathbf{d}_i] = \begin{bmatrix} \mathrm{d}u_i & 0 \\ 0 & \mathrm{d}v_i \end{bmatrix}. \tag{6.79b}$$

$\boldsymbol{\theta}_3$ is expressed in terms of the nodal displacements using the shape functions; specifically

$$\boldsymbol{\theta}_3 = \begin{Bmatrix} \partial u/\partial x \\ \partial v/\partial x \end{Bmatrix} = \sum_{i=1}^{5} \begin{Bmatrix} N_{i,x}\,u_i \\ N_{i,x}\,v_i \end{Bmatrix} = \Big[[\mathbf{h}_1][\mathbf{h}_2][\mathbf{h}_3][\mathbf{h}_4][\mathbf{h}_5]\Big] \left\{\mathbf{u}^{(e)}\right\} = \mathbf{H}_3\mathbf{u}^{(e)} \tag{6.80a}$$

where the components of $\mathbf{H}_3$ contains the derivatives of shape functions with respect to spatial variables, i.e.,

$$[\mathbf{h}_i] = \begin{bmatrix} N_{i,x} & 0 \\ 0 & N_{i,x} \end{bmatrix}. \tag{6.80b}$$

Therefore, the first nonlinear strain–displacement matrix $\mathbf{B}_{N3}$ can be written as

$$\mathbf{B}_{N3} = \mathbf{A}_3\,\mathbf{H}_3 = \Big[[\mathbf{b}_{N1}][\mathbf{b}_{N2}][\mathbf{b}_{N3}][\mathbf{b}_{N4}][\mathbf{b}_{N5}]\Big] \tag{6.81a}$$

where the components of $\mathbf{B}_{N3}$ are given as

$$[\mathbf{b}_{Ni}] = \begin{bmatrix} -\frac{1}{2}\,\partial u/\partial x & 0 \\ 0 & \partial v/\partial y \\ -2\,\partial u/\partial y & 0 \end{bmatrix} \begin{bmatrix} N_{i,x} & 0 \\ 0 & N_{i,x} \end{bmatrix}. \tag{6.81b}$$

The total nonlinear strain–displacement matrix is evaluated as the summation of its components $\mathbf{B}_{N1}$, $\mathbf{B}_{N2}$, and $\mathbf{B}_{N3}$. Now, with all the strain–displacement matrices evaluated, we are ready to compute the stiffness matrix for a planar membrane.

To obtain the stiffness matrix for a planar membrane, we need to compute the four constituent strain-displacement matrices $\mathbf{C}^s$, $\mathbf{C}^t$, $\mathbf{K}^s$ and $\mathbf{K}^t$, as mentioned earlier.

The tangent stiffness matrix $\mathbf{C}^s$, as established in Eqn. (6.50), becomes

$$\mathbf{C}^s = \int_{\pentagon} \mathbf{H}^{\mathsf{T}}\,\mathbf{S}^s\,\mathbf{H}\,H\,\mathrm{d}A = |\mathbf{J}_0| \sum_{i=1}^{n} \mathbf{H}^{\mathsf{T}}\,\mathbf{S}^s(\xi_i,\eta_i)\,\mathbf{H}\,H_{0\,i}\,w_i \tag{6.82a}$$

wherein

$$\mathbf{S}^s = \begin{bmatrix} \mathcal{S}_{11} & \mathcal{S}_{12} \\ \mathcal{S}_{21} & \mathcal{S}_{22} \end{bmatrix} \tag{6.82b}$$

where an isochoric response is assumed in that $H_0|\mathbf{J}_0| = H|\mathbf{J}|$. Here H_0 and H are the initial and current height or thickness of the septal membrane, and ξ_i, η_i and w_i are the co-ordinates and weights of quadrature for Gauss point i.

The stress vector $\boldsymbol{T} = \{s^\pi, s^\sigma, s^\tau\}^{\mathsf{T}}$ conjugate to strain vector $\boldsymbol{E} = \{\xi, \varepsilon, \gamma\}^{\mathsf{T}}$ has elements of a surface tension $s^\pi = \mathcal{S}_{11} + \mathcal{S}_{22}$, a normal-stress difference $s^\sigma = \mathcal{S}_{11} - \mathcal{S}_{22}$, and a shear stress $s^\tau = \frac{a}{b}\,\mathcal{S}_{12}$.

$$\mathcal{S}_{11} = \frac{1}{2}(s^\pi + s^\sigma), \quad \mathcal{S}_{22} = \frac{1}{2}(s^\pi - s^\sigma) \quad \text{and} \quad \mathcal{S}_{12} = \mathcal{S}_{21} = \frac{b}{a}s^\tau \tag{6.83}$$

such that $\mathbf{S} = \mathbf{P}\boldsymbol{\mathcal{U}}^{-1}\boldsymbol{\mathcal{S}}\boldsymbol{\mathcal{U}}^{-\mathsf{T}}\mathbf{P}^{\mathsf{T}}$ with $\mathbf{S}$ being the second Piola–Kirchhoff stress evaluated in the co-ordinate system of a pentagon, while $\boldsymbol{\mathcal{U}}$ is Laplace stretch, and $\mathbf{P}$ is a re-indexer of co-ordinate labeling needed to ensure invariance under a transformation of Laplace stretch.

The tangent stiffness matrix $\mathbf{C}^t$, as established in Eqn. (6.51), becomes

$$\mathbf{C}^t = \int_{\pentagon} \mathbf{B}^{\mathsf{T}}\,\boldsymbol{\mathcal{M}}^t\,\mathbf{B}\,|\mathbf{J}|\,H\,\mathrm{d}A = |\mathbf{J}_0| \sum_{i=1}^{n} \mathbf{B}^{\mathsf{T}}\,\boldsymbol{\mathcal{M}}^t(\xi_i,\eta_i)\,\mathbf{B}\,H_{0\,i}\,w_i \tag{6.84}$$

where its associated stress rate is described by a tangent modulus $\boldsymbol{\mathcal{M}}^t$.

The secant stiffness matrix $\mathbf{K}^s$, as established in Eqn. (6.48b), becomes

$$\mathbf{K}^s = \int_{\pentagon} \mathbf{B}^{\mathsf{T}}\,\boldsymbol{\mathcal{M}}^s\,\mathbf{B}\,H\,\mathrm{d}A = |\mathbf{J}_0| \sum_{i=1}^{n} \mathbf{B}^{\mathsf{T}}\,\boldsymbol{\mathcal{M}}^s(\xi_i,\eta_i)\,\mathbf{B}\,H_{0\,i}\,w_i \tag{6.85}$$

where its associated stress is described by a secant modulus $\boldsymbol{\mathcal{M}}^s$.

Likewise, a secant stiffness matrix $\mathbf{K}^t$, also established in Eqn. (6.51), becomes

$$\mathbf{K}^t = \int_{\pentagon} \mathbf{H}^{\mathsf{T}}\, \mathrm{d}\mathbf{S}^t\, \mathbf{H}\, H\, \mathrm{d}A = |\mathbf{J}_0| \sum_{i=1}^{n} \mathbf{H}^{\mathsf{T}}\, \mathrm{d}\mathbf{S}^t(\xi_i, \eta_i)\, \mathbf{H}\, H_{0\,i}\, w_i \tag{6.86}$$

where its associated stress rate is given by $\mathrm{d}\mathbf{S}^t := \mathbf{A}^{\mathsf{T}}\, \boldsymbol{\mathcal{M}}^t\, \mathrm{d}\mathbf{A}$.

6.2.4.3 Kinematic Matrices for a Tetrahedron

Let us consider a tetrahedron subjected to displacements of u, v and w in its three spatial directions, respectively. In terms of these displacements, elements of the deformation gradient can be written as

$$\mathbf{F} = \begin{bmatrix} 1 + \partial \mathrm{u}/\partial \mathrm{x} & \partial \mathrm{u}/\partial \mathrm{y} & \partial \mathrm{u}/\partial \mathrm{z} \\ \partial \mathrm{v}/\partial \mathrm{x} & 1 + \partial \mathrm{v}/\partial \mathrm{y} & \partial \mathrm{v}/\partial \mathrm{z} \\ \partial \mathrm{w}/\partial \mathrm{x} & \partial \mathrm{w}/\partial \mathrm{y} & 1 + \partial \mathrm{w}/\partial \mathrm{z} \end{bmatrix}. \tag{6.87}$$

The components of the right Cauchy–Green deformation tensor, viz., $\mathbf{C} := \mathbf{F}^{\mathsf{T}}\mathbf{F}$, becomes

$$\mathrm{C}_{11} = \left(\frac{\partial \mathrm{u}}{\partial x}\right)^2 + \left(\frac{\partial \mathrm{v}}{\partial x}\right)^2 + \left(\frac{\partial \mathrm{w}}{\partial x}\right)^2 + 2\,\frac{\partial \mathrm{u}}{\partial x} + 1 \tag{6.88a}$$

$$\mathrm{C}_{22} = \left(\frac{\partial \mathrm{u}}{\partial y}\right)^2 + \left(\frac{\partial \mathrm{v}}{\partial y}\right)^2 + \left(\frac{\partial \mathrm{w}}{\partial y}\right)^2 + 2\,\frac{\partial \mathrm{v}}{\partial y} + 1 \tag{6.88b}$$

$$\mathrm{C}_{33} = \left(\frac{\partial \mathrm{u}}{\partial z}\right)^2 + \left(\frac{\partial \mathrm{v}}{\partial z}\right)^2 + \left(\frac{\partial \mathrm{w}}{\partial z}\right)^2 + 2\,\frac{\partial \mathrm{w}}{\partial z} + 1 \tag{6.88c}$$

$$\mathrm{C}_{12} = \mathrm{C}_{21} = \frac{\partial \mathrm{u}}{\partial y} + \frac{\partial \mathrm{v}}{\partial x} + \frac{\partial \mathrm{u}}{\partial x} \cdot \frac{\partial \mathrm{u}}{\partial y} + \frac{\partial \mathrm{v}}{\partial x} \cdot \frac{\partial \mathrm{v}}{\partial y} + \frac{\partial \mathrm{w}}{\partial x} \cdot \frac{\partial \mathrm{w}}{\partial y} \tag{6.88d}$$

$$\mathrm{C}_{13} = \mathrm{C}_{31} = \frac{\partial \mathrm{u}}{\partial z} + \frac{\partial \mathrm{w}}{\partial x} + \frac{\partial \mathrm{u}}{\partial x} \cdot \frac{\partial \mathrm{u}}{\partial z} + \frac{\partial \mathrm{v}}{\partial x} \cdot \frac{\partial \mathrm{v}}{\partial z} + \frac{\partial \mathrm{w}}{\partial x} \cdot \frac{\partial \mathrm{w}}{\partial z} \tag{6.88e}$$

$$\mathrm{C}_{23} = \mathrm{C}_{32} = \frac{\partial \mathrm{v}}{\partial z} + \frac{\partial \mathrm{w}}{\partial y} + \frac{\partial \mathrm{u}}{\partial y} \cdot \frac{\partial \mathrm{u}}{\partial z} + \frac{\partial \mathrm{v}}{\partial y} \cdot \frac{\partial \mathrm{v}}{\partial z} + \frac{\partial \mathrm{w}}{\partial y} \cdot \frac{\partial \mathrm{w}}{\partial z}. \tag{6.88f}$$

The components of Laplace stretch $\boldsymbol{\mathcal{U}}$ are obtained in terms of displacement gradients through a Cholesky factorization of the right Cauchy–Green tensor as defined in Eqn. (2.15).

For computational ease, these strain attributes are additively decomposed into one linear

and five nonlinear components. The primary advantage of this decomposition is an emergence of a systematic structure in the strain-displacement matrix, which makes evaluation of the stiffness matrix much easier. The linear and nonlinear components for the strain attributes, thus obtained, are given by

$$\xi = \xi_L + \xi_{N1} + \xi_{N2} + \xi_{N3} + \xi_{N4} + \xi_{N5} \tag{6.89a}$$

$$\varepsilon_i = \varepsilon_{iL} + \varepsilon_{iN1} + \varepsilon_{iN2} + \varepsilon_{iN3} + \varepsilon_{iN4} + \varepsilon_{iN5} \tag{6.89b}$$

$$\gamma_i = \gamma_{iL} + \gamma_{iN1} + \gamma_{iN2} + \gamma_{iN3} + \gamma_{iN4} + \gamma_{iN5} \tag{6.89c}$$

where their linear and nonlinear components can be expressed in terms of elements arising from a matrix representation of the displacement gradient as

$$\xi_L = \frac{1}{3}\left(\frac{\partial \mathrm{u}}{\partial \mathrm{x}} + \frac{\partial \mathrm{v}}{\partial \mathrm{y}} + \frac{\partial \mathrm{w}}{\partial \mathrm{z}}\right) \tag{6.90a}$$

$$\xi_N = \frac{1}{6}\left(\frac{\partial \mathrm{u}}{\partial \mathrm{z}}\frac{\partial \mathrm{u}}{\partial \mathrm{z}} - \frac{\partial \mathrm{u}}{\partial \mathrm{x}}\frac{\partial \mathrm{u}}{\partial \mathrm{x}} - \frac{\partial \mathrm{v}}{\partial \mathrm{y}}\frac{\partial \mathrm{v}}{\partial \mathrm{y}} - \frac{\partial \mathrm{v}}{\partial \mathrm{z}}\frac{\partial \mathrm{v}}{\partial \mathrm{z}} + \frac{\partial \mathrm{w}}{\partial \mathrm{x}}\frac{\partial \mathrm{w}}{\partial \mathrm{x}} - \frac{\partial \mathrm{w}}{\partial \mathrm{y}}\frac{\partial \mathrm{w}}{\partial \mathrm{y}} - \frac{\partial \mathrm{w}}{\partial \mathrm{z}}\frac{\partial \mathrm{w}}{\partial \mathrm{z}} - 2\frac{\partial \mathrm{u}}{\partial \mathrm{y}}\frac{\partial \mathrm{v}}{\partial \mathrm{x}} - 4\frac{\partial \mathrm{v}}{\partial \mathrm{z}}\frac{\partial \mathrm{w}}{\partial \mathrm{y}}\right) \tag{6.90b}$$

$$\varepsilon_{1L} = \frac{1}{3}\left(\frac{\partial \mathrm{u}}{\partial \mathrm{x}} - \frac{\partial \mathrm{v}}{\partial \mathrm{y}}\right) \tag{6.90c}$$

$$\varepsilon_{1N} = \frac{1}{6}\left(2\frac{\partial \mathrm{v}}{\partial \mathrm{x}}\frac{\partial \mathrm{v}}{\partial \mathrm{x}} + \frac{\partial \mathrm{v}}{\partial \mathrm{y}}\frac{\partial \mathrm{v}}{\partial \mathrm{y}} - \frac{\partial \mathrm{u}}{\partial \mathrm{x}}\frac{\partial \mathrm{u}}{\partial \mathrm{x}} + \frac{\partial \mathrm{w}}{\partial \mathrm{x}}\frac{\partial \mathrm{w}}{\partial \mathrm{x}} - \frac{\partial \mathrm{w}}{\partial \mathrm{y}}\frac{\partial \mathrm{w}}{\partial \mathrm{y}} + 2\frac{\partial \mathrm{u}}{\partial \mathrm{y}}\frac{\partial \mathrm{v}}{\partial \mathrm{x}}\right) \tag{6.90d}$$

$$\varepsilon_{2L} = \frac{1}{3}\left(\frac{\partial \mathrm{v}}{\partial \mathrm{y}} - \frac{\partial \mathrm{w}}{\partial \mathrm{z}}\right) \tag{6.90e}$$

$$\varepsilon_{2N} = \frac{1}{6}\left(\frac{\partial \mathrm{w}}{\partial \mathrm{z}}\frac{\partial \mathrm{w}}{\partial \mathrm{z}} - \frac{\partial \mathrm{v}}{\partial \mathrm{x}}\frac{\partial \mathrm{v}}{\partial \mathrm{x}} - \frac{\partial \mathrm{v}}{\partial \mathrm{y}}\frac{\partial \mathrm{v}}{\partial \mathrm{y}} - \frac{\partial \mathrm{u}}{\partial \mathrm{z}}\frac{\partial \mathrm{u}}{\partial \mathrm{z}} + \frac{\partial \mathrm{v}}{\partial \mathrm{z}}\frac{\partial \mathrm{v}}{\partial \mathrm{z}} + 3\frac{\partial \mathrm{w}}{\partial \mathrm{y}}\frac{\partial \mathrm{w}}{\partial \mathrm{y}} - 2\frac{\partial \mathrm{u}}{\partial \mathrm{y}}\frac{\partial \mathrm{v}}{\partial \mathrm{x}} + 4\frac{\partial \mathrm{v}}{\partial \mathrm{z}}\frac{\partial \mathrm{w}}{\partial \mathrm{y}}\right) \tag{6.90f}$$

$$\gamma_{1L} = \frac{\partial \mathrm{v}}{\partial \mathrm{z}} + \frac{\partial \mathrm{w}}{\partial \mathrm{y}} \tag{6.90g}$$

$$\gamma_{1N} = 2\frac{\partial \mathrm{u}}{\partial \mathrm{x}}\frac{\partial \mathrm{v}}{\partial \mathrm{z}} - \frac{\partial \mathrm{u}}{\partial \mathrm{z}}\frac{\partial \mathrm{v}}{\partial \mathrm{x}} + 2\frac{\partial \mathrm{u}}{\partial \mathrm{x}}\frac{\partial \mathrm{w}}{\partial \mathrm{y}} - \frac{\partial \mathrm{u}}{\partial \mathrm{y}}\frac{\partial \mathrm{w}}{\partial \mathrm{x}} - \frac{\partial \mathrm{v}}{\partial \mathrm{y}}\frac{\partial \mathrm{v}}{\partial \mathrm{z}} - 2\frac{\partial \mathrm{v}}{\partial \mathrm{y}}\frac{\partial \mathrm{w}}{\partial \mathrm{y}} + \frac{\partial \mathrm{w}}{\partial \mathrm{y}}\frac{\partial \mathrm{w}}{\partial \mathrm{z}} \tag{6.90h}$$

$$\gamma_{2L} = \frac{\partial \mathrm{v}}{\partial \mathrm{z}} + \frac{\partial \mathrm{w}}{\partial \mathrm{y}} \tag{6.90i}$$

$$\gamma_{2N} = \frac{\partial \mathrm{u}}{\partial \mathrm{y}}\frac{\partial \mathrm{u}}{\partial \mathrm{z}} - 2\frac{\partial \mathrm{u}}{\partial \mathrm{x}}\frac{\partial \mathrm{v}}{\partial \mathrm{z}} - 2\frac{\partial \mathrm{u}}{\partial \mathrm{x}}\frac{\partial \mathrm{w}}{\partial \mathrm{y}} + \frac{\partial \mathrm{v}}{\partial \mathrm{y}}\frac{\partial \mathrm{v}}{\partial \mathrm{z}} + \frac{\partial \mathrm{w}}{\partial \mathrm{y}}\frac{\partial \mathrm{w}}{\partial \mathrm{z}} \tag{6.90j}$$

$$\gamma_{3L} = \frac{\partial \mathrm{u}}{\partial \mathrm{y}} + \frac{\partial \mathrm{v}}{\partial \mathrm{x}} \tag{6.90k}$$

$$\gamma_{3N} = -\frac{\partial \mathrm{u}}{\partial \mathrm{x}}\frac{\partial \mathrm{u}}{\partial \mathrm{y}} - 2\frac{\partial \mathrm{u}}{\partial \mathrm{x}}\frac{\partial \mathrm{v}}{\partial \mathrm{x}} + \frac{\partial \mathrm{v}}{\partial \mathrm{x}}\frac{\partial \mathrm{v}}{\partial \mathrm{y}} + \frac{\partial \mathrm{w}}{\partial \mathrm{x}}\frac{\partial \mathrm{w}}{\partial \mathrm{y}} \tag{6.90l}$$

The total stiffness matrix can be obtained as a sum of the linear and five nonlinear stiffness matrices.

First, the linear strain-displacement matrix $\mathbf{B}_L$ is obtained by expressing the strain attributes in terms of the nodal displacements through derivatives of the shape functions. Specifically, the linear strain-displacement matrix takes the form of

$$\mathbf{E}_L = \begin{Bmatrix} \xi_L \\ \varepsilon_{1L} \\ \varepsilon_{2L} \\ \gamma_{1L} \\ \gamma_{2L} \\ \gamma_{3L} \end{Bmatrix} = \begin{Bmatrix} \frac{1}{3}\,u_{,x} + \frac{1}{3}\,v_{,y} + \frac{1}{3}\,w_{,z} \\ \frac{1}{3}\,u_{,x} - \frac{1}{3}\,v_{,y} \\ \frac{1}{3}\,v_{,y} - \frac{1}{3}\,w_{,z} \\ v_{,z} + w_{,y} \\ v_{,z} + w_{,y} \\ u_{,y} + v_{,x} \end{Bmatrix} = \sum_{i=1}^{4} \begin{bmatrix} \frac{1}{3}\,N_{i,x} & \frac{1}{3}\,N_{i,y} & \frac{1}{3}\,N_{i,z} \\ \frac{1}{3}\,N_{i,x} & \frac{-1}{3}\,N_{i,y} & 0 \\ 0 & \frac{1}{3}\,N_{i,y} & \frac{-1}{3}\,N_{i,z} \\ 0 & N_{i,z} & N_{i,y} \\ 0 & N_{i,z} & N_{i,y} \\ N_{i,y} & N_{i,x} & 0 \end{bmatrix} \begin{Bmatrix} u_i \\ v_i \\ w_i \end{Bmatrix} \tag{6.91}$$

$$= \Big[[\mathbf{b}_{L1}][\mathbf{b}_{L2}][\mathbf{b}_{L3}][\mathbf{b}_{L4}] \Big] \left\{ \mathbf{u}^{(e)} \right\} = \mathbf{B}_L \mathbf{u}^{(e)}$$

wherein each component of $\mathbf{B}_L$ is given by

$$[\mathbf{b}_{Li}] = \begin{bmatrix} \frac{1}{3}\,N_{i,x} & \frac{1}{3}\,N_{i,y} & \frac{1}{3}\,N_{i,z} \\ \frac{1}{3}\,N_{i,x} & -\frac{1}{3}\,N_{i,y} & 0 \\ 0 & \frac{1}{3}\,N_{i,y} & -\frac{1}{3}\,N_{i,z} \\ 0 & N_{i,z} & N_{i,y} \\ 0 & N_{i,z} & N_{i,y} \\ N_{i,y} & N_{i,x} & 0 \end{bmatrix} \tag{6.92a}$$

and the nodal displacement vector for element e is given as

$$\mathbf{u}^{(e)} = \begin{Big\{} u_1 & v_1 & w_1 & u_2 & v_2 & w_2 & u_3 & v_3 & w_3 & u_4 & v_4 & w_4 \end{Big\}^{\mathsf{T}}. \tag{6.92b}$$

Note that the linear strain–displacement matrix $\mathbf{B_L}$ consists only of derivatives for the shape functions, and thus, remains the same throughout a deformation process.

Now we establish the nonlinear strain-displacement matrices that will be used to obtain the nonlinear stiffness matrix. The nonlinear components of each strain attribute have been additively decomposed into five components to make our computation easier. Components of each strain attribute are placed into an associated vector resulting in an additive decomposition of the total nonlinear strain $\mathbf{E}_N$. To obtain the nonlinear stiffness matrix corresponding to these nonlinear strain components, the nonlinear strains are written as a product of two quantities: a matrix $\mathbf{A}$ containing various components of the displacement gradient, and a vector $\boldsymbol{\theta}$ that contains the derivatives of displacement with respect to spatial location. The vector $\boldsymbol{\theta}$ essentially represents the slope of the body resulting from the deformation process. The components of the displacement gradient are placed in the matrix $\mathbf{A}$ in such a way so that its product with the slope vector yields the corresponding contribution to the nonlinear strain.

The slope vector $\boldsymbol{\theta}$ can further be expressed in terms of the corresponding nodal displacements by using the derivatives of the shape functions. Thus, the nonlinear strain components $\mathbf{E}_{Ni}, i = 1, 2, 3, 4$, can be expressed in terms of the nodal displacements, with the nonlinear strain-displacement matrix $\mathbf{B}_{Ni}$ corresponding to these strain components.

Now let us perform the procedure described above on all five nonlinear strain components.

For the first nonlinear strain, $\mathbf{E}_{N1}$ can be written as a product of the matrix $\mathbf{A}_1$ and the slope vector $\boldsymbol{\theta}_1$ as

$$\begin{aligned}
\mathbf{E}_{N1} &= \begin{Bmatrix} \xi_{1N} \\ \varepsilon_{1N} \\ \varepsilon_{2N} \\ \gamma_{1N} \\ \gamma_{2N} \\ \gamma_{3N} \end{Bmatrix} = \begin{Bmatrix} \frac{1}{6}\left(-u_{,x}^2 - v_{,y}^2 - w_{,z}^2\right) \\ \frac{1}{6}\left(-u_{,x}^2 + v_{,y}^2\right) \\ \frac{1}{6}\left(-v_{,y}^2 + w_{,z}^2\right) \\ -v_{,z}\, v_{,y} + w_{,y}\, w_{,z} \\ v_{,z}\, v_{,y} + w_{,y}\, w_{,z} \\ -u_{,x}\, u_{,y} + v_{,x}\, v_{,y} \end{Bmatrix} = \frac{1}{2} \begin{bmatrix} -\frac{1}{3}\,\partial u/\partial x & -\frac{1}{3}\,\partial v/\partial y & -\frac{1}{3}\,\partial w/\partial z \\ -\frac{1}{3}\,\partial u/\partial x & \frac{1}{3}\,\partial v/\partial y & 0 \\ 0 & -\frac{1}{3}\,\partial v/\partial y & \frac{1}{3}\,\partial w/\partial z \\ 0 & -2\,\partial v/\partial z & 2\,\partial w/\partial y \\ 0 & 2\,\partial v/\partial z & 2\,\partial w/\partial y \\ -2\,\partial u/\partial y & 2\,\partial v/\partial x & 0 \end{bmatrix} \begin{Bmatrix} \partial u/\partial x \\ \partial v/\partial y \\ \partial w/\partial z \end{Bmatrix} \\
&= \tfrac{1}{2}\,\mathbf{A}_1\,\boldsymbol{\theta}_1
\end{aligned} \tag{6.93}$$

with

$$\mathrm{d}\mathbf{A}_1 = \begin{bmatrix} -\frac{1}{3}\,\partial \mathrm{d}u/\partial x & -\frac{1}{3}\,\partial \mathrm{d}v/\partial y & -\frac{1}{3}\,\partial \mathrm{d}w/\partial z \\ -\frac{1}{3}\,\partial \mathrm{d}u/\partial x & \frac{1}{3}\,\partial \mathrm{d}v/\partial y & 0 \\ 0 & -\frac{1}{3}\,\partial \mathrm{d}v/\partial y & \frac{1}{3}\,\partial \mathrm{d}w/\partial z \\ 0 & -2\,\partial \mathrm{d}v/\partial z & 2\,\partial \mathrm{d}w/\partial y \\ 0 & 2\,\partial \mathrm{d}v/\partial z & 2\,\partial \mathrm{d}w/\partial y \\ -2\,\partial \mathrm{d}u/\partial y & 2\,\partial \mathrm{d}v/\partial x & 0 \end{bmatrix} = \sum_{i=1}^{4} \begin{bmatrix} -\frac{1}{3}\,N_{i,x}\,\mathrm{d}u_i & -\frac{1}{3}\,N_{i,y}\,\mathrm{d}v_i & -\frac{1}{3}\,N_{i,z}\,\mathrm{d}w_i \\ -\frac{1}{3}\,N_{i,x}\,\mathrm{d}u_i & \frac{1}{3}\,N_{i,y}\,\mathrm{d}v_i & 0 \\ 0 & -\frac{1}{3}\,N_{i,y}\,\mathrm{d}v_i & \frac{1}{3}\,N_{i,z}\,\mathrm{d}w_i \\ 0 & -2\,N_{i,z}\,\mathrm{d}v_i & 2\,N_{i,y}\,\mathrm{d}w_i \\ 0 & 2\,N_{i,z}\,\mathrm{d}v_i & 2\,N_{i,y}\,\mathrm{d}w_i \\ -2\,N_{i,y}\,\mathrm{d}u_i & 2\,N_{i,x}\,\mathrm{d}v_i & 0 \end{bmatrix}$$

$$= \Big[[\mathbf{l}_1][\mathbf{l}_2][\mathbf{l}_3][\mathbf{l}_4]\Big] \Big[[\mathbf{d}_1][\mathbf{d}_2][\mathbf{d}_3][\mathbf{d}_4]\Big]^{\mathsf{T}} = \mathbf{L}_1\mathbf{D}_1 \tag{6.94a}$$

wherein

$$[\mathbf{l}_i] = \begin{bmatrix} -\frac{1}{3}\,N_{i,x} & -\frac{1}{3}\,N_{i,y} & -\frac{1}{3}\,N_{i,z} \\ -\frac{1}{3}\,N_{i,x} & \frac{1}{3}\,N_{i,y} & 0 \\ 0 & -\frac{1}{3}\,N_{i,y} & \frac{1}{3}\,N_{i,z} \\ 0 & -2\,N_{i,z} & 2\,N_{i,y} \\ 0 & 2\,N_{i,z} & 2\,N_{i,y} \\ -2\,N_{i,y} & 2\,N_{i,x} & 0 \end{bmatrix} \quad \text{and} \quad [\mathbf{d}_i] = \begin{bmatrix} \mathrm{d}u_i & 0 & 0 \\ 0 & \mathrm{d}v_i & 0 \\ 0 & 0 & \mathrm{d}w_i \end{bmatrix}. \tag{6.94b}$$

The derivative of displacement with respect to spatial variables x, y and z, can be written as

$$\boldsymbol{\theta}_1 = \begin{Bmatrix} \partial u/\partial x \\ \partial v/\partial y \\ \partial w/\partial z \end{Bmatrix} = \sum_{i=1}^{4} \begin{Bmatrix} N_{i,x}\,u_i \\ N_{i,y}\,v_i \\ N_{i,z}\,w_i \end{Bmatrix} = \Big[[\mathbf{h}_1][\mathbf{h}_2][\mathbf{h}_3][\mathbf{h}_4]\Big] \left\{\mathbf{u}^{(e)}\right\} = \mathbf{H}_1\,\mathbf{u}^{(e)} \tag{6.95}$$

for element e, where

$$[\mathbf{h}_i] = \begin{bmatrix} N_{i,x} & 0 & 0 \\ 0 & N_{i,y} & 0 \\ 0 & 0 & N_{i,z} \end{bmatrix}. \tag{6.96}$$

Hence, the strain-displacement $\mathbf{B}_{N1}$ corresponding to the first nonlinear strain becomes

$$\mathbf{B}_{N1} = \mathbf{A}_1 \, \mathbf{H}_1 = \Big[[\mathbf{b}_{N1}][\mathbf{b}_{N2}][\mathbf{b}_{N3}][\mathbf{b}_{N4}] \Big] \tag{6.97}$$

wherein the components of $\mathbf{B}_{N1}$ are given as

$$[\mathbf{b}_i] = \begin{bmatrix} -\frac{1}{3}\,\partial u/\partial x & -\frac{1}{3}\,\partial v/\partial y & -\frac{1}{3}\,\partial w/\partial z \\ -\frac{1}{3}\,\partial u/\partial x & \frac{1}{3}\,\partial v/\partial y & 0 \\ 0 & -\frac{1}{3}\,\partial v/\partial y & \frac{1}{3}\,\partial w/\partial z \\ 0 & -2\,\partial v/\partial z & 2\,\partial w/\partial y \\ 0 & 2\,\partial v/\partial z & 2\,\partial w/\partial y \\ -2\,\partial u/\partial y & 2\,\partial v/\partial x & 0 \end{bmatrix} \begin{bmatrix} N_{i,x} & 0 & 0 \\ 0 & N_{i,y} & 0 \\ 0 & 0 & N_{i,z} \end{bmatrix}. \tag{6.98}$$

In a similar manner, we can obtain the strain-displacement matrices corresponding to the other nonlinear strain components. The second nonlinear strain terms can be written as

$$\begin{aligned} \mathbf{E}_{N2} &= \begin{Bmatrix} \xi_L \\ \varepsilon_{1N} \\ \varepsilon_{2N} \\ \gamma_{1N} \\ \gamma_{2N} \\ \gamma_{3N} \end{Bmatrix} = \begin{Bmatrix} \frac{1}{6}\left(u_{,z}^2 - v_{,z}^2 - w_{,y}^2\right) \\ \frac{-1}{6}\, w_{,y}^2 \\ \frac{1}{6}\left(-u_{,z}^2 + v_{,z}^2 + 3\, w_{,y}^2\right) \\ 0 \\ u_{,y}\, u_{,z} \\ w_{,x}\, w_{,y} \end{Bmatrix} = \frac{1}{2} \begin{bmatrix} \frac{1}{3}\,\partial u/\partial z & -\frac{1}{3}\,\partial v/\partial z & -\frac{1}{3}\,\partial w/\partial y \\ 0 & 0 & -\frac{1}{3}\,\partial w/\partial y \\ -\frac{1}{3}\,\partial u/\partial z & \frac{1}{3}\,\partial v/\partial z & \partial w/\partial y \\ 0 & 0 & 0 \\ 2\,\partial u/\partial y & 0 & 0 \\ 0 & 0 & 2\,\partial w/\partial x \end{bmatrix} \begin{Bmatrix} \partial u/\partial z \\ \partial v/\partial z \\ \partial w/\partial y \end{Bmatrix} \\ &= \tfrac{1}{2}\, \mathbf{A}_2\, \boldsymbol{\theta}_2 \end{aligned} \tag{6.99}$$

with

$$\mathrm{d}\mathbf{A}_2 = \begin{bmatrix} \frac{1}{3}\,\partial \mathrm{d}u/\partial z & -\frac{1}{3}\,\partial \mathrm{d}v/\partial z & -\frac{1}{3}\,\partial \mathrm{d}w/\partial y \\ 0 & 0 & -\frac{1}{3}\,\partial \mathrm{d}w/\partial y \\ -\frac{1}{3}\,\partial \mathrm{d}u/\partial z & \frac{1}{3}\,\partial \mathrm{d}v/\partial z & \partial \mathrm{d}w/\partial y \\ 0 & 0 & 0 \\ 2\,\partial \mathrm{d}u/\partial y & 0 & 0 \\ 0 & 0 & 2\,\partial \mathrm{d}w/\partial x \end{bmatrix} = \sum_{i=1}^{4} \begin{bmatrix} \frac{1}{3}\,N_{i,z}\,\mathrm{d}u_i & -\frac{1}{3}\,N_{i,z}\,\mathrm{d}v_i & -\frac{1}{3}\,N_{i,y}\,\mathrm{d}w_i \\ 0 & 0 & -\frac{1}{3}\,N_{i,y}\,\mathrm{d}w_i \\ -\frac{1}{3}\,N_{i,z}\,\mathrm{d}u_i & \frac{1}{3}\,N_{i,z}\,\mathrm{d}v_i & N_{i,y}\,\mathrm{d}w_i \\ 0 & 0 & 0 \\ 2\,N_{i,y}\,\mathrm{d}u_i & 0 & 0 \\ 0 & 0 & 2\,N_{i,x}\,\mathrm{d}w_i \end{bmatrix}$$

$$= \Big[[\mathbf{l}_1][\mathbf{l}_2][\mathbf{l}_3][\mathbf{l}_4] \Big] \Big[[\mathbf{d}_1][\mathbf{d}_2][\mathbf{d}_3][\mathbf{d}_4] \Big]^{\mathsf{T}} = \mathbf{L}_2 \mathbf{D}_2 \tag{6.100a}$$

wherein

$$[\mathbf{l}_i] = \begin{bmatrix} \frac{1}{3}\,N_{i,z} & -\frac{1}{3}\,N_{i,z} & -\frac{1}{3}\,N_{i,y} \\ 0 & 0 & -\frac{1}{3}\,N_{i,y} \\ -\frac{1}{3}\,N_{i,z} & \frac{1}{3}\,N_{i,z} & N_{i,y} \\ 0 & 0 & 0 \\ 2\,N_{i,y} & 0 & 0 \\ 0 & 0 & 2\,N_{i,x} \end{bmatrix} \quad \text{and} \quad [\mathbf{d}_i] = \begin{bmatrix} \mathrm{d}u_i & 0 & 0 \\ 0 & \mathrm{d}v_i & 0 \\ 0 & 0 & \mathrm{d}w_i \end{bmatrix}. \tag{6.100b}$$

The slope vector can further be expressed in terms of the nodal parameters via

$$\boldsymbol{\theta}_2 = \begin{Bmatrix} \partial u/\partial z \\ \partial v/\partial z \\ \partial w/\partial y \end{Bmatrix} = \sum_{i=1}^{4} \begin{Bmatrix} N_{i,z}\,u_i \\ N_{i,z}\,v_i \\ N_{i,y}\,w_i \end{Bmatrix} = \Big[[\mathbf{h}_1][\mathbf{h}_2][\mathbf{h}_3][\mathbf{h}_4] \Big] \left\{ \mathbf{u}^{(e)} \right\} = \mathbf{H}_2\,\mathbf{u}^{(e)} \tag{6.101}$$

where

$$[\mathbf{h}_i] = \begin{bmatrix} N_{i,z} & 0 & 0 \\ 0 & N_{i,z} & 0 \\ 0 & 0 & N_{i,y} \end{bmatrix}. \tag{6.102}$$

Hence, the strain-displacement matrix $\mathbf{B}_{N2}$ becomes

$$\mathbf{B}_{N2} = \mathbf{A}_2\,\mathbf{H}_2 = \Big[[\mathbf{b}_{N1}][\mathbf{b}_{N2}][\mathbf{b}_{N3}][\mathbf{b}_{N4}]\Big]\,. \tag{6.103}$$

The components of this strain-displacement matrix are given as

$$[\mathbf{b}_{Ni}] = \begin{bmatrix} \frac{1}{3}\,\partial u/\partial z & -\frac{1}{3}\,\partial v/\partial z & -\frac{1}{3}\,\partial w/\partial y \\ 0 & 0 & -\frac{1}{3}\,\partial w/\partial y \\ -\frac{1}{3}\,\partial u/\partial z & \frac{1}{3}\,\partial v/\partial z & \partial w/\partial y \\ 0 & 0 & 0 \\ 2\,\partial u/\partial y & 0 & 0 \\ 0 & 0 & 2\,\partial w/\partial x \end{bmatrix} \begin{bmatrix} N_{i,z} & 0 & 0 \\ 0 & N_{i,z} & 0 \\ 0 & 0 & N_{i,y} \end{bmatrix}. \tag{6.104}$$

For the third nonlinear strain term, i.e., $\mathbf{E}_{N3}$, can be written as

$$\begin{aligned} \mathbf{E}_{N3} &= \begin{Bmatrix} \xi_L \\ \varepsilon_{1N} \\ \varepsilon_{2N} \\ \gamma_{1N} \\ \gamma_{2N} \\ \gamma_{3N} \end{Bmatrix} = \begin{Bmatrix} \frac{1}{6}\,\left(-2\,v_{,x}\,u_{,y} - 4\,w_{,y}\,v_{,z} + w_{,x}^2\right) \\ \frac{1}{6}\,\left(2\,v_{,x}\,u_{,y} + w_{,x}^2\right) \\ \frac{1}{6}\,\left(-2\,v_{,x}\,u_{,y} + 4\,w_{,y}\,v_{,z}\right) \\ 0 \\ 0 \\ 0 \end{Bmatrix} \\ &= \frac{1}{2} \begin{bmatrix} -\frac{2}{3}\,\partial v/\partial x & -\frac{4}{3}\,\partial w/\partial y & \frac{1}{3}\,\partial w/\partial x \\ \frac{2}{3}\,\partial v/\partial x & 0 & \frac{1}{3}\,\partial w/\partial x \\ -\frac{2}{3}\,\partial v/\partial x & \frac{4}{3}\,\partial w/\partial y & 0 \\ 0 & 0 & 0 \\ 0 & 0 & 0 \\ 0 & 0 & 0 \end{bmatrix} \begin{Bmatrix} \partial u/\partial y \\ \partial v/\partial z \\ \partial w/\partial x \end{Bmatrix} = \tfrac{1}{2}\,\mathbf{A}_3\,\boldsymbol{\theta}_3 \end{aligned} \tag{6.105}$$

with

$$\mathrm{d}\mathbf{A}_3 = \begin{bmatrix} -\frac{2}{3}\,\partial \mathrm{d}v/\partial x & -\frac{4}{3}\,\partial \mathrm{d}w/\partial y & \frac{1}{3}\,\partial \mathrm{d}w/\partial x \\ \frac{2}{3}\,\partial \mathrm{d}v/\partial x & 0 & \frac{1}{3}\,\partial \mathrm{d}w/\partial x \\ -\frac{2}{3}\,\partial \mathrm{d}v/\partial x & \frac{4}{3}\,\partial \mathrm{d}w/\partial y & 0 \\ 0 & 0 & 0 \\ 0 & 0 & 0 \\ 0 & 0 & 0 \end{bmatrix} = \sum_{i=1}^{4} \begin{bmatrix} -\frac{2}{3}\,N_{i,x}\,\mathrm{d}v_i & -\frac{4}{3}\,N_{i,y}\,\mathrm{d}w_i & \frac{1}{3}\,N_{i,x}\,\mathrm{d}w_i \\ \frac{2}{3}\,N_{i,x}\,\mathrm{d}v_i & 0 & \frac{1}{3}\,N_{i,x}\,\mathrm{d}w_i \\ -\frac{2}{3}\,N_{i,x}\,\mathrm{d}v_i & \frac{4}{3}\,N_{i,y}\,\mathrm{d}w_i & 0 \\ 0 & 0 & 0 \\ 0 & 0 & 0 \\ 0 & 0 & 0 \end{bmatrix}$$

$$= \Big[[\mathbf{l}_1][\mathbf{l}_2][\mathbf{l}_3][\mathbf{l}_4]\Big] \Big[[\mathbf{d}_1][\mathbf{d}_2][\mathbf{d}_3][\mathbf{d}_4]\Big]^{\mathsf{T}} = \mathbf{L}_3\mathbf{D}_3 \tag{6.106a}$$

wherein

$$[\mathbf{l}_i] = \begin{bmatrix} -\frac{2}{3}\,N_{i,x} & -\frac{4}{3}\,N_{i,y} & \frac{1}{3}\,N_{i,x} \\ \frac{2}{3}\,N_{i,x} & 0 & \frac{1}{3}N_{i,x} \\ -\frac{2}{3}\,N_{i,x} & \frac{4}{3}\,N_{i,y} & 0 \\ 0 & 0 & 0 \\ 0 & 0 & 0 \\ 0 & 0 & 0 \end{bmatrix} \quad \text{and} \quad [\mathbf{d}_i] = \begin{bmatrix} \mathrm{d}v_i & 0 & 0 \\ 0 & \mathrm{d}w_i & 0 \\ 0 & 0 & \mathrm{d}w_i \end{bmatrix}. \tag{6.106b}$$

Here the slope vector $\boldsymbol{\theta}_3$ contains derivatives of displacements with respect to spatial variables y, z, x that relate to the nodal parameters via

$$\boldsymbol{\theta}_3 = \begin{Bmatrix} \partial u/\partial y \\ \partial v/\partial z \\ \partial w/\partial x \end{Bmatrix} = \sum_{i=1}^{4} \begin{Bmatrix} N_{i,y}\,u_i \\ N_{i,z}\,v_i \\ N_{i,x}\,w_i \end{Bmatrix} = \Big[[\mathbf{h}_1][\mathbf{h}_2][\mathbf{h}_3][\mathbf{h}_4]\Big] \big\{\mathbf{u}^{(e)}\big\} = \mathbf{H}_3\mathbf{u}^{(e)} \tag{6.107}$$

where

$$[\mathbf{h}_i] = \begin{bmatrix} N_{i,y} & 0 & 0 \\ 0 & N_{i,z} & 0 \\ 0 & 0 & N_{i,x} \end{bmatrix}. \tag{6.108}$$

Therefore, the strain-displacement matrix $\mathbf{B}_{N3}$ becomes

$$\mathbf{B}_{N3} = \mathbf{A}_3\,\mathbf{H}_3 = \Big[\,[\mathbf{b}_{N1}][\mathbf{b}_{N2}][\mathbf{b}_{N3}][\mathbf{b}_{N4}]\,\Big] \tag{6.109}$$

whose components are given as

$$\mathbf{b}_{Ni} = \begin{bmatrix} -\frac{2}{3}\,\partial v/\partial x & -\frac{4}{3}\,\partial w/\partial y & \frac{1}{3}\,\partial w/\partial x \\ \frac{2}{3}\,\partial v/\partial x & 0 & \frac{1}{3}\,\partial w/\partial x \\ -\frac{2}{3}\,\partial v/\partial x & \frac{4}{3}\,\partial w/\partial y & 0 \\ 0 & 0 & 0 \\ 0 & 0 & 0 \\ 0 & 0 & 0 \end{bmatrix} \begin{bmatrix} N_{i,y} & 0 & 0 \\ 0 & N_{i,z} & 0 \\ 0 & 0 & N_{i,x} \end{bmatrix}. \tag{6.110}$$

For the fourth nonlinear strain term, $\mathbf{E}_{N4}$ can be written as

$$\begin{aligned} \mathbf{E}_{N4} &= \begin{Bmatrix} \xi_L \\ \varepsilon_{1N} \\ \varepsilon_{2N} \\ \gamma_{1N} \\ \gamma_{2N} \\ \gamma_{3N} \end{Bmatrix} = \begin{Bmatrix} 0 \\ \frac{2}{6}\,v_{,x}^2 \\ -\frac{1}{6}\,v_{,x}^2 \\ 2\,v_{,z}\,u_{,x} + 2\,u_{,x}\,w_{,y} \\ -2\,v_{,z}\,u_{,x} - 2\,u_{,x}\,w_{,y} \\ -2\,v_{,x}\,u_{,x} \end{Bmatrix} = \frac{1}{2} \begin{bmatrix} 0 & 0 & 0 \\ 0 & \frac{2}{3}\,\partial v/\partial x & 0 \\ 0 & -\frac{1}{3}\,\partial v/\partial x & 0 \\ 4\,\partial v/\partial z & 0 & 4\,\partial u/\partial x \\ -4\,\partial v/\partial z & 0 & -4\,\partial u/\partial x \\ -4\,\partial v/\partial x & 0 & 0 \end{bmatrix} \begin{Bmatrix} \partial u/\partial x \\ \partial v/\partial x \\ \partial w/\partial y \end{Bmatrix} \\ &= \tfrac{1}{2}\,\mathbf{A}_4\,\boldsymbol{\theta}_4 \end{aligned} \tag{6.111}$$

with

$$\mathrm{d}\mathbf{A}_4 = \begin{bmatrix} 0 & 0 & 0 \\ 0 & \frac{2}{3}\,\partial \mathrm{d}v/\partial x & 0 \\ 0 & -\frac{1}{3}\,\partial \mathrm{d}v/\partial x & 0 \\ 4\,\partial \mathrm{d}v/\partial z & 0 & 4\,\partial \mathrm{d}u/\partial x \\ -4\,\partial \mathrm{d}v/\partial z & 0 & -4\,\partial \mathrm{d}u/\partial x \\ -4\,\partial \mathrm{d}v/\partial x & 0 & 0 \end{bmatrix} = \sum_{i=1}^{4} \begin{bmatrix} 0 & 0 & 0 \\ 0 & \frac{2}{3}\,N_{i,x}\,\mathrm{d}v_i & 0 \\ 0 & -\frac{1}{3}\,N_{i,x}\,\mathrm{d}v_i & 0 \\ 4\,N_{i,z}\,\mathrm{d}v_i & 0 & 4\,N_{i,x}\,\mathrm{d}u_i \\ -4\,N_{i,z}\,\mathrm{d}v_i & 0 & -4\,N_{i,x}\,\mathrm{d}u_i \\ -4\,N_{i,x}\,\mathrm{d}v_i & 0 & 0 \end{bmatrix}$$

$$= \Big[[\mathbf{l}_1][\mathbf{l}_2][\mathbf{l}_3][\mathbf{l}_4]\Big] \Big[[\mathbf{d}_1][\mathbf{d}_2][\mathbf{d}_3][\mathbf{d}_4]\Big]^{\mathsf{T}} = \mathbf{L}_4\mathbf{D}_4 \tag{6.112a}$$

wherein

$$[\mathbf{l}_i] = \begin{bmatrix} 0 & 0 & 0 \\ 0 & \frac{2}{3}\,N_{i,x} & 0 \\ 0 & -\frac{1}{3}\,N_{i,x} & 0 \\ 4\,N_{i,z} & 0 & 4\,N_{i,x} \\ -4\,N_{i,z} & 0 & -4\,N_{i,x} \\ -4\,N_{i,x} & 0 & 0 \end{bmatrix} \quad \text{and} \quad [\mathbf{d}_i] = \begin{bmatrix} \mathrm{d}v_i & 0 & 0 \\ 0 & \mathrm{d}v_i & 0 \\ 0 & 0 & \mathrm{d}u_i \end{bmatrix}. \tag{6.112b}$$

Here the slope vector $\boldsymbol{\theta}_4$ contains derivatives of displacements with respect to the spatial variables x and y that relate to the nodal parameters via

$$\boldsymbol{\theta}_4 = \begin{Bmatrix} \partial u/\partial x \\ \partial v/\partial x \\ \partial w/\partial y \end{Bmatrix} = \sum_{i=1}^{4} \begin{Bmatrix} N_{i,x}\,u_i \\ N_{i,x}\,v_i \\ N_{i,y}\,w_i \end{Bmatrix} = \Big[[\mathbf{h}_1][\mathbf{h}_2][\mathbf{h}_3][\mathbf{h}_4]\Big] \left\{\mathbf{u}^{(e)}\right\} = \mathbf{H}_4\mathbf{u}^{(e)} \tag{6.113}$$

where

$$[\mathbf{h}_i] = \begin{bmatrix} N_{i,x} & 0 & 0 \\ 0 & N_{i,x} & 0 \\ 0 & 0 & N_{i,y} \end{bmatrix}. \tag{6.114}$$

Therefore, the strain–displacement matrix $\mathbf{B}_{N4}$ becomes

$$\mathbf{B}_{N4} = \mathbf{A}_4\,\mathbf{H}_4 = \Big[\,[\mathbf{b}_{N1}][\mathbf{b}_{N2}][\mathbf{b}_{N3}][\mathbf{b}_{N4}]\,\Big] \tag{6.115}$$

whose components are given as

$$\mathbf{b}_{Ni} = \begin{bmatrix} 0 & 0 & 0 \\ 0 & \frac{2}{3}\,\partial v/\partial x & 0 \\ 0 & -\frac{1}{3}\,\partial v/\partial x & 0 \\ 4\,\partial v/\partial z & 0 & 4\,\partial u/\partial x \\ -4\,\partial v/\partial z & 0 & -4\,\partial u/\partial x \\ -4\,\partial v/\partial x & 0 & 0 \end{bmatrix} \begin{bmatrix} N_{i,x} & 0 & 0 \\ 0 & N_{i,x} & 0 \\ 0 & 0 & N_{i,y} \end{bmatrix}. \tag{6.116}$$

The last nonlinear strain term, $\mathbf{E}_{N5}$ can be written as

$$\begin{aligned} \mathbf{E}_{N5} &= \begin{Bmatrix} \xi_L \\ \varepsilon_{1N} \\ \varepsilon_{2N} \\ \gamma_{1N} \\ \gamma_{2N} \\ \gamma_{3N} \end{Bmatrix} = \begin{Bmatrix} 0 \\ 0 \\ 0 \\ -v_{,x}\,u_{,z} - 2\,w_{,y}\,v_{,y} - u_{,y}\,w_{,x} \\ 0 \\ 0 \end{Bmatrix} \\ &= \frac{1}{2} \begin{bmatrix} 0 & 0 & 0 \\ 0 & 0 & 0 \\ 0 & 0 & 0 \\ -2\,\partial v/\partial x & -4\,\partial w/\partial y & -2\,\partial u/\partial y \\ 0 & 0 & 0 \\ 0 & 0 & 0 \end{bmatrix} \begin{Bmatrix} \partial u/\partial z \\ \partial v/\partial y \\ \partial w/\partial x \end{Bmatrix} = \tfrac{1}{2}\,\mathbf{A}_5\,\boldsymbol{\theta}_5 \end{aligned} \tag{6.117}$$

with

$$\mathrm{d}\mathbf{A}_5 = \begin{bmatrix} 0 & 0 & 0 \\ 0 & 0 & 0 \\ 0 & 0 & 0 \\ -2\,\partial \mathrm{d}v/\partial x & -4\,\partial \mathrm{d}w/\partial y & -2\,\partial \mathrm{d}u/\partial y \\ 0 & 0 & 0 \\ 0 & 0 & 0 \end{bmatrix} = \sum_{i=1}^{4} \begin{bmatrix} 0 & 0 & 0 \\ 0 & 0 & 0 \\ 0 & 0 & 0 \\ -2\,N_{i,x}\,\mathrm{d}v_i & -4\,N_{i,y}\,\mathrm{d}w_i & -2\,N_{i,y}\,\mathrm{d}u_i \\ 0 & 0 & 0 \\ 0 & 0 & 0 \end{bmatrix}$$

$$= \Big[[\mathbf{l}_1][\mathbf{l}_2][\mathbf{l}_3][\mathbf{l}_4] \Big] \Big[[\mathbf{d}_1][\mathbf{d}_2][\mathbf{d}_3][\mathbf{d}_4] \Big]^{\mathsf{T}} = \mathbf{L}_5 \mathbf{D}_5 \tag{6.118a}$$

wherein

$$[\mathbf{l}_i] = \begin{bmatrix} 0 & 0 & 0 \\ 0 & 0 & 0 \\ 0 & 0 & 0 \\ -2\,N_{i,x} & -4\,N_{i,y} & -2\,N_{i,y} \\ 0 & 0 & 0 \\ 0 & 0 & 0 \end{bmatrix} \quad \text{and} \quad [\mathbf{d}_i] = \begin{bmatrix} \mathrm{d}v_i & 0 & 0 \\ 0 & \mathrm{d}w_i & 0 \\ 0 & 0 & \mathrm{d}u_i \end{bmatrix}. \tag{6.118b}$$

the slope vector $\boldsymbol{\theta}_5$ relates to the nodal parameters via

$$\boldsymbol{\theta}_5 = \begin{Bmatrix} \partial u/\partial z \\ \partial v/\partial y \\ \partial w/\partial x \end{Bmatrix} = \sum_{i=1}^{4} \begin{Bmatrix} N_{i,z}\,u_i \\ N_{i,y}\,v_i \\ N_{i,x}\,w_i \end{Bmatrix} = \Big[[\mathbf{h}_1][\mathbf{h}_2][\mathbf{h}_3][\mathbf{h}_4] \Big] \big\{ \mathbf{u}^{(e)} \big\} = \mathbf{H}_5 \mathbf{u}^{(e)} \tag{6.119}$$

where

$$[\mathbf{h}_i] = \begin{bmatrix} N_{i,z} & 0 & 0 \\ 0 & N_{i,y} & 0 \\ 0 & 0 & N_{i,x} \end{bmatrix}. \tag{6.120}$$

Therefore, the strain-displacement matrix $\mathbf{B}_{N5}$ becomes

$$\mathbf{B}_{N5} = \mathbf{A}_5\,\mathbf{H}_5 = \Big[[\mathbf{b}_{N1}][\mathbf{b}_{N2}][\mathbf{b}_{N3}][\mathbf{b}_{N4}]\Big] \tag{6.121}$$

whose components are given as

$$\mathbf{b}_{Ni} = \begin{bmatrix} 0 & 0 & 0 \\ 0 & 0 & 0 \\ 0 & 0 & 0 \\ -2\,\partial v/\partial x & -4\,\partial w/\partial y & -2\,\partial u/\partial y \\ 0 & 0 & 0 \\ 0 & 0 & 0 \end{bmatrix} \begin{bmatrix} N_{i,z} & 0 & 0 \\ 0 & N_{i,y} & 0 \\ 0 & 0 & N_{i,x} \end{bmatrix}. \tag{6.122}$$

The total nonlinear strain-displacement matrix $\mathbf{B}_N$ can be obtained as a sum of its five components, i.e., $\mathbf{B}_N = \sum_{i=1}^{5} \mathbf{B}_{Ni}$.

To obtain the stiffness matrix for a tetrahedron, we need to compute the four constituent strain-displacement matrices $\mathbf{C}^s$, $\mathbf{C}^t$, $\mathbf{K}^s$ and $\mathbf{K}^t$, as mentioned earlier. The tangent stiffness matrix $\mathbf{C}^s$, as established in Eqn. (6.50), becomes

$$\mathbf{C}^s = \int_V \mathbf{H}^\mathsf{T}\,\mathbf{S}^s\,\mathbf{H}\,\mathrm{d}V = |\mathbf{J}| \sum_{i=1}^{n} \mathbf{H}^\mathsf{T}\,\mathbf{S}^s(\xi_i, \eta_i, \zeta_i)\,\mathbf{H}\,w_i \tag{6.123a}$$

wherein ξ_i, η_i, ζ_i and w_i are the co-ordinates and weights of quadrature at the i^{th} Gauss point, and

$$\mathbf{S}^s = \begin{bmatrix} \mathcal{S}_{11} & \mathcal{S}_{12} & \mathcal{S}_{13} \\ \mathcal{S}_{21} & \mathcal{S}_{22} & \mathcal{S}_{23} \\ \mathcal{S}_{31} & \mathcal{S}_{32} & \mathcal{S}_{33} \end{bmatrix}. \tag{6.123b}$$

The stress vector $\boldsymbol{T} = \{\pi, \sigma_1, \sigma_2, \tau_1, \tau_2, \tau_3\}^\mathsf{T}$ conjugate to strain $\boldsymbol{E}$ has elements that comprise

a pressure $\pi = \mathcal{S}_{11} + \mathcal{S}_{22} + \mathcal{S}_{33} = -3P$ where P denotes the common definition for pressure, two separate normal-stress differences $\sigma_1 = \mathcal{S}_{11} - \mathcal{S}_{22}$ and $\sigma_2 = \mathcal{S}_{22} - \mathcal{S}_{33}$, and three separate shear stresses $\tau_1 = \frac{b}{c}\mathcal{S}_{32}$, $\tau_2 = \frac{a}{c}\mathcal{S}_{31}$ and $\tau_3 = \frac{a}{b}\mathcal{S}_{21} - \alpha\tau_2$. Of these, only pressure has an initial value, viz., Π_0, which represents atmospheric pressure. In a reciprocal sense, the stress components are assigned via

$$\mathbf{S}^s = \begin{bmatrix} \frac{1}{3}(\pi + 2\sigma_1 + \sigma_2) & \frac{b}{a}(\tau_3 + \alpha\,\tau_2) & \frac{c}{a}\,\tau_2 \\ \frac{b}{a}(\tau_3 + \alpha\,\tau_2) & \frac{1}{3}(\pi - \sigma_1 + \sigma_2) & \frac{c}{a}\tau_1 \\ \frac{c}{a}\,\tau_2 & \frac{c}{a}\tau_1 & \frac{1}{3}(\pi - \sigma_1 - 2\sigma_2) \end{bmatrix} \tag{6.124}$$

The tangent stiffness matrix $\mathbf{C}^t$, as established in Eqn. (6.51), becomes

$$\mathbf{C}^t = \int_V \mathbf{B}^\mathsf{T}\,\boldsymbol{\mathcal{M}}^t\,\mathbf{B}\,\mathrm{d}V = |\mathbf{J}|\sum_{i=1}^{n}\mathbf{B}^\mathsf{T}\,\boldsymbol{\mathcal{M}}^t(\xi_i,\eta_i,\zeta_i)\,\mathbf{B}\,w_i \tag{6.125}$$

where the stress rate is described by its tangent modulus $\boldsymbol{\mathcal{M}}^t$.

The secant stiffness matrix $\mathbf{K}^s$, as established in Eqn. (6.48b), becomes

$$\mathbf{K}^s = \int_V \mathbf{B}^\mathsf{T}\,\boldsymbol{\mathcal{M}}^s\,\mathbf{B}\,\mathrm{d}V = |\mathbf{J}|\sum_{i=1}^{n}\mathbf{B}^\mathsf{T}\,\boldsymbol{\mathcal{M}}^s(\xi_i,\eta_i,\zeta_i)\,\mathbf{B}\,w_i \tag{6.126}$$

where the stress is described by its secant modulus $\boldsymbol{\mathcal{M}}^s$.

Likewise, a secant stiffness matrix $\mathbf{K}^t$, also established in Eqn. (6.51), becomes

$$\mathbf{K}^t = \int_V \mathbf{H}^\mathsf{T}\,\mathrm{d}\mathbf{S}^t\,\mathbf{H}\,\mathrm{d}V = |\mathbf{J}|\sum_{i=1}^{n}\mathbf{H}^\mathsf{T}\,\mathrm{d}\mathbf{S}^t(\xi_i,\eta_i,\zeta_i)\,\mathbf{H}\,w_i \tag{6.127}$$

where its stress rate is given by $\mathrm{d}\mathbf{S}^t := \mathbf{A}^\mathsf{T}\,\boldsymbol{\mathcal{M}}^t\,\mathrm{d}\mathbf{A}$.

6.2.5 Force Vector

The principle of stationary potential energy via the Rayleigh–Ritz approach, i.e., Eqn. (6.47), determines a basis for finite element stress analysis. The internal strain energy is balanced

with the potential energy of applied internal and external loads on the body.

The virtual work done by external forces δW in Eq. (6.47) can be expressed as

$$\delta W = \int_S \mathbf{t}\,\delta\mathbf{u}\,\mathrm{d}S = \int_S \mathbf{t}\,\mathbf{N}\,\mathrm{d}\boldsymbol{\Delta}\,\mathrm{d}S = \left(\int_S \mathbf{N}^\mathsf{T}\,\mathbf{t}\,\mathrm{d}S\right)\,\mathrm{d}\boldsymbol{\Delta} \tag{6.128a}$$

where $\mathrm{d}S$ denotes a surface element with $\mathbf{t}$ being its surface traction vector (per unit surface area) at current time. Hence, the external $\mathbf{F}_{BC}$ force vectors are

$$\mathbf{F}_{BC} = \int_S \mathbf{N}^\mathsf{T}\,\mathbf{t}\,\mathrm{d}S. \tag{6.128b}$$

The force needed to balance the residual stresses, i.e., $\boldsymbol{F}_0$, is evaluated as

$$\boldsymbol{F}_0 = \int_V \mathbf{B}_L^\mathsf{T}\,\boldsymbol{T}_0\,\mathrm{d}V + \int_V \mathbf{B}_N^\mathsf{T}\,\boldsymbol{T}_0\,\mathrm{d}V \tag{6.129}$$

where the first integral only needs to be evaluated once, as its argument is constant valued.

6.2.5.1 Force Vector for a Chord

Following the procedure described above, the force vector of a 1D alveolar chord is evaluated numerically in its natural co-ordinate system as

$$\mathbf{F}_{BC} = \int_L \mathbf{N}^\mathsf{T}\,\mathbf{t}\,\mathrm{d}L = \sum_{i=1}^{2} \mathbf{N}^\mathsf{T}\,\mathbf{t}\,|\mathbf{J}|\,w_i \tag{6.130}$$

where w_i are the weighting coefficients of the Gauss integration rule, $\mathbf{N}$ is the shape function matrix for chord, and $\mathbf{t}$ is the traction on the septal chord that is selected so that the traction can be additively decomposed into that carried by the collagen and elastin fibers.

The internal force $\boldsymbol{F}_0$ accounting for an initial residual stress of $\boldsymbol{T}_0$, expressed as two separate integrals, can be computed as

$$\boldsymbol{F}_0 = \int_L \mathbf{B}_L^\mathsf{T}\,\boldsymbol{T}_0\,A\,\mathrm{d}L + \int_L \mathbf{B}_N^\mathsf{T}\,\boldsymbol{T}_0\,A\,\mathrm{d}L = |\mathbf{J}| \sum_{i=1}^{2} \mathbf{B}_L^\mathsf{T}\,\boldsymbol{T}_0\,A_i\,w_i + |\mathbf{J}| \sum_{i=1}^{2} \mathbf{B}_N^\mathsf{T}\,\boldsymbol{T}_0\,A_i\,w_i \tag{6.131a}$$

where the first integral will only need to be evaluated once, as the argument is constant valued. The cross-sectional areas of biologic chords need not be the same at both Gauss points; hence, it cannot be pulled outside the sum (integration). Here the initial stress $\mathbf{T}_0 = [s_0] \mapsto \mathbf{S}_0 = [s_0]$ contains the initial stress s_0 carried by the collagen and elastin fibers; specifically,

$$s_0 = \left(\phi s_0^c + (1-\phi) s_0^e\right) \quad \text{where} \quad \phi := A_0^c/(A_0^c + A_0^e) = A_0^c/A_0 \tag{6.131b}$$

where A_0 and A are the initial and current cross-sectional areas of the chord. The superscripts 'c' and 'e' designate collagen and elastin.

6.2.5.2 Force Vector for a Pentagon

The boundary of a 2D pentagon consists of line segments, which can be considered as 1D chords. Hence, an evaluation of the boundary integrals of a pentagon amounts to evaluating the line integrals along these boundary lines. Once the interpolation function for a pentagon are evaluated on the boundary of a pentagon, we can obtain the corresponding chordal interpolation functions [65]. Thus, the force vector $\mathbf{F}_{BC}$ for a pentagon can be obtained by integrating the traction vectors multiplied by appropriate shape functions over all sides of pentagon. Specifically, force along the boundary of a membrane can be obtained as

$$\begin{aligned}
\mathbf{F}_{BC} = \oint_L \mathbf{N}^\mathsf{T}\,\mathbf{t}\,\mathrm{d}L &= \int_{L_{12}} \mathbf{N}^\mathsf{T}\,\mathbf{t}_{12}\,|\mathbf{J}|\,\mathrm{d}L + \int_{L_{23}} \mathbf{N}^\mathsf{T}\,\mathbf{t}_{23}\,|\mathbf{J}|\,\mathrm{d}L + \int_{L_{34}} \mathbf{N}^\mathsf{T}\,\mathbf{t}_{34}\,|\mathbf{J}|\,\mathrm{d}L \\
&\quad + \int_{L_{45}} \mathbf{N}^\mathsf{T}\,\mathbf{t}_{45}\;|\mathbf{J}|\,\mathrm{d}L + \int_{L_{51}} \mathbf{N}^\mathsf{T}\,\mathbf{t}_{51}\,|\mathbf{J}|\,\mathrm{d}L \\
&= |\mathbf{J}| \sum_{i=1}^{2} \mathbf{N}^\mathsf{T}\,\mathbf{t}_{12}\,w_i + |\mathbf{J}| \sum_{i=1}^{2} \mathbf{N}^\mathsf{T}\,\mathbf{t}_{23}\,w_i + |\mathbf{J}| \sum_{i=1}^{2} \mathbf{N}^\mathsf{T}\,\mathbf{t}_{34}\,w_i \\
&\quad + |\mathbf{J}| \sum_{i=1}^{2} \mathbf{N}^\mathsf{T}\,\mathbf{t}_{45}\,w_i + |\mathbf{J}| \sum_{i=1}^{2} \mathbf{N}^\mathsf{T}\,\mathbf{t}_{51}\,w_i
\end{aligned} \tag{6.132}$$

where $\mathbf{N}$ represents the shape function matrix of a chord, but with the matrix dimension of a pentagon, $|\mathbf{J}|$ is the determinant of the Jacobian for a 1-D chord, w_i denotes the natural weight of the chord, $\mathrm{d}S$ is the arc-length of an infinitesimal line element along the boundary,

and $\mathbf{t}$ is the traction vector on each edge of the pentagon defined as

$$\mathbf{t} = \mathbf{S}^{s\mathsf{T}} \cdot \mathbf{n} \tag{6.133}$$

where $\mathbf{n}$ is the normal vector to each sides of pentagon on which the traction acts, and $\mathbf{S}^s$ are established in Eqn. (6.82b).

The internal force $\boldsymbol{F}_0$ accounting for an initial residual stress of $\boldsymbol{T}_0$ becomes

$$\boldsymbol{F}_0 = \int_V \mathbf{B}_L^{\mathsf{T}}\, \boldsymbol{T}_0 \, \mathrm{d}V + \int_V \mathbf{B}_N^{\mathsf{T}}\, \boldsymbol{T}_0 \, \mathrm{d}V = |\mathbf{J}| \sum_{i=1}^{5} \mathbf{B}_L^{\mathsf{T}}\, \boldsymbol{T}_0 \, H_i \, w_i + |\mathbf{J}| \sum_{i=1}^{5} \mathbf{B}_N^{\mathsf{T}}\, \boldsymbol{T}_0 \, H_i \, w_i \tag{6.134}$$

where $\mathbf{B}$ and $\mathbf{J}$ are the strain displacement and Jacobian matrix of pentagon, respectively, whose thickness or height H_i can vary over the surface of the membrane, and as such, cannot be pulled outside the summation. Here the initial stress

$$\mathbf{T}_0 = \left\{ \begin{array}{c} s_0^{\pi} \\ s_0^{\sigma} = 0 \\ s_0^{\tau} = 0 \end{array} \right\} \mapsto \mathbf{S}_0 = \left[\begin{array}{cc} \frac{1}{2} s_0^{\pi} & 0 \\ 0 & \frac{1}{2} s_0^{\pi} \end{array} \right] \tag{6.135}$$

contains the initial surface tension s_0^{π} carried by the septal membrane.

6.2.5.3 Force Vector for a Tetrahedron

The force vector on the alveolar volume is computed by integrating the traction vector over the four boundary surfaces of the tetrahedron. Here the matrix of shape functions; Eq. (6.30), is used to obtain the force vector for tetrahedron; specifically,

$$\begin{aligned} \mathbf{F}_{BC} &= \oint_A \mathbf{N}^{\mathsf{T}}\, \mathbf{t} \, \mathrm{d}A = \int_{\triangle_1} \mathbf{N}^{\mathsf{T}}\, \mathbf{t}_{\triangle_1} \, \mathrm{d}A + \int_{\triangle_2} \mathbf{N}^{\mathsf{T}}\, \mathbf{t}_{\triangle_2} \, \mathrm{d}A + \int_{\triangle_3} \mathbf{N}^{\mathsf{T}}\, \mathbf{t}_{\triangle_3} \, \mathrm{d}A + \int_{\triangle_4} \mathbf{N}^{\mathsf{T}}\, \mathbf{t}_{\triangle_4} \, \mathrm{d}A \\ &= |\mathbf{J}| \sum_{i=1}^{3} \mathbf{N}^{\mathsf{T}}\, \mathbf{t}_{\triangle_1} \, w_i + |\mathbf{J}| \sum_{i=1}^{3} \mathbf{N}^{\mathsf{T}}\, \mathbf{t}_{\triangle_2} \, w_i + |\mathbf{J}| \sum_{i=1}^{3} \mathbf{N}^{\mathsf{T}}\, \mathbf{t}_{\triangle_3} \, w_i + |\mathbf{J}| \sum_{i=1}^{3} \mathbf{N}^{\mathsf{T}}\, \mathbf{t}_{\triangle_4} \, w_i \end{aligned} \tag{6.136}$$

where $\Delta_i, i = 1, 2, 3, 4$ represent the triangular boundary surfaces of a tetrahedron. Here $\mathbf{N}$ represents the shape function matrix for these associated triangular boundaries. $|\mathbf{J}|$ is the

determinant of the Jacobian for triangle, n denotes the number of Gauss points, w_i is the natural weight of the triangle from Table 6.2, and $\mathbf{t}$ is the surface traction on the triangle surface. Integral $\oint$ denotes an integration over the surface boundary of a tetrahedron.

Note: Except for the base of the tetrahedron, the tractions on its other sides have equal and opposite contributions to the total force vector. Therefore, contributions from opposite boundary surfaces of the tetrahedron nullify each other. Hence, in order to obtain the total force vector for a tetrahedron, it is sufficient to only consider the contributions due to the traction on its base. Therefore, the total force vector takes the form of

$$\mathbf{F}_{BC} = |\mathbf{J}| \sum_{i=1}^{3} \mathbf{N}^{\mathsf{T}} \, \mathbf{t}_{\triangle_1} \, w_i \quad \text{with} \quad \mathbf{t}_{\triangle_1} = \mathbf{S}^{s\mathsf{T}} \cdot \mathbf{n} \tag{6.137}$$

where $\mathbf{t}_{\triangle_1}$ is the traction vector on the surface of triangle, $\mathbf{n}$ is the normal vector to each sides of tetrahedron on which the traction acts, and $\mathbf{S}^s$ has been defined in Eqn. (6.123b).

The internal force $\boldsymbol{F}_0$ accounting for an initial residual stress of $\boldsymbol{T}_0$ becomes

$$\boldsymbol{F}_0 = \int_V \mathbf{B}^{\mathsf{T}} \, \boldsymbol{T}_0 \, \mathrm{d}V = |\mathbf{J}| \sum_{i=1}^{4} \mathbf{B}_L^{\mathsf{T}} \, \boldsymbol{T}_0 \, w_i + |\mathbf{J}| \sum_{i=1}^{4} \mathbf{B}_N^{\mathsf{T}} \, \boldsymbol{T}_0 \, w_i \tag{6.138a}$$

where $\mathbf{B}$ and $\mathbf{J}$ are the strain displacement and Jacobian matrices of a tetrahedron, respectively. Here the stress vector $\boldsymbol{T}_0 = \{\pi, \sigma_1, \sigma_2, \tau_1, \tau_2, \tau_3\}^{\mathsf{T}}$ is conjugate to strain $\boldsymbol{E} = \{\xi, \varepsilon_1, \varepsilon_2, \gamma_1, \gamma_2, \gamma_3\}^{\mathsf{T}}$, where

$$\mathbf{T}_0 = \begin{Bmatrix} \pi_0 \\ \sigma_{1\,0} = 0 \\ \sigma_{2\,0} = 0 \\ \tau_{1\,0} = 0 \\ \tau_{2\,0} = 0 \\ \tau_{3\,0} = 0 \end{Bmatrix} \mapsto \mathbf{S}_0 = \begin{bmatrix} \frac{1}{3}\pi_0 & 0 & 0 \\ 0 & \frac{1}{3}\pi_0 & 0 \\ 0 & 0 & \frac{1}{3}\pi_0 \end{bmatrix} \tag{6.139}$$

contains the residual pressure π_0 inside a tetrahedron.

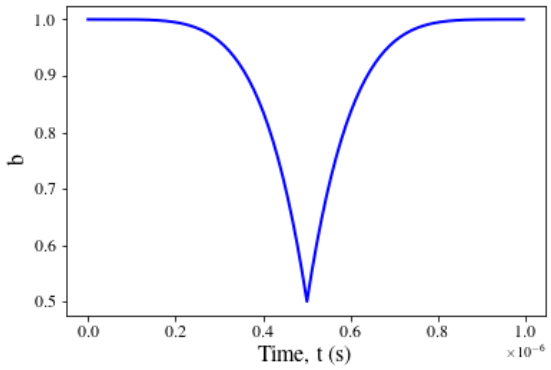

Figure 6.1: deformation history during the shock wave

6.3 Numerical Implementation

Here, the capabilities of the presented alveolar septa formulations and its finite element simulation subjected to shock waves that happened in a microsecond are demonstrated as an example.

The physical and material properties of alveolar membranes, along with their variance, are presented in Table 5.6. The material properties describing dilation, viz., M_1, M_2, and ξ_{1max}, were taken from Ref. [28] to model a visceral pleura membrane. The squeeze moduli, viz., N_1 and N_2, are in the same proportions as those of dilation, as reported in [28] for the visceral pleura. The shear properties, viz., G_1, G_2, and γ_{1max}, are our best estimates based upon very limited data [61].

Figure 6.1 presents the imposed deformation history to the alveolar membrane considering a compression first, and then an expansion as the alveolar septa is decompressed after the shock wave. The assumed deformation history illustrated here is described by

$$\boldsymbol{F}_0 = \begin{bmatrix} 1 & 0 \\ 0 & 1 \end{bmatrix} \qquad \rightarrow \qquad \boldsymbol{F}_N = \begin{bmatrix} 1 & 0 \\ 0 & b \end{bmatrix} \tag{6.140}$$

although, all elements of deformation gradients remain the same as their initial value, vis,

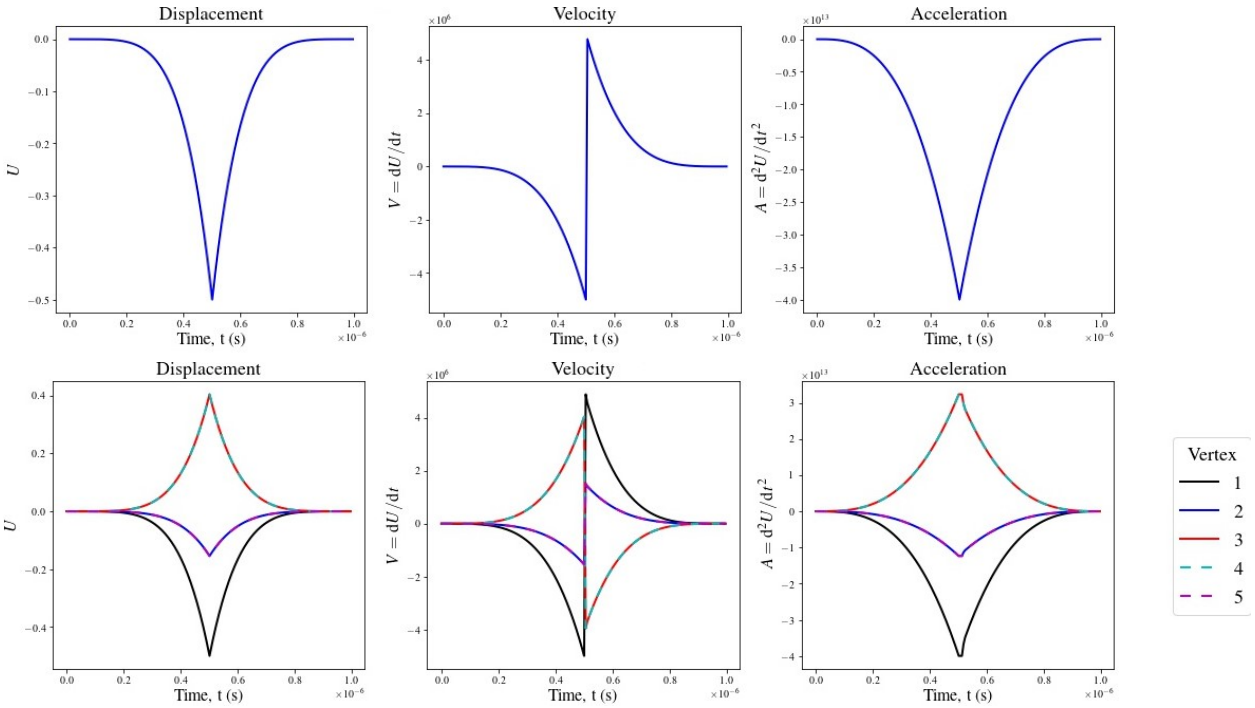

Figure 6.2: Alveolar membrane response for the squeeze mode caused by deformation histories.

$\boldsymbol{F}_0$, F_{22} varies exponentially from its initial value to its final value in $\boldsymbol{F}_N$.

The top row in Fig. 6.2 presents the displacement, velocity, and acceleration of node one as assigned in Fig. 5.2 through the imposed far-field deformation history that engages the squeeze modes. The second row demonstrates all vertices of the pentagon that appropriately show the behavior of alveolar septa when exposed to a traveling shock wave.

A ballistic impact produces a shock wave that rises rapidly to form over-pressure or peak pressure and then rapidly decreases to form a small pressure. Figure 6.3 illustrates the nodal forces for a 2D pentagon at node one during the time that shock wave happens. The black line is the nodal force from this theory written in Python with one pentagonal element. The blue points are the results from Ansys using the Neo-Hookean model written in FORTRAN, with 123 rectangular and triangular elements.

The simulation results in Fig. 6.4 present the equivalent stress distribution in the alveolar septa during the shock wave. Based on the simulation, the top and bottom parts of the

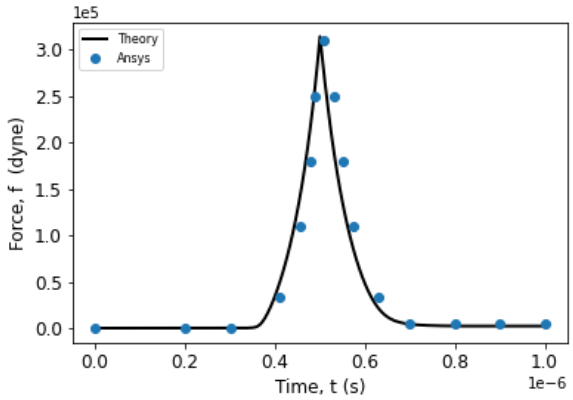

Figure 6.3: A comparison of the analytical solution and Ansys result of forces at node 1 of the pentagon.

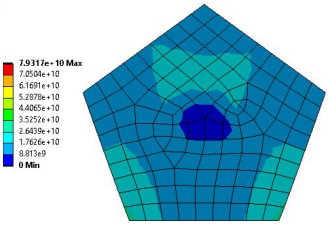

(a) Von Mises stress at time $t = 0.4\mu s$.

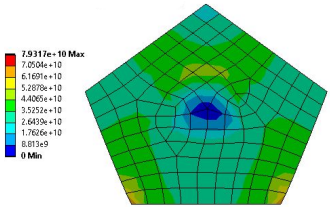

(b) Von Mises stress at time $t = 0.5\mu s$.

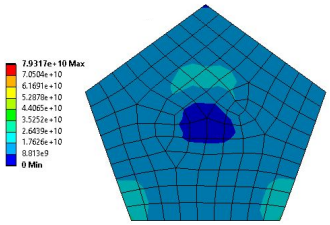

(c) Von Mises stress at time $t = 0.6\mu s$.

Figure 6.4: Simulation results

pentagon have the highest level of von Mises pressure.

7. SUMMARY

Through this dissertation, the components for a convected metric tensor and its inverse described in an oblique, Cartesian, coordinate system are derived whose axes are tangents to a triad of curvilinear coordinate axes originating at some particle of interest in a deforming body. Strains and strain rates are constructed in terms of these metrics, along with a velocity gradient, all quantified in this locally convected coordinate system. Quotient laws, and their associated Jacobians of transformation, are derived that map vector and tensor fields from this convected coordinate system in-to and out-of the Lagrangian and experimentor's coordinate systems.

We also derived two sets of thermodynamically admissible stress-strain pairs. The classical theory of elasticity and our two-mode theory of elasticity have two independent parameters for describing an isotropic elastic response, e.g., Young's modulus E and Poisson's ratio ν. Whereas, our three-mode elastic theory has three independent moduli for describing an uniform elastic response, viz., the bulk K, shear G, and squeeze N moduli. Whenever $N \equiv E/(1+\nu) = 2G$, the three-mode model reduces to the two-mode model, and to classical elasticity whenever the deformations are infinitesimal. So why are there three, independent, elastic moduli present in our three-mode elastic theory, while only two exist in the classical theory? Whenever stress power is described in terms of a symmetric strain rate, as in classic theory, the work done can be decomposed into two modes: volumetric and deviatoric. In this description, elastic responses are quantified through the bulk K and shear G moduli. Whereas, whenever stress power is described in terms of a triangular measure for strain rate, as in our theory, the work done can be decomposed into three modes: one volumetric mode and two deviatoric modes. One deviatoric mode describes motions of squeeze (e.g., pure shear), whose eigenvectors for stretch will not rotate in the body, while the other deviatoric mode describes motions of simple shear, whose eigenvectors for stretch will rotate in the body. The volumetric mode has an elastic response quantified through the bulk modulus K,

while the two deviatoric modes have elastic responses quantified through the squeeze N and shear G moduli, with N being unique to our theory.

Also, the Eulerian triangular decompositions of deformation has been analyzed. Physically observable stretch/strain components comprising the triangular Laplace stretch has been derived. Consideration of stress power, i.e., rate of working done by stretch rate, has enabled derivation of work conjugate stress-stretch tensors as-well-as thermodynamically conjugate scalar pairs of stress-strain attributes with physical meaning. Significantly, the Eulerian formulation containing an Eulerian, lower-triangular, stretch tensor has not been developed elsewhere in the mechanics literature.

The developed constitutive model is implemented as a microscopic alveolar model whose homogenized response describes the macroscopic behavior of parenchyma in lung. Such a model can be used in lieu of physical experiments to help develop and parameterize a better continuum lung model for use in finite element analyses. The need for such a model is to improved PPE to better protect a person from BABT and BLI when impacted by ballistic projectiles or blast waves.

The geometry of an individual alveolus is modeled as an irregular dodecahedron comprising 20 alveolar vertices, 30 1D alveolar chords, and 12 2D pentagonal alveolar septa, all enveloping a 3D alveolar sac. Implicit elastic constitutive equations are used to model these alveolar chords and septa. Alveolar chords are modeled as collagen and elastin fibers loaded in parallel. Damage is accounted for through the rupture of individual alveolar fibers and septa, and the tearing of capillaries that lead to blood and interstitial fluids leaking into its alveolar sac. Material properties for the individual fibers and septa are assigned through probability distribution functions to account for their biologic variability.

It is shown that geometric strains for the three physical dimensions that arise in this analysis are equivalent during uniform deformations when they are defined as geometric strains. Adopting Laplace stretch as our fundamental kinematic variable, thermodynamic conjugate pairs are established for these three geometric dimensions. These thermodynamic

strains equate with the above geometric strains under conditions of uniform deformation, plus they allow for the handling of nonuniform deformations, in particular, pure and simple shears. New to this implementation are the following: i) Sets of consistent interpolation/extrapolation procedures for 1D rods, 2D triangles and pentagons, and 3D tetrahedra, which allow physical fields to be mapped between the nodes and Gauss points of an element in a reproducible manner; ii) Shape functions and a Gauss integration formula suitable for constructing a pentagonal finite element, which is used to model alveolar septa; iii) Nonlinear strain-displacement matrices for 2D pentagons and 3D tetrahedra that employ Laplace stretch as their kinematic variable; and iv) A numerical algorithm that employs both secant and tangent stiffness matrices in its finite element solver.

REFERENCES

[1] W. Thomson, "II. On the thermoelastic, thermomagnetic, and pyroelectric properties of matter," *Philosophical Magazine*, vol. 5, pp. 4–27, 1878.

[2] S. D. Poisson, "Note sur l'Extension des Fils et des Plaques élastiques," *Annales de chimie et de physique*, vol. 36, pp. 384–387, 1827.

[3] J. H. Poynting, "On pressure perpendicular to the shear planes in finite pure shears, and on the lengthening of loaded wires when twisted," *Proceedings of the Royal Society, London A*, vol. 82, pp. 546–559, 1909.

[4] A. D. Freed and S. Zamani, "On the use of convected coordinate systems in the mechanics of continuous media derived from a **QR** factorization of **F**," *International Journal of Engineering Science*, vol. 127, pp. 145–161, 2018.

[5] A. D. Freed and S. Zamani, "Elastic Kelvin-Poisson-Poynting solids described through scalar conjugate stress/strain pairs derived from a **QR** factorization of **F**," *Journal of the Mechanics and Physics of Solids*, 2019.

[6] A. D. Freed, S. Zamani, L. Szabo, and J. D. Clayton, "Laplace stretch: Eulerian and lagrangian formulations," *Zeitschrift für angewandte Mathematik und Physik*, 2020.

[7] A. D. Freed, S. Zamani, S. Paul, and J. D. Clayton, "A dodecahedral model for alveoli," *to be submitted*, 2021.

[8] T. Josey, "Investigation of blast load characteristics on lung injury," Master's thesis, University of Waterloo, Waterloo, Ontario, Canada, 2010.

[9] L. R. G. Treloar, *The Physics of Rubber Elasticity*. Oxford: Clarendon Press, third ed., 1975.

[10] A. S. Lodge, *Body Tensor Fields in Continuum Mechanics: With applications to polymer rheology*. New York: Academic Press, 1974.

[11] A. S. Lodge, "On the use of convected coordinate systems in the mechanics of continuous media," *Proceedings of the Cambridge Philosophical Society*, vol. 47, pp. 575–584, 1951.

[12] L. Brillouin, "Les lois de l'élasticité sous forme tensorielle valable pour des coordonnées quelconques," *Annales de Physique*, vol. 3, pp. 251–298, 1925.

[13] H. Hencky, "Die Bewegungsgleichungen beim nichtstationären Fließen plastischer Massen," *Zeitschrift für angewandte Mathematik und Mechanik*, vol. 5, pp. 144–146, 1925.

[14] J. G. Oldroyd, "On the formulation of rheological equations of state," *Proceedings of the Royal Society, London A*, vol. 200, pp. 523–541, 1950.

[15] A. E. Green and W. Zerna, *Theoretical Elasticity*. Oxford: Clarendon Press, second ed., 1968.

[16] G. Lamé, *Leçons sur les coordonnées curvilignes et leurs diverses applications*. Paris: Mallet-Bachelier, 1859.

[17] A. S. Lodge and J. Meissner, "On the use of instantaneous strains, superposed on shear and elongational flows of polymeric liquids, to test the gaussian network hypothesis and to estimate the segment concentration and its variation during flow," *Rheologica Acta*, vol. 11, pp. 351–352, 1972.

[18] A. G. McLellan, *The Classical Thermodynamics of Deformable Materials*. Cambridge Monographs in Physics, Cambridge: Cambridge University Press, 1980.

[19] J. D. Clayton, *Nonlinear Mechanics of Crystals*. Dordrecht: Springer, 2011.

[20] A. D. Freed, D. R. Einstein, J. P. Carson, and R. E. Jacob, "Viscoelastic model for lung parenchyma for multi-scale modeling of respiratory system, Phase II: Dodecahedral micro-model," Tech. Rep. PNNL-21287, Pacific Northwest National Laboratory, Richland, WA, March 2012.

[21] J. P. Butler, H. Miki, S. Squarcia, R. A. Rogers, and J. L. Lehr, "Effect of macroscopic deformation on lung microstructure," *Journal of Applied Physiology*, vol. 81, pp. 1792–1799, 1996.

[22] A. S. Lodge, "A network theory of flow birefringence and stress in concentrated polymer solutions," *Transactions of the Faraday Society*, vol. 52, pp. 120–130, 1956.

[23] A. S. Lodge, "A network theory of constrained elastic recovery in concentrated polymer solutions," *Rheologica Acta*, vol. 1, pp. 158–163, 1958.

[24] A. S. Lodge, *Elastic Liquids: An introductory vector treatment of finite-strain polymer rheology*. London: Academic Press, 1964.

[25] C. Truesdell, *A First Course in Rational Continuum Mechanics*. Pure and Applied Mathematics, New York: Academic Press, 1977.

[26] A. R. Srinivasa, "On the use of the upper triangle (or **QR**) decomposition for developing constitutive equations for Green-elastic materials," *International Journal of Engineering Science*, vol. 60, pp. 1–12, 2012.

[27] A. D. Freed and A. R. Srinivasa, "Logarithmic strain and its material derivative for a **QR** decomposition of the deformation gradient," *ACTA Mechanica*, vol. 226, pp. 2645–2670, 2015.

[28] A. D. Freed, V. Erel, and M. R. Moreno, "Conjugate stress/strain base pairs for planar analysis of biological tissues," *Journal of Mechanics of Materials and Structures*, vol. 12, pp. 219–247, 2017.

[29] A. D. Freed, J. B. le Graverend, and K. R. Rajagopal, "A technical note: An elastic-inelastic decomposition of Laplace stretch," 2019. In review.

[30] A. G. McLellan, "Finite strain ccoordinate and the stability of solid phases," *Journal of Physics C: Solid State Physics*, vol. 9, pp. 4083–4094, 1976.

[31] S. Paul, K. R. Rajagopal, and A. D. Freed, "On coordinate indexing when using Laplace stretch," 2020. In review.

[32] A. D. Freed, "A note on stress/strain conjugate pairs: explicit and implicit theories of thermoelasticity for anisotropic materials," *International Journal of Engineering Science*, vol. 120, pp. 155–171, 2017.

[33] C. Carathéodory, "Untersuchungen über die Grundlagen der Thermodynamik," *Mathematische Annalen*, vol. 67, pp. 355–386, 1909. Translated in: J. Kestin (ed.), *The Second Law of Thermodynamics*, Dowden, Hutchinson and Ross, Stroudsberg, PA, 1976, pp. 229-256.

[34] S. Paul, A. D. Freed, and J. D. Clayton, "Coordinate indexing: On the use of eulerian and lagrangian laplace stretches," *Applications in Engineering Science*, vol. 5, 2021.

[35] K. Iwasawa, "On some types of topological groups," *Annals of Mathematics*, vol. 50, pp. 507–558, 1949.

[36] I. S. Sokolnikoff, *Tensor Analysis: Theory and applications to geometry and mechanics of continua*. Applied Mathematics Series, New York: Wiley, second ed., 1964.

[37] R. Hill, "Aspects of invariance in solid mechanics," *Advances in Applied Mechanics*, vol. 18, pp. 1–75, 1978.

[38] K. R. Rajagopal and A. R., Srinivasa, "Restrictions placed on constitutive relations by angular momentum balance and Galiean invariance," *Zeitschrift für angewandte Mathematik und Physik*, vol. 64, pp. 391–401, 2013.

[39] C. Truesdell and W. Noll, *The Non-Linear Field Theories of Mechanics*. Berlin: Springer-Verlag, third ed., 2004.

[40] F. G. Hoppin, Jr. and J. Hildebrandt, "Mechanical properties of the lung," in *Bioengineering Aspects of the Lung* (J. B. West, ed.), vol. 3 of *Lung Biology in Health and Disease*, pp. 83–162, New York: Marcel Dekker, 1977.

[41] E. Kimmel, R. D. Kamm, and A. H. Shapiro, "A cellular model of lung elasticity," *Journal of Biomechanical Engineering*, vol. 109, pp. 126–131, 1987.

[42] E. L. Wachspress, *A Rational Finite Element Basis*. New York: Academic Press, 1975.

[43] E. Wachspress, *Rational Bases and Generalized Barycentrics: Applications to finite elements and graphics*. Cham: Springer, 2016.

[44] N. Sukumar and E. A. Malsch, "Recent advances in the construction of polygonal finite element interpolants," *Archives of Computational Methods in Engineering*, vol. 13, pp. 129–163, 2006.

[45] G. Dasgupta, "Interpolants within convex polygons: Wachspress' shape functions," *Journal of Aerospace Engineering*, vol. 16, pp. 1–8, 2003.

[46] C. E. Perlman and J. Bhattacharya, "Alveolar expansion imaged by optical sectioning microscopy," *Journal of Applied Physiology*, vol. 103, pp. 1037–1044, 2007.

[47] F. Weinhold, "Metric geometry of equilibrium thermodynamics. III. Elementary formal structure of a vector-algebraic representation of equilibrium thermodynamics," *The Journal of Chemical Physics*, vol. 63, pp. 2488–2495, 1975.

[48] R. Gilmore, "Length and curvature in the geometry of thermodynamics," *Physical Review A*, vol. 30, pp. 1994–1997, 1984.

[49] S. Zamani, S. Paul, A. K. Akhilesh, J. Criscione, and A. D. Freed, "Application of **QR** framework in modeling the constitutive behavior of porcine coronary sinus tissue," *Mechanics Of Soft Materials*, 2021.

[50] Ames Research Staff, "Equations, tables, and charts for compressible flow," Tech. Rep. NACA 1135, National Advisory Committee for Aeronautics, 1953.

[51] S. S. Sobin, Y. C. Fung, and H. M. Tremer, "Collagen and elastin fibers in human pulmonary alveolar walls," *Journal of Applied Physiology*, vol. 64, no. 4, pp. 1659–1675, 1988.

[52] I. G. Fels, "Hydration and density of collagen and gelatin," *Journal of Applied Polymer Science*, vol. 8, pp. 1813–1824, 1964.

[53] J. R. Kanagy, "Specific heats of collagen and leather," *Journal of Research of the National Bureau of Standards*, vol. 55, pp. 191–195, 1955.

[54] C. E. Weir, "Effect of temperature on the volume of leather and collagen in water," *Journal of Research of the National Bureau of Standards*, vol. 41, pp. 279–285, 1948.

[55] M. A. Lillie and J. M. Gosline, "Unusual swelling of elastin," *Biopolymers*, vol. 64, pp. 115–126, 2002.

[56] R. E. Shadwick and J. M. Gosline, "Physical and chemical properties of rubber-like elastic fibres from the octopus aorta," *Journal of Experimental Biology*, vol. 114, pp. 239–257, 1985.

[57] S. R. Kakivaya and C. A. J. Hoeve, "The glass point of elastin," *Proceedings of the National Academy of Sciences, USA*, vol. 72, pp. 3505–3507, 1975.

[58] D. W. Urry, *Physicochemical properties of elastin and constituent peptides*, vol. 1 of *Elastin and Elastases*, pp. 141–173. Boca Raton: CRC Press, 1989.

[59] M. A. Lillie and J. M. Gosline, "Mechanical properties of elastin along the thoracic aorta in the pig," *Journal of Biomechanics*, vol. 40, pp. 2214–2221, 2007.

[60] H. Hörmann and H. Schlebusch, "Reversible and irreversible denaturation of collagen fibers," *Biochemistry*, vol. 10, no. 6, pp. 932–937, 1971.

[61] H. Saraf, K. T. Ramesh, A. M. Lennon, A. C. Merkle, and J. C. Roberts, "Mechanical properties of soft human tissues under dynamic loading," *Journal of Biomechanics*, vol. 40, pp. 1960–1967, 2007.

[62] A. D. Freed and K. R. Rajagopal, "A promising approach for modeling biological fibers," *ACTA Mechanica*, vol. 227, pp. 1609–1619, 2016.

[63] L. Davison, *Fundamentals of Shock Wave Propagation in Solids*. Shock Wave and High Pressure Phenomena, Berlin: Springer, 2008.

[64] J. S. Archer, "Consistent matrix formulations for structural analysis using finite-element techniques," *AIAA Journal*, vol. 3, pp. 1910–1918, 1965.

[65] J. N. Reddy, *An Introduction to the Finite Element Method*. McGraw-Hill, Inc.: McGraw.Hill series in mechanical engineering, 2nd ed., 1993.

[66] G. J. Y. Xiu-ying, Z. Jin-ch, "Stiffness matrix derivation of space beam element at elevated temperature," *J. Shanghai Jiaotong Univ.*, vol. 4, pp. 492–497, 2010.

[67] M. Elseifi, *A new scheme for the optimum design of stiffened composite panels with geometric imperfections*. PhD thesis, Virginia Polytechnic Institute and State University, Nov. 1998.

[68] T. Belytschko, W. K. Liu, and B. Moran, *Nonlinear Finite Elements for Continua and Structures*. Chichester: Wiley, 2000.

[69] A. D. Freed, *Soft Solids: A primer to the theoretical mechanics of materials*. Modeling and Simulation in Science, Engineering and Technology, Basel: Birkhäuser, 2014.

[70] G. Green, "On the propagation of light in crystallized media," *Transactions of the Cambridge Philosophical Society*, vol. 7, pp. 121–140, 1841.

[71] K. R. Rajagopal, "On implicit constitutive theories," *Applications of Mathematics*, vol. 48, no. 4, pp. 279–319, 2003.

[72] C. Truesdell, "Hypoelasticity," *Journal of Rational Mechanics and Analysis*, vol. 4, pp. 83–133, 1955.

APPENDIX A

QUOTIENT LAWS

Quotient laws determine how the components of vector and tensor fields map from one coordinate system into another coordinate system [36]. They are linear transformations. *They are not tensor equations* [10].

Usage of the word 'push' implicates moving a field forward through a linked set of configurations: Lagrangian $\mapsto$ convected $\mapsto$ experimentor's $\mapsto$ Eulerian. While usage of the word 'pull' implicates moving a field backwards through these configurations: Lagrangian $\leftarrow\!\shortmid$ convected $\leftarrow\!\shortmid$ experimentor's $\leftarrow\!\shortmid$ Eulerian.

The quotient laws preserve symmetry for covariant and contravariant tensors, whenever it exists, but not for mixed tensors (the exception being stretch $\mathbf{U}$ [69]). The quotient laws presented below preserve triangularity for mixed tensors, whenever it exists, but not for covariant or contravariant tensors.

A.1 Field Transfer: Convected Fields $\Leftrightarrow$ Experimentor's Fields

The transfer of vector and tensor fields between the oblique convected and the orthonormal experimentor's coordinate systems is governed by its Jacobian (or coordinate gradient) whose inverse exists. This Jacobian can appear in one of four forms

$$\mathbf{Y} := \left[\frac{\partial \tilde{x}^r}{\partial \xi^c}\right], \quad \mathbf{Y}^{-1} = \left[\frac{\partial \xi^r}{\partial \tilde{x}^c}\right], \quad \mathbf{Y}^{\mathsf{T}} = \left[\frac{\partial \tilde{x}^c}{\partial \xi^r}\right], \quad \mathbf{Y}^{-\mathsf{T}} = \left[\frac{\partial \xi^c}{\partial \tilde{x}^r}\right] \tag{A.1}$$

where coordinates $\tilde{x}^i$ locating a particle in the experimentor's coordinate system with base vectors $\{\tilde{\mathbf{e}}_i\}$, while coordinates ξ^i locate the same particle in the convected coordinate system with base vectors $\{\vec{\boldsymbol{g}}_i\}$. Matrices $\boldsymbol{\Lambda}$ and $\boldsymbol{\Gamma}$ do not commute, and as such, $\mathbf{Y} = \boldsymbol{\Gamma}\boldsymbol{\Lambda}$ is distinct from $\boldsymbol{\mathcal{U}} = \boldsymbol{\Lambda}\boldsymbol{\Gamma}$. Jacobian $\mathbf{Y}$ maps tangent vectors from the oblique convected basis $\{\vec{\boldsymbol{g}}_i\}$ into the orthonormal basis of the experimentalist $\{\tilde{\mathbf{e}}_i\}$, while Jacobian $\mathbf{Y}^{-\mathsf{T}}$ maps normal vectors

from the oblique convected basis into the orthonormal basis. Jacobians $\mathbf{Y}^{-1}$ and $\mathbf{Y}^{\mathsf{T}}$ run these maps in the reverse direction.

Given this set of Jacobian matrices, all covariant vectors $\tilde{\mathbf{w}} = \tilde{w}_i \, \tilde{\mathbf{e}}^i$ and $\boldsymbol{\omega} = \omega_i \, \vec{\boldsymbol{g}}^i$ push $\boldsymbol{\omega} \mapsto \tilde{\mathbf{w}}$ and pull $\boldsymbol{\omega} \mapsfrom \tilde{\mathbf{w}}$ via

$$\tilde{\mathbf{w}} = \mathbf{Y}^{-\mathsf{T}} \boldsymbol{\omega} \qquad \text{and} \qquad \boldsymbol{\omega} = \mathbf{Y}^{\mathsf{T}} \tilde{\mathbf{w}}, \tag{A.2a}$$

all contravariant vectors $\tilde{\mathbf{w}} = \tilde{w}^i \, \tilde{\mathbf{e}}_i$ and $\boldsymbol{\omega} = \omega^i \, \vec{\boldsymbol{g}}_i$ push $\boldsymbol{\omega} \mapsto \tilde{\mathbf{w}}$ and pull $\boldsymbol{\omega} \mapsfrom \tilde{\mathbf{w}}$ via

$$\tilde{\mathbf{w}} = \mathbf{Y} \boldsymbol{\omega} \qquad \text{and} \qquad \boldsymbol{\omega} = \mathbf{Y}^{-1} \tilde{\mathbf{w}}, \tag{A.2b}$$

all covariant tensors $\widetilde{\mathbf{W}} = \widetilde{W}_{ij} \, \tilde{\mathbf{e}}^i \otimes \tilde{\mathbf{e}}^j$ and $\boldsymbol{\Omega} = \Omega_{ij} \, \vec{\boldsymbol{g}}^i \otimes \vec{\boldsymbol{g}}^j$ push $\boldsymbol{\Omega} \mapsto \widetilde{\mathbf{W}}$ and pull $\boldsymbol{\Omega} \mapsfrom \widetilde{\mathbf{W}}$ via

$$\widetilde{\mathbf{W}} = \mathbf{Y}^{-\mathsf{T}} \boldsymbol{\Omega} \mathbf{Y}^{-1} \qquad \text{and} \qquad \boldsymbol{\Omega} = \mathbf{Y}^{\mathsf{T}} \widetilde{\mathbf{W}} \mathbf{Y}, \tag{A.2c}$$

all contravariant tensors $\widetilde{\mathbf{W}} = \widetilde{W}^{ij} \, \tilde{\mathbf{e}}_i \otimes \tilde{\mathbf{e}}_j$ and $\boldsymbol{\Omega} = \Omega^{ij} \, \vec{\boldsymbol{g}}_i \otimes \vec{\boldsymbol{g}}_j$ push $\boldsymbol{\Omega} \mapsto \widetilde{\mathbf{W}}$ and pull $\boldsymbol{\Omega} \mapsfrom \widetilde{\mathbf{W}}$ via

$$\widetilde{\mathbf{W}} = \mathbf{Y} \boldsymbol{\Omega} \mathbf{Y}^{\mathsf{T}} \qquad \text{and} \qquad \boldsymbol{\Omega} = \mathbf{Y}^{-1} \widetilde{\mathbf{W}} \mathbf{Y}^{-\mathsf{T}}, \tag{A.2d}$$

and all mixed (right covariant) tensors $\widetilde{\mathbf{W}} = \widetilde{W}^i_j \, \tilde{\mathbf{e}}_i \otimes \tilde{\mathbf{e}}^j$ and $\boldsymbol{\Omega} = \Omega^i_j \, \vec{\boldsymbol{g}}_i \otimes \vec{\boldsymbol{g}}^j$ push $\boldsymbol{\Omega} \mapsto \widetilde{\mathbf{W}}$ and pull $\boldsymbol{\Omega} \mapsfrom \widetilde{\mathbf{W}}$ via

$$\widetilde{\mathbf{W}} = \mathbf{Y} \boldsymbol{\Omega} \mathbf{Y}^{-1} \qquad \text{and} \qquad \boldsymbol{\Omega} = \mathbf{Y}^{-1} \widetilde{\mathbf{W}} \mathbf{Y}. \tag{A.2e}$$

These maps are for absolute vector and tensor fields, since the Jacobian determinant $\det \mathbf{Y} = abc$ plays no role here.

A.1.1 Derivatives

A time derivative $\mathrm{d}\bullet$ taken in the convected coordinate system pushes forward as a Lie derivative $\text{đ}\bullet$ in the experimentor's coordinate system. To quantify these Lie derivatives we need

$$\mathrm{d}\mathbf{H} := \mathrm{d}H^i_j \, \tilde{\mathbf{e}}_i \otimes \tilde{\mathbf{e}}^j \qquad \text{with} \qquad \mathrm{d}H^i_j = \frac{\partial \mathrm{d}\tilde{x}^i}{\partial \xi^k} \frac{\partial \xi^k}{\partial \tilde{x}^j} \tag{A.3}$$

or, alternatively, in terms of Jacobian $\mathbf{Y}$, $\mathrm{d}\mathbf{H} = \mathrm{d}\mathbf{Y} \cdot \mathbf{Y}^{-1}$ whose components populate an upper-triangular matrix.

With a velocity gradient $\mathrm{d}\mathbf{H}$ defined over $\{\tilde{\mathbf{e}}_i\}$ now in hand, the material derivative of a covariant vector described in $\{\vec{\boldsymbol{g}}_i\}$ pushes forward into the experimentor's frame with base vectors $\{\tilde{\mathbf{e}}_i\}$ as $\mathrm{d}\boldsymbol{\omega} \mapsto \text{đ}\tilde{\mathbf{w}}$, given that $\boldsymbol{\omega} \mapsto \tilde{\mathbf{w}}$, whose Lie derivative is defined by

$$\text{đ}\tilde{\mathbf{w}} = \mathbf{Y}^{-\mathsf{T}} \cdot \mathrm{d}\boldsymbol{\omega} \qquad\qquad \text{đ}\tilde{\mathbf{w}} := \mathrm{d}\tilde{\mathbf{w}} + \mathrm{d}\mathbf{H}^{\mathsf{T}} \cdot \tilde{\mathbf{w}}, \tag{A.4a}$$

the derivative of a contravariant vector pushes as $\mathrm{d}\boldsymbol{\omega} \mapsto \text{đ}\tilde{\mathbf{w}}$, given that $\boldsymbol{\omega} \mapsto \tilde{\mathbf{w}}$, whose Lie derivative is defined by

$$\text{đ}\tilde{\mathbf{w}} = \mathbf{Y} \cdot \mathrm{d}\boldsymbol{\omega} \qquad\qquad \text{đ}\tilde{\mathbf{w}} := \mathrm{d}\tilde{\mathbf{w}} - \mathrm{d}\mathbf{H} \cdot \tilde{\mathbf{w}}, \tag{A.4b}$$

the derivative of a covariant tensor pushes as $\mathrm{d}\boldsymbol{\Omega} \mapsto \text{đ}\widetilde{\mathbf{W}}$, given that $\boldsymbol{\Omega} \mapsto \widetilde{\mathbf{W}}$, whose Lie derivative is defined by

$$\text{đ}\widetilde{\mathbf{W}} = \mathbf{Y}^{-\mathsf{T}} \cdot \mathrm{d}\boldsymbol{\Omega} \cdot \mathbf{Y}^{-1} \qquad\qquad \text{đ}\widetilde{\mathbf{W}} := \mathrm{d}\widetilde{\mathbf{W}} + \mathrm{d}\mathbf{H}^{\mathsf{T}} \cdot \widetilde{\mathbf{W}} + \widetilde{\mathbf{W}} \cdot \mathrm{d}\mathbf{H}, \tag{A.4c}$$

the derivative of a contravariant tensor pushes as $\mathrm{d}\boldsymbol{\Omega} \mapsto \text{đ}\widetilde{\mathbf{W}}$, given that $\boldsymbol{\Omega} \mapsto \widetilde{\mathbf{W}}$, whose Lie derivative is defined by

$$\text{đ}\widetilde{\mathbf{W}} = \mathbf{Y} \cdot \mathrm{d}\boldsymbol{\Omega} \cdot \mathbf{Y}^{\mathsf{T}} \qquad\qquad \text{đ}\widetilde{\mathbf{W}} := \mathrm{d}\widetilde{\mathbf{W}} - \mathrm{d}\mathbf{H} \cdot \widetilde{\mathbf{W}} - \widetilde{\mathbf{W}} \cdot \mathrm{d}\mathbf{H}^{\mathsf{T}}, \tag{A.4d}$$

and the derivative of a mixed tensor pushes as $\mathrm{d}\boldsymbol{\Omega} \mapsto \text{đ}\widetilde{\mathbf{W}}$, given that $\boldsymbol{\Omega} \mapsto \widetilde{\mathbf{W}}$, whose LIE derivative is defined by

$$\text{đ}\widetilde{\mathbf{W}} = \mathbf{Y} \cdot \mathrm{d}\boldsymbol{\Omega} \cdot \mathbf{Y}^{-1} \qquad\qquad \text{đ}\widetilde{\mathbf{W}} := \mathrm{d}\widetilde{\mathbf{W}} - \mathrm{d}\mathbf{H} \cdot \widetilde{\mathbf{W}} + \widetilde{\mathbf{W}} \cdot \mathrm{d}\mathbf{H} \tag{A.4e}$$

wherein $\mathrm{d}\mathbf{H}^{\mathsf{T}}$ is taken to mean $\mathbf{Y}^{-\mathsf{T}} \cdot \mathrm{d}\mathbf{Y}^{\mathsf{T}} = \boldsymbol{\Gamma}^{-\mathsf{T}} \cdot \mathrm{d}\boldsymbol{\Gamma}^{\mathsf{T}} + \boldsymbol{\Gamma}^{-\mathsf{T}} (\mathrm{d}\boldsymbol{\Lambda} \cdot \boldsymbol{\Lambda}^{-1}) \boldsymbol{\Gamma}^{\mathsf{T}}$ whose components populate a lower-triangular matrix.

A.2 Field Transfer: Convected Fields ⇔ Lagrangian Fields

To push a Lagrangian field quantified in a coordinate system with base vectors $\{\vec{\boldsymbol{E}}_i\}$ into a convected field quantified in our locally, convected, coordinate system with base vectors $\{\vec{\boldsymbol{g}}_i\}$ or, vice versa, to pull a convected field back into the Lagrangian basis, one must first construct the quotient law that governs this particular type of field transfer. We begin with the fact that Laplace stretch $\boldsymbol{\mathcal{U}} = \mathcal{U}^i_j \, \tilde{\mathbf{e}}_i \otimes \vec{\boldsymbol{E}}_j$ is a gradient, which itself is a product of gradients in that

$$\mathcal{U}^i_j = \frac{\partial \tilde{x}^i}{\partial X^j} = \frac{\partial \tilde{x}^i}{\partial \xi^k} \frac{\partial \xi^k}{\partial X^j} \quad \text{or} \quad \boldsymbol{\mathcal{U}} = \mathbf{Y}\mathbf{Z} \quad \text{so that} \quad \mathbf{F} = \mathcal{R}\mathbf{Y}\mathbf{Z} \tag{A.5}$$

wherein Lagrangian coordinates X^i exist in basis $\{\vec{\boldsymbol{E}}_i\}$, experimentor's coordinates $\tilde{x}^i$ exist in basis $\{\tilde{\mathbf{e}}_i\}$, while physical coordinates ξ^k exist in basis $\{\vec{\boldsymbol{g}}_i\}$. We note that $\mathbf{F} = F^i_j \, \vec{\mathbf{e}}_i \otimes \vec{\boldsymbol{E}}_j$, $\mathcal{R} = \vec{\mathbf{e}}_i \otimes \tilde{\mathbf{e}}^j$, $\mathbf{Y} = Y^i_j \, \tilde{\mathbf{e}}_i \otimes \vec{\boldsymbol{g}}^j$, and $\mathbf{Z} = Z^i_j \, \vec{\boldsymbol{g}}_i \otimes \vec{\boldsymbol{E}}_j$.

Like $\mathbf{Y}$, $\mathbf{Z}$ is a Jacobian matrix pertaining to a coordinate transformation, this time between the convected and Lagrangian coordinate bases. It too appears in four forms

$$\mathbf{Z} := \left[\frac{\partial \xi^r}{\partial X^c}\right], \quad \mathbf{Z}^{-1} = \left[\frac{\partial X^r}{\partial \xi^c}\right], \quad \mathbf{Z}^{\mathsf{T}} = \left[\frac{\partial \xi^c}{\partial X^r}\right], \quad \mathbf{Z}^{-\mathsf{T}} = \left[\frac{\partial X^c}{\partial \xi^r}\right] \tag{A.6}$$

where $\mathbf{Z} = \mathbf{Y}^{-1}\boldsymbol{\mathcal{U}} = \boldsymbol{\Lambda}^{-1}\boldsymbol{\Gamma}^{-1}\boldsymbol{\Lambda}\boldsymbol{\Gamma}$, with transposes $\mathbf{Z}^{\mathsf{T}} = \boldsymbol{\mathcal{U}}^{\mathsf{T}}\mathbf{Y}^{-\mathsf{T}} = \boldsymbol{\Gamma}^{\mathsf{T}}\boldsymbol{\Lambda}\boldsymbol{\Gamma}^{-\mathsf{T}}\boldsymbol{\Lambda}^{-1}$ and $\mathbf{Z}^{-\mathsf{T}} = \mathbf{Y}^{\mathsf{T}}\boldsymbol{\mathcal{U}}^{-\mathsf{T}} = \boldsymbol{\Lambda}\boldsymbol{\Gamma}^{\mathsf{T}}\boldsymbol{\Lambda}^{-1}\boldsymbol{\Gamma}^{-\mathsf{T}}$ populating lower-triangular matrices.

Jacobian $\mathbf{Z}$ maps tangent vectors from the Lagrangian basis $\{\vec{\boldsymbol{E}}_i\}$ into the convected basis

$\{\vec{\boldsymbol{g}}_i\}$, while Jacobian $\mathbf{Z}^{-\mathsf{T}}$ maps normal vectors from the Lagrangian basis into the convected basis. Their inverses reverse the direction of these maps.

From this strategy, covariant vectors $\mathbf{w} = w_i\,\vec{\boldsymbol{E}}_i$ and $\boldsymbol{\omega} = \omega_i\,\vec{\boldsymbol{g}}^i$ have maps that pull $\mathbf{w} \leftarrow\!\shortmid\, \boldsymbol{\omega}$ and push $\mathbf{w} \mapsto \boldsymbol{\omega}$ as

$$\mathbf{w} = \mathbf{Z}^{\mathsf{T}}\boldsymbol{\omega} \qquad\qquad \boldsymbol{\omega} = \mathbf{Z}^{-\mathsf{T}}\mathbf{w}, \tag{A.7a}$$

contravariant vectors $\mathbf{w} = w^i\,\vec{\boldsymbol{E}}_i$ and $\boldsymbol{\omega} = \omega^i\,\vec{\boldsymbol{g}}_i$ have maps that pull $\mathbf{w} \leftarrow\!\shortmid\, \boldsymbol{\omega}$ and push $\mathbf{w} \mapsto \boldsymbol{\omega}$ as

$$\mathbf{w} = \mathbf{Z}^{-1}\boldsymbol{\omega} \qquad\qquad \boldsymbol{\omega} = \mathbf{Z}\mathbf{w}, \tag{A.7b}$$

covariant tensors $\mathbf{W} = W_{ij}\,\vec{\boldsymbol{E}}_i \otimes \vec{\boldsymbol{E}}_j$ and $\boldsymbol{\Omega} = \Omega_{ij}\,\vec{\boldsymbol{g}}^i \otimes \vec{\boldsymbol{g}}^j$ have maps that pull $\mathbf{W} \leftarrow\!\shortmid\, \boldsymbol{\Omega}$ and push $\mathbf{W} \mapsto \boldsymbol{\Omega}$ as

$$\mathbf{W} = \mathbf{Z}^{\mathsf{T}}\boldsymbol{\Omega}\mathbf{Z} \qquad\qquad \boldsymbol{\Omega} = \mathbf{Z}^{-\mathsf{T}}\mathbf{W}\mathbf{Z}^{-1}, \tag{A.7c}$$

contravariant tensors $\mathbf{W} = W^{ij}\,\vec{\boldsymbol{E}}_i \otimes \vec{\boldsymbol{E}}_j$ and $\boldsymbol{\Omega} = \Omega^{ij}\,\vec{\boldsymbol{g}}_i \otimes \vec{\boldsymbol{g}}_j$ have maps that pull $\mathbf{W} \leftarrow\!\shortmid\, \boldsymbol{\Omega}$ and push $\mathbf{W} \mapsto \boldsymbol{\Omega}$ as

$$\mathbf{W} = \mathbf{Z}^{-1}\boldsymbol{\Omega}\mathbf{Z}^{-\mathsf{T}} \qquad\qquad \boldsymbol{\Omega} = \mathbf{Z}\mathbf{W}\mathbf{Z}^{\mathsf{T}}, \tag{A.7d}$$

and mixed (right covariant) tensors $\mathbf{W} = W^i_j\,\vec{\boldsymbol{E}}_i \otimes \vec{\boldsymbol{E}}_j$ and $\boldsymbol{\Omega} = \Omega^i_j\,\vec{\boldsymbol{g}}_i \otimes \vec{\boldsymbol{g}}^j$ have maps that pull $\mathbf{W} \leftarrow\!\shortmid\, \boldsymbol{\Omega}$ and push $\mathbf{W} \mapsto \boldsymbol{\Omega}$ as

$$\mathbf{W} = \mathbf{Z}^{-1}\boldsymbol{\Omega}\mathbf{Z} \qquad\qquad \boldsymbol{\Omega} = \mathbf{Z}\mathbf{W}\mathbf{Z}^{-1}. \tag{A.7e}$$

APPENDIX B

NUMERICAL APPROXIMATIONS FOR LAPLACE STRETCH

Let the physical components for Laplace stretch at step n be denoted by

$$\boldsymbol{\mathcal{U}}_n = \boldsymbol{\Lambda}_n \boldsymbol{\Gamma}_n = \begin{bmatrix} \mathcal{U}^1_{1(n)} & \mathcal{U}^1_{2(n)} & \mathcal{U}^1_{3(n)} \\ 0 & \mathcal{U}^2_{2(n)} & \mathcal{U}^2_{3(n)} \\ 0 & 0 & \mathcal{U}^3_{3(n)} \end{bmatrix} = \begin{bmatrix} a_n & a_n\gamma_n & a_n\beta_n \\ 0 & b_n & b_n\alpha_n \\ 0 & 0 & c_n \end{bmatrix} \tag{B.1}$$

with analogous components assigned to steps $n-1$ and $n+1$, as required.

In a typical numerical application, one would be given the deformation gradient at the beginning and end of a time step of size h, say, denoted here as $\mathbf{F}_n$ and $\mathbf{F}_{n+1}$, whose affiliated Laplace stretch $\boldsymbol{\mathcal{U}}_n$ and $\boldsymbol{\mathcal{U}}_{n+1}$ would come from Eq. (2.15). With this information, finite difference formulæ can be constructed to acquire approximations for differential changes in the physical components of Laplace stretch a, b, c, α, β and γ.

The forward difference formula for Laplace stretch $\mathrm{d}\boldsymbol{\mathcal{U}}_n = \frac{\boldsymbol{\mathcal{U}}_{n+1}-\boldsymbol{\mathcal{U}}_n}{h} + \mathcal{O}(h)$ gives

$$\begin{aligned} \mathrm{d}a_n &\approx \frac{a_{n+1}-a_n}{h} & \mathrm{d}\alpha_n &\approx \frac{b_{n+1}}{b_n}\left(\frac{\alpha_{n+1}-\alpha_n}{h}\right) \\ \mathrm{d}b_n &\approx \frac{b_{n+1}-b_n}{h} & \mathrm{d}\beta_n &\approx \frac{a_{n+1}}{a_n}\left(\frac{\beta_{n+1}-\beta_n}{h}\right) \\ \mathrm{d}c_n &\approx \frac{c_{n+1}-c_n}{h} & \mathrm{d}\gamma_n &\approx \frac{a_{n+1}}{a_n}\left(\frac{\gamma_{n+1}-\gamma_n}{h}\right) \end{aligned} \tag{B.2}$$

while the backward difference formula $\mathrm{d}\boldsymbol{\mathcal{U}}_{n+1} = \frac{\boldsymbol{\mathcal{U}}_{n+1}-\boldsymbol{\mathcal{U}}_n}{h} + \mathcal{O}(h)$ gives

$$\begin{aligned} \mathrm{d}a_{n+1} &\approx \frac{a_{n+1}-a_n}{h} & \mathrm{d}\alpha_{n+1} &\approx \frac{b_n}{b_{n+1}}\left(\frac{\alpha_{n+1}-\alpha_n}{h}\right) \\ \mathrm{d}b_{n+1} &\approx \frac{b_{n+1}-b_n}{h} & \mathrm{d}\beta_{n+1} &\approx \frac{a_n}{a_{n+1}}\left(\frac{\beta_{n+1}-\beta_n}{h}\right) \\ \mathrm{d}c_{n+1} &\approx \frac{c_{n+1}-c_n}{h} & \mathrm{d}\gamma_{n+1} &\approx \frac{a_n}{a_{n+1}}\left(\frac{\gamma_{n+1}-\gamma_n}{h}\right) \end{aligned} \tag{B.3}$$

with there being a distinction in how the shear rates are approximated.

Equations (B.2 & B.3) are first-order approximations for these derivatives. Second-order approximations can be established whenever $n > 0$ and when the step size for step $[n, n+1]$ equals the step size for step $[n-1, n]$, where state $n = 0$ associates with an initial condition. The central difference formula for Laplace stretch $\mathrm{d}\boldsymbol{\mathcal{U}}_n = \frac{\boldsymbol{\mathcal{U}}_{n+1} - \boldsymbol{\mathcal{U}}_{n-1}}{2h} + \mathcal{O}(h^2)$ gives

$$\begin{aligned}
\mathrm{d}a_n &\approx \frac{a_{n+1} - a_{n-1}}{2h} & \mathrm{d}\alpha_n &\approx \frac{b_{n+1}}{b_n}\left(\frac{\alpha_{n+1} - \alpha_n}{2h}\right) + \frac{b_{n-1}}{b_n}\left(\frac{\alpha_n - \alpha_{n-1}}{2h}\right) \\
\mathrm{d}b_n &\approx \frac{b_{n+1} - b_{n-1}}{2h} & \mathrm{d}\beta_n &\approx \frac{a_{n+1}}{a_n}\left(\frac{\beta_{n+1} - \beta_n}{2h}\right) + \frac{a_{n-1}}{a_n}\left(\frac{\beta_n - \beta_{n-1}}{2h}\right) \\
\mathrm{d}c_n &\approx \frac{c_{n+1} - c_{n-1}}{2h} & \mathrm{d}\gamma_n &\approx \frac{a_{n+1}}{a_n}\left(\frac{\gamma_{n+1} - \gamma_n}{2h}\right) + \frac{a_{n-1}}{a_n}\left(\frac{\gamma_n - \gamma_{n-1}}{2h}\right)
\end{aligned} \tag{B.4}$$

while the backward difference formula $\mathrm{d}\boldsymbol{\mathcal{U}}_{n+1} = \frac{3\boldsymbol{\mathcal{U}}_{n+1} - 4\boldsymbol{\mathcal{U}}_n + \boldsymbol{\mathcal{U}}_{n-1}}{2h} + \mathcal{O}(h^2)$ gives

$$\begin{aligned}
\mathrm{d}a_{n+1} &\approx \frac{3a_{n+1} - 4a_n + a_{n-1}}{2h} & \mathrm{d}\alpha_{n+1} &\approx \frac{2b_n}{b_{n+1}}\left(\frac{\alpha_{n+1} - \alpha_n}{h}\right) - \frac{b_{n-1}}{b_{n+1}}\left(\frac{\alpha_{n+1} - \alpha_{n-1}}{2h}\right) \\
\mathrm{d}b_{n+1} &\approx \frac{3b_{n+1} - 4b_n + b_{n-1}}{2h} & \mathrm{d}\beta_{n+1} &\approx \frac{2a_n}{a_{n+1}}\left(\frac{\beta_{n+1} - \beta_n}{h}\right) - \frac{a_{n-1}}{a_{n+1}}\left(\frac{\beta_{n+1} - \beta_{n-1}}{2h}\right) \\
\mathrm{d}c_{n+1} &\approx \frac{3c_{n+1} - 4c_n + c_{n-1}}{2h} & \mathrm{d}\gamma_{n+1} &\approx \frac{2a_n}{a_{n+1}}\left(\frac{\gamma_{n+1} - \gamma_n}{h}\right) - \frac{a_{n-1}}{a_{n+1}}\left(\frac{\gamma_{n+1} - \gamma_{n-1}}{2h}\right)
\end{aligned} \tag{B.5}$$

both of which require values associated with state $n - 1$ to be stored.

APPENDIX C

PIVOTING STRATEGY

Paul *et al* [34] introduced a pivoting strategy that selects an optimal co-ordinate relabeling with respect to preserving the invariant directional qualities inherited through the **QR** factorization of a 3×3 matrix. The rotated 1 direction is selected to align with that axis which has minimal transverse shear, as determined through the functions

$$\mathcal{F}_1 := \sqrt{F_{21}^2 + F_{31}^2} \;\big/\; F_{11} \geqslant 0 \tag{C.1a}$$

$$\mathcal{F}_2 := \sqrt{F_{12}^2 + F_{32}^2} \;\big/\; F_{22} \geqslant 0 \tag{C.1b}$$

$$\mathcal{F}_3 := \sqrt{F_{13}^2 + F_{23}^2} \;\big/\; F_{33} \geqslant 0 \tag{C.1c}$$

after which the rotated 3 direction is selected so as to minimize the transverse shear acting across its 1-2 plane, with the F_{ij} being evaluated in basis $(\vec{\boldsymbol{\imath}}, \vec{\boldsymbol{\jmath}}, \vec{\boldsymbol{k}})$.

Algorithm 1 establishes the reference co-ordinate system that one ought to use for analysis. It is rectangular Cartesian with base vectors $(\vec{\boldsymbol{E}}_1, \vec{\boldsymbol{E}}_2, \vec{\boldsymbol{E}}_3)$.

There are six cases that can arise. Their associated orthogonal matrices are

$$[\mathbf{P}_0] = \begin{bmatrix} 1 & 0 & 0 \\ 0 & 1 & 0 \\ 0 & 0 & 1 \end{bmatrix} \qquad [\mathbf{P}_1] = \begin{bmatrix} 1 & 0 & 0 \\ 0 & 0 & 1 \\ 0 & 1 & 0 \end{bmatrix} \qquad [\mathbf{P}_2] = \begin{bmatrix} 0 & 1 & 0 \\ 1 & 0 & 0 \\ 0 & 0 & 1 \end{bmatrix}$$

$$[\mathbf{P}_3] = \begin{bmatrix} 0 & 0 & 1 \\ 1 & 0 & 0 \\ 0 & 1 & 0 \end{bmatrix} \qquad [\mathbf{P}_4] = \begin{bmatrix} 0 & 1 & 0 \\ 0 & 0 & 1 \\ 1 & 0 & 0 \end{bmatrix} \qquad [\mathbf{P}_5] = \begin{bmatrix} 0 & 0 & 1 \\ 0 & 1 & 0 \\ 1 & 0 & 0 \end{bmatrix} \tag{C.2a}$$

Algorithm 1 Co-ordinate Pivoting to get Upper-Triangle Dominance in $\hat{\mathbf{F}}$.

if $\mathcal{F}_1 \leqslant \mathcal{F}_2$ **and** $\mathcal{F}_1 \leqslant \mathcal{F}_3$ **then**
  if $|F_{32}| \leqslant |F_{23}|$ **then**
    $\hat{\mathbf{F}} := \mathbf{P}_0^{\intercal}\mathbf{F}\mathbf{P}_0$, $[\{\vec{\mathbf{E}}_1\}\{\vec{\mathbf{E}}_2\}\{\vec{\mathbf{E}}_3\}] := [\{\vec{\boldsymbol{\imath}}\}\{\vec{\boldsymbol{\jmath}}\}\{\vec{\boldsymbol{k}}\}] = [\{\vec{\boldsymbol{\imath}}\}\{\vec{\boldsymbol{\jmath}}\}\{\vec{\boldsymbol{k}}\}]\mathbf{P}_0$
  else
    $\hat{\mathbf{F}} := \mathbf{P}_3^{\intercal}\mathbf{F}\mathbf{P}_3$, $[\{\vec{\mathbf{E}}_1\}\{\vec{\mathbf{E}}_2\}\{\vec{\mathbf{E}}_3\}] := [\{\vec{\boldsymbol{\jmath}}\}\{\vec{\boldsymbol{\imath}}\}\{\vec{\boldsymbol{k}}\}] = [\{\vec{\boldsymbol{\imath}}\}\{\vec{\boldsymbol{\jmath}}\}\{\vec{\boldsymbol{k}}\}]\mathbf{P}_3$
  end if
else if $\mathcal{F}_2 \leqslant \mathcal{F}_1$ **and** $\mathcal{F}_2 \leqslant \mathcal{F}_3$ **then**
  if $|F_{13}| \leqslant |F_{31}|$ **then**
    $\hat{\mathbf{F}} := \mathbf{P}_1^{\intercal}\mathbf{F}\mathbf{P}_1$, $[\{\vec{\mathbf{E}}_1\}\{\vec{\mathbf{E}}_2\}\{\vec{\mathbf{E}}_3\}] := [\{\vec{\boldsymbol{\jmath}}\}\{\vec{\boldsymbol{k}}\}\{\vec{\boldsymbol{\imath}}\}] = [\{\vec{\boldsymbol{\imath}}\}\{\vec{\boldsymbol{\jmath}}\}\{\vec{\boldsymbol{k}}\}]\mathbf{P}_1$
  else
    $\hat{\mathbf{F}} := \mathbf{P}_4^{\intercal}\mathbf{F}\mathbf{P}_4$, $[\{\vec{\mathbf{E}}_1\}\{\vec{\mathbf{E}}_2\}\{\vec{\mathbf{E}}_3\}] := [\{\vec{\boldsymbol{k}}\}\{\vec{\boldsymbol{\jmath}}\}\{\vec{\boldsymbol{\imath}}\}] = [\{\vec{\boldsymbol{\imath}}\}\{\vec{\boldsymbol{\jmath}}\}\{\vec{\boldsymbol{k}}\}]\mathbf{P}_4$
  end if
else ($\mathcal{F}_3 \leqslant \mathcal{F}_1$ **and** $\mathcal{F}_3 \leqslant \mathcal{F}_2$)
  if $|F_{21}| \leqslant |F_{12}|$ **then**
    $\hat{\mathbf{F}} := \mathbf{P}_2^{\intercal}\mathbf{F}\mathbf{P}_2$, $[\{\vec{\mathbf{E}}_1\}\{\vec{\mathbf{E}}_2\}\{\vec{\mathbf{E}}_3\}] := [\{\vec{\boldsymbol{k}}\}\{\vec{\boldsymbol{\imath}}\}\{\vec{\boldsymbol{\jmath}}\}] = [\{\vec{\boldsymbol{\imath}}\}\{\vec{\boldsymbol{\jmath}}\}\{\vec{\boldsymbol{k}}\}]\mathbf{P}_2$
  else
    $\hat{\mathbf{F}} := \mathbf{P}_5^{\intercal}\mathbf{F}\mathbf{P}_5$, $[\{\vec{\mathbf{E}}_1\}\{\vec{\mathbf{E}}_2\}\{\vec{\mathbf{E}}_3\}] := [\{\vec{\boldsymbol{\imath}}\}\{\vec{\boldsymbol{k}}\}\{\vec{\boldsymbol{\jmath}}\}] = [\{\vec{\boldsymbol{\imath}}\}\{\vec{\boldsymbol{\jmath}}\}\{\vec{\boldsymbol{k}}\}]\mathbf{P}_5$
  end if
end if

whose affiliated components for the re-indexed deformation gradient are

$$
\begin{aligned}
[\hat{\mathbf{F}}_1] &= \begin{bmatrix} F_{11} & F_{12} & F_{13} \\ F_{21} & F_{22} & F_{23} \\ F_{31} & F_{32} & F_{33} \end{bmatrix} \qquad [\hat{\mathbf{F}}_2] = \begin{bmatrix} F_{11} & F_{13} & F_{12} \\ F_{31} & F_{33} & F_{32} \\ F_{21} & F_{23} & F_{22} \end{bmatrix} \qquad [\hat{\mathbf{F}}_3] = \begin{bmatrix} F_{22} & F_{21} & F_{23} \\ F_{12} & F_{11} & F_{13} \\ F_{32} & F_{31} & F_{33} \end{bmatrix} \\
[\hat{\mathbf{F}}_4] &= \begin{bmatrix} F_{22} & F_{23} & F_{21} \\ F_{32} & F_{33} & F_{31} \\ F_{12} & F_{13} & F_{11} \end{bmatrix} \qquad [\hat{\mathbf{F}}_5] = \begin{bmatrix} F_{33} & F_{31} & F_{32} \\ F_{13} & F_{11} & F_{12} \\ F_{23} & F_{21} & F_{22} \end{bmatrix} \qquad [\hat{\mathbf{F}}_6] = \begin{bmatrix} F_{33} & F_{32} & F_{31} \\ F_{23} & F_{22} & F_{21} \\ F_{13} & F_{12} & F_{11} \end{bmatrix}
\end{aligned} \tag{C.2b}
$$

where case 1 is the default case whose operator $\boldsymbol{P}_0$ is the identity tensor.

APPENDIX D

IMPLICIT ELASTICITY

Both explicit (i.e., Green [70]) and implicit (i.e., Rajagopal [71]) elastic material models are put forward in this appendix for one's consideration when choosing a material model to represent biologic fibers and membranes.

D.1 Alveolar Chords as Green (Explicit) Thermoelastic Fibers

A Green thermoelastic fiber has a Gibbs free-energy potential described by an explicit function of state, viz., $\mathcal{G}(\theta, F)$ where $\mathrm{d}\mathcal{G} = -\eta\,\mathrm{d}\theta - \frac{1}{\rho}e\,\mathrm{d}F$ (cf. Eqn. 5.26a), out of which one derives the governing thermoelastic constitutive equations, viz., for entropy

$$\eta = -\partial_\theta \mathcal{G}(\theta, F), \tag{D.1a}$$

and for strain

$$e := \ln(L/L_0) = -\rho\,\partial_F \mathcal{G}(\theta, F). \tag{D.1b}$$

Providing an energy function establishes a material model.

D.1.1 Hookean Fibers

Herein we consider a Gibbs free-energy potential suitable for describing a Hookean fiber

$$\mathcal{G}(\theta, F) \;=\; -\eta_0(\theta - \theta_0) - C\left(\theta \ln\left(\frac{\theta}{\theta_0}\right) - (\theta - \theta_0)\right) - \frac{F - F_0}{\rho}\left(\alpha \ln\left(\frac{\theta}{\theta_0}\right) + \frac{F - F_0}{2E}\right) \tag{D.2}$$

normalized so that $\mathcal{G}(\theta_0, F_0) = 0$ with initial conditions of $\eta_0 = -\partial_\theta \mathcal{G}(\theta_0, F_0)$ and $e_0 = -\rho\,\partial_F \mathcal{G}(\theta_0, F_0) = 0$ in our reference state associated with fields θ_0 and F_0. Introducing $\ln(\theta/\theta_0)$ presumes that temperature θ is absolute, i.e., it is measured in Kelvin, not centi-

grade, so in our application $\theta_0 = 310$ K is body temperature.

D.1.2 Secant Material Properties

Upon subtituting the Gibbs free-energy function (D.2) into the constitutive equations (D.1a & D.1b) governing entropy and strain, respectively, results in the matrix expression

$$\begin{Bmatrix} \eta - \eta_0 \\ \ln(L/L_0) \end{Bmatrix} = \begin{bmatrix} C_s & \alpha_s/\rho\theta \\ \alpha_s & 1/E_s \end{bmatrix} \begin{Bmatrix} \ln(\theta/\theta_0) \\ F - F_0 \end{Bmatrix}$$

which rearranges into a form that is more suitable for our needs, specifically

$$\begin{Bmatrix} \eta - \eta_0 \\ F - F_0 \end{Bmatrix} = \begin{bmatrix} C_s - \alpha_s^2 E_s/\rho\theta & \alpha_s E_s/\rho\theta \\ -\alpha_s E_s & E_s \end{bmatrix} \begin{Bmatrix} \ln(\theta/\theta_0) \\ \ln(L/L_0) \end{Bmatrix} \tag{D.3a}$$

with material properties: a specific heat (evaluated at some reference force F_0) of

$$C_s := \left. \frac{\eta - \eta_0}{\ln(\theta/\theta_0)} \right|_{F=F_0} \tag{D.3b}$$

with $C_s - \alpha_s^2 E_s/\rho\theta$ being a heat capacity (evaluated at some reference length L_0), plus a thermal strain coefficient (evaluated at some reference force F_0) of

$$\alpha_s := \left. \frac{\ln(L/L_0)}{\ln(\theta/\theta_0)} \right|_{F=F_0}, \tag{D.3c}$$

and an elastic compliance (evaluated at some reference temperature θ_0) of

$$\frac{1}{E_s} := \left. \frac{\ln(L/L_0)}{F - F_0} \right|_{\theta=\theta_0}. \tag{D.3d}$$

D.1.3 Tangent Material Properties

Upon differentiating the constitutive equations for entropy and strain found in Eqns. (D.1a & D.1b), respectively, assuming that they are both sufficiently differentiable functions

of state, while adopting the expression for Gibbs free energy found in Eqn. (D.2), results in the following constitutive equation

$$\begin{Bmatrix} \mathrm{d}\eta \\ L^{-1}\,\mathrm{d}L \end{Bmatrix} = -\begin{bmatrix} \partial_{\theta\theta}\,\mathcal{G} & \partial_{\theta F}\,\mathcal{G} \\ \rho\,\partial_{F\theta}\,\mathcal{G} & \rho\,\partial_{FF}\,\mathcal{G} \end{bmatrix} \begin{Bmatrix} \mathrm{d}\theta \\ \mathrm{d}F \end{Bmatrix} = \begin{bmatrix} C_t & \alpha_t/\rho\theta \\ \alpha_t & 1/E_t \end{bmatrix} \begin{Bmatrix} \theta^{-1}\,\mathrm{d}\theta \\ \mathrm{d}F \end{Bmatrix}$$

where we observe that the intensive and extensive variables now appear in rate or differential form; hence, this formulation is hypo-elastic. [72] The material properties are: a specific heat (at constant force) of

$$C_t := \left.\frac{\mathrm{d}\eta}{\theta^{-1}\,\mathrm{d}\theta}\right|_{\mathrm{d}F=0} = C_s - \frac{\alpha_s(F-F_0)}{\rho\,\theta} = -\theta\,\partial_{\theta\theta}\,\mathcal{G}(\theta,F) \tag{D.4a}$$

where the tangent response for specific heat C_t relates to the secant response for specific heat C_s via $C_t = C_s - \alpha_s(F-F_0)/\rho\theta$, with $C_t - \alpha_t^2 E_t/\rho\theta$ being a heat capacity (at constant strain), plus a thermal strain coefficient (at constant force) of

$$\alpha_t := \left.\frac{L^{-1}\,\mathrm{d}L}{\theta^{-1}\,\mathrm{d}\theta}\right|_{\mathrm{dF}=0} = -\rho\theta\,\partial_{F\theta}\,\mathcal{G}(\theta,F) = -\rho\theta\,\partial_{\theta F}\,\mathcal{G}(\theta,F) \tag{D.4b}$$

where, typically, $\alpha_t \equiv \alpha_s$, and an elastic compliance (at constant temperature) of

$$\frac{1}{E_t} := \left.\frac{L^{-1}\,\mathrm{d}L}{\mathrm{d}F}\right|_{\mathrm{d}\theta=0} = -\rho\,\partial_{FF}\,\mathcal{G}(\theta,F) \tag{D.4c}$$

D.2 Alveolar Chords as Rajagopal (Implicit) Thermoelastic Fibers

In 2003, Rajagopal [71] introduced the idea of an implicit elastic solid. In 2016, Freed & Rajagopal [62] constructed an elastic fiber model that convolves an explicit energy with an implicit energy. In their approach, they decomposed fiber strain $e := \ln(L/L_0)$ into a sum of two strains, viz., $e = e_1 + e_2$ wherein $e_1 := \ln(L_1/L_0)$ and $e_2 := \ln(L/L_1)$. Length L_0 is a reference fiber length, viz., its length whereat $F = F_0$. Length L_1 can be thought of as the fiber's length caused solely by a molecular reconfiguration under an applied load of F (e.g.,

an unraveling of crimp in collagen, a network reorientation in elastin, a reconformation in structural proteins, etc.).

Let the Gibbs free-energy potential be described by a function of the form

$$\mathcal{G}(\theta, e, F) := \mathcal{G}_1(e_1, F) + \mathcal{G}_2(\theta, F) \quad \text{with} \quad \mathrm{d}\mathcal{G} = -\eta\,\mathrm{d}\theta - \tfrac{1}{\rho} e\,\mathrm{d}F \tag{D.5}$$

where $\mathcal{G}_1$ is an implicit potential (a configuration energy) and $\mathcal{G}_2$ is an explicit potential (a strain energy). This energy function leads to the constitutive equation with the material properties of

$$C_t := \left.\frac{\mathrm{d}\eta}{\theta^{-1}\,\mathrm{d}\theta}\right|_{\mathrm{d}F=0} = -\theta\,\partial_{\theta\theta}\,\mathcal{G}(\theta, e, F) = -\theta\,\partial_{\theta\theta}\,\mathcal{G}_2(\theta, F) \tag{D.6a}$$

$$\alpha_t := \left.\frac{L^{-1}\,\mathrm{d}L}{\theta^{-1}\,\mathrm{d}\theta}\right|_{\mathrm{dF}=0} = -\rho\theta\,\partial_{F\theta}\,\mathcal{G}(\theta, e, F) = -\rho\theta\,\partial_{F\theta}\,\mathcal{G}_2(\theta, F) \tag{D.6b}$$

$$\frac{1}{E_t} := \left.\frac{L^{-1}\,\mathrm{d}L}{\mathrm{d}F}\right|_{\mathrm{d}\theta=0} = -\big(\rho\,\partial_{e_1}\mathcal{G}_1(e_1, F)\big)^{-1}\big(e + \rho\,\partial_F\,\mathcal{G}(\theta, e, F)\big) - \rho\,\partial_{FF}\,\mathcal{G}_2(\theta, F) \tag{D.6c}$$

where mass density ρ is a mass per unit length of line.

D.2.1 Biologic Fibers with Tangent Material Properties

The fiber model of Freed & Rajagopal [62] imposes a limiting constraint $e_{1_{\max}}$ onto the internal strain of reconfiguration e_1, viz., $e_1 \leqslant e_{1_{\max}}$. Their model, when cast in terms of a Gibbs free-energy function in the form of Eqn. (D.5), is described by an implicit energy contribution of

$$\mathcal{G}_1(e_1, F) = -\frac{1}{\rho}\Big(e_{1_{\max}}\big(E_1 e_1 - (F - F_0)\big) + 2e_1(F - F_0)\Big) \tag{D.7a}$$

and explicit energy contribution of

$$\mathcal{G}_2(\theta, F) = -\eta_0(\theta - \theta_0) - C\left(\theta \ln\left(\frac{\theta}{\theta_0}\right) - (\theta - \theta_0)\right) - \frac{F - F_0}{\rho}\left(\alpha \ln\left(\frac{\theta}{\theta_0}\right) + \frac{F - F_0}{2E_2}\right) \tag{D.7b}$$

that, collectively, depend upon temperature θ, force F, and an internal strain e_1, whose free energy is normalized so that $\mathcal{G}_1(e_{1,0}, F_0) = 0$ and $\mathcal{G}_2(\theta_0, F_0) = 0$ with initial conditions $e_{1,0} = 0$, $e_{2,0} = -\rho\,\partial_F \mathcal{G}_2(\theta_0, F_0) = 0$ and $\eta_0 = -\partial_\theta \mathcal{G}_2(\theta_0, F_0)$. In fact, the explicit contribution to the free energy adopted here is Hookean, cf. Eqn. (D.2). The resulting constitutive responses for entropy η and force F are therefore described by the following differential matrix equation

$$\begin{Bmatrix} \mathrm{d}\eta \\ \mathrm{d}F \end{Bmatrix} = \begin{bmatrix} C_t - \alpha_t^2 E_t/\rho\theta & \alpha_t E_t/\rho\theta \\ -\alpha_t E_t & E_t \end{bmatrix} \begin{Bmatrix} \theta^{-1}\,\mathrm{d}\theta \\ L^{-1}\,\mathrm{d}L \end{Bmatrix} \tag{D.7c}$$

whose elastic tangent compliance is now described by

$$\frac{1}{E_t(\theta, e, F)} = \frac{e_{1_{\max}} - e_1}{E_1 e_{1_{\max}} + 2(F - F_0)} + \frac{1}{E_2} \tag{D.7d}$$

wherein

$$e_1 = e - \alpha \ln\left(\frac{\theta}{\theta_0}\right) - \frac{F - F_0}{E_2} \tag{D.7e}$$

and whose initial tangent modulus $E_t(\theta_0, e_0, F_0)$ is $E_1 E_2/(E_1 + E_2)$ ($\approx E_1$ whenever $E_2 \gg E_1 > 0$) while its terminal tangent modulus $E_t(e_1 = e_{1_{\max}})$ is E_2. A transition strain occurs at $e_{1_{\max}}$ (> 0), which establishes the limiting state for internal strain e_1, i.e., $e_1 \leqslant e_{1_{\max}}$.

D.2.2 Biologic Fibers with Secant Material Properties

Material properties C_t, α_t and E_t for the above model, viz., those of Eqn. (D.7), describe tangents to material response functions. For the thermal properties, their secant counterparts C_s and α_s relate to their tangent properties C_t and α_t just as they do for a Green elastic fiber. Only the elastic compliance needs to be addressed.

The tangent modulus E_t is established through the relationship

$$\frac{1}{E_t} := \left.\frac{\mathrm{d}e}{\mathrm{d}F}\right|_{\mathrm{d}\theta=0} = \left.\frac{\mathrm{d}e_1}{\mathrm{d}F}\right|_{\mathrm{d}\theta=0} + \left.\frac{\mathrm{d}e_2}{\mathrm{d}F}\right|_{\mathrm{d}\theta=0} =: \frac{1}{E_{1t}} + \frac{1}{E_{2t}} \tag{D.8a}$$

so that a fiber's elastic compliance is described by

$$\mathrm{d}e = \frac{\mathrm{d}F}{E_t} \quad \text{where} \quad \frac{1}{E_t} = \frac{1}{E_{1t}} + \frac{1}{E_{2t}} \tag{D.8b}$$

and, consequently, its elastic modulus is described by

$$\mathrm{d}F = E_t\,\mathrm{d}e \quad \text{where} \quad E_t = \frac{E_{1t}E_{2t}}{E_{1t} + E_{2t}}. \tag{D.8c}$$

The implicit free-energy function introduced through Eqn. (D.7) produces a tangent compliance of

$$\frac{1}{E_t} = \frac{e_{1_{\max}} - e_1}{E_1 e_{1_{\max}} + 2(F - F_0)} + \frac{1}{E_2} \tag{D.8d}$$

whose internal strain caused by molecular reconfiguration comes from

$$e_1 = e - \alpha_t \ln\left(\frac{\theta}{\theta_0}\right) - \frac{F - F_0}{E_2}. \tag{D.8e}$$

The material properties of this model are: $E_1E_2/(E_1 + E_2)$ (> 0) is the initial tangent modulus, E_2 $(\gg E_1 > 0)$ is the terminal tangent modulus, $e_{1_{\max}}$ is the maximum strain that can arise from a molecular reconfiguration, and α_t is the thermal strain coefficient, all quantified against a reference state described by θ_0 and F_0.

It follows then that its associated secant compliance obeys

$$\frac{1}{E_s} := \left.\frac{e}{F - F_0}\right|_{\theta=\theta_0} = \left.\frac{e_1}{F - F_0}\right|_{\theta=\theta_0} + \left.\frac{e_2}{F - F_0}\right|_{\theta=\theta_0} =: \frac{1}{E_{1s}} + \frac{1}{E_{2s}} \tag{D.9a}$$

so the fiber's compliance representation is described by

$$e = \frac{F - F_0}{E_s} \quad \text{where} \quad \frac{1}{E_s} = \frac{1}{E_{1s}} + \frac{1}{E_{2s}} \tag{D.9b}$$

and, therefore, its modulus representation is described by

$$F = F_0 + E_s\, e \quad \text{where} \quad E_s = \frac{E_{1s} E_{2s}}{E_{1s} + E_{2s}}. \tag{D.9c}$$

where, upon integrating Eqn. (D.8d) by separation of variables, one arrives at a secant compliance comprising a sum between

$$\frac{1}{E_{1s}} = \frac{e_{1_{\max}}}{F - F_0} \left(1 - \frac{\sqrt{E_1 e_{1_{\max}}}}{\sqrt{E_1 e_{1_{\max}} + 2(F - F_0)}} \right) \tag{D.9d}$$

and

$$\frac{1}{E_{2s}} = \frac{1}{E_2} \tag{D.9e}$$

with $E_s(F \leqslant F_0) = E_1 E_2/(E_1 + E_2)$.

D.3 Alveolar Septa as Green (Explicit) Thermoelastic Membranes

For a 2D membrane with a mass density of ρ per unit area, its response is comprising uniform and non-uniform contributions. The thermodynamic conjugate fields pertaining to uniform behaviors are: temperature θ and entropy η, and surface tension π and dilation ξ, cf. Eqn. (5.37a). While the conjugate fields pertaining to non-uniform behaviors are: normal stress difference σ and squeeze strain ε, and shear stress τ and shear strain γ, cf. Eqn. (5.37b).

A Green thermoelastic membrane is assigned a Gibbs free-energy potential described by $\mathcal{G}(\theta, \pi, \sigma, \tau) = \mathcal{G}_u(\theta, \pi) + \mathcal{G}_n(\sigma, \tau)$ where $\mathrm{d}\mathcal{G} = -\eta\, \mathrm{d}\theta - \frac{1}{\rho}\big(\xi\, \mathrm{d}\pi + \varepsilon\, \mathrm{d}\sigma + \gamma\, \mathrm{d}\tau\big)$ from which one derives its governing thermoelastic constitutive equations; specifically, for entropy

$$\eta = -\partial_\theta\, \mathcal{G}(\theta, \pi, \sigma, \tau) = -\partial_\theta\, \mathcal{G}_u(\theta, \pi), \tag{D.10a}$$

for dilation

$$\xi = -\rho\,\partial_\pi \mathcal{G}(\theta,\pi,\sigma,\tau) = -\rho\,\partial_\pi \mathcal{G}_u(\theta,\pi), \tag{D.10b}$$

for squeeze

$$\varepsilon = -\rho\,\partial_\sigma \mathcal{G}(\theta,\pi,\sigma,\tau) = -\rho\,\partial_\sigma \mathcal{G}_n(\sigma,\tau), \tag{D.10c}$$

and for shear

$$\gamma = -\rho\,\partial_\tau \mathcal{G}(\theta,\pi,\sigma,\tau) = -\rho\,\partial_\tau \mathcal{G}_n(\sigma,\tau) \tag{D.10d}$$

whereby specifying energies $\mathcal{G}_u$ and $\mathcal{G}_n$ produces a material model for membranes.

D.3.1 Hookean Membranes

In this appendix, we consider a function for the Gibbs free-energy potential that is suitable for describing biologic Hookean membranes; specifically: for governing their uniform response, let

$$\mathcal{G}_u(\theta,\pi) = -\eta_0(\theta-\theta_0) - C\left(\theta\ln\left(\frac{\theta}{\theta_0}\right) - (\theta-\theta_0)\right) - \frac{\pi-\pi_0}{2\rho}\left(2\alpha\ln\left(\frac{\theta}{\theta_0}\right) + \frac{\pi-\pi_0}{4M}\right) \tag{D.11a}$$

and for governing their non-uniform response, let

$$\mathcal{G}_n(\sigma,\tau) = -\frac{1}{2\rho}\left(\frac{\sigma^2}{2N} + \frac{\tau^2}{G}\right) \tag{D.11b}$$

where symmetries $\mathcal{G}_n(\sigma,\tau) = \mathcal{G}_n(-\sigma,\tau) = \mathcal{G}_n(\sigma,-\tau) = \mathcal{G}_n(-\sigma,-\tau)$ must hold because the squeeze and shear variables can take on either sign. These free energies are normalized so that $\mathcal{G}_u(\theta_0,\pi_0) = 0$ and $\mathcal{G}_n(\sigma_0,\tau_0) = 0$ with initial conditions of $\eta_0 = -\partial_\theta \mathcal{G}_u(\theta_0,\pi_0)$, $\xi_0 = -\rho\,\partial_\pi \mathcal{G}_u(\theta_0,\pi_0) = 0$, $\varepsilon_0 = -\rho\,\partial_\sigma \mathcal{G}_n(0,0) = 0$ and $\gamma_0 = -\rho\,\partial_\tau \mathcal{G}_n(0,0) = 0$ for a reference state with fields θ_0, π_0, $\sigma_0 = 0$ and $\tau_0 = 0$.

D.3.2 Secant Material Properties

D.3.2.1 Uniform Response

Substituting the Gibbs free-energy function of Eqn. (D.11a) into the constitutive equations governing entropy Eqn. (D.10a) and dilation Eqn. (D.10b) results in a matrix expression of

$$\begin{Bmatrix} \eta - \eta_0 \\ \ln\sqrt{A/A_0} \end{Bmatrix} = \begin{bmatrix} C_s & \alpha_s/\rho\theta \\ \alpha_s & 1/4M_s \end{bmatrix} \begin{Bmatrix} \ln(\theta/\theta_0) \\ \pi - \pi_0 \end{Bmatrix}$$

where $\xi := \ln\sqrt{A/A_0}$. This matrix equation can be rearranged into a form that is more suitable for our needs, viz.,

$$\begin{Bmatrix} \eta - \eta_0 \\ \pi - \pi_0 \end{Bmatrix} = \begin{bmatrix} C_s - 4\alpha_s^2 M_s/\rho\theta & 4\alpha_s M_s/\rho\theta \\ -4\alpha_s M_s & 4M_s \end{bmatrix} \begin{Bmatrix} \ln(\theta/\theta_0) \\ \ln\sqrt{A/A_0} \end{Bmatrix} \tag{D.12a}$$

whose material properties are: a specific heat (evaluated at a reference surface tension π_0) of

$$C_s := \left.\frac{\eta - \eta_0}{\ln(\theta/\theta_0)}\right|_{\pi=\pi_0} \tag{D.12b}$$

with $C_s - 4\alpha_s^2 M_s/\rho\theta$ being a heat capacity in an absence of dilation, plus a thermal strain coefficient (evaluated at a reference surface tension π_0) of

$$\alpha_s := \left.\frac{\ln(L/L_0)}{\ln(\theta/\theta_0)}\right|_{\pi=\pi_0} = \frac{1}{2}\left.\frac{\ln(A/A_0)}{\ln(\theta/\theta_0)}\right|_{\pi=\pi_0}, \tag{D.12c}$$

where $\ln(A/A_0) = 2\ln(L/L_0)$ is the surface dilation, with L/L_0 being the stretch between any two points on its surface, plus an elastic membrane compliance (evaluated at a reference temperature θ_0) of

$$\frac{1}{M_s} := \left.\frac{\ln(A/A_0)}{T - T_0}\right|_{\theta=\theta_0} = 4 \left.\frac{\xi}{\pi - \pi_0}\right|_{\theta=\theta_0}, \tag{D.12d}$$

where $T := \frac{1}{2}(\sigma_{11} + \sigma_{22}) =: \frac{1}{2}\pi$ is the surface tension, with σ_{ij} being components of the Cauchy stress in this 2D space. These are *secant* material properties, hence the subscript 's', whose values can be measured in experiments.

D.3.2.2 Non-Uniform Response

Substituting the Gibbs free-energy function of Eqn. (D.11b) into the constitutive equations governing squeeze (D.10c) and shear (D.10d) leads to the following matrix equation

$$\begin{Bmatrix} \varepsilon \\ \gamma \end{Bmatrix} = \begin{bmatrix} 1/2N_s & 0 \\ 0 & 1/G_s \end{bmatrix} \begin{Bmatrix} \sigma \\ \tau \end{Bmatrix}$$

that when inverted becomes

$$\begin{Bmatrix} \sigma \\ \tau \end{Bmatrix} = \begin{bmatrix} 2N_s & 0 \\ 0 & G_s \end{bmatrix} \begin{Bmatrix} \varepsilon \\ \gamma \end{Bmatrix} \tag{D.13a}$$

whose material properties are: a squeeze compliance (in an absence of shear γ) of

$$\frac{1}{N_s} := \left.\frac{\ln(\Gamma/\Gamma_0)}{\sigma_{11} - \sigma_{22}}\right|_{g=g_0} = 2 \left.\frac{\varepsilon}{\sigma}\right|_{\gamma=0} \tag{D.13b}$$

where $\Gamma := a/b$ and $\Gamma_0 = a_0/b_0$ are the current and reference stretches of squeeze, with $\varepsilon := \ln\sqrt{\Gamma/\Gamma_0}$ being the squeeze strain, and where $\sigma := \sigma_{11} - \sigma_{22}$ establishes a normal stress difference, plus a shear compliance (in an absence of squeeze ε) of

$$\frac{1}{G_s} := \left.\frac{g - g_0}{\Gamma\sigma_{21}}\right|_{\Gamma=\Gamma_0} = \left.\frac{\gamma}{\tau}\right|_{\varepsilon=0} \tag{D.13c}$$

where g and g_0 are the current and reference magnitudes of shear, with $\gamma := g - g_0$ denoting shear strain, and where $\tau := \Gamma\sigma_{21}$ establishes the thermodynamic shear stress.

D.3.3 Tangent Material Properties

D.3.3.1 Uniform Response

Upon differentiating the constitutive equations for entropy and dilation found in Eqns. (D.10a & D.10b), respectively, assuming they are both sufficiently differentiable functions of state, while adopting the Gibbs free energy from Eqn. (D.11a), results in the following matrix constitutive equation

$$\begin{Bmatrix} \mathrm{d}\eta \\ \mathrm{d}\xi \end{Bmatrix} = -\begin{bmatrix} \partial_{\theta\theta}\,\mathcal{G}_u & \partial_{\theta\pi}\,\mathcal{G}_u \\ \rho\,\partial_{\pi\theta}\,\mathcal{G}_u & \rho\,\partial_{\pi\pi}\,\mathcal{G}_u \end{bmatrix} \begin{Bmatrix} \mathrm{d}\theta \\ \mathrm{d}\pi \end{Bmatrix} = \begin{bmatrix} C_t & \alpha_t/\rho\theta \\ \alpha_t & 1/4M_t \end{bmatrix} \begin{Bmatrix} \theta^{-1}\,\mathrm{d}\theta \\ \mathrm{d}\pi \end{Bmatrix}$$

which is hypo-elastic in its construction. [72] This expression can be rearranged into

$$\begin{Bmatrix} \mathrm{d}\eta \\ \mathrm{d}\pi \end{Bmatrix} = \begin{bmatrix} C_t - 4\alpha_t^2 M_t/\rho\theta & 4\alpha_t M_t/\rho\theta \\ -4\alpha_t M_t & 4M_t \end{bmatrix} \begin{Bmatrix} \theta^{-1}\,\mathrm{d}\theta \\ \frac{1}{2}A^{-1}\,\mathrm{d}A \end{Bmatrix} \tag{D.14a}$$

recalling that $\mathrm{d}\xi = \mathrm{d}A/2A$, and with material properties defined accordingly: a specific heat (at constant surface tension) of

$$C_t := \left.\frac{\mathrm{d}\eta}{\theta^{-1}\,\mathrm{d}\theta}\right|_{\mathrm{d}\pi=0} = C_s - \alpha_s(\pi - \pi_0)/\rho\theta = -\theta\,\partial_{\theta\theta}\,\mathcal{G}_u \tag{D.14b}$$

with $C_t - 4\alpha_t^2 M_t/\rho\theta$ denoting a heat capacity at constant dilation, and a lineal thermal strain coefficient (at constant surface tension) of

$$\alpha_t := \left.\frac{L^{-1}\,\mathrm{d}L}{\theta^{-1}\,\mathrm{d}\theta}\right|_{\mathrm{d}\pi=0} = \frac{1}{2}\left.\frac{A^{-1}\,\mathrm{d}A}{\theta^{-1}\,\mathrm{d}\theta}\right|_{\mathrm{d}\pi=0} = \begin{cases} -\rho\theta\,\partial_{\pi\theta}\,\mathcal{G}_u \\ -\rho\theta\,\partial_{\theta\pi}\,\mathcal{G}_u \end{cases} \tag{D.14c}$$

plus a compliance (at constant temperature) of

$$\frac{1}{M_t} := \left.\frac{A^{-1}\,\mathrm{d}A}{\mathrm{d}T}\right|_{\mathrm{d}\theta=0} = 4\left.\frac{\mathrm{d}\xi}{\mathrm{d}\pi}\right|_{\mathrm{d}\theta=0} = -4\rho\,\partial_{\pi\pi}\,\mathcal{G}_u. \tag{D.14d}$$

D.3.3.2 Non-Uniform Response

From $\mathrm{d}\mathcal{G} = \mathrm{d}\mathcal{G}_u + \mathrm{d}\mathcal{G}_n$ with $\mathrm{d}\mathcal{G}_u = -\eta\,\mathrm{d}\theta - \frac{1}{\rho}\xi\,\mathrm{d}\pi$ comes $\mathrm{d}\mathcal{G}_n = -\frac{1}{\rho}(\varepsilon\,\mathrm{d}\sigma + \gamma\,\mathrm{d}\tau)$ out of which one obtains the constitutive equations governing non-uniform responses in a Green elastic membrane, viz., $\varepsilon = -\rho\,\partial_\sigma\,\mathcal{G}_n$ and $\gamma = -\rho\,\partial_\tau\,\mathcal{G}_n$, that, assuming they are continuous and differentiable functions of state, can be expressed as the matrix differential equation

$$\begin{Bmatrix} \mathrm{d}\varepsilon \\ \mathrm{d}\gamma \end{Bmatrix} = -\rho \begin{bmatrix} \partial_{\sigma\sigma}\,\mathcal{G}_n & \partial_{\sigma\tau}\,\mathcal{G}_n \\ \partial_{\tau\sigma}\,\mathcal{G}_n & \partial_{\tau\tau}\,\mathcal{G}_n \end{bmatrix} \begin{Bmatrix} \mathrm{d}\sigma \\ \mathrm{d}\tau \end{Bmatrix} = \begin{bmatrix} 1/2N_t & 0 \\ 0 & 1/G_t \end{bmatrix} \begin{Bmatrix} \mathrm{d}\sigma \\ \mathrm{d}\tau \end{Bmatrix}$$

where $\partial_{\sigma\tau}\,\mathcal{G}_n = \partial_{\tau\sigma}\,\mathcal{G}_n = 0$, because the modes of squeeze and shear are taken to be decoupled. The resulting matrix is readily inverted into a form that is more useful for us, namely

$$\begin{Bmatrix} \mathrm{d}\sigma \\ \mathrm{d}\tau \end{Bmatrix} = \begin{bmatrix} 2N_t & 0 \\ 0 & G_t \end{bmatrix} \begin{Bmatrix} \mathrm{d}\varepsilon \\ \mathrm{d}\gamma \end{Bmatrix} \tag{D.15a}$$

whose associated material properties are established via

$$\frac{1}{N_t} := \left.\frac{\Gamma^{-1}\,\mathrm{d}\Gamma}{\mathrm{d}(\sigma_{11} - \sigma_{22})}\right|_{\mathrm{d}\gamma=0} = 2\left.\frac{\mathrm{d}\varepsilon}{\mathrm{d}\sigma}\right|_{\mathrm{d}\gamma=0} = -2\rho\,\partial_{\sigma\sigma}\,\mathcal{G}_n \tag{D.15b}$$

and

$$\frac{1}{G_t} := \frac{1}{\Gamma}\frac{\mathrm{d}g}{\mathrm{d}\sigma_{21}}\bigg|_{\mathrm{d}\Gamma=0} = \frac{\mathrm{d}\gamma}{\mathrm{d}\tau}\bigg|_{\mathrm{d}\varepsilon=0} = -\rho\,\partial_{\tau\tau}\mathcal{G}_n \tag{D.15c}$$

where the conjugate stresses are defined as $\sigma := \sigma_{11} - \sigma_{22}$ and $\tau := \Gamma\sigma_{21}$ with $\Gamma := a/b$ being the stretch of squeeze from which it follows that $\Gamma^{-1}\mathrm{d}\Gamma = 2\,\mathrm{d}\varepsilon$ because the strain of squeeze is given by $\varepsilon = \ln\sqrt{\Gamma/\Gamma_0}$. The squeeze compliance $1/N_t = 2\,\mathrm{d}\varepsilon/\mathrm{d}\sigma|_\gamma$ is evaluated at a constant shear γ, while the shear compliance $1/G_t = \mathrm{d}\gamma/\mathrm{d}\tau|_\varepsilon$ is evaluated at a constant squeeze ε.

D.4 Alveolar Septa as Rajagopal (Implicit) Thermoelastic Membranes

We employ implicit elasticity here to derive a constitutive theory suitable for describing biologic membranes.

D.4.1 Tangent Material Properties

D.4.1.1 Uniform Response

Like the implicit elastic fiber introduced in Eqn. (D.7), the uniform response of an implicit elastic membrane with a strain-limiting dilation can be modeled using a Gibbs free energy of the form $\mathcal{G}_u(\theta,\xi,\pi) := \mathcal{G}_1(\xi_1,\pi) + \mathcal{G}_2(\theta,\pi)$ where our definition for dilation $\xi := \ln\sqrt{A/A_0}$ decomposes into a sum of two dilations: $\xi_1 := \ln\sqrt{A_1/A_0}$ and $\xi_2 := \ln\sqrt{A/A_1}$ so that $\xi = \xi_1 + \xi_2$, with like interpretations as those from their 1D fiber counterparts, viz., e, e_1 and e_2. Such a membrane's tangent material properties are then given by

$$C_t := -\theta\,\partial_{\theta\theta}\mathcal{G}_u(\theta,\xi,\pi) = -\theta\,\partial_{\theta\theta}\mathcal{G}_2(\theta,\pi) \tag{D.16a}$$

$$\alpha_t := -\rho\theta\,\partial_{\pi\theta}\mathcal{G}_u(\theta,\xi,\pi) = -\rho\theta\,\partial_{\pi\theta}\mathcal{G}_2(\theta,\pi) = -\rho\theta\,\partial_{\theta\pi}\mathcal{G}_2(\theta,\pi) \tag{D.16b}$$

$$1/4M_t := -\big(\rho\,\partial_{\xi_1}\mathcal{G}_1(\xi_1,\pi)\big)^{-1}\big(\xi + \rho\,\partial_\pi\mathcal{G}_u(\theta,\xi,\pi)\big) - \rho\,\partial_{\pi\pi}\mathcal{G}_2(\theta,\pi) \tag{D.16c}$$

whose derivations are analogous to those for the implicit fiber derived in Eqn. (D.6).

D.4.1.2 Uniform Biologic Membrane Model

Like our model for a biologic fiber, we consider a Gibbs free-energy function for describing the uniform response of a biologic membrane whose implicit energy function takes on the form of

$$\mathcal{G}_1(\xi_1,\pi) = -\frac{1}{\rho}\Big(\xi_{1_{\max}}\big(4M_1\xi_1 - (\pi-\pi_0)\big) + 2\xi_1(\pi-\pi_0)\Big) \tag{D.17a}$$

and whose explicit energy function is

$$\mathcal{G}_2(\theta,\pi) = -\eta_0(\theta-\theta_0) - C_t\left(\theta\ln\left(\frac{\theta}{\theta_0}\right) - (\theta-\theta_0)\right) - \frac{\pi-\pi_0}{2\rho}\left(2\alpha_t\ln\left(\frac{\theta}{\theta_0}\right) + \frac{\pi-\pi_0}{4M_2}\right) \tag{D.17b}$$

thereby resulting an elastic tangent compliance, as established in Eqn. (D.16c), of

$$\frac{1}{4M_t(\theta,\xi,\pi)} = \frac{\xi_{1_{\max}}-\xi_1}{4M_1\xi_{1_{\max}} + 2(\pi-\pi_0)} + \frac{1}{4M_2} \tag{D.17c}$$

wherein

$$\xi_1 = \xi - \alpha_t\ln\left(\frac{\theta}{\theta_0}\right) - \frac{\pi-\pi_0}{4M_2} \tag{D.17d}$$

with $\xi_{1_{\max}} > 0$ being an upper bound on strain ξ_1, i.e., $\xi_1 \leqslant \xi_{\max}$. Such a membrane has an initial tangent stiffness $M_t(\theta_0,\xi_0,\pi_0)$ of $M_1M_2/(M_1+M_2)$ ($\approx M_1$ whenever $M_2 \gg M_1 > 0$) and it has a terminal tangent stiffness $M_t(\xi_1 = \xi_{1_{\max}})$ of M_2.

D.4.1.3 Non-Uniform Response

We seek an energetic construction that is consistent with the Freed & Rajagopal [62] fiber model, but which is applicable to the non-uniform responses that planar membranes can support. A Rajagopal elastic solid is implicit. Therefore, we choose a Gibbs free-energy

function for governing non-uniform behavior that looks like

$$\mathcal{G}_n(\varepsilon,\gamma,\sigma,\tau) = \mathcal{G}_1(\varepsilon_1,\sigma) + \mathcal{G}_2(\sigma) + \mathcal{G}_3(\gamma_1,\tau) + \mathcal{G}_4(\tau) \tag{D.18}$$

which depend upon three squeeze strains $\varepsilon := \ln\sqrt{\Gamma/\Gamma_0}$, $\varepsilon_1 := \ln\sqrt{\Gamma_1/\Gamma_0}$ and $\varepsilon_2 := \ln\sqrt{\Gamma/\Gamma_1}$, and three shear strains $\gamma := g - g_0$, $\gamma_1 := g_1 - g_0$, and $\gamma_2 := g - g_1$, both of which are additive in the sense that $\varepsilon = \varepsilon_1 + \varepsilon_2$ and $\gamma = \gamma_1 + \gamma_2$, and as such, so are their differential rates of change $\mathrm{d}\varepsilon = \mathrm{d}\varepsilon_1 + \mathrm{d}\varepsilon_2$ and $\mathrm{d}\gamma = \mathrm{d}\gamma_1 + \mathrm{d}\gamma_2$. Strains ε_1 and γ_1 may be thought of as describing an unraveling of molecular configuration, analogous to e_1 in the fiber model of Eqn. (D.7), and ξ_1 in the uniform membrane model of Eqn. (D.17). No coupling between squeeze and shear is assumed in this energy function. Energies $\mathcal{G}_1$ and $\mathcal{G}_3$ are Rajagopal elastic (they have implicit dependencies upon state), while energies $\mathcal{G}_2$ and $\mathcal{G}_4$ are Green elastic (they have explicit dependencies upon state).

From the thermodynamic expression $-\rho\,\mathrm{d}\mathcal{G}_n = \varepsilon\,\mathrm{d}\sigma + \gamma\,\mathrm{d}\tau$, the non-uniform Gibbs free energy $\mathcal{G}_n$, when expressed in the form of Eqn. (D.18), and given the definitions for squeeze $1/N$ and shear $1/G$ compliances put forward in Eqns. (D.15b & D.15c), one determines that the tangent squeeze compliance is described by

$$\frac{1}{2N_t} := \frac{\mathrm{d}\varepsilon}{\mathrm{d}\sigma} = -\big(\rho\,\partial_{\varepsilon_1}\mathcal{G}_1\big)^{-1}\big(\varepsilon + \rho\,\partial_\sigma(\mathcal{G}_1 + \mathcal{G}_2)\big) - \rho\,\partial_{\sigma\sigma}\mathcal{G}_2 \tag{D.19a}$$

and that the tangent shear compliance is described by

$$\frac{1}{G_t} := \frac{\mathrm{d}\gamma}{\mathrm{d}\tau} = -\big(\rho\,\partial_{\gamma_1}\mathcal{G}_3\big)^{-1}\big(\gamma + \rho\,\partial_\tau(\mathcal{G}_3 + \mathcal{G}_4)\big) - \rho\,\partial_{\tau\tau}\mathcal{G}_4 \tag{D.19b}$$

whose mathematical structure is similar to that of the Freed–Rajagopal fiber model presented in Eqn. (D.7). The first collection of terms on the right-hand side of both formulæ is Rajagopal elastic; the second is Green elastic.

D.4.1.4 Non-Uniform Biologic Membrane Model

We now specify the Gibbs free-energy functions of Eqn. (D.18) such that they produce tangent compliances $1/N_t$ and $1/G_t$ with like mathematical structure to Eqn. (D.17c) for dilation, viz., $1/M_t$. Specifically, we consider Gibbs free-energy functions of the form

$$-\rho\,\mathcal{G}_1(\varepsilon_1,\sigma) = \operatorname{sgn}(\varepsilon_1)\,\varepsilon_{1_{\max}}\big(2N_1\varepsilon_1 - \sigma\big) + 2\varepsilon_1\sigma \tag{D.20a}$$

$$-\rho\,\mathcal{G}_2(\sigma) = \sigma^2/4N_2 \tag{D.20b}$$

$$-\rho\,\mathcal{G}_3(\gamma_1,\tau) = \operatorname{sgn}(\gamma_1)\,\gamma_{1_{\max}}\big(G_1\gamma_1 - \tau\big) + 2\gamma_1\tau \tag{D.20c}$$

$$-\rho\,\mathcal{G}_4(\tau) = \tau^2/2G_2 \tag{D.20d}$$

where these energy functions have the same mathematical structure as the energies for biologic fibers (Eqn. D.7) and uniform membranes (Eqn. D.17), less their temperature dependence, and less their states of pre-stress, i.e., $\sigma_0 = 0$ and $\tau_0 = 0$.

The sign functions, viz., $\operatorname{sgn}(\varepsilon_1)$ and $\operatorname{sgn}(\gamma_1)$, account for the fact that squeeze and shear strains can be of either sign, but the Gibbs energy must remain negative. In effect, the sign functions flip the limiting state between tension and compression, i.e., they change the signs of $\varepsilon_{1_{\max}}$ and $\gamma_{1_{\max}}$ depending upon the respective signs of ε_1 and γ_1. As a consequence, $\mathcal{G}_1(\varepsilon_1,\sigma) = \mathcal{G}_1(-\varepsilon_1,-\sigma)$, $\mathcal{G}_2(\sigma) = \mathcal{G}_2(-\sigma)$, $\mathcal{G}_3(\gamma_1,\tau) = \mathcal{G}_3(-\gamma_1,-\tau)$ and $\mathcal{G}_4(\tau) = \mathcal{G}_4(-\tau)$.

When substituted into Eqn. (D.19), these energy functions produce the following thermoelastic compliances

$$\frac{1}{2N(\varepsilon,\sigma)} = \frac{\operatorname{sgn}(\varepsilon_1)\,\varepsilon_{1_{\max}} - \varepsilon_1}{2N_1\operatorname{sgn}(\varepsilon_1)\,\varepsilon_{1_{\max}} + 2\sigma} + \frac{1}{2N_2} \qquad \varepsilon_1 = \varepsilon - \frac{\sigma}{2N_2} \tag{D.21a}$$

$$\frac{1}{G(\gamma,\tau)} = \frac{\operatorname{sgn}(\gamma_1)\,\gamma_{1_{\max}} - \gamma_1}{G_1\operatorname{sgn}(\gamma_1)\,\gamma_{1_{\max}} + 2\tau} + \frac{1}{G_2} \qquad \gamma_1 = \gamma - \frac{\tau}{G_2} \tag{D.21b}$$

which provide the tangent operators that we will use to describe the non-uniform behavior of a biologic membrane.

D.4.2 Secant Material Properties

D.4.2.1 Uniform Response

Integrating by parts the tangent compliance governing dilation found in Eqn. (D.17c) results in a secant compliance of

$$\frac{1}{4M_s(\pi)} = \frac{\xi_{1_{\max}}}{\pi - \pi_0}\left(1 - \frac{\sqrt{M_1\xi_{1_{\max}}}}{\sqrt{M_1\xi_{1_{\max}} + \frac{1}{2}(\pi - \pi_0)}}\right) + \frac{1}{4M_2} \tag{D.22}$$

where $M_s(\pi \leqslant \pi_0) = M_1M_2/(M_1 + M_2)$. This compliance applies to the thermodynamic equations governing the uniform secant response of our membranes, as established in Eqn. (D.12a).

D.4.2.2 Non-Uniform Response

Integrating by parts the tangent compliance governing squeeze in Eqn. (D.21a) provides its secant compliance of

$$\frac{1}{2N_s(\sigma)} = \frac{\varepsilon_{1_{\max}}}{|\sigma|}\left(1 - \frac{\sqrt{N_1\varepsilon_{1_{\max}}}}{\sqrt{N_1\varepsilon_{1_{\max}} + |\sigma|}}\right) + \frac{1}{2N_2} \tag{D.23}$$

where $N_s(\sigma = 0) = N_1N_2/(N_1 + N_2)$, while integrating by parts the tangent compliance governing shear in Eqn. (D.21b) results in its secant compliance of

$$\frac{1}{G_s(\tau)} = \frac{\gamma_{1_{\max}}}{|\tau|}\left(1 - \frac{\sqrt{G_1\gamma_{1_{\max}}}}{\sqrt{G_1\gamma_{1_{\max}} + 2|\tau|}}\right) + \frac{1}{G_2} \tag{D.24}$$

where $G_s(\tau = 0) = G_1G_2/(G_1 + G_2)$. These compliances apply to the thermodynamic equations governing the non-uniform secant response of our membranes, as established in Eqn. (D.13a).